Journal of
Irrigation Sciences and Engineering(JISE)
ISSN 2588-5952
Iranian Hydraulic Association
Shahid Chamran University of Ahvaz
Faculty of Water and Environmental Engineering
Vol. 48(4) Winter 2026

Contents

------- Research Papers -------

**Experimental Study of Longitudinal Extension Effects on Scour Patterns Around Single and Grouped Piers** 1
Farinaz Erfani Fard, Seyed Amin Asghari Pari and Lotfollah Emadali

**Evaluating Environmental Impacts of Dam Construction Using an Enhanced Quantitative Checklist: A Case Study of Haleh Dam in Iran** 19
Nader Nabipour and Babak Lashkar-Ara

**Numerical investigation of Semicircular Sharp-Crested Weirs** 37
Abbas Parsaie, Mohammad Bahrami Yarahmadi and Mahziar BasitNejad

**Investigation of Changes in the Green and Blue Water Footprint of Wheat in Drought and Rainy Seasons (A Case Study on Wheat under the Dez Irrigation Network, Southwestern Iran)** 49
Mahkameh Mansouri, Esfandiar Fateh, Amir Aynehband and Ali Shahbazi

**Assesment the adaptability of Jacaranda mimosifolia L. to Ahvaz climete condition under salinity and water stresses** 65
Khalil Asadivafa, Mousa Mousavi, Abdul-kadhm N. S. Al-Showily, Mohammad Albaji and Naser Alemzadeh Ansari

**Estimation of Transmissivity and Storage Coefficients in a Dual-Aquifer System Using Combined Field and Analytical Methods** 79
Sheyda Mohammadi Fard, Jahangir Abedi-Koupai and Saeid Eslamian

**Debris Blockage Risk of Modified Stepped Spillways: A Laboratory Study on Obstacle Configuration** 105
Seyed Amin Asghari Pari, Seyed Ali Asghari Pari, Mohammad Amin Mokarram and Mojtaba Kordnaeij

**Environmental Water Diplomacy between Iran and Turkey: Challenges and Strategic Priorities** 117
Fatemeh Lashkari, Mir Mehrdad Mirsanjari and Fatemeh Mohammadyari

------- Review Papers-------

**Modern Filtration Technologies for Nutrient Removal from Domestic Wastewaters: A Review** 133
Saeid Eslamian and Mousa Maleki

**Microplastics: The Invisible Invaders – Unveiling Sources, Journeys, Impacts, and Cutting-Edge Remedies in a Plastic-Choked World** 145
Fatemeh Elyasi, Laleh divband hafshejani and Parvaneh Tishehzan

**In The Name of God**

# Irrigation Sciences and Engineering

(Scientific)

**Vol. 48 (4)** **Winter 2026**

**Board of Editors**

| | | |
|---|---|---|
| **AkhondAli, A. M.** | **Professor** | **Faculty of Water and Environmental Engineering, Shahid Chamran University of Ahvaz, Ahvaz, Iran** |
| **Ghomeshi, M** | **Professor** | **Faculty of Water and Environmental Engineering, Shahid Chamran University of Ahvaz, Ahvaz, Iran** |
| **Heydarpour, M.** | **Professor** | **Faculty of Agriculture, Isfahan University of Technology** |
| **Kashefipour, S. M.** | **Professor** | **Faculty of Water and Environmental Engineering, Shahid Chamran University of Ahvaz, Ahvaz, Iran** |
| **Liaghat, A. M.** | **Professor** | **Faculty of Agriculture, University of Tehran** |
| **Hosseinzadeh Dalir, A.** | **Professor** | **Professor, Water Engineering Department, Faculty of Agriculture, University of Tabriz, Iran.** |
| **Naseri, A. A.** | **Professor** | **Faculty of Water and Environmental Engineering, Shahid Chamran University of Ahvaz, Ahvaz, Iran** |
| **Zand Parsa, Sh.** | **Professor** | **Faculty of Agriculture, Shiraz University of Technology** |
| **Pagliara, Stefano.** | **Professor** | **Department of Civil Engineering, University of Pisa,Italy** |
| **Sai Hin, L.** | **Associate Professor** | **Department Of Civil Engineering, Faculty of Engineering, University of Malaya, Maliysia** |
| **Ahmadian, R.** | **Professor** | **Department of Civil Engineering, School of Engineering, Cardiff University, UK** |
| **Ritzema, H.** | **Associate Professor** | **Water Resources Management Group, Environmental Sciences Group, Wageningen University & Research, Netherland** |

**Published by: Shahid Chamran University of Ahvaz, Faculty of Water Sciences Engineering, Ahvaz, Iran.**
**Director: BoromandNasab, S.**
**Editor-in-Chief: Kashefipour, S.M.**
**Editorial Manager: Yazdani, N**
**Type Setting: Yazdani, N.**

**E–mail: JISE.Water@Scu.ac.ir**
**JISE.Water@yahoo.com**

Publication license of the Ministry of Culture and Islamic Guidance No. 10362/124 on 29/12/1998 and license of the Journal Review Office of the Ministry of Science, Research and Technology No. 11/3/1264 on 21/10/2009 for the Journal of Irrigation Sciences and Engineering.

## The Names of The Reviewers of The Articles In This Issue

| | |
|---|---|
| Anvari | Sedigheh |
| Bahmani | Omid |
| Gorgizade | Ali |
| Khoramian | Amin |
| Khoramian | Mohammad |
| Mahdi | Sarai Tabrizi |
| Nozari | Hamed |
| Olapour | Masoud |
| Parsaei | Abbas |
| Ramezani | Yosef |
| Rasoul | Mirabbasi |
| Sajjadi | Mohsen |
| Sayadi | Atefeh |
| Younesi | Hojat allah |

# Preface

Praise be to the Almighty God who blessed us, with the efforts and perseverance of the editorial board, the journal staff, and the cooperation of the reviewers and editors, the Journal of Irrigation Sciences and Engineering (JISE) publishes the Vol.48 No.4 in English.

The JISE journal has a history about 43 years and The Ministry of Science, Research and Technology issued the license for this journal in 2009 as a scientific-research journal in present form. This journal is indexed on the ISC and Doaj international sites.

The editorial board of the JISE journal hopes that the esteemed colleagues in all universities, scientific and research centers by sending their valuable scientific and practical articles in specialties of water engineering, irrigation and drainage, water resources, hydraulic structures, sediment hydraulics, aquatic environment, watershed management, meteorology, hydrology, groundwater, water economics, and the related sciences cooperate with the JISE. Also we hope those people who are specialist in these fields of study assist us for the continuity of journal printing and publishing and providing more valuable researches of water sciences and engineering. We sincerely thank all the experts and reviewers of the articles who have played a role in improving the quality of the journal on various occasions by providing their valuable opinions.

**Editor-in-chief**

**S.M. Kashefipour**

| Contents | Page |
|---|---|


**Experimental Study of Longitudinal Extension Effects on Scour Patterns Around Single and Grouped Piers** 1
Farinaz Erfani Fard, Seyed Amin Asghari Pari and Lotfollah Emadali

**Evaluating Environmental Impacts of Dam Construction Using an Enhanced Quantitative Checklist: A Case Study of Haleh Dam in Iran** 19
Nader Nabipour and Babak Lashkar-Ara

**Numerical investigation of Semicircular Sharp-Crested Weirs** 37
Abbas Parsaie, Mohammad Bahrami Yarahmadi and Mahziar BasitNejad

**Investigation of Changes in the Green and Blue Water Footprint of Wheat in Drought and Rainy Seasons (A Case Study on Wheat under the Dez Irrigation Network, Southwestern Iran)** 49
Mahkameh Mansouri, Esfandiar Fateh, Amir Aynehband and Ali Shahbazi

**Assesment the adaptability of Jacaranda mimosifolia L. to Ahvaz climete condition under salinity and water stresses** 65
Khalil Asadivafa, Mousa Mousavi, Abdul-kadhm N. S. Al-Showily, Mohammad Albaji and Naser Alemzadeh Ansari

**Estimation of Transmissivity and Storage Coefficients in a Dual-Aquifer System Using Combined Field and Analytical Methods** 79
Sheyda Mohammadi Fard, Jahangir Abedi-Koupai and Saeid Eslamian

**Debris Blockage Risk of Modified Stepped Spillways: A Laboratory Study on Obstacle Configuration** 105
Seyed Amin Asghari Pari, Seyed Ali Asghari Pari, Mohammad Amin Mokarram and
Mojtaba Kordnaeij

**Environmental Water Diplomacy between Iran and Turkey: Challenges and Strategic Priorities** 117
Fatemeh Lashkari, Mir Mehrdad Mirsanjari and Fatemeh Mohammadyari

**Modern Filtration Technologies for Nutrient Removal from Domestic Wastewaters: A Review** 133
Saeid Eslamian and Mousa Maleki

**Microplastics: The Invisible Invaders – Unveiling Sources, Journeys, Impacts, and Cutting-Edge Remedies in a Plastic-Choked World** 145
Fatemeh Elyasi, Laleh divband hafshejani and Parvaneh Tishehzan

Shahid Chamran University of Ahvaz

**Irrigation Sciences and Engineering (JISE)**
**Vol. 48, No. 4, Winter 2026, p. 1-17**

Journal homepage: https://jise.scu.ac.ir

**Research Paper**

# Experimental Study of Longitudinal Extension Effects on Scour Patterns Around Single and Grouped Piers

Farinaz Erfani Fard[1], Seyed Amin Asghari Pari[2*] and Lotfollah Emadali[3]

1- *Department of Civil Engineering, Behbahan Khatam Alanbia University of Technology, Behbahan, Iran*
2*- *Corresponding Author, Associate Professor, Department of Civil Engineering, Behbahan Khatam Alanbia University of Technology, Behbahan, Iran (asghari_amin@bkatu.ac.ir)*
3- *Assistant Professor, Department of Civil Engineering, Behbahan Khatam Alanbia University of Technology, Behbahan, Iran.*

ARTICLE INFO

*Artlcle history:*
Received: 15 February 2025
Revised: 10 May 2025
Accepted: 18 May 2025
Available online: 04 January 2026

*Keywords:*
Local scour, Square pier, Maximum scour depth, Single pier, pier group.

TO CITE THIS ARTICLE:

Erfani Fard, F., Asghari Pari, S. A., Emadali, L. 2026. 'Experimental Study of Longitudinal Extension Effects on Scour Patterns Around Single and Grouped Piers', *Irrigation Sciences and Engineering*, 48(4), pp. 1-17. doi: 10.22055/jise.2025.49041.2155

**Abstract**

Scour, defined as the erosion of a streambed around obstructions, poses significant risks to bridge piers, leading to structural failures and causing economic and human losses. This study investigates the effects of pier shape (modified by adding triangular and rounded noses to rectangular piers) and longitudinal extension on scour depth around single piers and pier groups. Experiments were conducted on rectangular single piers with a fixed width of 0.03 meters and varying lengths (length-to-width ratios, L/D = 1–9), as well as on groups of three-square piers with a side length of 0.03 meters and varying center-to-center distances (S/D = 2–5). The results demonstrate that adding a nose significantly reduces scour depth. The triangular nose on a rectangular pier (L/D = 9) achieved the highest reduction, decreasing the maximum scour depth by 80% compared to the benchmark model. In pier group configurations, increasing the distance between piers generally led to greater scour depths, as each pier began to act independently. The maximum scour depth observed in the S/D = 3 model increased by 25% relative to the benchmark. As pier spacing increased, scour holes became more distinct. Additionally, equipping the first pier in a group with a nose effectively diverted flow away from the piers, reducing scour more effectively than in nose-less configurations, with the triangular nose proving most effective. Overall, pier groups exhibited significantly higher scour depths than single piers.

## Introduction

Local scour around bridge piers, resulting from complex interactions between hydrodynamic forces and sediment transport, remains a critical challenge in hydraulic engineering. This phenomenon is primarily driven by three key mechanisms: (1) the formation of a horseshoe vortex at the pier's upstream face, (2) the downward flow that accelerates sediment entrainment, and (3) the wake vortices propagating downstream, which further erode the riverbed (Ahmed, 1995; Dey and Raikar, 2007; Wang et al., 2017). Given its potential to compromise bridge stability, extensive research has characterized scour dynamics, with emphasis on the influence of flow conditions, sediment properties, and pier geometry (Melville and Raudkivi, 1977; Breusers et al., 1977; Dey and Raikar, 1995; Pandey et al., 2020; Vijayasree and Eldho, 2021). Recent experimental and numerical advancements have deepened insights into scour processes. Guan et al. (2019), for instance, demonstrated that the horseshoe vortex system evolves from a single vortex to a complex multi-vortex structure during scour development. Their findings revealed that the primary vortex intensifies in strength and size

as the scour hole deepens, highlighting the dynamic nature of flow-pier interactions. To mitigate scour risks, countermeasures such as collars (Farooq et al., 2023; Heidarpour et al., 2010), slots (Moncada et al., 2009), and optimized pier geometries have been explored (added for parallel structure). Streamlined shapes (e.g., elliptical piers) reduce scour depth by up to 29.16% compared to square piers (Khan et al., 2024), while octagonal configurations disrupt vortex formation more effectively (Farooq and Grumman, 2019).

Pier dimensions and alignment relative to flow direction significantly influence scour characteristics. Experimental studies by Khan et al. (2017) demonstrated that increasing pier size from 0.03 × 0.03 m to 0.05 × 0.05 m elevates scour depth, highlighting the sensitivity of scour to structural scale. Similarly, Fenocchi and Natale (2016) used numerical and physical modeling to investigate rectangular piers of different lengths and flow attack angles. According to their results, for rectangular piers with different length-to-width ratios ($L/D$ = 1, 1.5, 2, and 3), scour increases significantly as the flow attack angle increases. Omara et al. (2022) studied scour around rectangular piers with length ratios $L/D$ = 1-9 in shallow flow. Their research showed that the maximum scour occurred in rectangular piers with $L/D$ = 4.5. These findings collectively emphasize the importance of geometric considerations in pier design.

While most research focuses on single pier configurations, modern bridge designs often employ pier groups to accommodate wider spans. This necessitates a thorough understanding of the interplay between multiple piers, including vortex interference, spacing effects, and collective scour patterns. Research on tandem and side-by-side arrangements has revealed that scour depth depends critically on the dimensionless spacing ratio ($S/D$), where $S$ represents the center-to-center distance between piers and $D$ denotes the pier width. For instance, Ataie-Ashtiani and Aslani-kordkandi (2013) compared the flow patterns around a tandem circular pier group and single piers. Their results showed that the turbulent kinetic energy, turbulence intensity, and vortex strength around the piers group were lower than around single piers. They also stated that the bed shear stress between the two piers is about twice that around the piers, and the scour between them is approximately 15% greater than for the single pier case. Complementary numerical investigations by Habibi et al. (2023) identified $S/D$ = 2 as a critical threshold for tandem pier groups, beyond which pier interactions diminish significantly. The configuration of pier groups also plays a pivotal role in scour development. A comparative study by Vijayasree and Eldho (2016) demonstrated that oblong pier arrangements reduce scour volume by 55.63% relative to twin circular piers, illustrating the benefits of aerodynamic shaping. Zhou et al. (2020) examined the influence of the angled pier arrangement and spacing in the group of three cylindrical piers. They said that when piers are placed in a line, the distance between the piers does not determine the scour depth. However, when the flow attack angle is greater than zero, depending on the attack angle, pier diameter, and pier spacing, the maximum scour depth shifts from the first pier to the second and third piers, which they attributed to a reinforcing effect. They also came up with an equation for predicting maximum scour depth based on their data and data from other experiments.

Overall, Recent research on scour patterns around bridge piers highlights key influences of pier geometry, flow conditions, and pier arrangements. Experimental studies demonstrate that rectangular piers induce the deepest scour due to intensified horseshoe vortices, whereas streamlined shapes (e.g., sharp-nosed or lenticular) minimize scour depth (Baranwal et al., 2023; Al-Jubouri et al., 2024). Scour depth correlates positively with flow velocity and frontal area (Baranwal et al., 2023), as well as water depth and discharge (Kadam and Dawari, 2024). For grouped piers, spacing critically affects scour dynamics: increasing the distance between side-by-side piers reduces scour depth (Movahedi et al., 2011), and in tandem arrangements, maximum

scour depth at the upstream pier occurs at a spacing of two pier diameters, with reduced scour at the downstream pier due to sheltering effects (Hassan et al., 2020). Lenticular piles consistently outperform circular and square shapes in scour mitigation (Tariq et al., 2022), and non-uniform twin piers further underscore spacing-dependent scour variations (Ravanfar et al., 2024).

The primary objective of this paper is to investigate the combined effects of two factors, pier length extension and nose shape alteration, on scour depth. This topic has received limited attention in previous studies, which typically examine either pier nose shape or pier length in isolation. In contrast, this study systematically analyzes the interaction between these two parameters and presents their simultaneous effects on scour depth and patterns. Moreover, it includes a comparative analysis of scour around square pier groups with various nose shapes (such as triangular and circular) at different distances. This innovative approach contributes to the design of more erosion-resistant bridge piers. 36 experiments were conducted on rectangular single piers of varying lengths and groups of three piers at different spacings, with configurations including no nose, triangular noses, and round noses under consistent laboratory conditions.

**Experimental Setup**

The experiments for this study were conducted in a flume with glass walls, 0.6 meters in width and height, and 6 meters in straight length at the Hydraulics Research Laboratory of Behbahan Khatam Alanbia University of Technology. At the flume inlet, two perpendicular metal mesh screens and a Styrofoam piece installed on the water surface were used to minimize fluctuations caused by water pumping. A gate was installed at the flume outlet to adjust the water level. The maximum flow rate of the current was 90 liters per second, measured by an ultrasonic flowmeter with an accuracy of ± 0.01. The flowmeter's sensors were positioned on the outlet pipe from the pump, just before entering the flume. The sediment particles used were non-cohesive sedimentary particles with a specific gravity of $\rho_s$ = 2650 kg/m³ and a median diameter of $d_{50}$ = 0.0012 m. All experiments were performed under constant conditions: clear water, a discharge of 25.7 liters per second, the average approach velocity, $u$, was 0.285 m/s, and the velocity ratio, $u/u_c$ = 0.96. The water depth was maintained 0.15 meters above the sediment surface. This study used rectangular single piers with a constant width of 0.03 meters, varying lengths (length-to-width ratios $L/D$ = 1, 2, 3, 4, 5, 6, 7, 9), and a height of 0.45 meters. Three square piers, each measuring 0.03 meters in both length and width, were utilized in the pier group experiments. The center-to-center distance between piers in the pier groups, experiments was chosen as 2, 3, 4, and 5 times the pier width ($S/D$ = 2, 3, 4, 5). Additionally, to examine the effect of the nose on scour, all experiments were conducted in three conditions: rectangular cross-section (Rec), with a triangular nose (Tria), and with a round nose (Round). In this study, the $L/D$ =1, Rec test is adopted as the benchmark model. An Acoustic Doppler Velocimeter (ADV) was used to investigate flow development. Due to the instrument's operational constraints—requiring full submersion of its probes—the first measurable point was 0.5 m below the water surface. Velocity profiles were plotted along the flume's centerline within the pier-installed region. As shown in Fig. (1), the velocity profiles remain uniform along the channel's longitudinal direction, with profiles at different locations overlapping. Under the current experimental conditions, the flow was fully developed along the straight section containing the bridge piers.

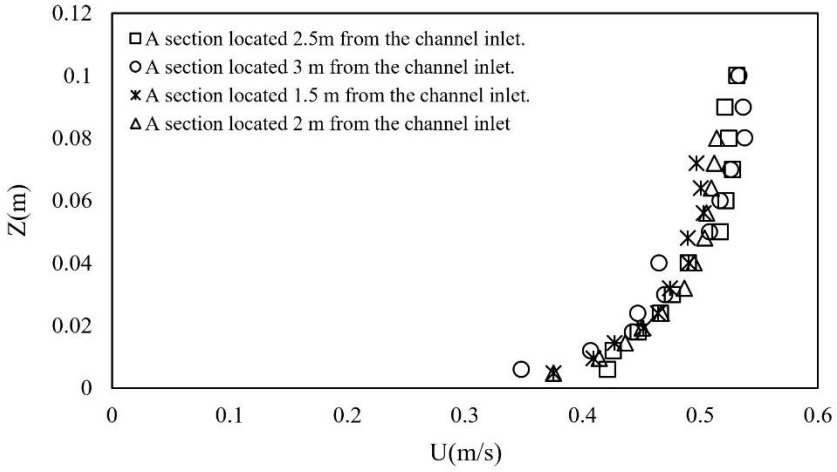



**Fig. 1- Velocity profiles at various distances from the channel inlet.**

In this study, Melville's equation was employed to estimate the critical flow velocity (Melville, 1997); subsequently, Kramer's mean transport criterion was applied to verify the threshold at which sediment initiation occurs. According to the Kramer sediment transport criterion, this threshold is usually characterized by the displacement of medium-sized sediment particles within the bed material (Kramer, 1935). While this method is primarily qualitative, it effectively captures the initial stages of sediment transport, providing a reliable indicator of when sediment begins to shift. Since laboratory observations were specifically conducted for the study in question, they were generally considered more reliable, and the results matched to real experimental conditions. The methodology was as follows: First, an experiment without a pier (to prevent localized scour due to the presence of a pier) was conducted to determine the critical velocity. The water depth was set (0.15 m in this study), and the flow discharge was gradually increased until, at a point in the channel and bed where the flow was fully developed and unaffected by side walls, the first bed particle was dislodged and transported downstream. Using the relation $Q = Au_c$, the average $u_c$ was determined as the critical velocity. Subsequently, experiments were conducted at a specified discharge (25.7 L/s), lower than the critical discharge, and $u/u_c$ = 0.96 to ensure clear-water scour conditions.

**Dimensional Analysis**

The parameters influencing local scour around bridge piers are diverse. Extensive studies have been conducted in this regard, with Ettema et al. (1998) and Ansari et al. (2002) identifying scour depth as a function of influential parameters, including flow characteristics, channel properties, pier specifications, bed conditions, and fluid properties. The present study aims to investigate the impact of longitudinal pier development, both as single and group configurations, as well as the effect of nose placement on local scour around piers. Consequently, the parameters affecting the scour hole depth ($d_s$) are as follows: flow depth ($y$), flow velocity ($u$), fluid density ($\rho$), the kinematic viscosity of flow ($\nu$), median sediment size ($d_{50}$), bed sediment density ($\rho_s$), bridge pier width ($D$), pier length ($L$), geometric standard deviation of bed particle distribution ($\sigma_g$), time ($t$), gravitational acceleration ($g$), the center-to-center spacing between piers ($S$), and nose shape parameter ($\beta$).

$$d_s = f(u, \rho, \nu, d_{50}, \rho_s, D, L, \sigma_g, t, g, S, \beta,) = 0 \quad (1)$$

For dimensional analysis in this study, the Buckingham π theorem was employed. Based on this method, 11 dimensionless parameters were formed. The flow depth for this study was

selected based on criteria established by Breusers et al. (1977), Ettema (1980), and Raudkivi (1986), which indicate that when $y/D > 3$ to 4, the maximum scour depth becomes independent of flow depth. According to Xie (2011) and Fael et al. (2016), the equilibrium scour depth does not depend on sediment coarseness for $D/d_{50} \geq 25$–50. Additionally, Lee and Sturm (2009) demonstrated that the maximum relative pier scour depth occurs at $b/d_{50} \approx 25$. To eliminate the channel wall effect on scour depth, $B/D \geq 10$ should be maintained (Melville and Chiew, 1999). The discharge rate, duration, flow depth, and median sediment size remain constant in all experiments. Finally, the dimensional analysis of parameters affecting scour depth is obtained as follows:

$$\frac{d_s}{D} = f(\frac{L}{D}, \frac{S}{D}, \beta) \quad (2)$$

**Test Conditions**

After preparing the bed, the pump was activated, and the gate installed downstream was adjusted to achieve a height of 0.15 meters above the bed. To prevent initial scour caused by the flow, water entry into the flume began with a low discharge, and then, after establishing the necessary flow depth, the discharge was gradually increased to reach the intended 25.7 liters per second. Once the flow reached the desired conditions, the scour experiment commenced, marking the initial time. In previous studies (Melville and Chiew, 1999; Sheppard et al., 2014; Lança et al., 2013), various criteria were stated for equilibrium scour depth under steady flow. According to Kumar et al. (1999), equilibrium time is defined as the point when the scour rate is equal to or less than one millimeter over 3 hours. Mia and Mago (2003) halted their experiments when the rate of scour advancement became less than 1 mm/hr. Moncada et al. (2009) selected a criterion where the changes in scour depth over 2 hours are less than 1 mm to define the onset of the equilibrium state. To achieve equilibrium in the scouring experiments of the present research, the equilibrium time for all experiments was considered to be approximately 72 hours. In this study, the equilibrium depth was defined as a depth at which, in the last 8 hours of each test, the changes in the depth of the hole are equal to or less than 1 mm. Fig.(2)demonstrates that scour depth progression around the benchmark model stabilized over time, with marginal fluctuations, confirming the establishment of equilibrium conditions in the experiment. At the end of the experiment, the water supply system was turned off, and the water level adjustment gate was lowered to allow for gentle drainage. After the complete drainage of water, a bed profiler device was employed to measure topographic changes caused by bed scouring. This device consists of a mobile, intelligent carriage equipped with a laser with a measurement error of ±1 mm. Fig.(3)shows the setup before starting tests, and Fig.(4)shows a selected test.

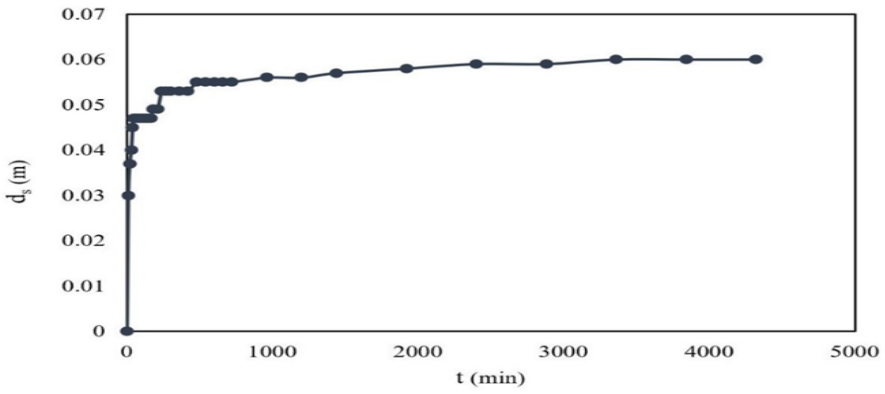



**Fig. 2- Equilibrium Scour Depth Progression: Benchmark Model test**

 *DOI:* 10.22055/jise.2025.49041.2155




**Fig. 3- Setup and Calibration of Experimental Apparatus for Laboratory Testing: a) Smoothing of bed sediment, b) placement of the pier in the bed sediment, c) leveling of the pier.**

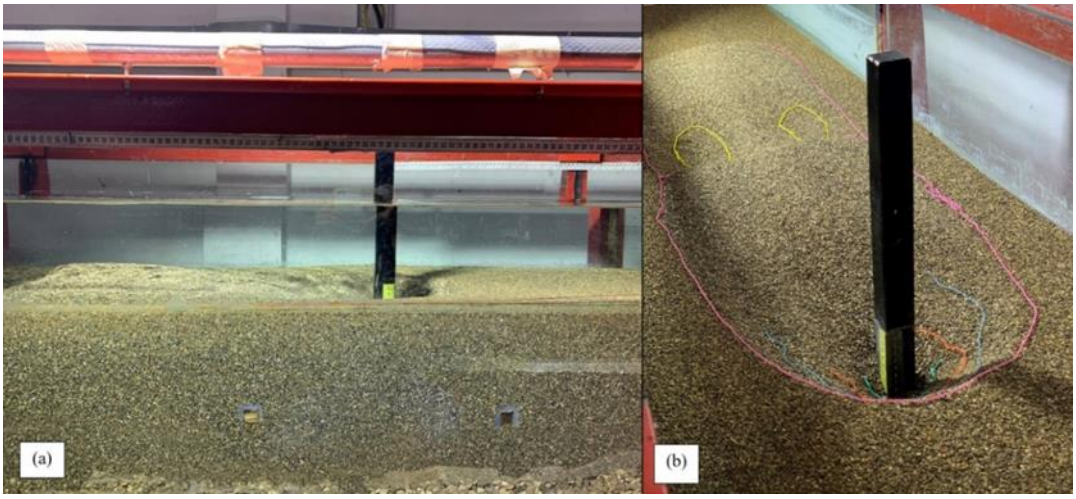



**Fig. 4- L/D = 1, Rec Test: a) In-Progress Testing, b) Scouring Completed.**

## Results and Discussion

### Flow Pattern

The presence of a bridge pier in the river cross-section leads to the formation of complex turbulent structures around the pier. This study examined changes in surface flow paths by analyzing wood chip movements on the water surface. Small wood chips were sprinkled on the surface, revealing flow patterns as they passed near piers. To illustrate the changes in the surface flow path caused by the bridge piers, wood chips were first sprinkled on the water. Then, a video was recorded from above. The recorded video was converted into sequential images, which were then analyzed using the PIVLab code in MATLAB software. Fig. (5)and Fig. (6)show the output images from PIVLab.

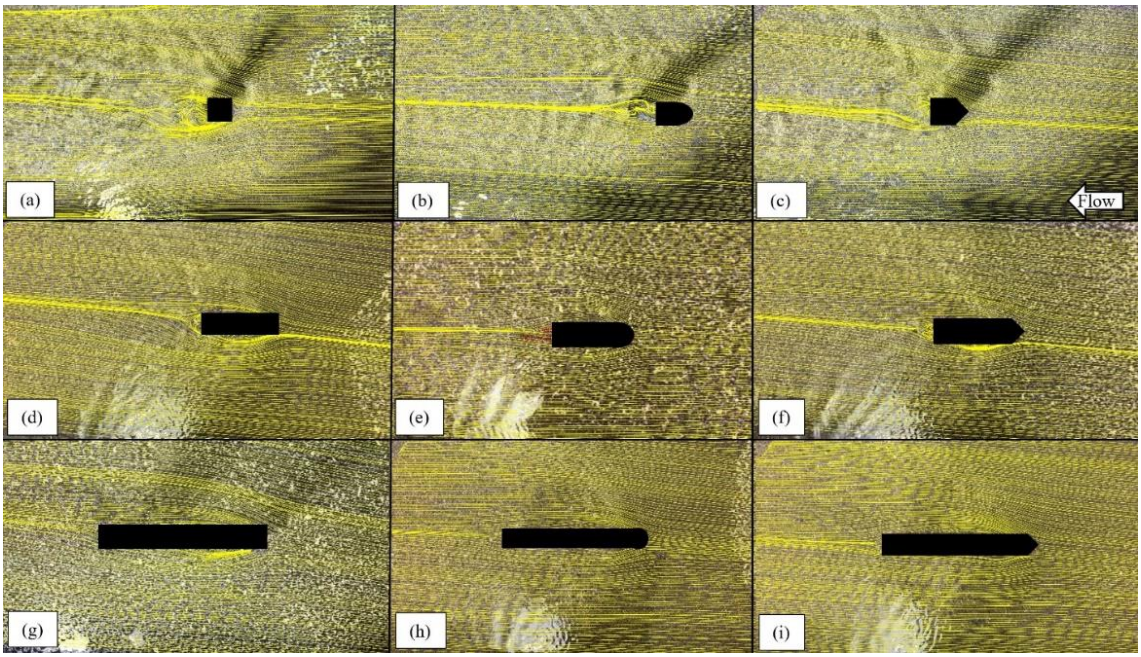



**Fig. 5- Surface flow conditions around single pier: a) L/D = 1, Rec, b) L/D = 1, Round, c) L/D = 1, Tria, d) L/D = 4, Rec, e) L/D = 4, Round, f) L/D = 4, Tria, g) L/D = 9, Rec, h) L/D = 9, Round, and i) L/D = 9, Tria.**

As shown in Fig. (5a), when the flow impacts a single pier with an *L/D* ratio of 1, it symmetrically deflects around the pier, forming two downstream vortices. As the pier length increases, the surface flow mechanism changes, reducing the size of the surface vortices and consequently decreasing the oscillations downstream of the pier. For an extended single pier with an L/D ratio of 9, the flow, after striking the pier, is deflected to the sides and continues along and beyond the pier without noticeable oscillation. The addition of a nose to the single pier, which alters the surface area impacted by the flow, results in smaller vortices forming behind the pier and a reduction in oscillations over a shorter downstream distance. In extended single piers, the combination of elongation and the presence of a nose causes the flow, after striking the nose, to be diverted and then to continue along a straight path without oscillation beside the pier. As illustrated in Fig. (6), in experiments involving a group of piers, the upstream pier initially deflects the flow to the sides, allowing it to enter the space between the two piers. This interaction leads to the formation of surface oscillations and vortices behind each pier. When the spacing between piers increases, the flow first impacts the upstream pier, then deflects to the side, and subsequently flows between the two piers. In this case, the larger spacing increases both the flow area and the volume of flow passing through. As depicted in Fig. (5), this results in more pronounced surface oscillations and turbulence between the piers compared to cases with smaller pier spacing.

 *DOI:* 10.22055/jise.2025.49041.2155

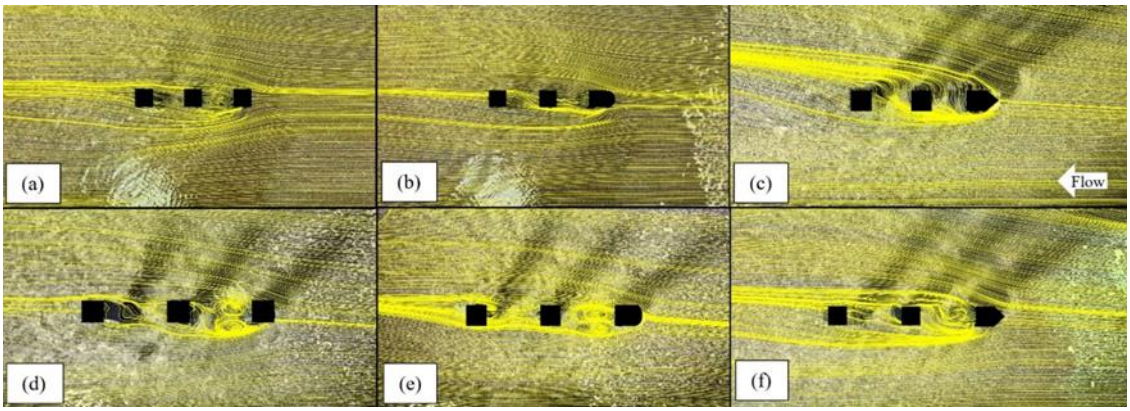



**Fig. 6- Surface flow conditions around pier groups: a) *S/D* = 3, Rec, b) *S/D* =3, Round, c) *S/D* = 3, Tria, d) *S/D* = 5, Rec, e) *S/D* = 5, Round, and f) *S/D* = 5, Tria.**

It was observed that adding a nose to the upstream pier in the pier group reduced surface oscillations between the two piers compared to configurations without a nose. Furthermore, the triangular nose, due to its smaller contact area with the flow, was more effective in minimizing surface oscillations between the piers than the round nose.

**Scour Pattern**

Comparison of the results in Fig. (7)reveals a direct correlation between pier length and scour depth reduction. The *L/D* = 9, Rec model, which features the longest pier, exhibits a 35% reduction in maximum scour depth compared to the benchmark case. This decrease can be attributed to the weakened interaction of primary vortices, reducing their collective intensity. Additionally, the increased pier length promotes smoother flow passage around the structure, thereby decreasing turbulence. As a result, both vortex strength and localized scour are mitigated. The observed trend—where scour depth decreases with increasing pier length (while pier width remains constant)—is consistent with established flow dynamics and vortex behavior (Vijayasree and Eldho, 2016; Chibana et al., 2022; Tao et al., 2013; Muzzammil et al., 2004). These findings are further supported by Kharbeche (2022), Guemou et al. (2016), and Omara et al. (2022), who demonstrated that lengthening the pier while maintaining a constant width alters scour mechanisms, ultimately reducing scour depth. As illustrated in Fig. (7a) triangular nose on the upstream side of the shortest pier (*L/D* = 1, Tria) reduces the maximum scour depth by 60% compared to the benchmark model, whereas a rounded nose (*L/D* = 1, Round) achieves a 50% reduction. Notably, the triangular nose yields a 20% lower scour depth than the rounded nose for *L/D* = 1, confirming that pier shape significantly influences scour depth and flow dynamics. Consistent with prior studies (Baranwal et al., 2023; Elshahat and Elnikhely, 2023; Vijayasree et al., 2019), sharp or triangular noses outperform round and rectangular designs in scour mitigation. This improvement stems from the nose's flow-deflecting effect, which reduces pressure buildup on the pier surface. For piers with short longitudinal extensions, the triangular nose promotes lateral flow deflection, isolating the horseshoe vortex from downstream vortices and weakening vortex intensity. In contrast, rectangular piers with flat faces exhibit the deepest scour due to unmitigated vortex development (Farooq and Gumman, 2019; Ismael et al., 2015; Tao et al., 2013). In this study, the triangular nose (sharp nose) also showed better results in minimizing the scour hole depth than the round nose. The simultaneous effects of nose geometry and pier length on maximum scour depth were also examined. The results indicate that both the addition of a nose and an increase in pier length significantly reduce scour depth. Specifically, the *L/D* =9, Tria

model reduced scour depth by 80%, while the *L/D* =9, Round model achieved a reduction of 68% compared to the benchmark model. These findings demonstrate a strong synergistic effect from elongating the pier and incorporating a nose. Among the models tested, the *L/D* =9, Tria model emerged as the best performer, reducing maximum scour depth by 69% compared to the *L/D* =9, Rec model, 33% compared to the *L/D* =9, Round model, and 50% compared to the *L/D* =1, Tria model.

Fig. (8)shows the bed profile changes at the end of the experiment for some single pier tests. The longitudinal extension of the pier significantly reduces both the depth of scour and the extent of erosion on the bed, while also reducing the volume of sediment mounds formed downstream Moreover, the combined effects of the pier's longitudinal extension and the design of its nose—whether triangular or round— reduce scoured area, limiting scouring to the bed adjacent to the pier

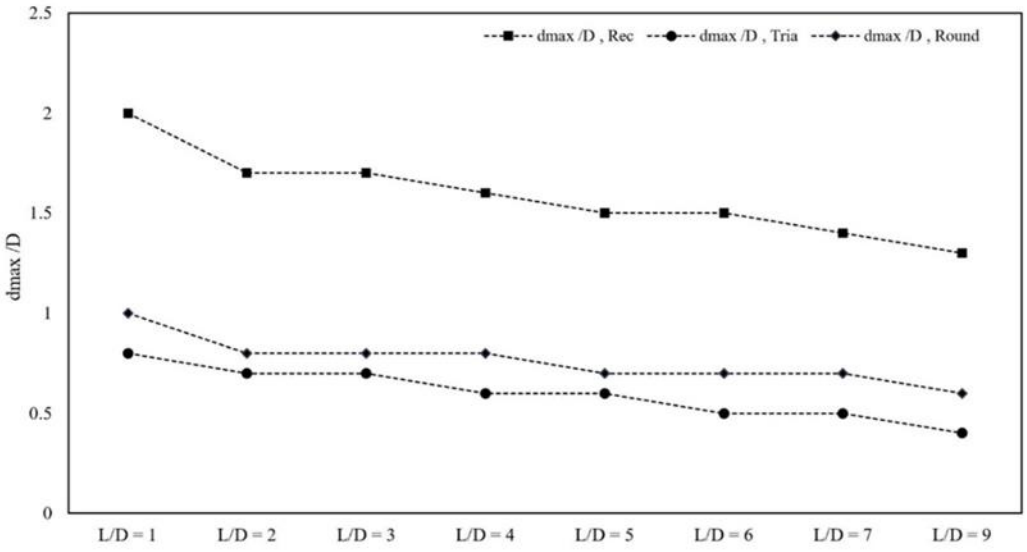



**Fig. 7- The maximum scour depth in single piers**

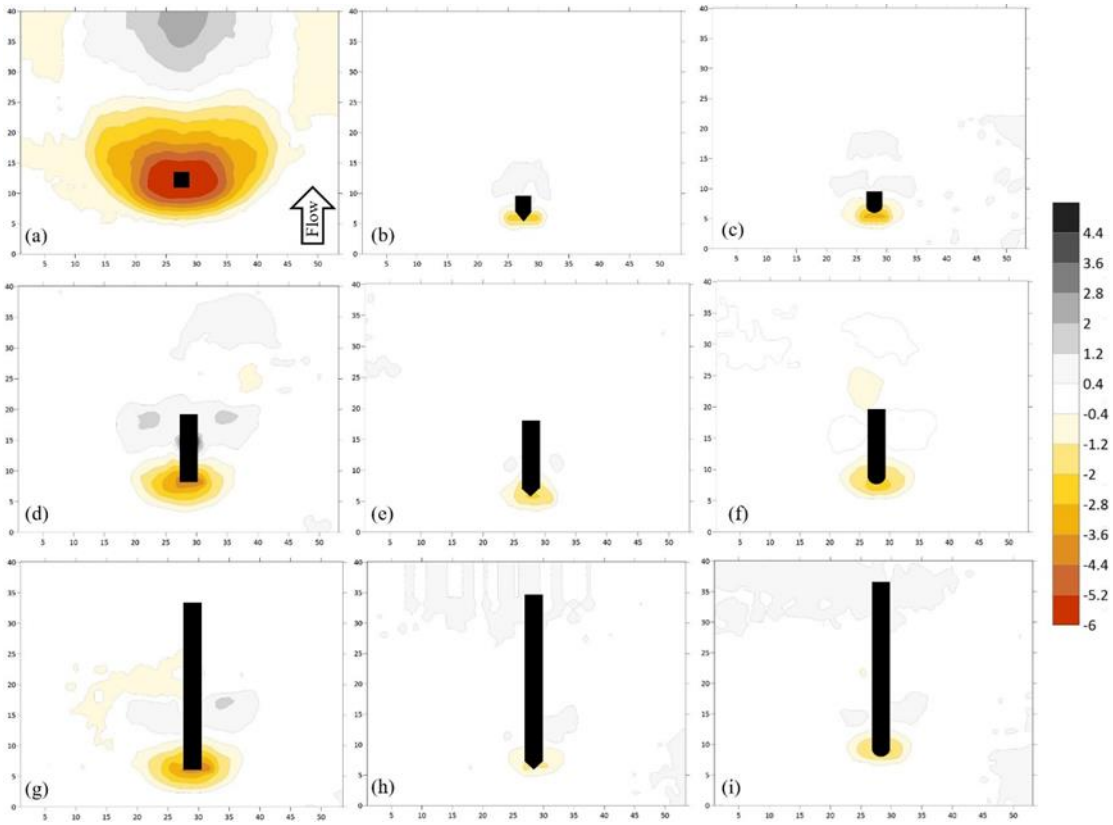



**Fig. 8- Topographic status of the single pier: a) L/D = 1, Rec, b) L/D = 1, Tria, c) L/D = 1, Round, d) L/D = 4, Rec, e) L/D = 4, Tria, f) L/D = 4, Round, g) L/D = 9, Rec, h) L/D = 9, Tria, and i) L/D = 9, Round.**

As illustrated in Fig. (9), in the pier group experiments without noses, the maximum scour depth occurred at the first pier, followed by the second and third piers. This pattern occurs because unobstructed flow impacts the first pier at maximum intensity, making it act as a defensive barrier for downstream piers. The shielding effect of the upstream pier reduces scour at the subsequent piers, consistent with previous findings (Salim and Jones, 1996; Ataie-Ashtiani and Beheshti, 2006; Kim et al., 2014; Hassan et al., 2020). Further analysis of Fig. (9) indicates that in nose-less tests, the maximum scour depth (observed at the first pier) increases with the spacing ratio (*S/D*) from 2 to 4, driven by interactions between the horseshoe vortex systems of adjacent piers. Specifically, increasing *S/D* from 2 to 3 elevates the scour rate by 14%, while a further increase to *S/D* = 4 results in a 9% rise compared to the *S/D* = 2 test. However, at *S/D* = 5, the vortex interaction weakens, reducing the maximum scour depth. The diminished overlap of vortices around each pier contributes to this decline. In the *S/D* = 5 Rec model, the maximum scour depth decreased by 4.5% compared to the *S/D* = 2, Rec model, though it remained 15% higher than the benchmark model. These results align with prior studies (Habibi et al. 2024; Hassan et al., 2020), reinforcing the relationship between pier spacing, vortex dynamics, and scour depth. This is evident in the topographic images of the pier group without a nose in Fig. (10), whereas the distance between the piers in the group increases, the scour holes also become separated, with each pier having its own scour hole. According to previous studies (Dargahi, 1990; Das et al., 2016) and the analysis of single piers presented in this research, the shape of the bridge pier nose significantly influences the vortex pattern and scour distribution. As illustrated in Fig. (9), in the experiments conducted on piers with noses, both the triangular and round noses resulted in the highest transfer of scour from the first pier

to the second. This phenomenon can be attributed to the effect of the nose shape on the flow impact dynamics. Based on the analysis of Fig. (9), the addition of a nose to the first pier in the group configuration significantly reduced the maximum scour depth across all piers compared to the no-nose scenario. The triangular nose design yielded substantial reductions in scour depth relative to the *S/D* = 2, Rec model: 59% (*S/D* = 2, Tria), 23% (*S/D* = 3, Tria), 64% (*S/D* = 4, Tria), and 68% (*S/D* = 5, Tria). Similarly, the rounded nose design demonstrated reductions of 50%, 27%, 23%, and 65% for *S/D* = 2, 3, 4, and 5, respectively. In addition, the maximum scour depths for pier groups with triangular and round noses at various spacing distances were compared. It was observed that in the *S/D* = 2 and *S/D* = 3 models, the round nose outperformed the triangular nose. Conversely, in the *S/D* = 4 model, the triangular nose demonstrated superior performance. At a spacing distance of *S/D* = 5, the effectiveness of both nose designs was nearly equivalent. The topographic images of pier groups with various nose designs, as illustrated in Fig.(10), indicate that the presence of a nose on the first pier minimizes the bed area exposed to scour both upstream and downstream of the piers.

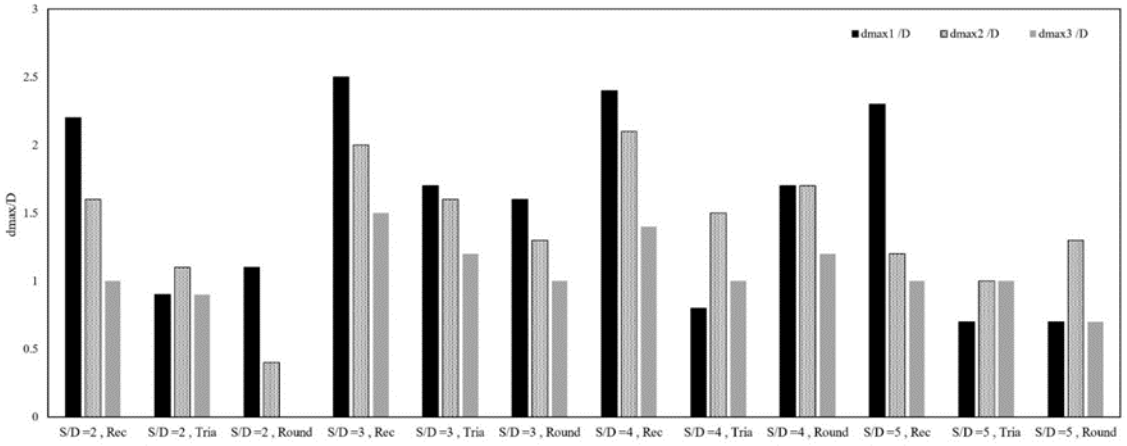



**Fig. 9- The maximum scour depth in pier groups.**

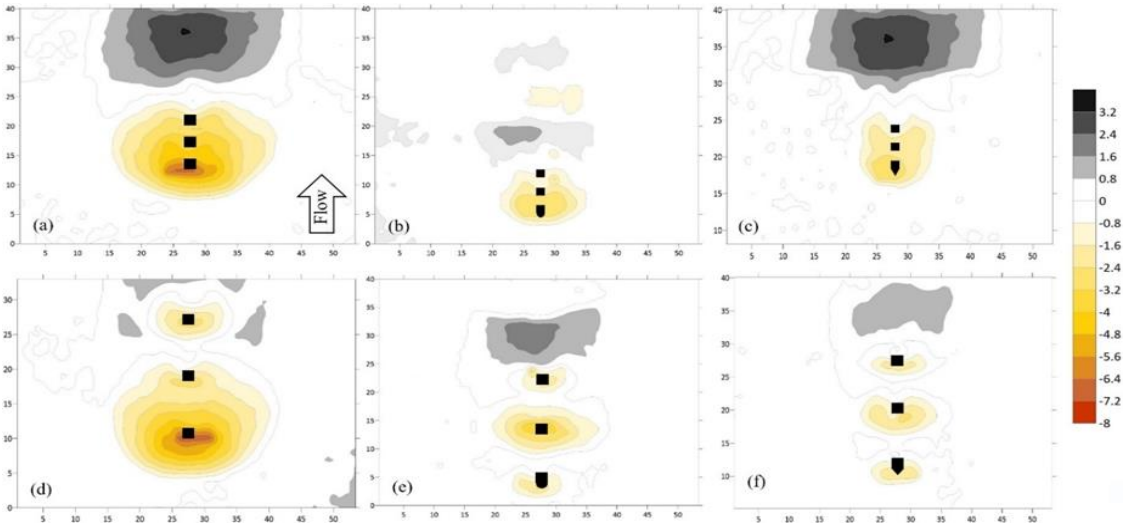



**Fig. 10- Topographic status of the pier groups: a) S/D = 2, Rec, b) S/D = 2, Round, c) S/D = 2, Tria, d) S/D = 5, Rec, e) S/D = 5, Round, and f) S/D = 5, Tria.**

 *DOI:* 10.22055/jise.2025.49041.2155

Comparing the results of the extended single pier tests with those of the corresponding pier group tests, it can be concluded that the maximum scour depth for the extended single pier is consistently less than that of the first pier in the corresponding group. This is most probably due to the interference effect of the second downstream pier in the pier group experiments. Overlapping of scour holes is observed due to the presence of a downstream pier, and as the bed level behind the upstream pier decreases, it helps transport the bed sediment eroded from the front of the first pier. As a result, the maximum scour depth at the upstream pier is higher than in the case when the flow is not constricted. It is also important to note that the upstream pier is subjected to the reinforcing effect of the downstream pier (Amini et al., 2013). Also, the topographic images reveal that the extended single piers, compared to the corresponding extended pier groups, have a smaller surface area of the sediment bed affected by scour. scour result for all experiments is shown in Table (1).

**Table. 1- Scour results**.

| Type of piers | *L*/*D* | Pier shape | *S*/*D* | $d_{max1}$ /*D* | $d_{max2}$ /*D* | $d_{max3}$/*D* |
|---|---|---|---|---|---|---|
| Single pier | 1 | Rec | * | 2 | * | * |
| | 2 | Rec | * | 1.7 | * | * |
| | 3 | Rec | * | 1.7 | * | * |
| | 4 | Rec | * | 1.6 | * | * |
| | 5 | Rec | * | 1.5 | * | * |
| | 6 | Rec | * | 1.5 | * | * |
| | 7 | Rec | * | 1.4 | * | * |
| | 9 | Rec | * | 1.3 | * | * |
| | 1 | Tria | * | 0.8 | * | * |
| | 2 | Tria | * | 0.7 | * | * |
| | 3 | Tria | * | 0.7 | * | * |
| | 4 | Tria | * | 0.6 | * | * |
| | 5 | Tria | * | 0.6 | * | * |
| | 6 | Tria | * | 0.5 | * | * |
| | 7 | Tria | * | 0.5 | * | * |
| | 9 | Tria | * | 0.4 | * | * |
| | 1 | Round | * | 1 | * | * |
| | 2 | Round | * | 0.8 | * | * |
| | 3 | Round | * | 0.8 | * | * |
| | 4 | Round | * | 0.8 | * | * |
| | 5 | Round | * | 0.7 | * | * |
| | 6 | Round | * | 0.7 | * | * |
| | 7 | Round | * | 0.7 | * | * |
| | 9 | Round | * | 0.6 | * | * |
| Group pier | 1 | Rec | 2 | 2.2 | 1.6 | 1 |
| | 1 | Rec | 3 | 2.5 | 2 | 1.5 |
| | 1 | Rec | 4 | 2.4 | 2.1 | 1.4 |
| | 1 | Rec | 5 | 2.3 | 1.2 | 1 |
| | 1 | Tria | 2 | 0.9 | 1.1 | 0.9 |
| | 1 | Tria | 3 | 1.7 | 1.6 | 1.2 |
| | 1 | Tria | 4 | 0.8 | 1.5 | 1 |
| | 1 | Tria | 5 | 0.7 | 1 | 1 |
| | 1 | Round | 2 | 1.1 | 0.4 | 0.0 |
| | 1 | Round | 3 | 1.6 | 1.3 | 1 |
| | 1 | Round | 4 | 1.7 | 1.7 | 1.2 |
| | 1 | Round | 5 | 0.7 | 1.3 | 0.7 |

## Conclusion

This study investigated the effects of longitudinal pier extensions and nose shape modifications on local scour under controlled conditions. Key findings include:

Pier Elongation (No Nose): Increasing the length-to-width ratio (*L/D*) up to 9 effectively reduced scour by up to 35% by separating upstream and downstream vortex systems.

Nose Modification (*L/D* = 1): Adding a triangular or round nose reduced scour by 60% and 50%, respectively, with the triangular shape proving more effective at deflecting flow.

Combined Effects (*L/D* = 9 with Nose): A strong synergistic effect was observed—triangular and round-nosed piers reduced scour by 80% and 68%, respectively, compared to the benchmark.

Pier Groups: Upstream piers experienced the most scour; nose modifications reduced scour across all piers, with round noses performing better at close spacing (*S/D* = 2–3) and triangular noses at intermediate spacing (*S/D* = 4).

Spacing Effects: Scour increased at *S/D* = 2–4 due to vortex interference, but decreased at *S/D* = 5 as vortex interaction weakened and distinct scour holes formed.

Single vs. Group Piers: Pier groups showed deeper scour than single piers due to flow interaction between multiple piers.

These results emphasize the benefits of combining pier elongation with nose shaping to significantly reduce scour risk. Future work should focus on field validation and scaling effects.

## Acknowledgment

This research has no acknowledgments.

## Conflict of Interest

The authors declared no potential conflicts of interest concerning the research, authorship, and publication of this article. Confirmation.

## Funding

The authors received no financial support for the research, authorship, and publication of this article.

## Data Availability Statements

Data Availability Statement: All information and results are presented in the text of the article.

## Authors' contribution

**First Author: Farinaz Erfanifard** (50%): Responsible for writing the manuscript, conducting the experiments, and analyzing the results.

**Second Author: Seyed Amin Asghari Pari** (Corresponding Author, 40%): Served as the thesis supervisor, controlled the overall work, and reviewed the results.

**Third Author: Lotfala Emadali** (10%): Provided consultation and overall review.

## Notation

The following symbols are used in this paper:

*A = flow cross-section*
*B = flume width;*
*D = pier width;*
$d_{50}$ *= median grain diameter;*
*ds = local scour depth;*
$d_{maxi}$ *= the maximum scour depth around the ith pier;*
*g = gravitational acceleration;*
*L = pier length;*
*n = number of piers;*
*S = center-to-center spacing between piers;*
*t= time;*
*u = flow velocity;*
$u_c$ *= critical flow velocity;*
*y = flow depth;*
$\rho$ *= fluid density;*
$\rho_s$ *= bed sediment density;*
$\beta$ *= nose shape parameter;*
$\sigma_g$ *= geometric standard deviation of bed particle distribution;*
$\nu$ *= kinematic viscosity of flow.*

**References**

1- Ahmed, F. 1995. Flow and erosion around bridge piers. Dissertation, University of Alberta.

2- Aksoy, A.O., Bombar, G., Arkis, T. and Guney, M.S., 2017. Study of the time-dependent clear water scour around circular bridge piers. *Journal of hydrology and hydromechanics*, *65*(1), p.26. DOI: 10.1515/johh-2016-0048.

3- Al-Jubouri, M., Ray, R.P. and Abbas, E.H., 2024. Prediction of scour depth for diverse pier shapes utilizing two-dimensional Hydraulic Engineering Center's River Analysis System sediment model. *Fluids*, *9*(11), p.247. doi.org/10.3390/fluids9110247.

4- Amini, A., Melville, B.W., Ali, T.M. and Ghazali, A.H., 2013. Closure to "Clear-Water Local Scour around Pile Groups in Shallow-Water Flow" by Ata Amini, Bruce W. Melville, Thamer M. Ali, and Abdul H. Ghazali. *Journal of Hydraulic Engineering*, *139*(6), pp.680-681. doi.org/10.1061/(ASCE)HY.1943-7900.00007.

5- Ansari, S.A., Kothyari, U.C. and Ranga Raju, K.G., 2002. Influence of cohesion on scour around bridge piers. *Journal of hydraulic research*, *40*(6), pp.717-729. doi.org/10.1080/00221680209499918

6- Ataie-Ashtiani, B. and Aslani-Kordkandi, A., 2013. Flow field around single and tandem piers. *Flow, turbulence and combustion*, *90*, pp.471-490.

7- Ataie-Ashtiani, B. and Beheshti, A.A., 2006. Experimental investigation of clear-water local scour at pile groups. *Journal of Hydraulic Engineering*, *132*(10), pp.1100-1104. doi.org/10.1061/(ASCE)0733-9429(2006)132:10(1100)

8- Baranwal, A., Das, B.S. and Setia, B., 2023. A comparative study of scour around various shaped bridge pier. *Engineering Research Express*, *5*(1), p.015052. DOI 10.1088/2631-8695/acbfa1.

9- Breusers, H.N.C., Nicollet, G. and Shen, H.W., 1977. Local scour around cylindrical piers. *Journal of hydraulic research*, *15*(3), pp.211-252. doi.org/10.1080/00221687709499645

10- Das, S., Das, R. and Mazumdar, A., 2016. Comparison of local scour characteristics around two eccentric piers of different shapes. *Arabian Journal for Science and Engineering*, *41*, pp.1199-1213.

11- Dargahi, B., 1990. Controlling mechanism of local scouring. *Journal of hydraulic engineering*, *116*(10), pp.1197-1214. doi.org/10.1061/(ASCE)0733-9429(1990)116:10(119.

12- Dey, S. and Raikar, R.V., 2007. Characteristics of horseshoe vortex in developing scour holes at piers. *Journal of Hydraulic Engineering*, *133*(4), pp.399-413. doi.org/10.1061/(ASCE)0733-9429(2007)133:4(399).

13- Dey, S., Bose, S.K. and Sastry, G.L., 1995. Clear water scour at circular piers: a model. *Journal of Hydraulic Engineering*, *121*(12), pp.869-876. doi.org/10.1061/(ASCE)0733-9429(1995)121:12(869.

14- Chibana, T., Quiocho, R. and Watanabe, K., 2022. Role of grain size distribution and pier aspect ratio in scouring and sorting around bridge piers. *Water*, *14*(13), p.2066. doi.org/10.3390/w14132066.

15- Elshahat, E. and Elnikhely, E., 2023. Influence of the Shape and Properties of the Bridge Pier's Nose on Scour Depth. *The Egyptian International Journal of Engineering Sciences and Technology*, *42*(1), pp.15-22. Doi: 10.21608/EIJEST.2022.150217.1167.

16- Ettema, R., Melville, B.W. and Barkdoll, B., 1998. Scale effect in pier-scour experiments. *Journal of Hydraulic Engineering*, *124*(6), pp.639-642. doi.org/10.1061/(ASCE)0733-9429(1998)124:6(639).

17- Ettema, R. 1980. Scour at bridge piers, Report No. 216, University of Auckland, New Zealand.

18- Fael, C., Lança, R. and Cardoso, A., 2016. Effect of pier shape and pier alignment on the equilibrium scour depth at single piers. *International Journal of Sediment Research*, *31*(3), pp.244-250. doi.org/10.1016/j.ijsrc.2016.04.001.

19- Farooq, R. and Ghumman, A.R., 2019. Impact assessment of pier shape and modifications on scouring around bridge pier. *Water*, *11*(9), p.1761. doi.org/10.3390/w11091761.

20- Farooq, R., Azimi, A.H., Tariq, M.A.U.R. and Ahmed, A., 2023. Effects of hooked-collar on the local scour around a lenticular bridge pier. *International Journal of Sediment Research*, *38*(1), pp.1-11. doi.org/10.1016/j.ijsrc.2022.07.002.

21- Fenocchi, A. and Natale, L., 2016. Using numerical and physical modeling to evaluate total scour at bridge piers. *Journal of Hydraulic Engineering*, *142*(3), p.06015021. doi.org/10.1061/(ASCE)HY.1943-7900.0001096.

22- Guan, D., Chiew, Y.M., Wei, M. and Hsieh, S.C., 2019. Characterization of horseshoe vortex in a developing scour hole at a cylindrical bridge pier. *International journal of sediment research*, *34*(2), pp.118-124. doi.org/10.1016/j.ijsrc.2018.07.001.

23- Guemou, B., Seddini, A. and Ghenim, A.N., 2016. Numerical investigations of the round-nosed bridge pier length effects on the bed shear stress. *Progress in Computational Fluid Dynamics, An International Journal*, *16*(5), pp.313-321. doi.org/10.1504/PCFD.2016.078753.

24- Habibi, K., Fard, F.E. and Pari, S.A.A., 2023. Investigation of the flow field around bridge piers on a non-eroding bed using FLOW-3D. In *22nd Iranian Conference on Hydraulics*.

25- Habibi, K., Fard, F.E., Pari, S.A.A. and Shafai-Bejestan, M., 2024. Experimental and theoretical study of sediment scour around angled bridge piers. *Canadian Journal of Civil Engineering*, *51*(10), pp.1091-1108. doi.org/10.1139/cjce-2023-0277.

26- Hassan, Z.F., Karim, I.R. and Al-Shukur, A.H.K., 2020. Effect of interaction between bridge piers on local scouring in cohesive soils. *Civil Engineering Journal*, *6*(4), pp.659-669. DOI: 10.28991/cej-2020-03091498.

27- Heidarpour, M., Afzalimehr, H. and Izadinia, E., 2010. Reduction of local scour around bridge pier groups using collars. *International Journal of Sediment Research*, *25*(4), pp.411-422. doi.org/10.1016/S1001-6279(11)60008-5.

28- Ismael, A., Gunal, M. and Hussein, H., 2015. Effect of bridge pier position on scour reduction according to flow direction. *Arabian Journal for Science and Engineering*, *40*, pp.1579-1590.

29- Kadam, G. and Dawari, B., 2024. Experimental, analytical, and numerical evaluation of Bridge Pier scouring. *Civ Environ Eng*, *20*(1), pp.411-425. DOI: 10.2478/cee-2024-0032.

30- Khan, M., Tufail, M., Ajmal, M., Haq, Z.U. and Kim, T.W., 2017. Experimental analysis of the scour pattern modeling of scour depth around bridge piers. *Arabian Journal for Science and Engineering*, *42*, pp.4111-4130.

31- Khan, K.A., Waseem, M. and Alam, M., 2024. Experimental investigation of pier scour depth and its scour hole pattern for different shapes. *Journal of Infrastructure, Policy and Development*, *8*(4), p.3096.

32- Kharbeche, M., 2022. *The Role of Pier Shape and Aspect Ratio on Local Scour with and Without Sacrificial Piles* (Master's thesis, University of Windsor (Canada)).

33- Kim, H.S., Nabi, M., Kimura, I. and Shimizu, Y., 2014. Numerical investigation of local scour at two adjacent cylinders. *Advances in water resources*, *70*, pp.131-147. doi.org/10.1016/j.advwatres.2014.04.018.

34- Kramer, H., 1935. Sand mixtures and sand movement in fluvial model. *Transactions of the American Society of Civil Engineers*, *100*(1), pp.798-838. doi.org/10.1061/TACEAT.000465.

35- Kumar, V., Raju, K.G.R. and Vittal, N., 1999. Reduction of local scour around bridge piers using slots and collars. *Journal of hydraulic engineering*, *125*(12), pp.1302-1305. doi.org/10.1061/(ASCE)0733-9429(1999)125:12(1302).

36- Lança, R., Fael, C., Maia, R., Pêgo, J.P. and Cardoso, A.H., 2013. Clear-water scour at pile groups. *Journal of Hydraulic Engineering*, *139*(10), pp.1089-1098. doi.org/10.1061/(ASCE)HY.1943-7900.0000770.

37- Lee, S.O. and Sturm, T.W., 2009. Effect of sediment size scaling on physical modeling of bridge pier scour. *Journal of hydraulic engineering*, *135*(10), pp.793-802. doi.org/10.1061/(ASCE)HY.1943-7900.0000091.

38- Melville, B.W. and Chiew, Y.M., 1999. Time scale for local scour at bridge piers. *Journal of Hydraulic Engineering*, *125*(1), pp.59-65. doi.org/10.1061/(ASCE)0733-9429(1999)125:1(59).

39- Melville, B.W., 1997. Pier and abutment scour: integrated approach. *Journal of hydraulic Engineering*, *123*(2), pp.125-136. doi.org/10.1061/(ASCE)0733-9429(1997)123:2(125).

40- Melville, B.W. and Raudkivi, A.J., 1977. Flow characteristics in local scour at bridge piers. *Journal of Hydraulic Research*, *15*(4), pp.373-380. doi.org/10.1080/00221687709499641

41- Mia, M.F. and Nago, H., 2003. Design method of time-dependent local scour at circular bridge pier. *Journal of Hydraulic Engineering*, *129*(6), pp.420-427. doi.org/10.1061/(ASCE)0733-9429(2003)129:6(420).

42- Moncada-M, A.T., Aguirre-Pe, J., Bolivar, J.C. and Flores, E.J., 2009. Scour protection of circular bridge piers with collars and slots. *Journal of Hydraulic Research*, *47*(1), pp.119-126. doi.org/10.3826/jhr.2009.3244

43- Movahedi, N., Dehghani, A.A., Aarabi, M.J. and Zahiri, A.R., 2011. Temporal evolution of local scour depth around side-by-side piers. *Journal homepage: http://www. ojceu. ir/main*, *82*, p.86.

44- Muzzammil, M., Gangadharaiah, T. and Gupta, A.K., 2004, June. An experimental investigation of a horseshoe vortex induced by a bridge pier. In *Proceedings of the institution of civil engineers-water management* (Vol. 157, No. 2, pp. 109-119). Thomas Telford Ltd. doi.org/10.1680/wama.2004.157.2.109.

45- Omara, H., Ookawara, S., Nassar, K.A., Masria, A. and Tawfik, A., 2022. Assessing local scour at rectangular bridge piers. *Ocean Engineering*, *266*, p.112912. doi.org/10.1016/j.oceaneng.2022.112912.

46- Pandey, M., Azamathulla, H.M., Chaudhuri, S., Pu, J.H. and Pourshahbaz, H., 2020. Reduction of time-dependent scour around piers using collars. *Ocean Engineering*, *213*, p.107692. doi.org/10.1016/j.oceaneng.2020.107692.

47- Raudkivi, A.J., 1986. Functional trends of scour at bridge piers. *Journal of hydraulic engineering*, *112*(1), pp.1-13. doi.org/10.1061/(ASCE)0733-9429(1986)112:1(1).

48- Ravanfar, S.M., Mohammadpour, R. and Sabzevari, T., 2024. Experimental study of local scour around non-uniform twin piers. *International Journal of River Basin Management*, *22*(3), pp.429-444. doi.org/10.1080/15715124.2023.2167823

49- Salim, M. and Jones, J.S., 1996. Scour around exposed pile foundations. In *North American water and environment congress & destructive water* (pp. 2202-2211). ASCE.

50- Sheppard, D.M., Melville, B. and Demir, H., 2014. Evaluation of existing equations for local scour at bridge piers. *Journal of Hydraulic Engineering*, *140*(1), pp.14-23. doi.org/10.1061/(ASCE)HY.1943-7900.0000800.

51- Tao, J., Gao, Q. and Yu, X., 2013. *Assessment of the Effects of Pier Configurations on the Flow Pattern and Scour: A CFD Modeling Approach* (No. 13-2840).

52- Tariq, M., Khan, A. and Khan, M., 2022. Experimental study of scour hole depth around bridge pile using efficient cross-section. *Applied Sciences*, *12*(10), p.5205. doi.org/10.3390/app12105205.

53- Vijayasree, B. and Eldho, T., 2016. Experimental study of scour around bridge piers of different arrangements with same aspect ratio.

54- Vijayasree, B.A., Eldho, T.I., Mazumder, B.S. and Ahmad, N., 2019. Influence of bridge pier shape on flow field and scour geometry. *International Journal of River Basin Management*, *17*(1), pp.109-129. doi.org/10.1080/15715124.2017.1394315

55- Vijayasree, B.A. and Eldho, T.I., 2021. A modification to the Indian practice of scour depth prediction around bridge piers. *Current Science*, *120*(12), pp.1875-1881.

56- Wang, C., Yu, X. and Liang, F., 2017. A review of bridge scour: mechanism, estimation, monitoring and countermeasures. *Natural Hazards*, *87*, pp.1881-1906.

57- Xie, Z., 2011. *Theoretical and numerical research on sediment transport in pressurized flow conditions*. The University of Nebraska-Lincoln.

58- Zhou, K., Duan, J.G. and Bombardelli, F.A., 2020. Experimental and theoretical study of local scour around three-pier group. *Journal of Hydraulic Engineering*, *146*(10), p.04020069. doi.org/10.1061/(ASCE)HY.1943-7900.0001794.

© 2026 The Author(s). Published by Shahid Chamran University of Ahvaz. This is an open-access article distributed under the terms of the Creative Commons Attribution License (http://creativecommons.org/licenses/by/4.0), which permits unrestricted use, distribution, and reproduction in any medium, provided the original work is properly cited.

Shahid Chamran University of Ahvaz

**Irrigation Sciences and Engineering (JISE)**
**Vol. 48, No. 4, Winter 2026, p. 19-36**

**Research Paper**

Journal homepage: https://jise.scu.ac.ir

# Evaluating Environmental Impacts of Dam Construction Using an Enhanced Quantitative Checklist: A Case Study of Haleh Dam in Iran

Nader Nabipour[1] and Babak Lashkar-Ara[2*]

*1- Ph.D. Student, Department of Water Engineering, College of Civil Engineering, Jundi-Shapur University of Technology, Dezful, Iran.*
*2*- Corresponding Author, Associate Professor, Department of Water Engineering, College of Civil Engineering, Jundi-Shapur University of Technology, Dezful, Iran. (Lashkarara@jsu.ac.ir)*

**ARTICLE INFO**

*Artlcle history:*
Received: 19 August 2025
Revised: 06 November 2025
Accepted: 30 November 2025
Available online: 04 January 2026

*Keywords:*
Environmental monitoring; Checklist; Integrated method; Water resources; Leopold matrix

**TO CITE THIS ARTICLE:**

Nabipour, N., Lashkar-Ara, B. 2026. 'Evaluating Environmental Impacts of Dam Construction Using an Enhanced Quantitative Checklist: A Case Study of Haleh Dam in Iran', *Irrigation Sciences and Engineering*, 48(4), pp. 19-36. doi: 10.22055/jise.2025.50440.2178.

**Abstract**

The construction of dams, as one of the fundamental strategies for water resources management, has always been accompanied by environmental challenges. This study conducts a comprehensive environmental impact assessment (EIA) of the Haleh Dam located in Kuhdasht County, Lorestan Province, Iran. The methodological approach integrates a quantified checklist with the modified Iranian Leopold matrix to enable a precise and comparative analysis of impacts during both construction and operation phases. Evaluations were performed based on three criteria—significance, intensity, and nature of effects—across four environmental dimensions: physical, biological, socio-economic, and cultural.

The findings indicate that during the construction phase, the implementation scenario (−146) demonstrated a relatively lower adverse impact compared to the non-implementation scenario (−160), while the operation phase (+378) revealed long-term positive effects mainly in the socio-economic dimension (+155), such as improved water supply, flood regulation, and job generation. Nevertheless, several components, particularly terrestrial habitats and surface water quality, experienced moderate to high negative impacts during construction.

Therefore, the study suggests that the Haleh Dam may be considered environmentally justifiable, conditional upon the effective implementation of mitigation and monitoring measures. It also acknowledges inherent methodological limitations, including reliance on expert judgment for scoring and the lack of post-implementation monitoring data. Despite these constraints, the proposed integrated approach provides a practical framework for EIA in data-limited contexts and can support sustainable assessment of similar water infrastructure projects in developing regions.

## Introduction

In recent decades, pressures stemming from population growth, industrial expansion, shifting consumption patterns, and climate crises have compelled governments and societies to develop extensive plans for vital infrastructure, particularly in the domain of water resources. Among these, dam construction projects have played a crucial role as a key instrument in water resource management, contributing to potable water supply, flood control, hydropower generation, and agricultural support (World Commission on Dams, 2000; Ansar et al., 2014). However, the vast scale and complexity of such projects have rendered them among the most controversial forms of human intervention in nature. Although dams offer benefits, they can cause significant ecological, social, and economic impacts, which has led to the global

adoption of Environmental Impact Assessment (EIA) to guide sustainable project decisions (Fearnside, 2016; Lerer and Scudder, 1999).

The primary objective of EIA is to identify, predict, and analyze the direct and indirect impacts of proposed projects on environmental components prior to implementation. It aims to reduce environmental damage and optimize the socio-economic benefits of projects by proposing corrective and mitigation strategies (Glasson et al., 2013; Canter and Wood, 1996). EIA has not only become a tool for environmental protection but has also evolved into an integral part of development policy-making (Morgan, 2012; Pope et al., 2013).

In Iran, EIA studies officially started in the mid-1990s after the ratification of relevant regulations (Makhdoum, 2008). However, experiences from several dam projects, including Karkheh, Gotvand, Sivand, and Karun-4, show that merely following the administrative EIA process does not ensure impact mitigation or sustainable development (Makhdoum, 2008; Khodabakhshi et al., 2011). Common shortcomings include weak methodological design, neglect of cumulative impacts, limited stakeholder engagement, and lack of post-implementation monitoring, all of which reduce assessment effectiveness (Bragagnolo et al., 2017; Sánchez and Morrison-Saunders, 2011). Dam construction projects require rigorous and multidimensional analysis. Their impacts occur in two main phases: construction and operation. The construction phase often causes temporary but severe effects, such as vegetation loss, noise pollution, geomorphological changes, and threats to wildlife. The operation phase, however, leads to longer-term consequences, including altered flow regimes, water quality degradation, species loss, and persistent social impacts (World Commission on Dams, 2000; Lyu et al., 2018). Therefore, the use of integrated and quantitative EIA tools is essential.

Traditional EIA methods such as simple checklists, the Leopold matrix (1971), and qualitative forms while straightforward, lack the ability to prioritize and quantify impacts and are often influenced by subjective judgments of evaluators (Sadler and Verheem, 1996). In Iran, some dam construction projects have also employed these traditional approaches, such as the ICOLD and Leopold matrices. For instance, in the study by Sayadi et al. (2009) on the Gotvand Dam, a combination of the ICOLD and Leopold matrices was applied to assess environmental impacts across three domains: physico chemical, biological, and socio–cultural. The results indicated that although the applied method was effective in identifying a broad spectrum of environmental impacts, it lacked quantitative weighting and prioritization among various effects, thereby limiting the precision of stepwise decision-making. Moreover, the authors emphasized the necessity of integrating Geographic Information System (GIS) data and local participation to enhance the reliability of results. These findings highlight the inherent limitations of traditional matrix-based EIA methods and underscore the need for adopting more quantitative and scored approaches in environmental impact assessment. Likewise, the environmental assessment of the Zhaveh Dam in western Iran (Karimi et al., 2019) employed both the checklist and ICOLD matrix approaches to evaluate the project's biophysical and socio-economic impacts. The results indicated that while the ICOLD matrix identified broad environmental categories, it remained largely descriptive and lacked any systematic weighting or prioritization of parameters. Similarly, the checklist method could detect direct and indirect biological impacts, but its qualitative and non-comparative nature prevented an integrated evaluation of the project's overall environmental condition. The study concluded that both approaches failed to provide a transparent basis for decision-making or to capture cumulative, long-term effects. Such methodological deficiencies, consistent with those observed in the Gotvand Dam case (Sayadi et al., 2009), reinforce the necessity for a more quantitative, structured, and rank-based checklist such as the one proposed in the present study to improve the reliability, traceability, and reproducibility of EIA

outcomes for large dam projects. To address these limitations, researchers have increasingly turned to advanced approaches such as scoring-based checklists, the modified ICOLD matrix, Analytical Hierarchy Process (AHP), multi-criteria decision-making (MCDM) models, and the integration of spatial data (GIS) to support more evidence-based and precise decision-making processes (Geneletti, 2005; Modak and Biswas, 1999; Dehnavi and Kouzehgar, 2019).

Recent advances in multi-criteria decision-making (MCDM) have expanded the methodological rigor of dam-related environmental assessments through hybrid weighting and ranking schemes that balance objective and subjective inputs. For instance, Eslami et al. (2021) applied the IDOCRIW–COCOSO framework to evaluate and prioritize mitigation strategies for the Nohob Dam (Iran), achieving improved balance between entropy-based weights and expert judgment. While such approaches reduce bias in criteria weighting, integration of cumulative impacts and post-2020 adaptive monitoring indicators within a unified GIS-MCDM workflow remains limited a gap addressed in the present study for the Haleh Dam.

One Emerging framework in this domain is the use of quantified checklists incorporating indicators such as intensity, spatial extent, reversibility, duration, likelihood, and interaction with other impacts. These allow for better prioritization of negative impacts and identification of mitigation actions (Valizadeh and Shekari, 2015). Additionally, matrix-based methods especially in localized versions such as the Iranian modified matrix have gained traction due to their flexibility and adaptability to dam construction projects in Iran (Javadi et al., 2007; Valizadeh and Shekari, 2015). By combining these two methods, it becomes possible to achieve a more comprehensive assessment of project impacts across different time periods and domains including physical, biological, economic, and social aspects. It is noteworthy that in addition to environmental impacts, the social and cultural dimensions of dam projects have gained increasing attention. Neglecting human-related issues such as forced displacement, disruption of local livelihoods, social dissatisfaction, and erosion of community cohesion can significantly affect the overall effectiveness of a project (Mostert, 2003; Lerer and Scudder, 1999). Therefore, effective EIA studies must transcend a purely environmental perspective and move toward an interdisciplinary framework that actively involves stakeholders.

Unlike previously reported hybrid approaches such as the ICOLD Leopold combination, AHP, MCDM, or GIS-based assessments, the present integration was specifically designed to preserve the operational simplicity of a quantified checklist while incorporating the multi-dimensional analytical capacity of the Iranian modified Leopold matrix. This design eliminates the need for complex hierarchical weighting or extensive spatial datasets, making it particularly effective for large dam projects in data-limited contexts. Moreover, it allows scoring at the activity component interaction level, which directly supports prioritization of impacts and selection of mitigation measures a capability not explicitly addressed in earlier hybrid models.

In this context, the present study adopts a combined framework of scoring-based checklists and the Iranian modified matrix to offer a structured, quantitative, and localized methodology for assessing the environmental impacts of a dam construction project. The model evaluates the effects of each project activity during both construction and operation phases on key environmental components including water quality, vegetation cover, wildlife habitats, soil resources, and socio-economic sustainability. By employing a criteria-based scoring system and comparing the scenarios of implementation versus non-implementation, the approach provides a decision-making platform grounded in comparable and evidence-based data. In this study, the approach referred to as the "Advanced Checklist" is not intended as an entirely new framework but rather as a methodological enhancement of the quantified checklist technique. Three additional evaluation criteria importance (I), magnitude (M), and nature (N) of the impacts were

incorporated, and the scoring logic of the Iranian Modified Leopold Matrix was systematically integrated into the checklist structure. This incremental improvement maintains the quantitative simplicity of the original checklist while enriching it with analytical depth, localization, and multidimensional interpretability for dam-related environmental impact assessments in Iran.

Ultimately, the selection of the advanced checklist method in this study is driven by the need to integrate analytical rigor, ease of application, tool localization, and result interpretability. The findings of this research are expected not only to provide an objective assessment of the case study project, but also to serve as a replicable model for conducting EIA in other dam construction projects in Iran, especially in ecologically and hydrologically sensitive areas.

## Materials and Methods

This study evaluates the environmental impacts of the Haleh Dam construction project, located in Kuhdasht County, Lorestan Province, Iran. Considering the significance of dam construction in securing water resources and promoting sustainable development, the need for systematic and efficient assessment approaches in this region was evident. Accordingly, an integrated methodology combining a quantified checklist and the Iranian-modified Leopold matrix was selected to perform a comprehensive Environmental Impact Assessment (EIA). The objective of this study is to provide an interpretable and holistic picture of the environmental impacts across the various phases of the project namely construction and operation.

### Study Area

Haleh Dam is situated in Kuhdasht County, Lorestan Province, Iran, approximately 12 kilometers from the city center, at geographic coordinates of approximately 47°35′ E and 33°25′ N. Nestled within the Zagros Mounta ins, the surrounding region is renowned for its pristine natural landscapes, scenic valleys, and ecological richness, making it a popular local ecotourism destination. The dam area encompasses the catchment basins of the Madianrud River and the Darreh-Dezdan Valley, both of which play a crucial role in regional water management and development. From an engineering perspective, Haleh Dam is a homogeneous earth-fill structure with a maximum height of 44 meters and a total reservoir volume of 3.5 million cubic meters, while its regulated water storage capacity reaches approximately 7.2 million cubic meters. The irrigation command area and associated water distribution networks cover roughly 250 hectares, contributing significantly to local water resource utilization and management. The dam is critical for agricultural water supply, flood control, and the protection of natural resources in the region. Additionally, it provides opportunities for recreational activities, aquaculture development, and broader economic growth. Balancing ecological integrity with economic exploitation is of particular importance in this context. As a vital infrastructural investment in the domains of water and environmental management, the construction of Haleh Dam also serves as a key driver for sustainable development, improving the quality of life and supporting regional economic progress. Preliminary estimates indicate that the dam can annually provide around 5 million cubic meters of water for agricultural use, enabling irrigation of approximately 500 hectares of farmland. This has already contributed to the expansion of agricultural and industrial activities, facilitated flood control, enabled land reclamation, and fostered fish farming and tourism development. The region’s semi-arid climate, coupled with its diverse flora and fauna, increases the ecological vulnerability of the ecosystem. From a socio-economic perspective, local communities largely rely on natural resources, agriculture, and animal husbandry. For the purpose of environmental assessment and analysis, data were collected through a combination of approaches, including literature review, existing technical reports, field surveys, and interviews with experts and local stakeholders. Fig. (1) Illustrates the geographical location of Haleh Dam within Lorestan Province.

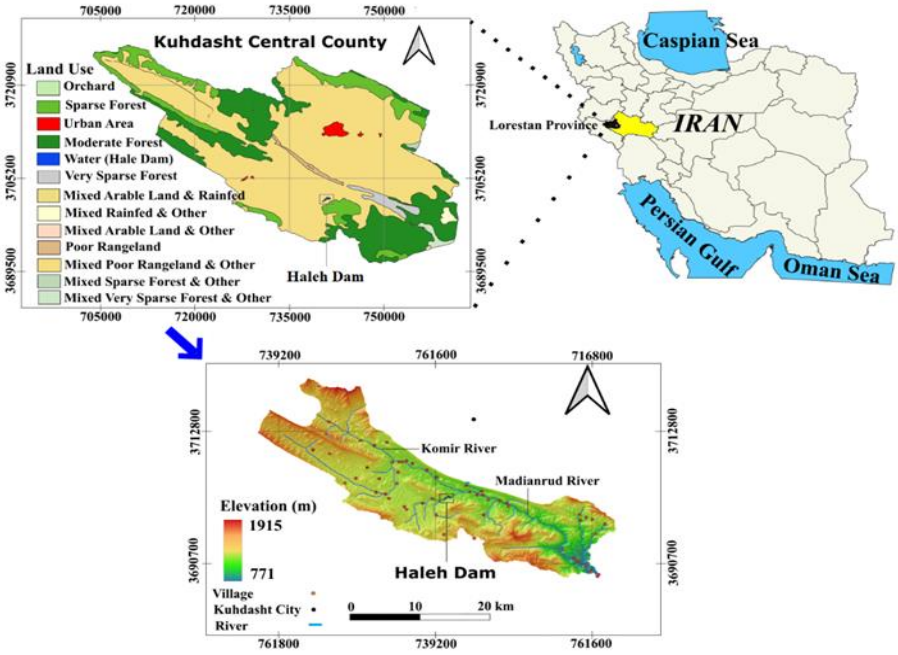



**Fig. 1- Geographical location of the Hale Dam – Kohdasht, Lorestan, Iran.**

**Scoring Methods Quantified Checklist Method**

In the process of environmental impact analysis, the initial stage aimed to identify, categorize, and prioritize potential interactions between project activities and various environmental components. For this purpose, the quantified checklist method was used to convert qualitative observations into numerical values. This method provides a structured and comparable analysis and serves as a practical tool, especially during the screening phase and for stakeholder engagement. Within this method, all potential interactions between project activities and environmental components were systematically assessed. These interactions were evaluated using a set of key indicators and quantitative criteria designed to express the relative weight and significance of each impact within the overall assessment process.

**Scoring Framework**

At this stage, for each specific interaction between a project activity and an environmental component, a set of evaluation metrics was defined based on three primary and essential indicators. The first indicator, Importance of Effect (I), reflects the relative weight and significance of each impact on a numeric scale from 0 to 5. This score plays a pivotal role in prioritizing environmental effects and enables decision-makers to focus on more critical and influential impacts in the Mitigation and management process. The second indicator, Magnitude of Effect (M), quantifies the extent or potential severity of the impact that each activity may exert on a given environmental component. It is assessed on a scale from 1 to 3, with higher values indicating stronger and more substantial effects. The third indicator, Nature of Effect (N), denotes the direction and type of the impact. Positive impacts are assigned a score of +1, while negative impacts are given a value of −1. This indicator allows for a combined analysis of both beneficial and adverse project outcomes within a single integrated framework. The final score for each interaction is calculated and recorded using Equation (1):

$$\text{Score} = \text{Importance of Effect (I)} \times \text{Magnitude of Effect (M)} \times \text{Nature of Effect (N)} \quad (1)$$

Equation (1) essentially applies a weighting mechanism to the core indicators, expressing

the degree of influence of each interaction as a function of its importance, magnitude, and nature. This composite scoring system forms a foundational reference for subsequent analyses and for constructing the project's environmental impact matrices.

**Data Collection and Expert Consultation**

To ensure the accuracy and reliability of the evaluation results, data were collected through structured questionnaires distributed among 36 domain experts involved in the study. The panel included six experts from the Regional Water Authority, four from the Water and Wastewater Company, nine agricultural specialists, four environmental experts, six structural civil engineers, two university professors specializing in structural engineering, and five hydraulic engineers focusing on water structures The mean of all expert scores was used to determine the final quantitative values applied in the matrices All expert opinions were assigned equal weight, while the views of local stakeholders were incorporated qualitatively, based on field observations and semi-structured interviews conducted within the project area. Experts were selected purposively based on their direct experience in environmental impact assessment and dam construction projects, with a minimum of five years of professional background in related fields. The selection aimed to include a balanced representation of governmental, academic, and private-sector perspectives to minimize disciplinary bias and ensure methodological rigor. Prior to data collection, a short calibration session was organized to ensure a common understanding of each evaluation criterion and scoring scale among all experts. Significant discrepancies in individual scores were reviewed through group discussion, and the mean values were adopted as the final quantitative inputs to minimize evaluator bias and enhance scoring consistency.

**Activities and Environmental Components Assessed**

In the process of environmental impact assessment, the main activities and operations during both construction and operation phases of the project were identified and listed. These included: earth excavation and soil compaction, construction of access roads, heavy machinery operations and mechanized activities, generation of construction and industrial waste, development of green spaces and restoration of natural habitats, as well as the presence and behavior of the workforce at the project site. Each of these activities was evaluated in relation to four principal and critical environmental dimensions: the physical dimension, including land, water, and air; the biological dimension, comprising vegetation cover and wildlife; the socio-economic dimension, encompassing employment, migration, livelihoods, and regional economic development; and finally, the cultural dimension, which addressed cultural heritage, natural landscape, and social interactions within the local community. This assessment served as a foundation for deeper and more structured analyses in the subsequent stages of the evaluation process, and played a significant role in identifying key impacts and prioritizing environmental management actions.

**Modified Iranian Leopold Matrix**

In the subsequent step, to conduct a more structured and multidimensional analysis of environmental impacts, a localized version of the Leopold Matrix was employed. Originally introduced in 1971 by Leopold, this tool was adapted in the present study to better suit the climatic, ecological, and socio-cultural conditions of Iran, based on the modifications proposed by Makhdoum (2008). The primary objective of this adaptation was to establish an analytical framework capable of assessing project impacts more accurately and effectively within local and regional contexts.

**Structure and Characteristics of the Matrix**

The modified Leopold Matrix employed in this study adopts a two-dimensional structure, wherein the rows represent the main project activities and the columns denote various environmental components. Within each cell of the matrix, the indicators of importance, magnitude, and nature of impact are recorded

based on the results of prior assessments. This flexible structure allows for the evaluation of direct, indirect, cumulative, and long-term impacts of the project. Notably, the scoring range in this adapted version is confined to ±5, in order to facilitate a more intuitive and locally ontextualized interpretation of the results at both local and regional scales. Moreover, due to the critical relevance of long-term and cumulative effects in large-scale infrastructure projects, special attention was given to indirect impacts and background interactions, such as pollutant dispersion, ecological shifts, and transport-induced effects, throughout the assessment process.

**Integrated Approach: Advanced Checklist**

In light of previous approaches, both the Quantified Checklist and the Modified Leopold Matrix have been recognized for their respective advantages and limitations. While the checklist method will facilitate simplicity and the numerical representation of impacts, it will remain constrained in delivering a comprehensive and multi-dimensional evaluation. Conversely, the Leopold matrix will enable more structured and multi-dimensional interpretations but may initially exhibit certain structural shortcomings. To address these limitations and to harness the strengths of both methods, an integrated approach, hereafter referred to as the "Advanced Checklist", is introduced as an incremental methodological improvement over the quantified checklist method. This hybrid approach will combine the simplicity and quantifiability of the checklist with the multi-dimensional and structured analysis offered by the Leopold matrix. In implementing the integrated framework for environmental impact assessment of the project, five critical stages will be followed, each playing a vital role in structuring and deepening the analytical process. First, the key project activities across the construction, operation, and upgrading phases will be identified and listed. These activities will then be classified according to four principal environmental dimensions: physical (land, water, air), biological (vegetation, wildlife), socio-economic (employment, migration, livelihoods, regional development), and cultural (cultural heritage, natural landscape, and local community interactions). Subsequently, the potential interactions between each activity and the environmental components will be assessed and scored based on the three criteria: importance (I), magnitude (M), and nature (N) of the impact. These assessments will serve as the foundation for more detailed and comprehensive analyses in subsequent stages. Thereafter, the final score for each interaction will be calculated using the numerical expression: $I \times M \times N$, enabling a structured and quantitative depiction of each activity's level of impact on different components.

The results will then be organized into two-dimensional matrices, where the aggregate scores corresponding to each activity and component will be determined, thereby identifying critical patterns and impact hotspots. In the final stage, two practical scenarios "Project Implementation" and "No-Action" will be designed and formalized to facilitate comparative analysis and informed strategic decision-making. Although numerical analyses of these scenarios will not yet be executed at this stage, the necessary infrastructure for such advanced evaluations will have been thoroughly established and will be ready for future use.

This integrated approach will preserve both simplicity and numerical capacity while enabling comprehensive, multi-dimensional impact analyses. Moreover, the method will enhance the precision and Efficiency of the evaluation process and allow for the identification of complex relationships and indirect project effects. It will empower managers and decision-makers to better understand project impacts across various spatial and temporal scales and adopt appropriate strategies for mitigating adverse consequences.

Additionally, the approach will provide a robust foundation for developing quantitative models, long-term predictions, and sensitivity analyses throughout the planning and implementation phases-ultimately contributing

to the effective and sustainable management of environmental projects.

In conclusion, this intelligent and precise integration of methods and tools will offer a comprehensive, flexible, and locally adaptable framework with a critical role in the holistic management of environmental project impacts. It will not only support a deeper and clearer understanding of environmental effects but also promote a transparent, evidence-based decision-making process ultimately leading to sustainable project development in harmony with the environment.

## Findings

In this study, a hybrid advanced checklist framework was utilized to conduct a Quantitative analysis of the environmental impacts resulting from the implementation of the Haleh Dam project. To this end, numerical values assigned to each interaction between project activities and environmental components were calculated, and the algebraic sum of the scores in each column of the matrix was derived and recorded for the four principal environmental dimensions: physical, biological, Socio-economic, and cultural. This methodology enabled a structured, data-driven, and comparative evaluation of the impacts and provided a solid foundation for interpreting the detailed findings across the construction and operational phases of the project.

### Environmental Impact Assessment during the Construction Phase

To conduct a precise and quantitative analysis of the environmental impacts associated with the construction phase of the Haleh Dam project, a structured and enhanced-format table was utilized. This table systematically evaluates the effects of each construction activity based on four main environmental dimensions: physical, biological, socio-economic, and cultural Table (1). It is built upon data derived from the advanced scoring checklist model and enables a comparative and analyzable quantitative representation of the ecosystem status, providing insight into both favorable and adverse impacts of various development activities. The findings from this stage indicate that, within the physical dimension, activities such as excavation and embankment, workshop construction, and the operation of heavy machinery exert the most significant negative impacts on the environment. These adverse effects, clearly reflected in the negative numerical scores in Table 1, primarily degrade soil quality, air conditions, and surface water resources. Subsequent assessments of the other environmental dimensions followed the same analytical framework, with the results presented in Table (2). In the biological dimension, wastewater generation, excavation and embankment, and the construction of access roads were identified as major sources of negative impact, whereas actions such as green space development and vegetation restoration showed considerable positive effects. In the socio-economic dimension, most activities were found to yield beneficial outcomes, including the creation of temporary employment, increased economic interactions, and improvement of local infrastructure. Within the cultural dimension, the construction of access roads enhanced connectivity to cultural and historical areas, although extensive excavation and wastewater discharge had detrimental effects on the natural landscape and cultural heritage of the region. Tables (1) and (2) collectively provide a comprehensive overview of the environmental consequences during the construction phase, serving as a foundation for the comparative analysis of project implementation versus non-implementation scenarios in the subsequent section.

### Analysis of the Implementation and Non-Implementation Scenarios during the Construction Phase

The findings derived from Table 2 indicate that the total environmental impact score associated with construction-related activities of the Haleh Dam project, within the physical dimension, amounted to −146. This figure reflects the substantial negative effects of activities such as excavation, material transport, and the operation of heavy machinery on the physical integrity of the

regional ecosystem. Subsequently, the cumulative environmental impact assessment was conducted across the four principal dimensions physical, biological, socio-economic, and cultural for two scenarios: "project implementation" and "project non-implementation" during the construction phase. The results yielded total scores of −146 and −160, respectively Fig. (2). The relatively small difference between the two scenarios suggests that, while the regional ecosystem is affected by human interventions in both cases, project implementation offers greater potential for environmental management and mitigation through targeted strategies. Notably, many of the adverse effects associated with the non-implementation scenario stem from the persistence of pre-existing unfavorable conditions, including destructive flooding events, limited economic development, and weak local infrastructure. In contrast, project implementation despite initial environmental costs can be accompanied by structured monitoring programs and mitigation measures, making the impacts more manageable. Therefore, from a strategic perspective, the implementation scenario is more defensible. It allows for the control, reduction, and possible compensation of negative impacts, whereas the non-implementation scenario risks the continuation of chronic, unmanaged environmental threat.

**Table 1- Assessment of environmental impacts in the physical environment, construction phase**

| Activities | Excavation and backfilling | | | | Establishment of workshop equipment | | | | Operation of machinery | | | | Construction of access road | | | | Solid waste generation | | | |
|---|---|---|---|---|---|---|---|---|---|---|---|---|---|---|---|---|---|---|---|---|
| Environmental parameter | I | M | N | effect | I | M | N | effect | I | M | N | effect | I | M | N | effect | I | M | N | effect |
| Air quality | 4 | 3 | - | -12 | 3 | 2 | - | -6 | 3 | 3 | - | -9 | 2 | 2 | - | -4 | 2 | 2 | - | -4 |
| Ambient noise | 3 | 3 | - | -9 | 3 | 2 | - | -6 | 3 | 3 | - | -9 | 2 | 2 | - | -4 | 0 | 0 | 0 | 0 |
| Surface water quality | 2 | 1 | - | -2 | 2 | 1 | - | -2 | 1 | 1 | - | -1 | 1 | 1 | - | -1 | 2 | 3 | - | -6 |
| Landform | 4 | 3 | - | -12 | 3 | 3 | - | -9 | 3 | 3 | - | -9 | 2 | 2 | - | -4 | 0 | 0 | 0 | 0 |
| Soil erosion | 4 | 3 | - | -12 | 3 | 3 | - | -9 | 3 | 2 | - | -6 | 2 | 3 | - | -6 | 0 | 0 | 0 | 0 |
| Cumulative effect | | | | -47 | | | | -32 | | | | -34 | | | | -19 | | | | -10 |

$$\sum(I \times N \times M) = -142$$

**Table 2- Summation of the environmental impact assessment of Haleh Dam during the**

| Activities | Physical | | | | | Biological | | | | | Socio-economic | | | Cultural | | |
|---|---|---|---|---|---|---|---|---|---|---|---|---|---|---|---|---|
| Environmental parameter | Excavation and backfilling | Establishment of workshop equipment | Operation of machines | Construction of access road | Solid waste production | Excavation and backfilling | Construction of access road | Creating green space | Establishment of workshop equipment | Solid waste production | Hiring a worker | Construction of access road | Creating green space | Solid waste production | Construction of access road | Excavation and backfilling |
| Air quality | -12 | -6 | -12 | -4 | -4 | 0 | 0 | 0 | 0 | 0 | 0 | 0 | 0 | 0 | 0 | 0 |
| Ambient noise | -9 | -6 | -9 | -4 | 0 | 0 | 0 | 0 | 0 | 0 | 0 | 0 | 0 | 0 | 0 | 0 |
| Surface water quality | -2 | -2 | -1 | -1 | -6 | 0 | 0 | 0 | 0 | 0 | 0 | 0 | 0 | 0 | 0 | 0 |
| Landform | -12 | -9 | -6 | -4 | 0 | 0 | 0 | 0 | 0 | 0 | 0 | 0 | 0 | 0 | 0 | 0 |
| Soil erosion | -12 | -9 | -6 | -6 | 0 | 0 | 0 | 0 | 0 | 0 | 0 | 0 | 0 | 0 | 0 | 0 |
| Plant habitat | 0 | 0 | 0 | 0 | 0 | -6 | -4 | +12 | -4 | -4 | 0 | 0 | 0 | -6 | +6 | -4 |
| pest insects | 0 | 0 | 0 | 0 | 0 | -4 | -4 | +9 | -4 | -4 | 0 | 0 | 0 | 0 | +4 | 0 |
| Creepy crawlies | 0 | 0 | 0 | 0 | 0 | 0 | 0 | 0 | -1 | -6 | 0 | 0 | 0 | -4 | 0 | -9 |
| Income and expenses | 0 | 0 | 0 | 0 | 0 | 0 | 0 | 0 | 0 | 0 | +9 | +6 | +1 | 0 | 0 | 0 |
| Transportation | 0 | 0 | 0 | 0 | 0 | 0 | 0 | 0 | 0 | 0 | -4 | +9 | 0 | 0 | 0 | 0 |
| Employment | 0 | 0 | 0 | 0 | 0 | 0 | 0 | 0 | 0 | 0 | +12 | 0 | +1 | 0 | 0 | 0 |
| Agriculture | 0 | 0 | 0 | 0 | 0 | 0 | 0 | 0 | 0 | 0 | -4 | -1 | 0 | 0 | 0 | 0 |
| Algebraic sum of effects | -47 | -32 | -34 | -19 | -10 | -10 | -8 | +21 | -9 | -14 | +13 | +14 | +2 | -10 | +10 | -13 |
| Total values | -142 | | | | | -20 | | | | | +29 | | | -13 | | |

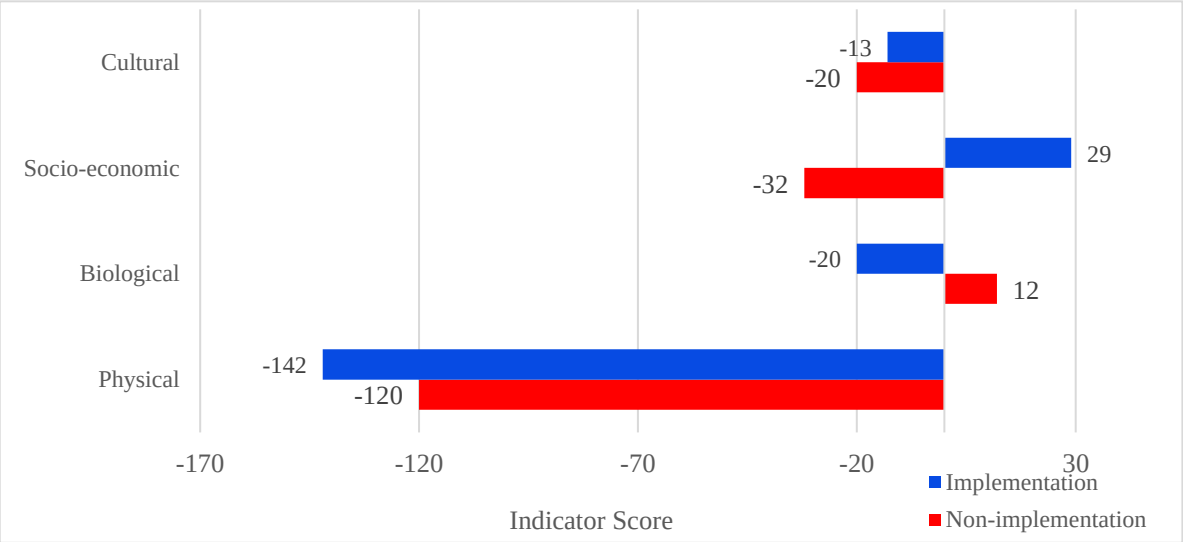



**Fig. 2- Implementation and Non-Implementation Options for the Project during the Construction Phase**

**Environmental Impact Assessment during the Operational Phase**

During the operational phase of the Haleh Dam, the environmental impact assessment summarized in Table (3) yields a total cumulative score of +378, indicating a net positive effect of the project on the surrounding ecosystem and various environmental dimensions. A detailed analysis of the results reveals that the socio-economic environment experienced the most substantial positive impact, with a cumulative score of +155, highlighting the project's significant contribution to regional development and improved well-being. Within the socio-economic dimension, activities such as water supply, flood control, development of recreational areas, maintenance of access roads, and green space management generated the highest positive impacts. The provision of water led to population growth, job creation, adequate supply for agriculture, drinking, and industrial use, land-use change from rain-fed to irrigated farming, and overall enhancement of social welfare. Additionally, flood control contributed to the protection of agricultural lands, reduced soil erosion, and minimized economic losses resulting from flood events. The development of recreational facilities facilitated tourism, sports, and leisure activities centered on the reservoir.

In the cultural dimension, despite some negative effects associated with increased chemical fertilizer use, the overall score reached +92. Key positive outcomes included improved public health indicators, enhanced scenic landscapes, and promotion of tourism, made possible by improved water access and the expansion of cultural-recreational amenities.

The physical environment also recorded a net positive impact of +84, despite some adverse effects due to agricultural chemical inputs. The most notable positive impact was related to flood control, which led to reduced erosion, improved surface water quality, and protection of agricultural productivity. Additionally, water provision facilitated the conversion of dryland to irrigated farmland, while green space maintenance improved air quality and further reduced soil degradation.

In the biological dimension, a total of +47 positive impacts were identified. The primary contributors were, respectively, water provision, flood control, and green space maintenance. Water availability promoted the restoration of plant and animal habitats and encouraged the return of wildlife species. Flood control enhanced ecological resilience, and green space conservation not only improved air quality but also supported vegetation preservation in the region.

**Analysis of Implementation and Non-Implementation Options during the Operational Phase**

According to the findings summarized in Table (3), the total cumulative score from the environmental impact assessment during the operational phase of the Haleh Dam across the four key dimensions (physical, biological, socio-economic, and cultural) amounts to +378, reflecting the predominance of positive environmental impacts resulting from the dam's operation. In contrast, the hypothetical scenario of "non-implementation of the project" during the same phase yields a cumulative negative score of –360. A comparative analysis of these two scenarios implementation versus non-implementation is illustrated in Fig. (3), clearly demonstrating that the operational phase of the project has yielded substantial positive impacts, particularly in terms of enhancing socio-economic indicators and mitigating adverse physical and biological effects. These results strongly support the necessity of implementing the project, provided that environmental requirements are observed and continuous monitoring is conducted throughout the operational period.

**Final Evaluation of Implementation and Non-Implementation Options across the Construction and Operational Phases**

To provide a more comprehensive assessment of the project's impacts, a comparative analysis was conducted between the implementation and non-implementation scenarios across both the construction and operational phases. The outcomes, illustrated in Fig. (4), reveal significant differences between the two alternatives across various environmental dimensions:

- In the physical environment, project implementation resulted in a total of –58 negative impacts, whereas the non-implementation scenario projected a far higher magnitude of –200 negative effects. This indicates that, while the project introduces some adverse effects, it effectively mitigates the severity of naturally occurring environmental degradation.
- In the biological environment, implementation yielded a positive score of +27, while non-implementation corresponded to –28, underscoring the project's ecological restoration benefits.
- In the socio-economic environment, the contrast is particularly significant: implementation led to +184 positive impacts, in stark contrast to –202 negative impacts under the non-implementation scenario highlighting the project's critical role in enhancing livelihoods, employment, and water security.
- In the cultural environment, the project contributed to +79 positive impacts, compared to –90 under the non-implementation case.

Ultimately, the aggregate assessment across both phases demonstrates a total of +232 positive effects for the implementation option, versus –452 negative effects for non-implementation. These findings clearly affirm that, despite some temporary adverse effects associated with project development, its overall contribution to sustainable regional development and mitigation of latent environmental risks strongly justifies its execution.

**Table 3- Summary of the Environmental Impact Assessment during the Operational Phase of the Haleh Dam**

| Activities | Physical | | | | Biological | | | Socio-economic | | | | | Cultural | | | | | |
|---|---|---|---|---|---|---|---|---|---|---|---|---|---|---|---|---|---|---|
| Environmental parameter | Water supply | Flood control | Fertilizer usage | Green space maintenance | Water supply | Flood control | Green space maintenance | Water supply | Flood control | Recreational development | Green space maintenance | Access road maintenance | Water supply | Flood control | Recreational development | Fertilizer usage | Green space maintenance | Access road maintenance |
| Air quality | 0 | 0 | 0 | +10 | 0 | 0 | 0 | 0 | 0 | 0 | 0 | 0 | 0 | 0 | 0 | 0 | 0 | 0 |
| Surface water quality | +12 | +9 | -6 | 0 | 0 | 0 | 0 | 0 | 0 | 0 | 0 | 0 | 0 | 0 | 0 | 0 | 0 | 0 |
| Upstream groundwater quality | +4 | +4 | -2 | 0 | 0 | 0 | 0 | 0 | 0 | 0 | 0 | 0 | 0 | 0 | 0 | 0 | 0 | 0 |
| Groundwater quality | +4 | +6 | -2 | 0 | 0 | 0 | 0 | 0 | 0 | 0 | 0 | 0 | 0 | 0 | 0 | 0 | 0 | 0 |
| Low-flow regime | +4 | +6 | 0 | -2 | 0 | 0 | 0 | 0 | 0 | 0 | 0 | 0 | 0 | 0 | 0 | 0 | 0 | 0 |
| Flood regime | +6 | +6 | 0 | 0 | 0 | 0 | 0 | 0 | 0 | 0 | 0 | 0 | 0 | 0 | 0 | 0 | 0 | 0 |
| Landform | 0 | +2 | -1 | +4 | 0 | 0 | 0 | 0 | 0 | 0 | 0 | 0 | 0 | 0 | 0 | 0 | 0 | 0 |
| Soil erosion | 0 | +9 | -4 | +15 | 0 | 0 | 0 | 0 | 0 | 0 | 0 | 0 | 0 | 0 | 0 | 0 | 0 | 0 |
| Plant habitat | 0 | 0 | 0 | 0 | +9 | +9 | +4 | 0 | 0 | 0 | 0 | 0 | 0 | 0 | 0 | 0 | 0 | 0 |
| Animal habitat | 0 | 0 | 0 | 0 | +9 | +9 | +4 | 0 | 0 | 0 | 0 | 0 | 0 | 0 | 0 | 0 | 0 | 0 |
| Pest insects | 0 | 0 | 0 | 0 | 0 | -6 | 0 | 0 | 0 | 0 | 0 | 0 | 0 | 0 | 0 | 0 | 0 | 0 |
| Animal migration | 0 | 0 | 0 | 0 | +9 | +4 | +1 | 0 | 0 | 0 | 0 | 0 | 0 | 0 | 0 | 0 | 0 | 0 |
| Population of the area | 0 | 0 | 0 | 0 | 0 | 0 | 0 | +15 | +6 | +6 | +1 | +1 | 0 | 0 | 0 | 0 | 0 | 0 |
| Employment | 0 | 0 | 0 | 0 | 0 | 0 | 0 | +12 | +4 | +4 | 0 | +9 | 0 | 0 | 0 | 0 | 0 | 0 |
| Agriculture | 0 | 0 | 0 | 0 | 0 | 0 | 0 | +15 | +12 | 0 | 0 | +1 | 0 | 0 | 0 | 0 | 0 | 0 |
| Land use | 0 | 0 | 0 | 0 | 0 | 0 | 0 | +9 | +12 | +4 | 0 | +4 | 0 | 0 | 0 | 0 | 0 | 0 |
| Income and expenditures | 0 | 0 | 0 | 0 | 0 | 0 | 0 | +9 | +12 | +9 | +1 | +6 | 0 | 0 | 0 | 0 | 0 | 0 |
| Migration | 0 | 0 | 0 | 0 | 0 | 0 | 0 | +9 | -12 | +6 | +6 | -6 | 0 | 0 | 0 | 0 | 0 | 0 |
| Health | 0 | 0 | 0 | 0 | 0 | 0 | 0 | 0 | 0 | 0 | 0 | 0 | +12 | +6 | +4 | -4 | +2 | 0 |
| Educational | 0 | 0 | 0 | 0 | 0 | 0 | 0 | 0 | 0 | 0 | 0 | 0 | 0 | 0 | 0 | 0 | 0 | +4 |
| Tourism | 0 | 0 | 0 | 0 | 0 | 0 | 0 | 0 | 0 | 0 | 0 | 0 | +8 | +2 | +15 | 0 | +12 | +6 |
| Landscapes | 0 | 0 | 0 | 0 | 0 | 0 | 0 | 0 | 0 | 0 | 0 | 0 | +4 | +2 | +9 | 0 | +9 | +1 |
| Algebraic sum of impacts | +30 | +42 | -15 | +27 | +27 | +11 | +9 | +69 | +34 | +29 | +8 | +15 | +24 | +10 | +28 | -4 | +23 | +11 |
| Total value | +84 | | | | +47 | | | +155 | | | | | +92 | | | | | |

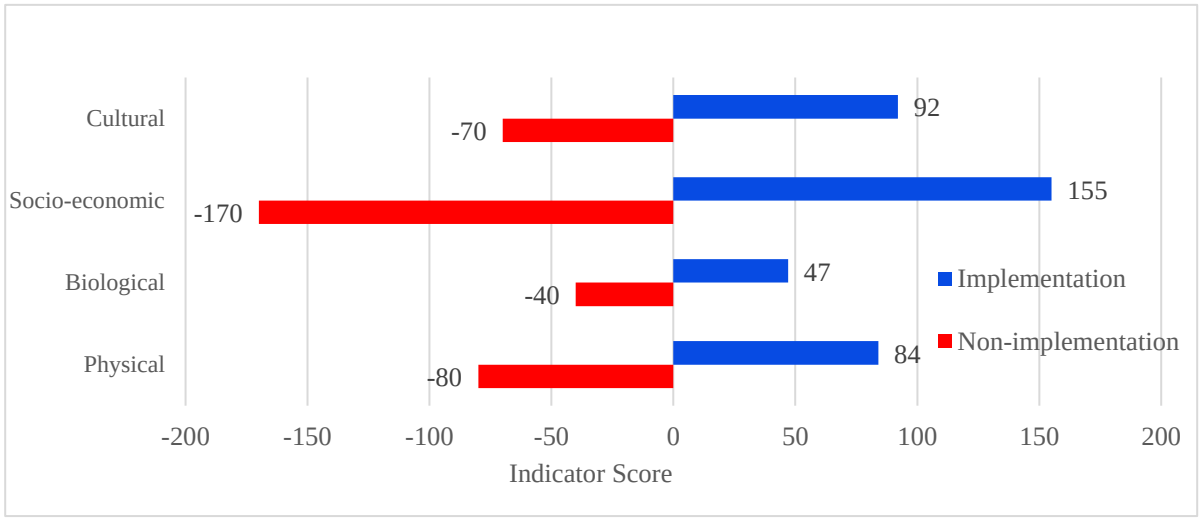



**Fig. 3- Comparison of Implementation and Non-Implementation Options during the Operational Phase of the Haleh Dam Proje**

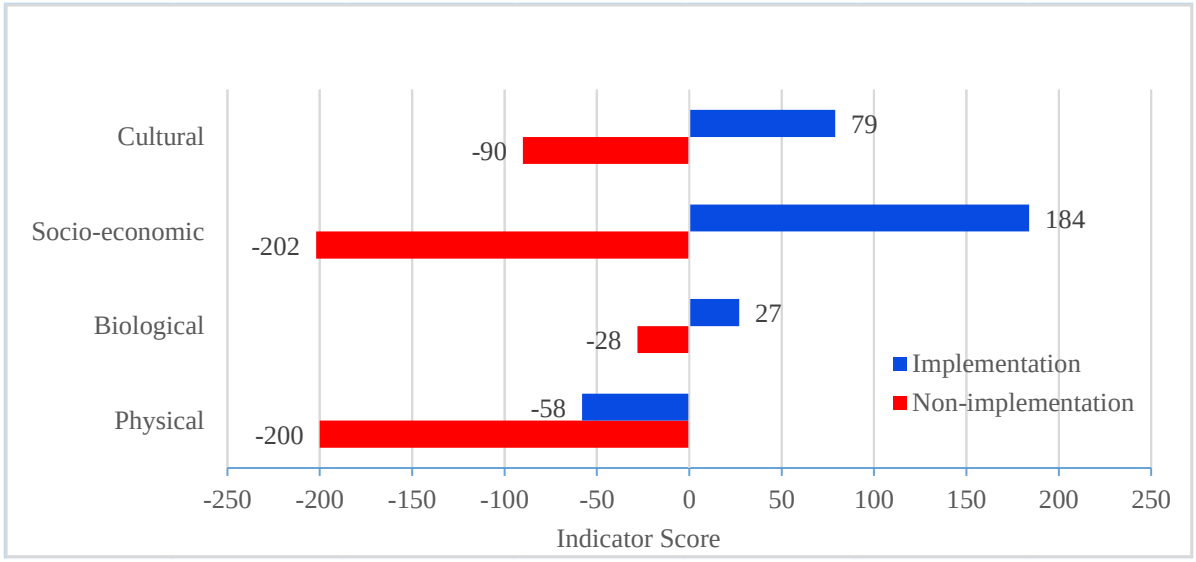



**Fig. 4- Final Comparison of Implementation and Non-Implementation Options during the Construction and Operational Phases of the Haleh Dam Project**

## Discussion and Conclusion

This study conducted a comprehensive and quantitative environmental impact assessment (EIA) of the Haleh Dam project during both the construction and operation phases, utilizing an integrated approach based on an advanced scoring checklist. The adopted methodology enabled a multidimensional evaluation by quantitatively analyzing the project's effects across four key environmental domains: physical, biological, socio-economic, and cultural. In the construction phase, the implementation scenario recorded a cumulative negative score of –146, demonstrating a relatively lower adverse impact compared to the non-implementation scenario (–160). The most substantial negative effects were associated with the physical environment, primarily driven by excavation and embankment operations, the use of heavy machinery, and wastewater generation. However, in the operation phase, the implementation scenario resulted in a significant cumulative positive score of +378,

underscoring the long-term environmental benefits of the project. The socio-economic environment exhibited the highest positive contribution (+155), reflecting improvements in water availability, flood control, tourism development, job creation, and enhancement of community welfare. Additional positive impacts were also observed in the cultural (+92), physical (+84), and biological (+47) environments, indicating ecological recovery and improved infrastructure conditions.

The final comparative evaluation of the two scenarios implementation (+232) and non-implementation (–520) across both project phases suggests the potential environmental justification for the dam project, conditional upon the effective implementation of mitigation and monitoring measures. These findings indicate that, despite some temporary adverse effects during construction, the project has the potential to contribute to sustainable regional development if ecological and cultural limitations are properly mitigated and monitored, alongside enhanced agricultural productivity, reliable water supply for domestic, agricultural, and industrial uses, flood damage mitigation, and the strengthening of the local ecosystem. Moreover, the optimal use of the reservoir for recreational, tourism, and sport activities offers valuable socio-economic development opportunities for local communities.

The Gotvand Dam project in Iran is a clear example where significant negative environmental effects were identified after construction, particularly the salinization of the Karun River. Nevertheless, management reforms such as controlled reservoir operation, salt-layer isolation, and long-term monitoring were developed and implemented to mitigate the impacts (Sayadi et al., 2009). Similar adaptive management strategies were also proposed for the Zhoveh Dam project (Karimi et al., 2019). These lessons underline the necessity of adopting an adaptive management pathway for the Haleh Dam as well, ensuring that identified ecological risks remain under control throughout its operational lifespan.

Compared with the hybrid IDOCRIW–COCOSO approach by Eslami et al. (2021), the present study extends the weighting ranking integration by embedding adaptive monitoring indicators and cumulative effect analysis in the GIS environment. While both frameworks employ entropy-based criteria weighting to minimize subjective bias, our Haleh Dam model reveals higher criterion sensitivity under semi-arid conditions, highlighting the contextual dependency of socio-ecological priorities.

In developing regions, the integration of cumulative and cross-project effects into Environmental Impact Assessment (EIA) remains a persistent limitation. For instance, a recent study conducted around the Campo-Ma'a National Park in Cameroon (Zo'obo Engolo et al. 2024) applied the Sorensen and Rau framework to evaluate multiple development projects near a protected area. Despite moderate consideration of direct impacts ($\geq 79\%$), cumulative effects and integrated management were addressed to a limited extent ($\approx 52\%$), largely due to insufficient data and fragmented monitoring systems. The authors proposed combining matrix and network-based approaches, alongside digital platforms, to strengthen impact tracking. These findings align with the rationale of the present study, which emphasizes quantified and adaptive assessment tools as an effective means of overcoming similar data and integration challenges.

Nevertheless, to minimize the negative impacts during the construction phase, it is recommended to implement effective control measures such as frequent water spraying to reduce dust, afforestation in erosion-prone zones, use or retrofitting of modern machinery, installation of pollution-control filters, and provision of proper sanitation infrastructure (e.g., septic tanks). During the operational phase, training farmers in the judicious use of fertilizers and pesticides, along with promoting biological pest control methods, can play a crucial role in reducing ecological pressures and enhancing the resilience of the local ecosystem.

**Limitations**

Despite the robustness of the proposed analytical framework, several inherent limitations should be noted. First, the scoring process inevitably involves a degree of subjectivity, as it relies on expert judgment despite efforts to standardize criteria through quantitative checklists. However, this subjectivity was minimized by involving a multidisciplinary panel of 36 experts and by applying uniform weighting and inter-rater reliability calibration during the scoring process.

Second, although the Haleh Dam project has now entered its operational phase, comprehensive long-term environmental monitoring data are still being accumulated, which currently limits the empirical verification of all predicted impacts.

Third, the evaluation did not include direct participation of affected local communities, which may limit the integration of socio-cultural concerns and local knowledge. Nonetheless, a participatory extension phase has been planned during the ongoing monitoring stage to incorporate local stakeholders' feedback and traditional ecological knowledge (TEK) into adaptive management.

Finally, while cumulative effects were conceptually considered, the framework has not yet been extended to transboundary or large-scale cumulative interactions. Future research should expand this component through GIS-based regional frameworks and shared environmental databases, ensuring more comprehensive ecosystem-level accountability.

Overall, the proposed analytical framework owing to its flexibility, quantification capacity, and transparency demonstrates strong potential as a practical and reliable decision-support tool for environmental impact assessments of infrastructure projects. By providing objective numerical comparability across project alternatives, it contributes to evidence-based decision-making aligned with the principles of sustainable development. Therefore, the 'Advanced Checklist' may be viewed as a structured enhancement and modernization of existing EIA tools rather than a fundamentally new model.

**Acknowledgments**

The authors would like to express their sincere appreciation to Lorestan Regional Water Company for their valuable support and for providing essential data and access to the project site. Special thanks are also extended to the engineering consulting firm Abdan Faraz Consulting Engineers for their technical guidance and collaboration during the environmental impact assessment process. Furthermore, the authors gratefully acknowledge the Jundi-Shapur University of Technology, Dezful, Iran for providing the academic environment and resources necessary for the preparation of this article.

**Conflict of Interest**

The authors declared no potential conflicts of interest concerning the research, authorship, and publication of this article. Confirmation

**Funding**

The authors received no financial support for the research, authorship, and publication of this article.

**Data Availability Statements**

Data Availability Statement: All information and results are presented in the text of the article.

**Authors' contribution**

**First Author:** Nader Nabipour, Study design, data collection, initial drafting; revise methods/results.

**Second Author:** Babak Lashkar-Ara Overall supervision, final study structure, full data analysis/interpretation, final edits/submission.

**Reference**

1- Ansar, A., Flyvbjerg, B., Budzier, A. and Lunn, D., 2014. Should we build more large dams? The actual costs of hydropower megaproject development. *Energy Policy*, 69, pp. 43–56. doi: 10.1016/j.enpol.2013.10.069.

2- Bragagnolo, C., do Nascimento, N. and Geneletti, D., 2017. Streamlining or sidestepping? Political pressure to revise environmental licensing and EIA in Brazil. *Environmental Impact Assessment Review*, 65, pp. 86–90. doi: 10.1016/j.enpol.2013.10.069.

3- Canter, L. W. and Wood, C., 1996. *Environmental impact assessment*. 2nd ed. London: McGraw-Hill.

4- Dehnavi, R. and Kouzehgar, R., 2019. Evaluation of ICOLD Matrix for Environmental Impact Assessment of the Peyghamchay Dam. *Environmental Monitoring and Assessment*, 191(10), article 607. doi: doi:10.1007/s10661-019-7767-4.

5- Eslami, V., Ashofteh, P.-S., Golfam, P. and Loáiciga, H.A., 2021. A multi-criteria decision-making approach for managing environmental impacts of dam construction using the IDOCRIW–COCOSO method: Case of Nohob Dam, Iran. *Water Resources Management*, 35(12), pp. 4231–4246. doi: 10.1007/s11269-021-02932-1.

6- Fearnside, P. M., 2016. Environmental and social impacts of hydroelectric dams in Brazilian Amazonia: Implications for the aluminum industry. *World Development*, 77, pp. 48–65. doi: 10.1016/j.worlddev.2015.08.015.

7- Geneletti, D., 2005. Formalising expert opinion through multi-attribute value functions: an application in landscape ecology. *Journal of Environmental Management*, 76(3), pp. 255–262. doi: 10.1016/j.jenvman.2005.01.025.

8- Glasson, J., Therivel, R. and Chadwick, A., 2013. *Introduction to Environmental Impact Assessment*. 4th edn. London: Routledge.

9- Javadi, S., Mohammadi, K. and Khodadadi, A., 2007. The environmental impact assessment of Gotvand Upper Dam using the combination of two methods of ICOLD and Leopold matrix. *Environmental Sciences*, 4(3), pp. 35–48 [In Persian].

10- Karimi, S., Bouzari, S. and Saadat Foomani, M., 2019. Environmental impact assessment of Zhaveh Dam construction using checklist and ICOLD matrix methods: Case study of Zhoveh Dam. *In: Proceedings of the Conference on Environmental Science, Engineering and Technologies (CESET 2019)*, Faculty of Environment, University of Tehran, Tehran, Iran. (In Persian).

11- Khodabakhshi, M., Zahraee, B. and Malekmohammadi, B., 2011. Environmental impact assessment of dam construction using multi-criteria ELECTRE and decision matrix methods. *Environmental Sciences*, 8(2), pp. 115-128. (In Persian).

12- Leopold, L. B., 1971. *A procedure for evaluating environmental impact*. Vol. 645. Washington, DC: US Department of the Interior.

13- Lerer, L. B. and Scudder, T., 1999. Health impacts of large dams. *Environmental Impact Assessment Review*, 19(2), pp. 113–123. doi: 10.1016/S0195-9255(98)00040-9.

14- Lyu, H. M., Sun, W. J., Shen, S. L. and Arulrajah, A., 2018. Flood risk assessment in metro systems of mega-cities using a GIS-based modeling approach. *Science of the Total Environment*, 626, pp. 1012–1025. doi: 10.1016/j.scitotenv.2018.01.138.

15- Makhdoum, M., 2008. Problems arising from non-compliance with environmental considerations in water projects. in *Proceedings of the Conference on Environmental Impact Assessment of Water Resource Development Projects* . (In Persian).

16- Modak, P. and Biswas, A. K., 1999. *Conducting environmental impact assessment for developing countries*. Tokyo: UNU Press.

17- Morgan, R. K., 2012. Environmental impact assessment: The state of the art. *Impact Assessment and Project Appraisal*, 30(1), pp. 5–14. doi: 10.1080/14615517.2012.661557.

18- Mostert, E., 2003. The challenge of public participation. *Water Policy*, 5(2), pp. 179–197. doi: 10.2166/wp.2003.0014.

19- Pope, J., Bond, A., Morrison-Saunders, A. and Retief, F., 2013. Advancing the theory and practice of impact assessment: Setting the research agenda. *Environmental Impact Assessment Review*, 41, pp. 1–9. doi: 10.1016/j.eiar.2013.01.008.

20- Sadler, B. and Verheem, R., 1996. *Strategic environmental assessment: Status, challenges and future directions*. Ministry of Housing, Spatial Planning and the Environment, the Netherlands: International Study of the Effectiveness of Environmental Assessment.

21- Sánchez, L. E. and Morrison-Saunders, A., 2011. Learning about knowledge construction in environmental impact assessment follow-up. *Environmental Impact Assessment Review*, 31(3), pp. 211–218. doi: 10.1016/j.eiar.2010.12.002.

22- Sayadi, A., Khodadadi, D. A., and Partani, S., 2009. Environmental impact assessment of gotvand hydro-electric dam on the Karoon River using ICOLD technique. *International Journal of Environmental and Ecological Engineering*, 3(6), pp.118-123. doi: 10.5281/zenodo.1339949.

23- Valizadeh S. and Shekari Z., 2015. Evaluation of Iranian Leopold matrix application in the environmental impact assessment (EIA) of solid waste management options in Birjand city. *Health and Environment*, 8(2), pp. 249–262. (In Persian).

24- World Commission on Dams (WCD)., 2000. *Dams and development: A new framework for decision-making*. London: Earthscan Publications.

25- Zo'obo Engolo, G.M., Dieudonné, S., Mbog Mbog, S., Polmbaye, P. and Bitondo, B., 2024. Cumulative Impact Assessment of Development Projects Around Campo-Ma'an National Park in Cameroon. *Journal of Environmental Assessment and Management*. doi: 10.37256/epr.4220244571.

© 2026 The Author(s). Published by Shahid Chamran University of Ahvaz. This is an open-access article distributed under the terms of the Creative Commons Attribution License (http://creativecommons.org/licenses/by/4.0), which permits unrestricted use, distribution, and reproduction in any medium, provided the original work is properly cited.

Shahid Chamran University of Ahvaz

**Irrigation Sciences and Engineering (JISE)**
**Vol. 48, No. 4, Winter 2026, p. 37-48**

**Research Paper**

Journal homepage: https://jise.scu.ac.ir

# Numerical investigation of Semicircular Sharp-Crested Weirs

Abbas Parsaie[1*], Mohammad Bahrami Yarahmadi[2] and Mahziar BasitNejad[3]

*1*-Corresponding Author, Assistant Professor, Department of Water Structures, Faculty of Water and Environmental Engineering, Shahid Chamran University of Ahvaz, Ahvaz, Iran. (parsaie@scu.ac.ir)*

*2-Associate professor, Department of Water Structures, Faculty of Water and Environmental Engineering, Shahid Chamran University of Ahvaz, Ahvaz, Iran.*

*3- Ph.D Student, Department of Water Structures, Faculty of Water and Environmental Engineering, Shahid Chamran University of Ahvaz, Ahvaz, Iran.*

**ARTICLE INFO**

*Article history:*
Received: 22 April 2025
Revised: 06 September 2025
Accepted: 27 September 2025
Available online: 04 January 2026

*Keywords:*
Discharge Coefficient, Simpson's rule, Flow Measurement, Confidence Interval, Sharp Crested Weirs.

**TO CITE THIS ARTICLE:**

Parsaie, A., Bahrami Yarahmadi, M., Basitnejad, M. 2026. 'Numerical investigation of Semicircular Sharp-Crested Weirs', *Irrigation Sciences and Engineering*, 48(4), pp. 37-48. doi: 10.22055/jise.2025.49460.2161.

**Abstract**

Sharp-crested weirs (SCWs) are widely used hydraulic structures for measuring discharge in small and confined channels. Their hydraulic performance is primarily governed by the relationship between flow head and discharge (H-Q), along with the associated discharge coefficient ($C_d$). The derivation of the H-Q relationship typically involves the integration of the velocity profile over the flow cross-section. However, for semicircular sharp-crested weirs (SCCWs), this process becomes analytically complex due to the emergence of elliptic integrals. To address this, the present study employed Simpson's numerical integration rule to approximate the relevant elliptic integrals with high accuracy, with a specific focus on determining $C_d$. A simplified analytical expression for the H-Q relationship was developed and thoroughly validated against an extensive dataset obtained from laboratory experiments. The model exhibited strong agreement with observed data, confirming its predictive capability. Furthermore, dimensional analysis using Buckingham's π-theorem revealed that the discharge coefficient is a function of the dimensionless ratios H/P, H/D, and D/P, where H is the upstream flow head, P is the weir height, and D is the crest diameter. The observed $C_d$ values ranged between 0.95 and 0.97 within a 95% confidence interval for flow conditions where H/P varied from 0.06 to 1.1 and D/P from 0.33 to 3.54. In addition, a nonlinear empirical model was formulated to estimate Cd, achieving a mean absolute percentage error (MAPE) of approximately 7.4%, indicating the robustness and applicability of the proposed methodology for semicircular weir configurations.

## Introduction

Weirs are hydraulic structures commonly used in water engineering for various purposes, such as flow measurement, increasing upstream flow depth at water intake structures, and controlling flow rates in open channels. Among the various types of weirs, sharp-crested weirs are especially prevalent for flow measurement in small irrigation canals. These can be designed with different cross-sectional shapes, including rectangular, triangular, trapezoidal, and circular (Bos, 1976). Recently, innovative cross-sectional designs for weirs have been introduced, including full and half-cycle cosine weirs Azimi and Salehi (2022); Salehi et al. (2019), compound weirs Ansari et al., (2019); Zahiri et al., (2014), and combinations with other flow measurement

 *DOI:* 10.22055/jise.2025.49460.2161

structures like gates and orifices (e.g., weir-gate and weir-orifice configurations) (Zeinivand et al. 2024 b & a). According to hydraulic principles, the flow rate over these weirs depends on the upstream flow head and the length of the weir's crest. While the discharge capacity relates linearly to crest length, it follows a power function concerning the upstream flow head (Akan and Iyer 2021). Notably, the accuracy and sensitivity of flow measurements are influenced by this power relationship. For example, the discharge capacity of rectangular weirs is proportional to the upstream head raised to the power of 1.5 ($Q_{rec} \propto h^{1.5}$). In contrast, for triangular weirs, it is proportional to the power of 2.5 ($Q_{trn} \propto h^{2.5}$) (Bos, 1976). However, these relations indicate that triangular weirs offer more precision and sensitivity than rectangular weirs. Although triangular weirs provide greater measurement accuracy, following a power function of 2.5, they have a significantly lower discharge capacity than rectangular weirs(Akan and Iyer, 2021). Consequently, triangular weirs are not suitable for measuring large flow rates. From a hydraulic standpoint, achieving the same flow rate through a triangular weir requires a 30% increase in the upstream head compared to a rectangular weir (Akan and Iyer, 2021). To overcome these limitations, trapezoidal weirs, which combine features of both rectangular and triangular shapes, have been proposed as an effective solution. The Cipolletti weir is a notable example of this design, successfully balancing measurement accuracy and discharge capacity (Akan and Iyer, 2021). Recent advancements in hydraulics have deepened our understanding of flow dynamics and the design of hydraulic structures. Research on crown wheel spillways highlights crucial hydrodynamic processes that influence discharge coefficients. Lashkar-Ara and Sheikhi (2022) investigate the performance of spillways under free flow conditions, while Habibi and Lashkar-Ara (2018) examine how floating debris accumulation affects hydraulic efficiency, finding that increased slenderness coefficients reduce overflow blockage and enhance discharge capacity. Additionally, denil fishways are explored as effective solutions for facilitating fish migration, utilizing baffles to minimize turbulence (Mahmoudian et al., 2023). Furthermore, the analysis of shear stress distributions in rectangular open channels (Lashkar-Ara and Fathi-Moghadam, 2023) provides critical insights into the impact of geometric and physical factors on boundary shear. Collectively, these studies advance our understanding of hydraulic parameters and support the optimization of hydraulic designs and modeling techniques in the field. Another type of weir that provides a good balance of accuracy and discharge capacity is the circular (or semicircular) weir. However, limited comprehensive analytical and laboratory research on its hydraulics has been performed. The complexity of the relationship between the upstream flow head and flow rate for this type of weir poses challenges that can hinder its practical use by operators. Bos (1976) and Staus (1930) developed an equation to estimate the discharge capacity of SCCWs. They formulated the following equation (Eq. 1) using the auxiliary parameters *w* and *wi*(.

$$w = 1.467\left(\frac{h}{D}\right)^2 + 0.664\left(\frac{h}{D}\right) - 0.059 \quad (1)$$

$$w_i = \frac{4}{15}\sqrt{2g} \times w \quad (2)$$

$$Q = c_d w_i D^{2.5} \quad (3)$$

where Q is the flow rate, $C_d$ is the discharge coefficient, $h$ is the upstream flow head, and $D$ is the diameter of the weir. Balachandar et al., (1991) proposed a simple method for calculating semicircular weirs' $C_d$. Using experimental results from previous studies, they created graphs to determine $C_d$ across various dimensionless parameters, including the contraction ratio (D/b), the ratio of upstream flow head to the weir height (H/P), and the ratio of upstream flow head to the weir diameter (H/D). In an analytical study, Vatankhah(2010) examined the H-Q relationship of a semicircular weir (SCCW). He noted that solving the H-Q for SCCWs involves dealing with elliptic integrals, which

can be cumbersome for operators. By implementing a change of variable, he derived a simple and practical formula, demonstrating good accuracy (with a mean absolute percentage error of less than 5%). Additionally, he presented an empirical formula (Eq. 4) for these weirs' $C_d$.

$$C_d = \frac{0.728 + 0.240\frac{H}{P}}{1 + 0.688\sqrt{\frac{H}{P}}} \quad (4)$$

Ghadba (2011) conducted a study to investigate the hydraulic characteristics of flow in SCCWs and using dimensional analysis, he derived the parameters influencing the $C_d$. To validate his analytical results, Ghadba (2011) performed experiments on 16 weir models with varying crest heights and radii. His findings revealed that changes in the weir radius had a more significant impact than crest height; specifically, as the weir radius increased, the flow volume over the crest also increased. Ghobadian and Meratifashi (2012) proposed a modified theoretical relationship for the H-Q relationship of SCCWs. They presented an empirical H-Q relationship that accounts for flow pattern complexity. They conducted experiments on six semicircular weirs with varying diameters and heights, reporting a correlation coefficient of 0.889 between experimental and theoretical results. Irzooki et al. (2014) conducted a laboratory study on the flow parameters of SCCWs, utilizing weirs with four different radii and three crest heights. Their results indicated that, under consistent conditions, an increase in weir radius led to a higher $C_d$, while an increase in the height of the SCCW resulted in decreased $C_d$.

As noted, deriving the H-Q relationship for SCCWs poses challenges, which accounts for the limited research on this type of weir. This study aims to derive the H-Q relationship in a simplified manner using Simpson's rule, apply dimensional analysis through Buckingham's Π-Theory to identify the dimensionless parameters affecting $C_d$, and ultimately propose an empirical relationship for calculating $C_d$.

## Material and Methods

This study aims to provide a simple H-Q relationship for semicircular weirs (SCCWs). A schematic sketch of the SCCW is shown in Fig. (1). As shown in this figure, $R$ indicates the radius of the weir crest cross-section, the flow depth over the crest by $y$, and the weir height by $P$.

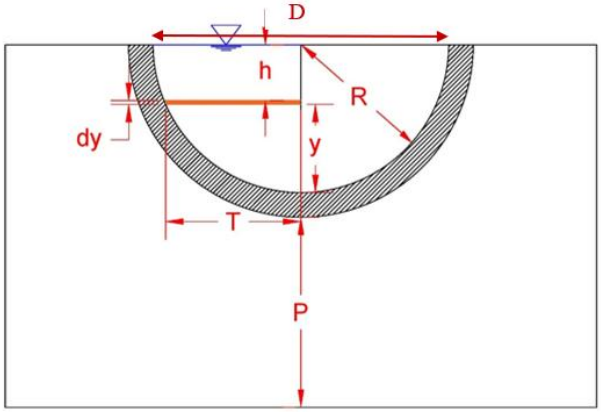



**Fig. 1- Sketch of the semicircular sharp-crested weir**

 *DOI:* 10.22055/jise.2025.49460.2161

To derive the H-Q relationship, referring to Figure (1), A thin element with a thickness of *dy* and width *T* is considered within the cross-sectional area of the flow passing through the weir. The theoretical discharge ($Q_{th}$) through this element is calculated using Equation (5).

$$\mathrm{Q_{th}} = 2\int_{\mathrm{o}}^{\mathrm{R}} u\mathrm{T}\mathrm{dy} \tag{5}$$

Where $u$ is the velocity of the considered element flow (determined using the Bernoulli equation: Eq. 6).

$$u \cong \sqrt{2gh} \tag{6}$$

Where *h* is the upstream flow head over the element. Substituting Equation (6) into Equation (5) yields the integral form of the H-Q relationship, presented in Equation (7).

$$\begin{aligned} Q_{th} = 2\int_{o}^{R} uT\,dy \xrightarrow{u\cong\sqrt{2gh}} Q_{th} \\ = 2\int_{0}^{R} \sqrt{2gh}\ T\ dy \\ Q_{th} = 2\sqrt{2g}\int_{0}^{R} \sqrt{h}\ T\ dy \end{aligned} \tag{7}$$

As given in Equation (7), this integral ranges from zero to the radius of the crest (R), meaning the flow depth can vary from zero to *R*. To solve Equation (7), both parameters of *h* and *T* are expressed as functions of the flow depth (*y*). Since the cross-sectional geometry is semicircular, there is a direct relationship between *h*, *T*, and *y*, as indicated in Equation (8).

$$\begin{aligned} &T^2 + (R-y)^2 = R^2 \\ &T = \sqrt{2yR - y^2} \\ &h = R - y \end{aligned} \tag{8}$$

By substituting Equation (8) into Equation (7), Equation (9) is obtained.

$$Q_{th} = 2\sqrt{2g}\int_{0}^{R} \sqrt{R-y}\sqrt{2Ry-y^2}\,dy \tag{9}$$

Solving equation (9) leads to an elliptical integral, which is not easy to use. One way to simplify such an integral is to use Simpson's rule. Simpson's rule Chapra and Canale, (2011) evaluates the given integral, which requires numerical approximation. Simpson's rule is a numerical method for approximating definite integrals (Equation 10). It involves dividing the integration interval into smaller subintervals and approximating the function in each subinterval using a second-degree polynomial.

$$\begin{aligned} \int_a^b f(y)dy \approx \frac{h}{3}\Bigg( & f(y_0) \\ & + 4\sum_{i=1,3,5,\dots}^{n-1} f(y_i) \\ & + 2\sum_{i=2,4,6,\dots}^{n} f(y_i) \\ & + f(y_n)\Bigg) \end{aligned} \tag{10}$$

$$\begin{aligned} \int_a^b f(y)dy \approx \frac{h}{3}\big( & f(y_0) + 4f(y_1) \\ & + 2f(y_2) + 4f(y_3) \\ & + \cdots + 2f(y_{n-2}) \\ & + 4f(y_{n-1}) \\ & + f(y_n)\big) \end{aligned}$$

where $h = \frac{b-a}{n}$is the width of each subinterval, $n$ is the number of subintervals (which must be even), and $y_i = a + ih, i = 0,1,2,\cdots,n$ are the discretized integration points and $f(y_i) = \sqrt{R-y_i}\sqrt{2Ry_i - y_i^2}$.

Due to the certain simplifications, such as ignoring energy loss and estimating integral parameters with Simpson's rule, the results from the theoretical equation may differ from the experimental data (measured discharge: $Q_m$). As a result, the values obtained from the theoretical equation ($Q_{th}$) are multiplied by a coefficient known as the discharge coefficient ($C_d$), as shown in Equation (11).

$$Q_m = C_d Q_{th} \tag{11}$$

The $C_d$, as given in Eq. (12), depends on the upstream flow head ($h$), the radius ($R$) of the crest, and the height of the weir ($P$). Additionally, $C_d$ is influenced by the flow regime (turbulent and subcritical flow conditions, represented by flow depth $y$ and velocity $V$) and flow properties (viscosity $\mu$, density $\rho$, and surface tension $\sigma$).

$$C_d = \varphi(y, P, R, V, \mu, \rho, \sigma) \quad (12)$$

Using Buckingham Π theory, the dimensionless parameters affecting the $C_d$ are derived ( Eq. 13).

$$C_d = \varphi\left(\frac{H}{P}, \frac{H}{D}, \frac{D}{P}, Fr, Re, We\right) \quad (13)$$

where $H$ represents the total head of the flow over the crest, which encompasses both the flow depth over the crest and the velocity head of the approaching flow. Therefore, instead of using $y$ (the flow depth), $H$, which denotes the total head, is used.

**Evaluation of the Developed Model**

After developing the numerical model based on Simpson's rule, its results were evaluated using the statistical index MAPE. The MAPE (Mean Absolute Percentage Error) is the mean of the absolute percentage errors and is one of the most commonly used indicators for assessing the accuracy of predictive or estimation models. This metric is widely applied in time series forecasting, regression modeling, and numerical model analysis. The MAPE index is defined by the following equation(Neysi et al, 2025):

$$MAPE = \sum_{i=1}^{n} \frac{1}{n} \left|\frac{A_i - F_i}{A_i}\right| \times 100 \quad (14)$$

In this equation, Ai represents the actual value at time, Fi denotes the predicted value by the model at time , and n is the total number of data points.

**Validation of the proposed formula**

Data from various researchers, including Ghobadian and Meratifashi (2012), Irzooki et al. (2014), and Ghadba (2011), were used to calibrate and validate Equation (10) against laboratory data and to determine $C_d$. Table (1) lists the geometric dimensions of the weirs and the hydraulic parameters from their experiments.

## Results and discussion

This section presents the calibration results of the proposed formula (Equation 10) and the discharge coefficient ($C_d$) calculation. The equation was calibrated using experimental data derived from over 43 laboratory models comprising 240 experimental runs. Selected calibration results for various weir geometries are shown in Figure (2), which demonstrates a strong correlation between the observed data and the results generated by the proposed formula. To calibrate the proposed formula with the laboratory data, 10 subinterval was considered. Notably the modeling accuracy was approximately 7%.

**Table 1- The range of geometric and hydraulic data collected concerning SCCWs**

| Authors | Range | P(m) | D(m) | Q(l/s) |
|---|---|---|---|---|
| Ghobadian and Meratifashi (2012) | min | 0.198 | 0.15 | 1.8 |
| | max | 0.25 | 0.25 | 15.7 |
| Irzooki et al. 2014 | min | 0.14 | 0.31 | 1.34 |
| | max | 0.248 | 0.515 | 28.86 |
| Ghadba (2011) | min | 0.15 | 0.1 | 1.64 |
| | max | 0.3 | 0.4 | 46.38 |

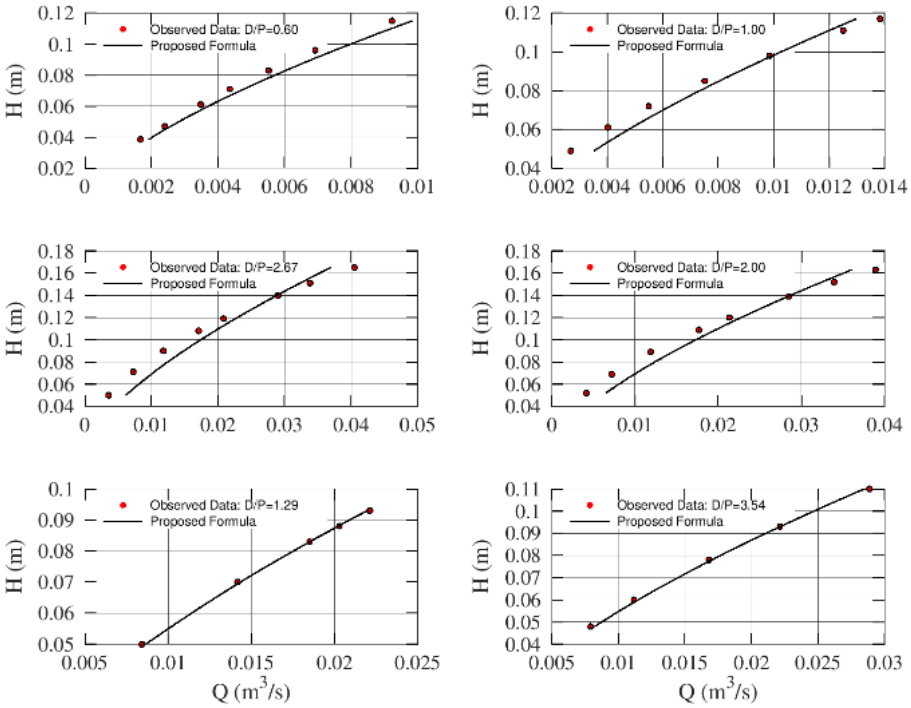



**Fig. 2 – H-Q relation of SCCWs: observed data and proposed formula**

During the calibration of Eq. (10) for each laboratory weir model, a value of $C_d$ was determined for each relative upstream head, with values ranging from 0.6 to 1.10.

As shown in Figure 4, the discharge coefficient exhibits a direct logarithmic relationship with the relative flow head parameters. Initially, its value increases and then remains constant.The semicircular geometry of the weir causes the discharge coefficient to initially increase and then stabilize at an almost constant value. As the H/P ratio increases, energy losses become greater, leading to a reduction in the discharge coefficient. However, with further increases in H/P, since both energy loss and flow velocity increase simultaneously, their combined effect results in little to no change in the discharge coefficient. This behavior has also been observed in the studies by Ghobadian and Meratifashi (2012) and Irzooki et al. (2014).

The histogram and violin plot of the $C_d$ values are presented in Figure (3).

As illustrated in Figure (3), the average value of $C_d$ is approximately 0.96 (≈1), with a 95% confidence interval ranging from 0.95 to 0.97. As detailed in the Materials and Methods section, various parameters influence $C_d$ (Eq. 13), including $H/P$, $H/D$, and $D/P$. The values of $C_d$ for the same models (shown in Figure 2) were plotted versus $H/P$ and are shown in Figure (4).

According to Eq. (13), in addition to $H/P$, the geometric parameter $D/P$ also influences $C_d$. To illustrate the variation of $C_d$ regarding D/P, an average value of $C_d$ was calculated for each laboratory model, and the results were plotted against $D/P$, as shown in Fig. (5). This figure demonstrates that for nearly all models, the average value of $C_d$ is clustered around one.

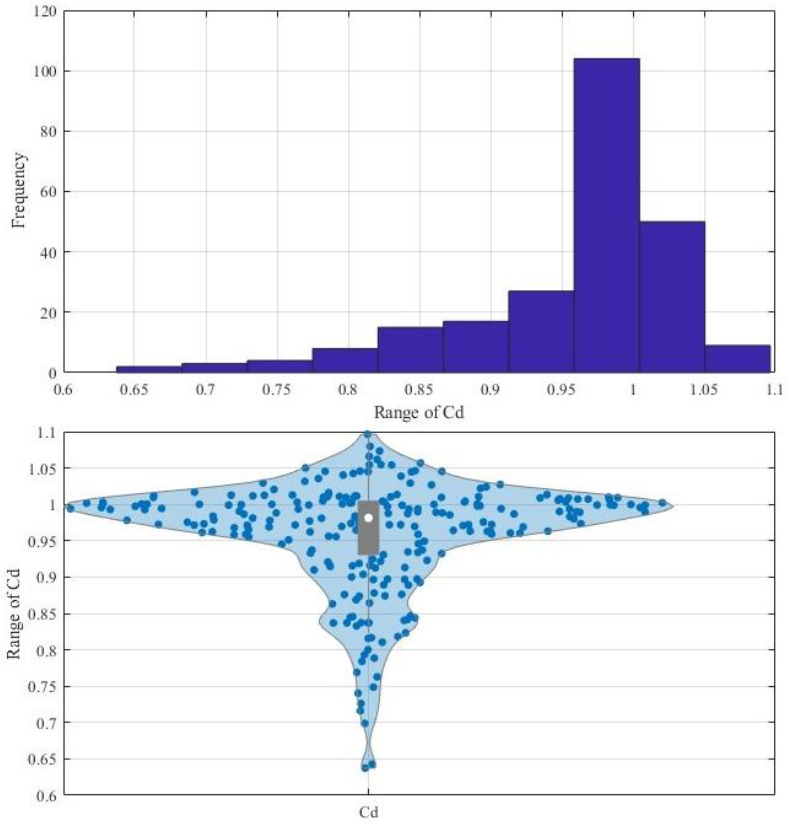



**Fig. 3- The histogram and violin graph of the obtained $C_d$ of SCCWs**

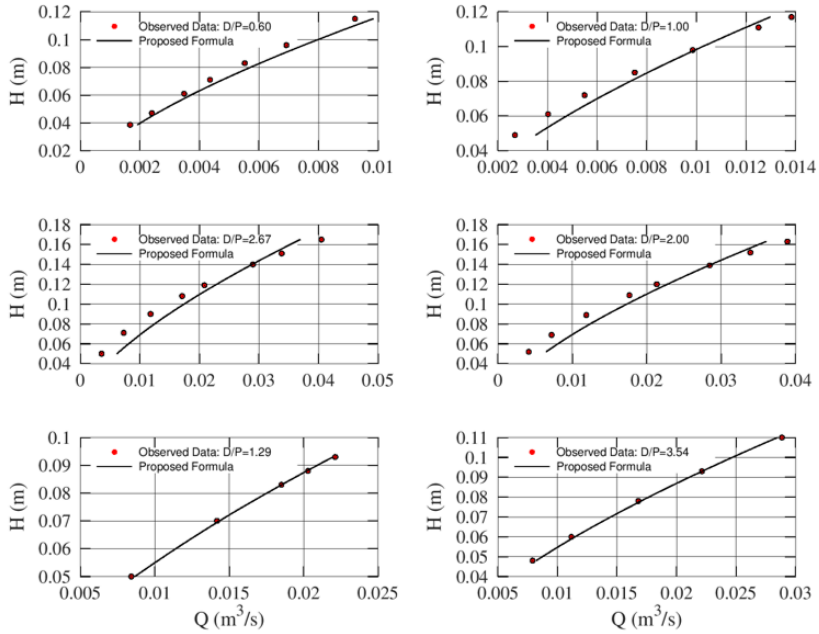



**Fig. 4- The values of $C_d$ versus the $H/P$ for some models of SCCWs**

 *DOI:* 10.22055/jise.2025.49460.2161

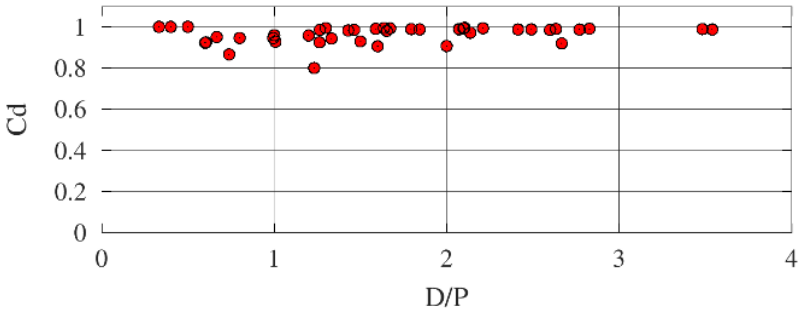



**Fig. 5 – The average values of $C_d$ of SCCWs versus the D/P**

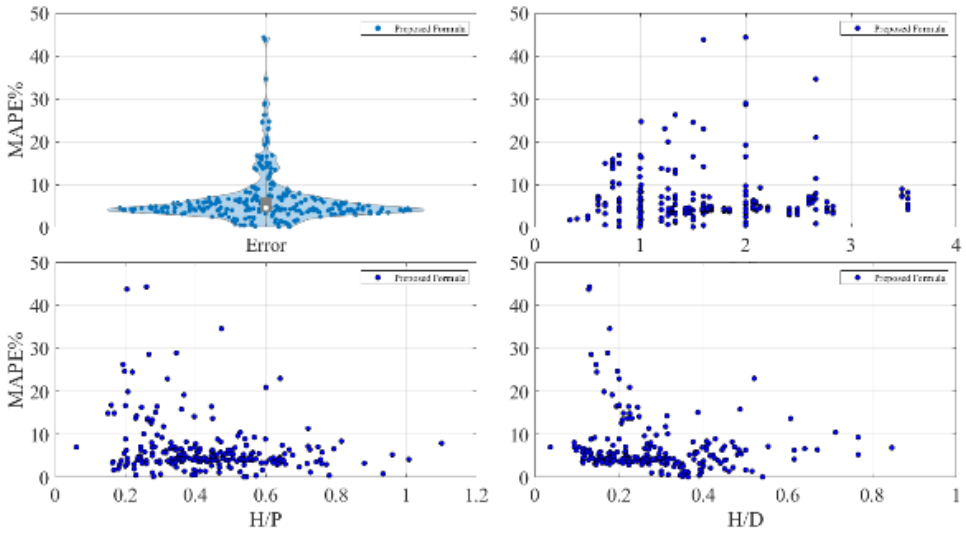



**Fig. 6 – The values of the MAPE of the proposed formula versus the involved parameters**

**The developed formula for $C_d$**

In this part, according to Table 1 and using the nonlinear regression technique, a nonlinear equation given in Eq. (14) was proposed to calculate the $C_d$ for semicircular sharp-crested weirs.

$$Cd = \left(\frac{H}{P}\right)^{0.31\frac{D}{P}} \quad (14)$$

As presented in Table 1, Eq. (14) was utilized for D/P between 0.33 and 3.54, while H/P ranges between 0.06 and 1.10. Noteworthy that in the same condition (same ranges of D/P and H/P), the H/D changes between 0.34 and 0.85. The proposed formula's average error (MAPE) is about 7.4 percent (%). The Violon graph of MAPE results of the proposed formula and its variation versus the involved parameters (H/P, H/D, and D/P) are shown in Fig. (6). As shown in Fig. 6, most errors accumulated between 0 and 10 percent. Increasing the H/P or H/D reduces the MAPE (error of the proposed formula). Fig. 6 shows that no significant relation exists between the variation of H/P and MAPE.

**Compared with previous research**

In this section, the results of this study are compared with those of previous researchers. For this purpose, the results of two researchers, including Vatankhah(2010) and "Staus (1930)" (Bos, 1976), were selected. As mentioned, for any weir, including SCCWs, two essential components are the H-Q and the

$C_d$. The results of the $C_d$ based on the two approaches of the mentioned researchers are presented in Fig. (7). As is evident from these figures, the range of the calculated $C_d$ based on the Vatankhah(2010) and Staus (1930) approaches for the data published by Ghobadian and Meratifashi (2012) and Ghadba (2011) is in the range of 0.6 and 0.7, while the results of $C_d$ calculated by "Staus(1930)" approach for Irzooki et al.(2014) ranges between 1.00 and 2.54.

The value of $C_d$ calculated by the proposed formula is between 0.6 and 0.9, and its average value is about 0.96; at a 95% confidence level, it is between 0.95 and 0.97. Well, of course, the difference between the range of the proposed formula and the range of calculated $C_d$ by the approaches of Vatankhah (2010) and Staus(1930) is due to the final equation and the powers considered for the flow head. The H-Q curve was considered for a more accurate comparison of these formulas. The performance of the proposed formulas (all tested formulas in this study) for the H-Q curve of all the models was evaluated. For example, the results of six modules (presented in Figure 2) are shown in Figure (8). On average, the MAPE of Vatankhah (2010) formula is about 3 percent, the error of the Staus(1930) approach is about 5 percent, and the error of the formula presented in this study is about seven percent.

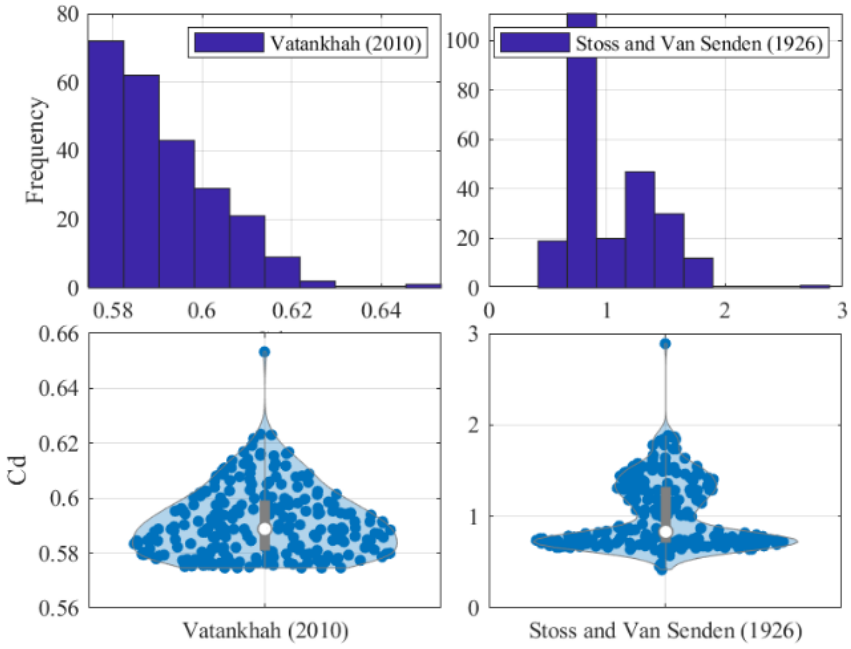



**Fig. 7 – The histogram and violin graph of the obtained $C_d$ of the semicircular sharp-crested weir**

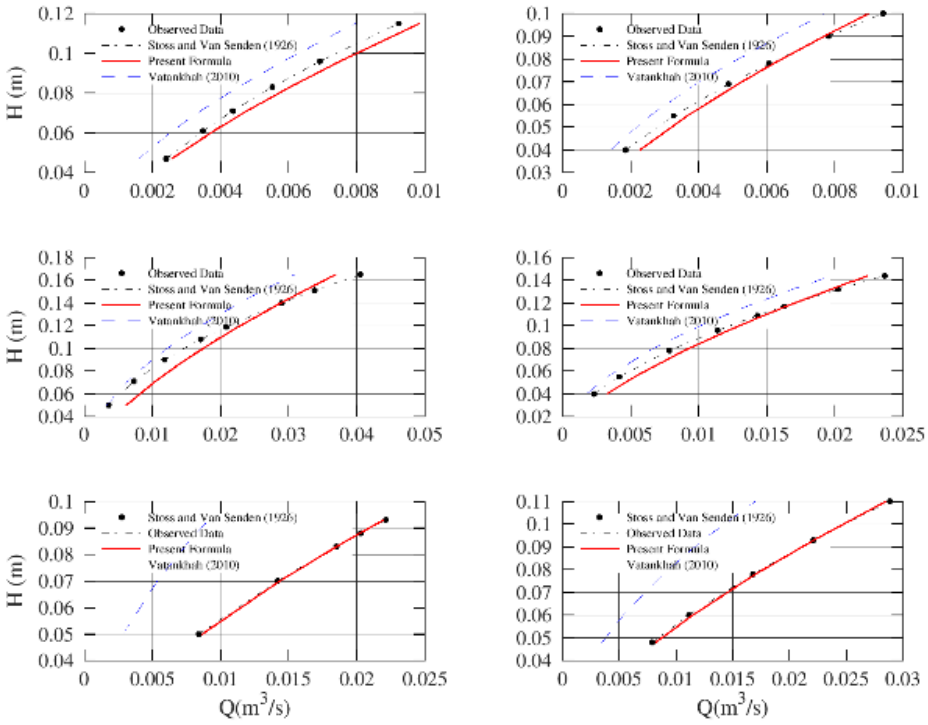



**Fig. 8- The results of head discharge simulation through the present study, Vatankhah(2010), and Staus (1930)**

## Conclusion

Here, an effort has been made to present a straightforward solution to the integral form of the H-Q curve for SCCWs. To achieve this, both components under the square root in the integral form of the H-Q equation were approximated using Simpson's rule. The resulting formula was calibrated against various geometries of SCCWs. Notably, the variable geometric parameters for this type of weir are the crest's diameter and the weir's height. The results indicate a good agreement between the proposed formula and the observed data (average error of about 7.5%). Dimensional analysis reveals that two parameters, including the relative upstream head (H/P) and the ratio of the crest diameter to the height of the weir (D/P), are involved in $C_d$. The findings indicate that $C_d$ varies between 0.6 and 1.1, with an average value of approximately 0.96, accompanied by a 95% confidence interval of (0.95, 0.97), considering the ranges of H/P between 0.06 and 1.1, and D/P between 0.33 and 3.5. Plotting the average discharge coefficient against D/P demonstrates no significant trend in their variations. For most values of D/P, $C_d$ remains approximately 0.96.

## Notations

| | |
|---|---|
| $Q_m$ | measured discharge |
| $Q_{th}$ | theoretical discharge |
| $C_d$ | discharge coefficient |
| D | Diameter |
| $dy$ | Thickness of an element |
| $H$,$h$ | Total upstream head |
| H-Q | Head discharge |
| MAPE | mean absolute percentage error |
| max | Maximum |
| min | Minimum |
| P | Weir Height |
| $Q$ | discharge |
| R | Radius |
| SCCWs | Semicircular sharp-crested weirs |
| T | The top width of the surface of the flow |

| | |
|---|---|
| u | Flow velocity |
| y | Flow depth |

**Acknowledgments**

We are grateful to the Research Council of Shahid Chamran University of Ahvaz for financial support.

**Conflict of Interest**

The authors declared no potential conflicts of interest concerning the research, authorship, and publication of this article. Confirmation.

**Funding**

The financial support of this research has been provided by Grant number .SCU.WH1404.72091 and we hereby thank the Honorable Vice Chancellor of Research from Shahid Chamran University of Ahvaz for their support.

**Data Availability Statements**

Data Availability Statement: All information and results are presented in the text of the article.

**Authors' contribution**

**First Author:** Abbas Parsaie: idea, writing.
**Second Author:** Mohammad Bahram Yarahmadi: edit and revise
**Third Author:** Mahziar Basit Nejad: collection of data, revise.

**References**

1- Akan, A. O., and S. Iyer. 2021. "Hydraulic structures." *Open Channel Hydraulics*, 213–304. Elsevier. https://doi.org/10.1016/B978-0-12-821770-2.00004-X

2- Ansari, M.A., Hussain, A., Shariq, A. and Alam, F., 2019. Experimental and numerical studies for estimating coefficient of discharge of side compound weir. *Canadian Journal of Civil Engineering*, *46*(10), pp.887-895. https://doi.org/10.1139/cjce-2017-0689.

3- Azimi, A.H. and Salehi, S., 2022. Hydraulics of flow over full-cycle cosine and rectangular sharp-crested weirs. *Canadian Journal of Civil Engineering*, *49*(6), pp.954-968. https://doi.org/10.1139/cjce-2020-0581.

4- Balachandar, R., Sorbo, S. and Ramamurthy, A.S., 1991. A note on circular sharp-crested weirs. *Canadian Journal of Civil Engineering*, *18*(5), pp.881-885. https://doi.org/10.1139/l91-106.

5- Bos, M. G. 1976. *Discharge measurement structures*. 464. Netherlands: International Institute for Land Reclamation and Improvement (ILRI).

6- Ghadba, E.I., 2011. Hydraulic characteristics of semi-circular sharp crested weirs. *Tikrit Journal of Engineering Sciences*, *18*(1), pp.58-68.

7- Ghadba, E. I. 2011. "Hydraulic characteristics of semi-circular sharp crested weirs." *Tikrit Journal of Engineering Sciences*, 18 (1): 58–68. https://doi.org/10.25130/tjes.18.1.11

8- Ghobadian, R., and E. Meratifashi. 2012. "Modified Theoretical Stage-Discharge Relation for Circular Sharp-Crested Weirs." *Water Science and Engineering*, 5 (1): 26–33. https://doi.org/10.3882/j.issn.1674-2370.2012.01.003.

9- Habibi, S. and Lashkara-Ara, B., 2018. Laboratory Evaluation of the Effect of Floating Debris Accumulation at Crown Wheel Weirs on the Hydraulic Characteristics under Cumulative Test. *Irrigation and Drainage Structures Engineering Research*, *19*(72), pp.15-32. https://doi.org/10.22092/idser.2017.114730.1237.

10- Irzooki, R.H., Akib, S.M. and Fayyadh, M.M., 2014. Experimental study of characteristics of flow over weirs with semicircular openings. *Arabian Journal for Science and Engineering*, *39*(11), pp.7599-7608. https://doi.org/10.1007/s13369-014-1360-8.

11- Lashkar-Ara, B., Sheikhi, Y. 2011. 'Introduce of CPK Spillway and Study of Its Discharge Coefficient under Free Flow Regime', *Irrigation Sciences and Engineering*, 40(2), pp. 209-221. doi: 10.22055/jise.2017.13180.

12- Lashkar-Ara, B. and Fathi-Moghadam, M., 2014. Analysis of shear stress in rectangular open channels using force balance method. *Journal of Hydraulics*, *9*(3), pp.33-44. 10.30482/JHYD.2014.10174

13- Mahmoudian, Z., Baharvand, S. and Lashkar-Ara, B., 2019. Investigating the flow pattern in baffle fishway denil type. *Irrigation Sciences and Engineering*, *42*(3), pp.179-196. DOI: 10.22055/jise.2019.23693.1689.

14- Neysi, K. , Daryaee, M. , Kashefipour, S. M. , Shahriari, A. and Zayeri, M. 2025. Improving Water Diversion Efficiency in Converging Side Weirs through Side Vane Installation: a numerical simulation. *Irrigation Sciences and Engineering*, *47*(4), 93-104. doi: 10.22055/jise.2025.48446.2145

15- Salehi, S., K. Esmaili, and A. H. Azimi. 2019. "Mean velocity and turbulent characteristics of flow over half-cycle cosine sharp-crested weirs." *Flow Measurement and Instrumentation*, 66: 99–110. https://doi.org/10.1016/j.flowmeasinst.2019.02.002.

16- *STAUS, A. 1930. Zur Berechnung kreisrunder Uberfalle. Wasserkraft und Wasserwirtschaft, 25(11): 122-123*

17- Vatankhah, A. R. 2010. "Flow measurement using circular sharp-crested weirs." *Flow Measurement and Instrumentation*, 21 (2): 118–122. https://doi.org/10.1016/j.flowmeasinst.2010.01.006.

18- Zahiri, A., Tang, X. and Azamathulla, H.M., 2014. Mathematical modeling of flow discharge over compound sharp-crested weirs. *Journal of Hydro-Environment Research*, *8*(3), pp.194-199. https://doi.org/10.1016/j.jher.2014.01.001.

19- Zeinivand, M. and Ghomeshi, M., 2024 a. The discharge coefficient of sharp triangular weir pierced by orifices. *Flow Measurement and Instrumentation*, *97*, p.102560.https://doi.org/10.1016/j.flowmeasinst.2024.102560.

20- Zeinivand, M., S. Barani, and M. Ghomeshi. 2024b. "Investigating the process of changing the discharge coefficient of the flow passing through the combined structure of rectangular sharp-crested weir with multiple-gates." *Ain Shams Engineering Journal*, 15 (2): 102418. https://doi.org/10.1016/j.asej.2023.102418.

© 2026 The Author(s). Published by Shahid Chamran University of Ahvaz. This is an open-access article distributed under the terms of the Creative Commons Attribution License (http://creativecommons.org/licenses/by/4.0), which permits unrestricted use, distribution, and reproduction in any medium, provided the original work is properly cited.

Shahid Chamran University of Ahvaz

**Irrigation Sciences and Engineering (JISE)**
**Vol. 48, No. 4, Winter 2026, p. 49-64**

**Research Paper**

Journal homepage: https://jise.scu.ac.ir

# Investigation of Changes in the Green and Blue Water Footprint of Wheat in Drought and Rainy Seasons (A Case Study on Wheat under the Dez Irrigation Network, Southwestern Iran)

Mahkameh Mansouri[1], Esfandiar Fateh[2*], Amir Aynehband[3] and Ali Shahbazi[4]

*1- PhD student in Agrotechnology, Department of Plant Production and Genetics, Shahid Chamran University of Ahvaz, Ahvaz, Iran.*
*2*- Corresponding Author, Department of Plant Production and Genetics, Shahid Chamran University of Ahvaz, Ahvaz, Iran. (E.fateh@scu.ac.ir)*
*3- Department of Plant Production and Genetics, Shahid Chamran University of Ahvaz, Ahvaz, Iran.*
*4- Deputy Director of Basic Studies of Water Resources, Khuzestan Water and Power Authority (KWPA)*

ARTICLE INFO

*Artlcle history:*
Received: 22 April 2025
Revised: 10 June 2025
Accepted: 18 June 2025
Available online: 04 January 2026

*Keywords:*
Blue water footprint, Green water footprint, Drought indices, Water resource management

TO CITE THIS ARTICLE:
Mansoouri, M., Fateh, E., Aynehband, A., Shahbazi, A. 2026. 'Investigation of Changes in the Green and Blue Water Footprint of Wheat in Drought and Rainy Seasons (A Case Study on Wheat under the Dez Irrigation Network, Southwestern Iran)', *Irrigation Sciences and Engineering*, 48(4), pp. 49-64. doi: 10.22055/jise.2025.49468.2162

**Abstract**

Water resource management in agriculture, especially in arid and semi-arid regions, is a major global challenge. This study examines the impact of drought and wet periods on the blue water footprint (WFblue) and green water footprint (WFgreen) of wheat within the Dez irrigation network in Southwest Iran (1993–2023). The objective is to analyze variations in the water footprint using 30 years of meteorological data, wheat yield, and water input to the Dez network. Data were evaluated through WFblue/WFgreen models and ANOVA Results show that severe drought significantly increases WFblue by approximately 121.07% (375.20 $m^3ton^{-1}$) compared to the normal condition (169.59 $m^3ton^{-1}$), while reducing WFgreen, exerting substantial stress on groundwater and surface water resources. Variance analysis indicates that drought indices (RDI, SPI) significantly affect water resources, with SPI as the primary driver of variability. This study builds on Hoekstra's water footprint theory by integrating adaptive management strategies for drought and wet periods, emphasizing temporal variations in water use. The findings highlight the urgent need for smart water management and advanced meteorological forecasting to guide policies that mitigate drought impacts and enhance water-use efficiency.

## Introduction

Approximately half of global agricultural production relies on irrigation systems, with agriculture consuming 71% of freshwater resources, making it the largest water consumer worldwide, compared to 18% for industry and 8% for urban use (Nalbantis and Tsakiris, 2009; Burton, 2010). Optimizing water management in agriculture can significantly alleviate water shortages in other sectors and improve agricultural productivity.

Climate change, reduced precipitation, and altered rainfall patterns have heightened the need for optimized water management strategies. Traditional water management methods are no longer sufficiently effective. Agricultural water management comprises two main components: supply management (e.g., harnessing surface water, utilizing groundwater, and transferring water via irrigation channels) and demand management (e.g., modifying consumption patterns, input adjustments, and stakeholder participation). Given water resource constraints, demand management has become a key strategy for improving efficiency.

 *DOI:* 10.22055/jise.2025.49468.2162

he water footprint concept, introduced by Hoekstra in 2002, serves as a metric to assess water consumption in producing goods, particularly in agriculture, and has been applied to evaluate water security (Hoekstra et al., 2011; Veettil and Mishra, 2016). However, initial water footprint models, such as those developed by Hoekstra and colleagues before the standardized framework of 2011, often relied on annual average data, neglecting seasonal and inter-annual variations in blue and green water resources (Borzoo et al., 2024). For instance, these models typically overlooked fluctuations in precipitation and evapotranspiration, leading to inaccurate estimates of crop water requirements and inefficient irrigation planning, particularly during drought and wet periods. Evaluating crop water requirements and their variations under these conditions is essential for effective water management. The blue water footprint (WFblue) represents freshwater directly sourced from surface and groundwater, while the green water footprint (WFgreen) refers to rainwater stored in soil and vegetation. Assessing these resources can significantly enhance sustainable water management. This study examines changes in the blue and green water footprints of wheat over a 30-year period (1993–2023) in the Dez irrigation network, addressing a research gap in the region where prior studies, such as Panahi and Malik Muhammadi (2008) and Salarian (2014), focused on general water consumption and irrigation development but overlooked temporal variations in blue and green water footprints under drought and wet conditions. The main research question is: Can the network's water supply during drought compensate for green water shortages and prevent yield reductions?

## Materials and Methods

### Study Area

The study was conducted in the modern Dez irrigation network, located in northern Khuzestan Province, Iran, recognized as one of the largest and oldest modern irrigation networks in the country. Construction began in 1957 and was fully operational by the 1976–1977 agricultural season, aimed at supplying agricultural water and controlling floods from the Dez River, utilizing water from the Dez Dam. It is bounded by the northern Dezful hills to the north, Haft-Tappeh lands and the Shavoor River to the south, the Shoor River (Gelal Kohnag) to the east, and the Karkheh River to the west, covering the cities of Dezful, Andimeshk, and Shush. The network spans a gross area of approximately 111,674 hectares and a net area of 93,599 hectares, divided into three regions: Sabili (6,000 hectares, with water pumped due to elevated lands, featuring five pumping stations and a 12.8 km main canal), East Dez (37,000 hectares), and West Dez (50,000 hectares), based on the agricultural lands' positions relative to the Dez River and the regulating dam (North Khuzestan Irrigation Networks Operation Company). The region experiences a semi-arid climate with an average annual rainfall of 327 mm, a potential evapotranspiration of about 2,460 mm, and an average annual temperature of 24.6°C, based on 30-year data (1993–2023) from the Safiabad Dezful station (Details are provided in Table (1). The Dez River exhibits a perennial hydrological regime with seasonal fluctuations, with higher flows in the wet season (spring) and lower flows in the dry season (summer). Wheat constitutes approximately 36% of the cropping pattern in the Dez irrigation network (not the entire northern Khuzestan region), making it the dominant crop, based on cultivated area data from the North Khuzestan Irrigation Networks Operation Company and corroborated by the Khuzestan Agricultural Organization's statistical yearbook (NKINOC, n.d.; Khuzestan Agricultural Organization, 2023). Wheat planting in the Dez network typically occurs from mid-November to mid-December, with harvesting from late April to mid-May. The average irrigated wheat yield in the Dez network, used for water footprint calculations on an annual basis (1993–2023), is approximately 4,000 kg/ha (NKINOC, n.d.). The network employs diverse structures such as regulating dams, diversion dams, canals, and drains, including concrete-lined canals and 76 irrigation gates in the Sabili region, making it a distinguished and efficient irrigation system. Its selection for this study was driven by its historical significance, vast coverage, progressive farmers facilitating better

cooperation in surveys, and the need to redefine cropping patterns due to aging infrastructure, potential structural damage, and reduced water inflow caused by climate change, upstream water transfers, and multiple upstream dams. Meteorological data were collected from the Safiabad Dezful station (48°38'24"E, 32°40'12"N, 143 m above sea level), chosen for its proximity and reliable long-term data. The location of the network is shown in Figure (1).

**Table 1- Average 30-Year Meteorological Data (1993–2023) from Safiabad Dezful Station**

| Year | Tmin (°C) | Tmax (°C) | RH (%) | Wind (Km/day) | Sun (hours) | Rain (mm) | Evaporation (mm) |
|---|---|---|---|---|---|---|---|
| 1993-2023 | 16.5 | 32.6 | 55.25 | 329 | 3.4 | 327 | 2459.6 |

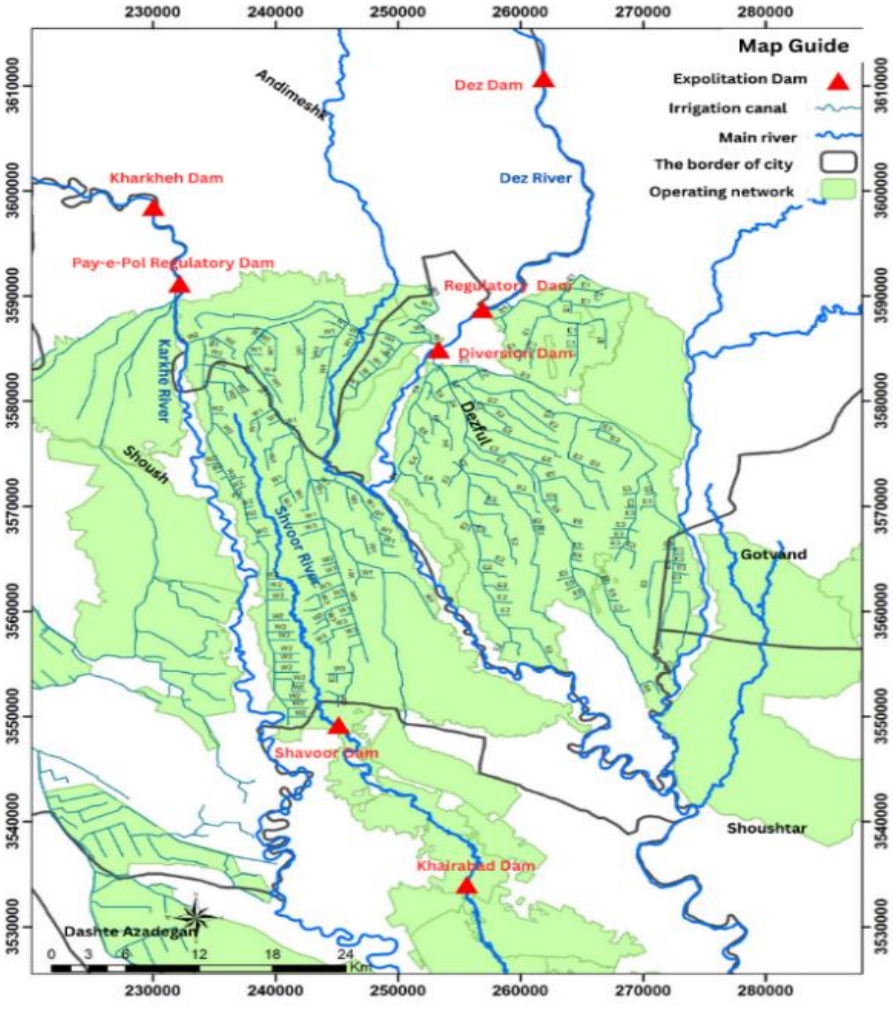



**Fig.1- location of Dez network**

**Data and Tools**

The study utilized a dataset comprising climatic parameters (maximum and minimum temperature, precipitation, wind speed, sunshine hours, and evaporation), 30-year meteorological data (1993–2023) from Safiabad Dezful station, 30-year wheat yield data (1993–2023) from the Khuzestan Agricultural Organization, and water input data to the Dez irrigation network from the North District Irrigation and Drainage Operation Company.

Data were processed using two software tools:

DrinC (version 1.7) to calculate drought indices (RDI, SPI, SDI) and assess wet and dry conditions, and Cropwat (version 8.0) to compute blue and green water footprints (WFblue and WFgreen).

**Blue and Green Water Footprint Calculation**

The blue and green water footprints were calculated following the global water footprint standard by Hoekstra et al. (2011). Cropwat was used to determine WFblue and WFgreen based on crop yield data from the Khuzestan Agricultural Organization. The calculations followed these equations:

$$WF_{Blue} = \frac{ET_{Blue}}{Y} \times 10 \quad (1)$$

$$WF_{Green} = \frac{ET_{Green}}{Y} \times 10 \quad (2)$$

Where:

$WF_{Blue}$, $WF_{Green}$: Blue and green water footprints ($m^3 ton^{-1}$).

$ET_{Blue}$, $ET_{Green}$: Blue and green evapotranspiration (mm), calculated using:

Y: Crop yield (ton $ha^{-1}$).

$$ET_{Blue} = \begin{cases} 0, & Eff \geq ETc \\ ETc - Eff\ Rain, & other\ wise \end{cases} \quad (3)$$

$$ET_{Green} = \begin{cases} ETc, & Irr.Req = 0 \\ Eff\ Rain, & other\ wise \end{cases} \quad (4)$$

Where:

$ETc$: Crop evapotranspiration (mm $day^{-1}$).

$Eff\ Rain$: Effective rainfall (mm), calculated using the USDA SCS method as configured in Cropwat (version 8.0). This method estimates effective rainfall based on total rainfall (P) by accounting for runoff and deep percolation, following the approach outlined by Allen et al (1998). The average effective rainfall over the 30-year period (1993–2023) was 162.2 mm.

Equation (1) states that if effective rainfall exceeds crop evapotranspiration, the blue evapotranspiration ($ET_{Blue}$)is considered zero; otherwise, it equals the difference between crop evapotranspiration ($ETc$) and effective rainfall ($Eff\ Rain$).

Equation (2) indicates that the green evapotranspiration ($ET_{Green}$) equals the crop water requirement when irrigation demand is zero; in all other cases, it is equivalent to the effective rainfall ($Eff\ Rain$).

The parameter $ETc$ (crop evapotranspiration) in the above equations was estimated using the reference evapotranspiration ($ET_o$) as described by Allen et al. (1998) and supported by alternative methods evaluated by Fisher and Pringle (2013); (Equation 6).

$$ET_C = ET_o \times Kc \quad (5)$$

Where:

$Kc$: Crop coefficient, adjusted based on local planting and harvesting dates and climatic parameters for wheat over 30 years, as per FAO guidelines (Allen et al., 1998).

$ET_o$: Reference evapotranspiration, calculated using the Penman-Monteith equation (Allen et al., 1998).

$$ET_0 = \frac{0.408(R_n - G) + \gamma \frac{900}{T+273} u_2 (e_s - e_a)}{\Delta + \gamma(1 + 0.3u_2)} \quad (6)$$

Where:

Rn:Net radiation (MJ $m^{-2} day^{-1}$).

G: Soil heat flux (MJ $m^{-2} day^{-1}$).

γ: Psychrometric constant (kPa°$C^{-1}$).

T:Air temperature (°C).

$u_2$:Wind speed at 2 m height (m $s^{-1}$)

$e_s, e_a$:Saturation and actual vapor pressure (kPa)

Δ: Slope of the vapor pressure curve (kPa°$C^{-1}$)

Drought and Wet Period Assessment

Drought intensity was evaluated using three indices:

Reconnaissance Drought Index (RDI): Calculated using cumulative precipitation (P) and potential evapotranspiration (PET) to assess water balance (Hargreaves & Samani, 1985; Tsakiris et al., 2007). PET was computed using the Hargreaves method, as implemented in the DrinC software (version 1.7), due to its simplicity and reduced data requirements compared to the Penman-Monteith method. The Hargreaves method estimates PET as follows:

$$PET = 0.023(0.408) \times (T_{mean} + 17.8) \times \sqrt{T\,max - T\,min} \times R_a \quad (7)$$

Where:

PET: Potential evapotranspiration (mm day$^{-1}$)

$T_{mean}$: Mean daily temperature (°C)

T max, T min: Maximum and minimum daily temperatures (°C)

$R_a$:Extraterrestrial radiation (MJ m$^{-2}$day$^{-1}$), calculated based on latitude and calendar day of the year as per Hargreaves and Samani (1985).

0.408: Conversion factor from MJ m$^{-2}$ to mm.

The classification of climatic and hydrological conditions based on SPI, RDI, and SDI indices is presented in Table (2).

Note: Potential evapotranspiration ($ET_0$) was calculated using the Penman-Monteith method, and effective rainfall (Eff. rain) using the USDA SCS method (average Eff. rain: 162.2 mm). $ET_0$ represents annual values, whereas crop evapotranspiration (ETc) for wheat during the growing season (approximately 600 mm) is lower due to the crop coefficient (Kc).

Positive values indicate wet periods, while negative values indicate dry periods. RDI was computed for 3, 6, 9, and 12-month periods within a hydrological year. RDI was selected over alternatives like the Standardized Precipitation Evapotranspiration Index (SPEI) due to its direct compatibility with DrinC software and its focus on water balance, as outlined by Tsakiris et al. (2007). Additionally, the meteorological monitoring network design for RDI was optimized based on approaches by Tsakiris et al. (2008).

Standardized Precipitation Index (SPI): A statistical tool based on long-term precipitation data, fitted to a gamma distribution and transformed to a normal distribution (Hayes et al., 2007). Positive SPI values indicate above-average precipitation, while negative values indicate drought. SPI was chosen for its simplicity and standardized approach to analyzing precipitation and identifying climatic droughts.

Streamflow Drought Index (SDI): Used to assess hydrological drought based on cumulative streamflow volume (Vangelis et al., 2013). Due to data availability constraints, only 20 years of streamflow data (2001–2021) were available for computing SDI, compared to the 30-year period (1993–2023) used for climatic indices (RDI and SPI). This shorter timeframe may limit capturing long-term hydrological drought trends in the earlier (1993–2000) and later (2022–2023) years, but SDI was included as a complementary index to evaluate hydrological drought, enhancing the climatic analyses provided by RDI and SPI. In this study, climatic drought and water footprint data were analyzed using the SPI and RDI indices over a 30-year period (1993–2023). Precipitation data and related information for these indices were fully available for this period. On the other hand, to analyze hydrological drought and assess water inflow in the irrigation network, the SDI index was used. Due to limitations in the availability of water inflow data for the network, these analyses were conducted based on a 20-year dataset (2001–2021). The difference in time periods reflects data availability constraints but does not compromise the primary focus on climatic drought impacts, as SDI serves as a supplementary index.

**Table 2- Classification of Climatic and Hydrological Conditions Based on SPI, RDI, and SDI Indices**

| Classification | SPI, RDI, SDI Value |
|---|---|
| Extremely wet | ≥ 2.0 |
| Very wet | 1.5 to 1.99 |
| Moderate wet | 1.0 to 1.49 |
| Near normal | -0.99 to 0.99 |
| Mild drought | -1.0 to -1.49 |
| Moderate drought | -1.5 to -1.99 |
| Severe drought | ≤ -2.0 |

Note: Classification criteria are based on global standards (McKee et al., 1993 for SPI; Tsakiris et al., 2007 for RDI; Nalbantis and Tsakiris, 2008 for SDI) and applied to SPI, RDI, and SDI indices calculated using DrinC software (version 1.7) for the October–September period. SPI is based on precipitation, RDI on the precipitation-to-potential evapotranspiration ratio (P/PET), and SDI on river flow. Data normalization for SPI and RDI was performed using DrinC's standard process, fitting precipitation (for SPI) and P/PET ratios (for RDI) to a gamma distribution and transforming them to a normal distribution(Abramovitz and Stegun, 1965; Thom, 1958).
SDI normality was confirmed through visual inspection (histograms and Q-Q plots), supported by the Central Limit Theorem due to the large sample size (20 years). SDI data are available for 2001–2021.

## Methodology

Statistical analysis was performed using a two-way ANOVA to evaluate the individual and interactive effects of drought indices on water resources. The independent variables were the drought indices (RDI, SPI, and SDI), while the dependent variables were the blue and green water footprints (WFblue and WFgreen). The interactive effects between SPI and RDI, as well as other combinations of indices (e.g., SPI-SDI, RDI-SDI), were examined to understand their combined impact on the water footprints. All climatic data (e.g., precipitation, temperature, wind speed, sunshine hours, and potential evapotranspiration) used as inputs to compute SPI and RDI were normalized by the DrinC software (version 1.7) as part of its standard computation process. This process ensures robust statistical analysis by fitting precipitation (for SPI) and P/PET ratios (for RDI) to a gamma distribution and transforming them to a normal distribution, meeting the normality assumptions required for ANOVA. For SDI, which relies on streamflow data, normality was assessed through visual inspection using histograms and Q-Q plots, and the large sample size (20 years) supported the assumption of approximate normality based on the Central Limit Theorem. The analysis also assumed homogeneity of variances (confirmed using Levene's test) and independence of observations (ensured by the study design and data collection across different years). Post-hoc tests, such as Tukey's test, were not conducted, as the study focused on the overall significance of main and interactive effects; however, such tests could be considered in future studies for pairwise comparisons of drought severity levels.

### Results and Discussion

The use of a 20-year period (2001–2021) for SDI, compared to the 30-year period (1993–2023) for RDI and SPI, may have limited the ability to capture long-term hydrological drought trends in the earlier (1993–2000) and later (2022–2023) years. In this research, SPI and RDI were employed to assess climatic drought and its impact on the water footprint, while SDI was used to evaluate hydrological drought and the water inflow to the irrigation network, complementing the climatic analyses. Since SDI was used as a complementary index, its shorter time frame is unlikely to have significantly impacted the overall findings, which primarily focus on water footprint dynamics influenced by climatic variations.

### Comparison of SPI and RDI

Comparison of the SPI and RDI indices in (3) revealed that both indices generally provide similar interpretations of drought and wet conditions in most years. For instance, in 2019, which experienced widespread flooding in Khuzestan, both indices indicated wet conditions (SPI = 1.80, Very Wet; RDI = 1.50, Very Wet), consistent with a decrease in the blue water footprint (WFblue = 50.0 $m^3ton^{-1}$) and an increase in the green water footprint (WFgreen = 376.5 $m^3ton^{-1}$). However, in drought years such as 1995 (SPI

= -1.83, Moderate Drought; RDI = -1.75, Severe Drought) and 2021 (SPI = -2.58, Severe Drought; RDI = -2.57, Extremely Drought), the RDI index indicated a greater severity of drought.

**Water Footprint and Drought Analysis**

The blue and green water footprints (calculated using Cropwat 8.0) and drought/wet conditions (assessed using DrinC 1.7) are summarized in Table (3) and illustrated in Figure (2).

Figure (2) illustrates a consistent increase in WFblue, indicating greater reliance on blue water resources (groundwater and surface water). Reduced effective precipitation is a primary driver of this trend, increasing pressure on blue water to compensate for deficits. This raises concerns about overexploitation of groundwater and sustainable management. Conversely, WFgreen shows a declining trend, reflecting limited access to effective rainfall during wheat planting, possibly due to reduced soil infiltration, uneven rainfall distribution, or suboptimal farm management practices (e.g., non-optimal crop rotation delaying planting).

**Table 3 - Exit code of DrinC and Cropwat**

| Year | SPI | RDI | SPI interpretation | RDI interpretation | Wfblue ($m^3\ ton^{-1}$) | Wfgreen ($m^3\ ton^{-1}$) |
|---|---|---|---|---|---|---|
| 1993 | 1.12 | 1.21 | Moderately Wet | Moderately Wet | 133.2 | 220.1 |
| 1994 | 0.92 | 0.97 | Near Normal | Near Normal | 123.5 | 220 |
| 1995 | -1.83 | -1.75 | Moderate Drought | Moderate Drought | 222.3 | 139 |
| 1996 | 0.73 | 0.71 | Near Normal | Near Normal | 58.4 | 351.7 |
| 1997 | 1.37 | 1.4 | Moderately Wet | Moderately Wet | 43.6 | 324 |
| 1998 | 0.37 | 0.3 | Near Normal | Near Normal | 57.3 | 306.3 |
| 1999 | 0.63 | 0.56 | Near Normal | Near Normal | 112.6 | 279.6 |
| 2000 | 0.18 | 0.16 | Near Normal | Near Normal | 111.7 | 360.2 |
| 2001 | 0.37 | 0.3 | Near Normal | Near Normal | 174 | 236.5 |
| 2002 | -0.04 | -0.03 | Near Normal | Near Normal | 119.5 | 254.5 |
| 2003 | -0.64 | -0.61 | Near Normal | Near Normal | 212.2 | 204.6 |
| 2004 | 0.55 | 0.56 | Near Normal | Near Normal | 112.4 | 280.1 |
| 2005 | -0.05 | -0.06 | Near Normal | Near Normal | 86.6 | 260.9 |
| 2006 | 1.12 | 1.09 | Moderately Wet | Moderately Wet | 80.8 | 281.8 |
| 2007 | -0.04 | -0.04 | Near Normal | Near Normal | 79 | 284.2 |
| 2008 | -1.38 | -1.37 | Mild Drought | Moderate Drought | 314.2 | 88.7 |
| 2009 | -0.6 | -0.53 | Near Normal | Near Normal | 267.5 | 124 |
| 2010 | -0.7 | -0.73 | Near Normal | Near Normal | 265.2 | 151.8 |
| 2011 | 0.06 | 0.07 | Near Normal | Near Normal | 200.6 | 227.7 |
| 2012 | -0.09 | -0.09 | Near Normal | Near Normal | 211.3 | 192.4 |
| 2013 | -0.56 | -0.52 | Near Normal | Near Normal | 318.9 | 132.6 |
| 2014 | 0.21 | 0.26 | Near Normal | Near Normal | 152 | 249.9 |
| 2015 | -0.17 | -0.14 | Near Normal | Near Normal | 243.6 | 202.1 |
| 2016 | -1.28 | -1.25 | Mild Drought | Mild Drought | 202.8 | 178.9 |
| 2017 | -1.33 | -1.4 | Mild Drought | Mild Drought | 402.3 | 108.3 |
| 2018 | 1.41 | 1.32 | Moderately Wet | Moderate Drought | 188 | 281.1 |
| 2019 | 1.8 | 1.50 | Very Wet | Very Wet | 0.4 | 376.5 |
| 2020 | 0.81 | 0.76 | Near Normal | Near Normal | 197.5 | 252.7 |
| 2021 | -2.58 | -2.57 | Severe Drought | Severe Drought | 331.9 | 101.1 |
| 2022 | -1.38 | -1.43 | Mild Drought | Mild Drought | 375.2 | 174.5 |
| 2023 | -135 | -1.4 | Mild Drought | Mild Drought | 464.9 | 79.4 |

Note: Interpretation based on standard thresholds; WF values in $m^3$/ton. RDI calculations adapted from (Tsakiris et al., 2008)

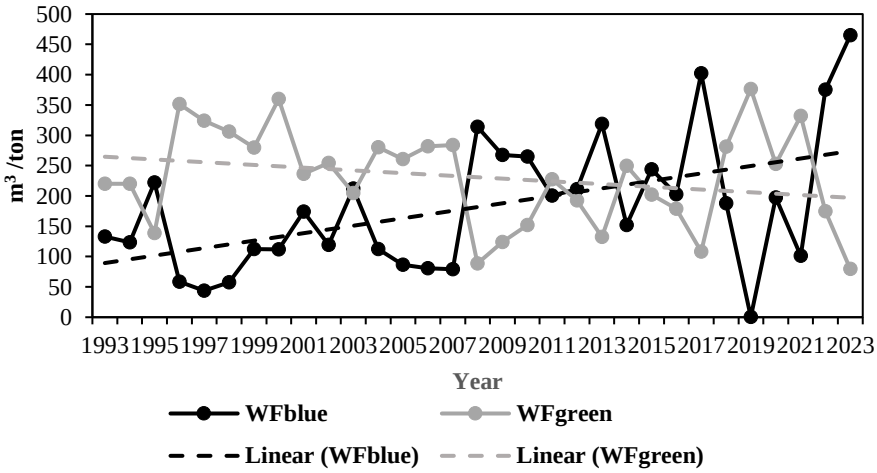



**Fig. 2- 30-year changes in the blue and green water footprint of wheat in the cultivated lands of the Dez irrigation network**

**Table 4- Correlation analysis and relationship between drought indicators and blue and green footprints**

| Indicators | SPI | RDI | WFblue | WFgreen |
|---|---|---|---|---|
| SPI | 1 | 0.998505 | -0.58726 | 0.380326 |
| RDI | 0.998505 | 1 | -0.58075 | 0.362443 |
| WFblue | -0.58726 | -0.58075 | 1 | -0.88924 |
| WFgreen | 0.380326 | 0.362443 | -0.88924 | 1 |

The results indicated a significant interactive effect between SPI and RDI on the blue water footprint (WFblue) of wheat, particularly during drought periods Table (4). The underlying mechanism of this relationship stems from the reduction in effective rainfall (Eff. rain) during drought conditions, as reflected by negative SPI and RDI values. When Eff. rain decreases below the crop evapotranspiration requirement (ETc), the shortfall in water availability must be compensated through irrigation, thereby increasing ETblue. As per the water footprint calculation framework (Equations 3 and 4), ETblue is calculated as ETblue = ETc − Eff. rain when Eff. rain < ETc. For instance, in a drought year like 2008 (SPI = -1.2), the effective rainfall (Eff. rain) was 169.2 mm, significantly below the average crop evapotranspiration (ETc) during the growing season of approximately 600 mm Table (1), resulting in a higher ETblue to meet the water needs of wheat. This increased ETblue directly contributes to a higher WFblue, indicating a greater reliance on blue water resources (e.g., river water from the Dez River or groundwater) to sustain crop production under water-scarce conditions. Conversely, in wetter years like 2018 (SPI = 1.4), Eff. rain increased to 211.9 mm, reducing the irrigation demand and consequently lowering ETblue. This mechanism underscores the vulnerability of wheat production in the Dez Irrigation Network to climatic variations, emphasizing the need for adaptive water management strategies—such as optimizing irrigation scheduling or enhancing water storage—to mitigate the increased stress on blue water resources during drought periods. The details presented in Table (4) are clearly reflected in Figures (2) and (3). Figure (3) illustrates the trends in the drought indices RDI and SDI, annual rainfall (Rain), and network water input (NIW) over a 20-year period. The alignment between the table values and figures enables a comprehensive examination of the impacts of rainfall and drought on water resources. Figure (4) compares rainfall (mm) and net irrigation water (NIW, $m^3 year^{-1}$) requirements under three climatic conditions (dry, normal, and wet), highlighting increased irrigation demand as rainfall decreases.

**Table 5 - Regional and accounting parameters of the country during the 30th period**

| Year | Tmin ℃ | Tmax ℃ | RH % | Wind Km/day | Sun hours | Rain mm | Eff.rain mm | Etblue mm/day | Etgreen mm/day | Y Kg/ha |
|---|---|---|---|---|---|---|---|---|---|---|
| 1993 | 15.5 | 31.3 | 50.6 | 131.4 | 2 | 230.8 | 220.1 | 133.2 | 220.1 | 2781.07 |
| 1994 | 15.8 | 31.6 | 50 | 165.9 | 2.6 | 265.8 | 220.1 | 123.5 | 220 | 2922.84 |
| 1995 | 15.1 | 31.9 | 51.6 | 152.9 | 2.4 | 254 | 139.2 | 222.3 | 139 | 4558.79 |
| 1996 | 16.4 | 32.6 | 48.8 | 169 | 2.6 | 379.8 | 289.7 | 58.4 | 289.7 | 4282.57 |
| 1997 | 15.6 | 31.5 | 48.2 | 159.6 | 2.5 | 257.4 | 333 | 43.6 | 324 | 5314.69 |
| 1998 | 16.6 | 33.3 | 47.2 | 153.4 | 2.4 | 252.9 | 306.4 | 57.3 | 306.3 | 3538.01 |
| 1999 | 16.7 | 33.1 | 46 | 168.1 | 2.6 | 266.5 | 279.8 | 112.6 | 279.6 | 4670.31 |
| 2000 | 16 | 32.3 | 47.2 | 183.2 | 2.8 | 281.6 | 208 | 111.7 | 360.2 | 4252.72 |
| 2001 | 16.4 | 33.1 | 48.2 | 176.8 | 2.7 | 277.3 | 236.7 | 174 | 236.5 | 4294.45 |
| 2002 | 13.3 | 28 | 57.1 | 210.2 | 3.3 | 311.9 | 254.5 | 119.5 | 254.5 | 3598.68 |
| 2003 | 16.5 | 32.5 | 47.7 | 179.6 | 2.8 | 279.1 | 204.6 | 212.2 | 204.6 | 4151.45 |
| 2004 | 16.2 | 32.2 | 53.3 | 177.7 | 2.8 | 282.2 | 280 | 112.4 | 280.1 | 4346.1 |
| 2005 | 16.2 | 32.6 | 51.3 | 198.5 | 3.1 | 301.7 | 260.9 | 86.6 | 260.9 | 4379.5 |
| 2006 | 16.7 | 32.3 | 53.2 | 241.2 | 3.7 | 347 | 281.8 | 80.8 | 281.8 | 4445.78 |
| 2007 | 16.3 | 32.5 | 53.8 | 242.8 | 3.8 | 349.1 | 284.4 | 79 | 284.2 | 4031.95 |
| 2008 | 16.8 | 33 | 52.2 | 244.1 | 3.8 | 349.8 | 88.7 | 314.2 | 88.7 | 3050.32 |
| 2009 | 16.9 | 32.4 | 56.8 | 256.5 | 4 | 366.6 | 124 | 267.5 | 124 | 3365.71 |
| 2010 | 17.8 | 34 | 48.2 | 254.4 | 3.9 | 358.3 | 151.8 | 265.2 | 151.8 | 2986.01 |
| 2011 | 16.4 | 32.3 | 47.5 | 245.3 | 3.8 | 345.3 | 222.7 | 200.6 | 227.7 | 3021.55 |
| 2012 | 17 | 32.7 | 46.5 | 223 | 3.5 | 322.6 | 192.3 | 211.3 | 192.4 | 2892.62 |
| 2013 | 16.1 | 32.3 | 50.4 | 220.3 | 3.4 | 322.4 | 132.6 | 318.9 | 132.6 | 3961.41 |
| 2014 | 16.9 | 32.3 | 51.4 | 238.9 | 3.7 | 343.3 | 249.9 | 152 | 249.9 | 4857.76 |
| 2015 | 17.7 | 32.9 | 72.2 | 228.4 | 3.5 | 354.6 | 202.1 | 243.6 | 202.1 | 4807 |
| 2016 | 16.7 | 32.8 | 72.1 | 237.9 | 3.7 | 363.2 | 179 | 202.8 | 178.9 | 5693.6 |
| 2017 | 16.9 | 34 | 68.3 | 315.2 | 4.9 | 439.2 | 108.3 | 402.3 | 108.3 | 5190.9 |
| 2018 | 17.5 | 33.4 | 74.1 | 363.4 | 5.6 | 494.1 | 281.1 | 188 | 281.1 | 4841.1 |
| 2019 | 16.7 | 32.6 | 74.7 | 236.2 | 3.7 | 363.9 | 376.5 | 0.4 | 376.5 | 4480 |
| 2020 | 16.7 | 32.8 | 74.1 | 200.2 | 3.1 | 326.8 | 252.7 | 197.5 | 252.7 | 3761 |
| 2021 | 17.2 | 34.6 | 68.4 | 207.6 | 3.2 | 331 | 79.4 | 101.1 | 331.9 | 3816 |
| 2022 | 17.3 | 33.9 | 49.1 | 272.8 | 4.2 | 377.3 | 174.5 | 375.2 | 174.5 | - |
| 2023 | 17.6 | 33.7 | 52.4 | 335.3 | 5.2 | 444.2 | 79.4 | 464.9 | 79.4 | - |

**Table 6-Descriptive status of drought indices (RDI and SDI), annual rainfall, and water input to the irrigation network during the wheat growing season over a 20-year period**

| Year | NIW (m3 year$^{-1}$) | Rain (mm) | RDI | SDI | RDI Interpretation | SDI Interpretation |
|---|---|---|---|---|---|---|
| 2001-2002 | 12723.1 | 292.7 | -0.03 | -0.19 | Near Normal | Near Normal |
| 2002-2003 | 17561.7 | 235.9 | -0.61 | 0.42 | Near Normal | Near Normal |
| 2003-2004 | 13453.5 | 357.8 | 0.56 | 0.17 | Near Normal | Near Normal |
| 2004-2005 | 13330.4 | 292.0 | -0.06 | 0.17 | Near Normal | Near Normal |
| 2005-2006 | 16663.0 | 428.3 | 1.09 | 1.08 | Moderately Wet | Moderately Wet |
| 2006-2007 | 16838.2 | 292.7 | -0.04 | 0.68 | Near Normal | Near Normal |
| 2007-2008 | 15591.8 | 176.0 | -1.37 | -1.56 | Moderate Drought | Moderate Drought |
| 2008-2009 | 7030.2 | 239.2 | -0.53 | -2.39 | Near Normal | Severe Drought |
| 2009-2010 | 17525.0 | 230.2 | -0.73 | 0.45 | Near Normal | Near Normal |
| 2010-2011 | 16217.8 | 303.6 | 0.07 | 0.55 | Near Normal | Near Normal |
| 2011-2012 | 18753.7 | 287.6 | -0.09 | 0.24 | Near Normal | Near Normal |
| 2012-2013 | 18195.3 | 242.7 | -0.52 | 1.14 | Near Normal | Moderately Wet |
| 2013-2014 | 20672.5 | 319.0 | 0.26 | 1.32 | Near Normal | Moderately Wet |
| 2014-2015 | 17960.9 | 279.5 | -0.14 | 0.80 | Near Normal | Near Normal |
| 2015-2016 | 15084.4 | 183.2 | -1.25 | 0.22 | Mild Drought | Near Normal |
| 2016-2017 | 18266.8 | 179.8 | -1.40 | 0.68 | Mild Drought | Near Normal |
| 2017-2018 | 10850.5 | 468.1 | 1.32 | -1.52 | Moderately Wet | Moderate Drought |
| 2018-2019 | 9311.8 | 434.9 | 1.50 | -0.36 | Very Wet | Near Normal |
| 2019-2020 | 15234.1 | 389.4 | 0.76 | 0.61 | Near Normal | Near Normal |
| 2020-2021 | 16673.3 | 103.4 | -2.57 | -0.80 | Severe Drought | Near Normal |

Note: RDI values are calculated for the hydrological year (October–September) using DrinC, reflecting annual climatic conditions, except for 2018–2019, where RDI is based on localized data reflecting the severe flooding in Khuzestan, classified as Very Wet. SDI, annual rainfall, and network water input (NIW) are calculated for the wheat growing season (October–May) for 2001–2021. RDI values were previously misaligned by one year in earlier versions and have been corrected using validated DrinC outputs. These values may differ from water footprint calculations Table (7), which تare based on calendar year data (January–December) from Cropwat.

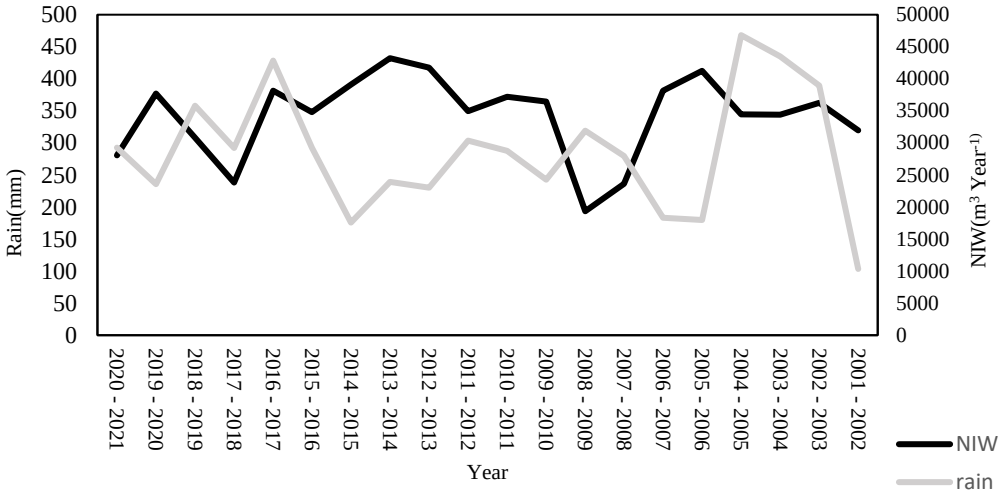



**Fig. 3 - Trends in changes in water entering the Dez irrigation network and rainfall over a 20-year statistical period**

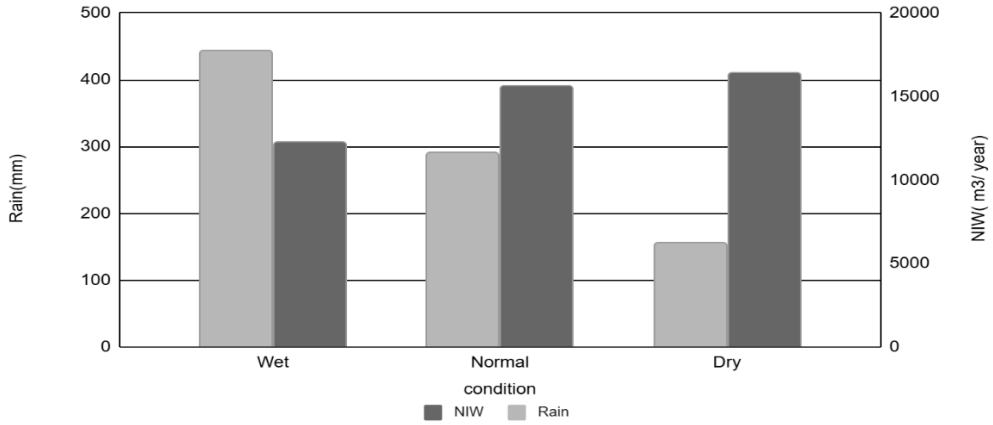



**Fig. 4- compares rainfall and net irrigation water (NIW) requirements under three climatic conditions (dry, normal, and wet)**

**Impact of Climatic Variations on Water Footprints**

The RDI reflects precipitation deficits. In years with negative RDI (e.g., 2008–2009, RDI = -0.42), insufficient rainfall led to reduced NIW (7030.2 m³). The SDI indicates hydrological drought severity (e.g., 2008–2009, SDI = -2.39), exerting significant pressure on water resources. In wet years (e.g., 2005–2006, rainfall = 428.3 mm, RDI = -0.02), NIW increased to 16,663 m³, reflecting favorable conditions.

To evaluate the individual and interactive effects of the drought indices SDI and RDI on water resources, a statistical analysis of variance (ANOVA) was conducted. This analysis enabled the assessment of each index's impact independently as well as their interactions under varying climatic conditions. The results of these analyses are presented in Table (7) and visualized in Figures (5) and (6) to clarify the relationships between the indices and water resources with greater precision.

Figures (5,6) provide a comparative analysis of the blue and green water footprints of wheat under varying climatic conditions. Figure 5 compares the average WFblue (99.12 $m^3ton^{-1}$in wet conditions vs. 202.78 $m^3ton^{-1}$ in dry conditions) and WFgreen (296.7 m3ton-1 in wet conditions vs. 223.49 $m^3ton^{-1}$in dry conditions), highlighting the increased reliance on blue water resources during dry periods. Figure (6) illustrates the trends in WFblue and WFgreen across a spectrum of conditions from Very Wet to Severe Drought, showing a clear upward trend in WFblue and a

corresponding decline in WFgreen as drought intensity increases. These visualizations underscore the vulnerability of wheat production in the Dez Irrigation Network to climatic variations, emphasizing the need for adaptive water management strategies.

**ANOVA Results for the Blue Water Footprint**

The ANOVA results presented in Table (7) indicate that the Standardized Precipitation Index (SPI) has a highly significant effect on the blue water footprint (WFblue) (P-value ≈ 0.000206), suggesting that variations in standardized precipitation play a critical role in the utilization of blue water resources within the Dez Irrigation Network. In contrast, the individual effect of the Reconnaissance Drought Index (RDI) was not statistically significant (P-value = 0.3). This does not necessarily indicate a lack of effect but rather suggests uncertainty in the result, potentially due to factors such as the sample size or high variance in the data. For instance, the 30-year dataset (1993–2023) for RDI may include variability influenced by local climatic fluctuations (e.g., severe flooding in 2019), which could affect the statistical power of the analysis. The interaction between SPI and RDI, however, approached statistical significance under certain climatic conditions, indicating a potential combined influence that warrants further investigation with a larger or more controlled dataset.

**ANOVA Results for the Green Water Footprint**

The results obtained from the statistical analyses Table (8) indicate that the Standardized Precipitation Index (SPI) has a significant effect on the green water footprint (WFgreen), whereas the Reconnaissance Drought Index (RDI) exhibits a lesser impact. These findings highlight the critical role of effective rainfall and its temporal distribution in meeting crop water requirements. As drought intensity increases, reliance on blue water resources intensifies, exerting considerable stress on water resources. Figure (5) illustrates the green and blue water footprints of wheat during drought and wet periods over the 30-year study period, showing a clear pattern of increased WFblue and decreased WFgreen during drought conditions.

.

**Table 7 -ANOVA analysis of variance of simple and interaction effects of drought indices SDI and RDI on blue water footprint**

| Term | Df | Sum Sq | Mean Sq | F Value | Pr (>F) |
|---|---|---|---|---|---|
| SPI | 1 | 136780 | 136780 | 18.384 | 0.000206* |
| RDI | 1 | 8234 | 8234 | 1.107 | 0.302125 |
| SPI: RDI | 1 | 23422 | 23422 | 3.148 | 0.087294 |
| Residuals | 27 | 200880 | 7440 | - | - |

** signification in 0.01, * signification in 0.05

**Table 8 - ANOVA analysis of variance of simple and interaction effects of drought indices SDI and RDI on green water footprint**

| Term | Df | Sum Sq | Mean Sq | F Value | Pr (>F) |
|---|---|---|---|---|---|
| SPI | 1 | 65998 | 65998 | 16.814 | 0.000339* |
| RDI | 1 | 3622 | 3622 | 0.923 | 0.345296 |
| SPI:RDI | 1 | 19666 | 19666 | 5.010 | 0.033639* |
| Residuals | 27 | 105978 | 3925 | | |

** signification in 0.01, * signification in 0.05

**Table 9- Average green and blue water footprints under different drought and wet conditions based on RDI and SPI drought indices**

| Year's Drought Condition | Frequency | Ave.WFgreen | Ave.WFblue | WFgreen/WFblue |
|---|---|---|---|---|
| Very Wet | 1 | 376.5 | 50.0 | 7.53 |
| Moderately Wet | 4 | 276.63 | 111.4 | 2.48 |
| Near Normal | 19 | 241.7 | 152.8 | 1.22 |
| Mild Drought | 5 | 125.96 | 351.88 | 0.36 |
| Moderate Drought | 1 | 139 | 222.3 | 0.63 |
| Severe Drought | 1 | 101.1 | 331.9 | 0.30 |

Note: Values are based on calendar year data (January–December) from Cropwat, aligned with drought conditions derived from RDI and SPI in Table 3. For 2018–2019, RDI and SPI are based on localized data reflecting the severe flooding in Khuzestan. Frequencies reflect the number of years within each drought condition category over the study period (1993–2023).

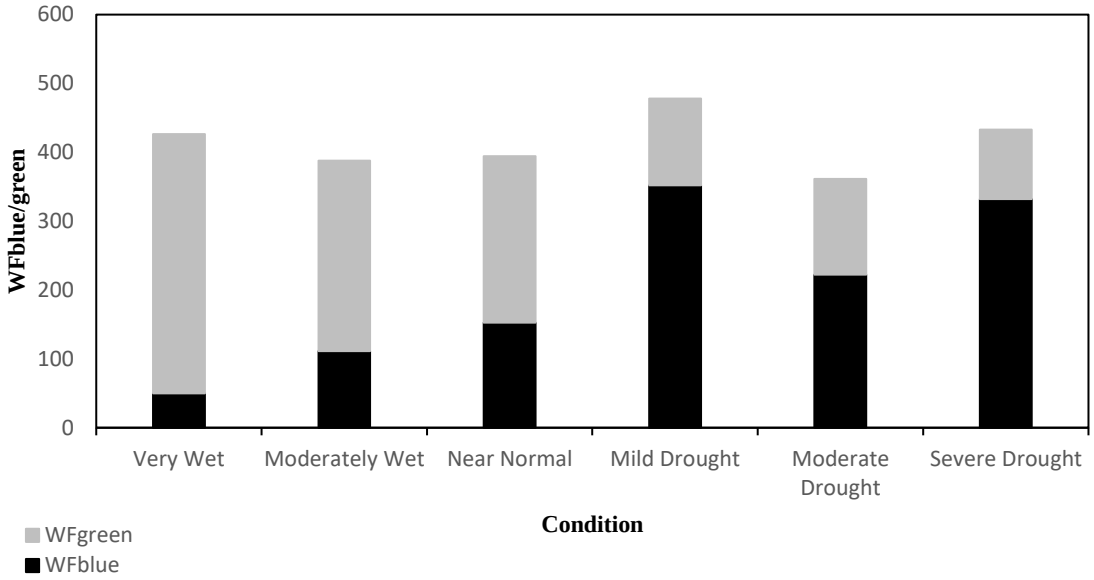



**Fig. 5 - Green and blue water footprint of wheat during drought and wet periods over a 30-year statistical period**

**Blue Water Footprint of Wheat in Severe Drought**

The analyses reveal that severe drought significantly increases the blue water footprint (WFblue) while reducing the green water footprint (WFgreen). In severe drought conditions, WFblue reached 375.20 $m^3ton^{-1}$, an increase of approximately 121.07% compared to normal conditions (169.59 $m^3ton^{-1}$), exerting substantial stress on blue water resources. This increase reflects a heightened dependence on water resources, underscoring the critical need for precise water management during severe drought. Indeed, this represents the most sensitive condition for water resource management.

The findings derived from the analysis of Table (9) highlight significant challenges and opportunities in water resource management under varying climatic conditions. In low-precipitation and drought years, dependence on blue water resources increases substantially, indicating greater stress on stored water reserves and elevated water inputs to the Dez irrigation network to compensate for deficits. The reduction in the green water footprint (WFgreen) during these conditions is associated with decreased precipitation, reduced soil water infiltration, and limited access to natural water resources, potentially causing severe impacts on agriculture without artificial irrigation. Concurrently, the increase in the blue water

footprint (WFblue) during severe drought reflects heightened extraction from groundwater or surface water sources and greater reliance on artificial irrigation systems. This underscores the critical need for precise planning and the development of efficient management strategies to ensure the sustainable use of water resources in the face of drought.

**Blue Water Footprint of Wheat in Moderately Wet Conditions**

In moderately wet conditions, WFgreen peaked at 276.63 $m^3ton^{-1}$, indicating effective utilization of green water resources. These conditions impose the least stress on irrigation systems and represent the optimal scenario for meeting crop water requirements.

**Blue Water Footprint of Wheat in Near Normal, Mild and Modearte Drought Conditions**

Over the 30-year study period (1993–2023), the prevalence of 'moderately wet' (4 years), 'near normal' (19 years), and 'mild drought' (5 years) conditions indicates a relative balance between wet and mildly dry years. However, a notable shift occurs in 'mild drought' conditions, where WFblue sharply rises to 351.88 $m^3ton^{-1}$—more than double the 163.36 $m^3ton^{-1}$ observed in 'near normal' years—while WFgreen drops to 125.96 $m^3ton^{-1}$. This significant increase in blue water footprint underscores the heightened dependence on irrigation during these periods, highlighting the urgent need for enhanced resource management strategies to sustainably address water stress. Figure (4) illustrates that as drought intensity increases, the average WFblue exhibits an upward trend, while WFgreen declines. These changes reflect reduced effective rainfall and increased stress on storage and irrigation systems, as well as higher water inputs to the Dez irrigation network during drought conditions. These findings emphasize the importance of developing management strategies tailored to climatic variations.

## Conclusion

The findings of this study demonstrate that climatic variations significantly influence wheat production in the Dez Irrigation Network, challenging the ability of irrigation systems to fully address water deficits during drought. In response to the research question—whether the network's water supply and release can compensate for effective rainfall shortages and maintain crop yields—the results indicate that this is not feasible. Drought affects water resources through two primary mechanisms: heightened reliance on irrigation due to diminished rainfall and reduced availability of soil moisture from natural precipitation. These dynamics reveal the limitations of even advanced irrigation networks in sustaining normal cultivation levels under drought conditions, as the increased demand for irrigation water places substantial pressure on available resources. The study underscores the critical need for adaptive water management strategies that prioritize efficient use of rainfall and innovative resource allocation to mitigate drought impacts and ensure agricultural sustainability in arid and semi-arid regions. For future research, the following investigations are recommended: first, evaluating the economic implications of the increased WFblue during severe drought to determine whether the additional water use and associated pumping costs are justified by the market value of wheat; second, replicating the current analysis for other irrigation networks located in different basins with more severe water resource constraints and higher temperature stress both within the province and in other regions of the country, to enhance understanding of challenges and potential solutions in diverse environmental conditions. Additionally, future studies should incorporate climate change projections to further refine water management strategies. These results underscore the critical need for precise water management, emphasizing rainfall quality, temporal distribution, and intelligent resource use to mitigate drought impacts and sustain agricultural productivity in arid and semi-arid regions like Southwestern Iran.

## Conflict of Interest

The authors declared no potential conflicts of interest concerning the research,

authorship, and publication of this article. Confirmation.

**Funding**

The financial support of this research has been provided by Grant number 309 and we hereby thank the Honorable Vice Chancellor of Research from Shahid Chamran University of Ahvaz for their support.

**Data Availability Statements**

The datasets generated and/or analyzed during the current study are available from the corresponding author on reasonable request.

**Authors' contribution**

**First Author:**Mahkameh Mansoori, Writing and executing articles-60%

**Second Author:** Esfandiar Fateh, Study of the article and revised-30%

**Third Author:** Amir Aynehband, Giving advice-5%

**Fourth Author:** Ali Shahbazi, Giving advice-5%

**Acknowledgments**

This research was made possible through the support and collaboration of Eng. Nasser Behmanshfar, Deputy of Technical and Engineering at the North District Operation Company, who generously shared his knowledge, expertise, and energy. We sincerely thank him and other esteemed specialists at the company for their valuable guidance and advice. Additionally, we express our gratitude to the Khuzestan Water and Power Authority and Shahid Chmaran University of Ahvaz for providing essential resources and substantial support.

**References**

1- Abramowitz, M. and Stegun, I.A., 1965. With formulas, graphs, and mathematical tables. *National Bureau of Standards Applied Mathematics Series. e*, *55*, p.953.

*2*- Allen, R. G., Pereira, L. S., Raes, D., & Smith, M. 1998. *Crop evapotranspiration: Guidelines for computing crop water requirements* (FAO Irrigation and Drainage Paper 56). Food and Agriculture Organization.

*3*- Borzoo, F., Ramezani Etedali, H., Kaviani, A., and Kalanaki, M.2024. Investigating green water footprint in spring wheat under climate change conditions and different crop dates. *Iranian Journal of irrigation and drainage*, 18(3),pp. 393-408.

4- Burton, M. 2010. Irrigation management principles and practices. *CABI Publishing*. https://doi.org/10.1079/9781845935160.0000

5- Fisher, D.K. and Pringle III, H.C., 2013. Evaluation of alternative methods for estimating reference evapotranspiration. *Agricultural Sciences*, *4*(8), pp.51-60. https://doi.org/10.4236/as.2013.48A008

6- Hargreaves, G. H., & Samani, Z. A. 1985. Reference crop evapotranspiration from temperature. *Applied Engineering in Agriculture*, 1 (2), 96–99. https://doi.org/10.13031/2013.26773.

7-Hayes, M. J., Alvord, C., & Lowrey, J. 2007. Drought indices. *Intermountain West Climate Summary*, 3 (6), 2–6.

8- Hoekstra, A. Y., Chapagain, A. K., Aldaya, M. M., & Mekonnen, M. M. (2011). *The water footprint assessment manual: Setting the global standard*. Routledge. https://doi.org/10.4324/9781849775526

9- McKee, T. B., Doesken, N. J., & Kleist, J. 1993. The relationship of drought frequency and duration to time scale. In *Proceedings of the Eighth Conference on Applied Climatology* (pp. 179–184). American Meteorological Society.

10- Nalbantis, I., & Tsakiris, G. 2009. Assessment of hydrological drought revisited. *Water Resources Management, 23(5), 881–897. https://doi.org/10.1007/s11269-008-9305-1.

11- Panahi, F., & Malik Muhammadi, A. 2008. Optimization of agricultural water in the region. In *Proceedings of the National Conference on Water Harvesting* (pp. 489–498). (In Persian).

12- Ramezani Etedali, H., Kalanaki, M., & van Oel, P. 2022. Evaluation of future climate component changes from north to southwest Iran. *Journal of Ecohydrology, 9*(2), 373–386. https://doi.org/10.22059/ije.2022.90424.

13- Salarian, M. 2014. Development of water resources and transformations in modern irrigation. **Water Harvesting Journal*, 2, 83–90. (In Persian).

14- Thom, H. C. S. 1958. A note on the gamma distribution. *Monthly Weather Review*, 86(4), 117–122. https://doi.org/10.1175/1520-0493(1958)086<0117:ANOTGD>2.0.CO;2.

15- Tsakiris, G., Loukas, A., Pangalou, D., Vangelis, H., Tigkas, D., Rossi, G., & Cancelliere, A. 2007. Drought characterization. In A. Iglesias et al. (Eds.), Drought Management Guidelines Technical Annex (pp. 85–102). CIHEAM / ECMEDA Water, Zaragoza.

16- Tsakiris, G., Nalbantis, I., Pangalou, D., Tigkas, D., & Vangelis, H. 2008. Drought meteorological monitoring network design for the reconnaissance drought index (RDI). In A. Franco Lopez (Ed.), Proceedings of the 1st International Conference "Drought Management: Scientific and Technological Innovations" (pp. 57–62). Zaragoza, Spain: Option Méditerranéennes, Series A, No. 80, 12-14 June 2008.

17- Vangelis, H., Tigkas, D., & Tsakiris, G. 2013. The effect of PET method on Reconnaissance Drought Index (RDI) calculation. *Journal of Arid Environments*, 88, 130–140. https://doi.org/10.1016/j.jaridenv.2012.09.002.

18- Veettil, A. V., & Mishra, A. K. 2016. Water security assessment using blue and green water footprint concepts. *Journal of Hydrology*, 542, 589–602. https://doi.org/10.1016/j.jhydrol.2016.09.034

© 2026 The Author(s). Published by Shahid Chamran University of Ahvaz. This is an open-access article distributed under the terms of the Creative Commons Attribution License (http://creativecommons.org/licenses/by/4.0), which permits unrestricted use, distribution, and reproduction in any medium, provided the original work is properly cited.

Shahid Chamran University of Ahvaz

**Irrigation Sciences and Engineering (JISE)**
**Vol. 48, No. 4, Winter 2026, p. 65-78**
Journal homepage: https://jise.scu.ac.ir

**Research Paper**

# Assesment the adaptability of *Jacaranda mimosifolia* L. to Ahvaz climete condition under salinity and water stresses

Khalil Asadivafa[1], Mousa Mousavi[2]*, Abdul-kadhm N. S. Al-Showily[3], Mohammad Albaji[4] and Naser Alemzadeh Ansari[5]

*1- Ph.D. Student, Department of Horticultural Science, Faculty of Agriculture, Shahid Chamran University of Ahvaz, Ahvaz, Iran.*
*2*- Corresponding Author, Associate Professor, Department of Horticultural Science, Faculty of Agriculture, Shahid Chamran University of Ahvaz, Ahvaz, Iran.(m.mousavi@scu.ac.ir ).*
*3- Assistant Professor, Department of Horticultural Science, College of Agriculture, University of Basrah, Iraq.*
*4- Professor, Department of Irrigation and Drainage, Faculty of Water and Environmental Science, Shahid Chamran University of Ahvaz, Ahvaz, Iran.*
*5- Associate Professor, Department of Horticultural Science, Faculty of Agriculture, Shahid Chamran University of Ahvaz, Ahvaz, Iran.*

**ARTICLE INFO**

*Artlcle history:*
Received: 25 December 2024
Revised: 11 August 2025
Accepted: 02 September 2025
Available online: 04 January 2026

*Keywords:*
Drought, Jacaranda, Salinity.

**TO CITE THIS ARTICLE:**
Asadivafa, K., Mousavi, M., N. S. Al-Showily, A., Albaji, M., Alemzadeh Ansari, N. 2026. 'Assesment the adaptability of Jacaranda mimosifolia L. to Ahvaz climete condition under salinity and water stresses', *Irrigation Sciences and Engineering*, 48(4), pp. 65-78. doi: 10.22055/jise.2025.48612.2151

**Abstract**

To enrich the plant diversity of the landscape, introducing new ornamental trees such as Jacaranda tree is a useful solution. Therefore, it is essential to investigate Jacaranda compatibility with the limiting factors of different regions. This research was aimed at elucidating the influence of combined salinity levels (1, 2.5, 4, and 5.5 ds.m$^{-1}$ NaCl) and low irrigation levels (100, 80, and 60% FC) on the some morpho-physiological characteristics, consist of fresh and dry weight of areal part, relative water content (RWC), malondialdehyde (MDA), electrolyte leakage (EL), sodium (Na) and potassium (K) content of Jacaranda plants under field condition as a factorial experiment based on randomized complete block design with 4 replicates in 2023. The results indicated that, the growth of Jacaranda decreased gradually under both salinity and drought stress depending on the severity of the stress. The fresh and dry weight of the aerial part showed the greatest reduction under 5.5 dS.m$^{-1}$ NaCl and 60% (FC) compared to 1 dS.m$^{-1}$ NaCl and 100% FC. Low irrigation as accompanied with salinity significantly affected on EL enhancement and the highest EL was attained in 5.5 ds.m$^{-1}$ and 60%FC. Similarly, the highest MDA and Na content have been obtained in the interaction effect of 5.5 ds.m$^{-1}$ NaCl×60% FC. Conversely, the plants exposed to drought and salinity, indicated lower RWC and K content by severity-dependent changes. Overall, to produce Jacaranda seedlings in tropical and sub tropical nurseries, one should carefully use non-saline water and soil.

## Introduction

Abiotic stresses exhibit progressive development under the global climatic changes in the current era (Nadeem et al., 2019). These stresses often correlate with a reduction in the soil water and cultivable capacity of the soil (Bhat et al., 2021). Water deficit is one of the most important limiting factors in agronomic production especially in arid and semi-arid regions. Iran with about 250 mm annual rainfall average, is classified as an arid and semi-arid area in the world and thereby exposes to drought unquestionably (Fathian et al., 2015).

Water stress affecting plant growing and has negative consequences on plant growth parameters and metabolic pathways including water relations, photosynthetic assimilation, antioxidant defense and mineral absorption resulting in reduction of crop quality and yield considerably (De Vries et al., 2020). In a study, reduced growth resulted of drought stress caused changes in several morphological traits such as reduced shoot length, shoot diameter, leaf area and fresh weight of fig tree leaves. The authors explained the vegetative growth retardation in fig trees is related to the reduced relative water content (RWC) (Darwish et al., 2015).

 *DOI:* 10.22055/jise.2025.48612.2151

Drought negatively affected on plant water potential, cell division and photosynthesis, therefore both plant growth and yield are impacted by drought stress (Brito et al., 2019). The reason of the restriction in growth rate due to water deficit is ascribed to the adverse effect of this stress on the photosynthetic activity (Proietti et al., 2013). Reduced relative water content as an important indicator of water status in plants is directly associated with soil water content (Mohamed and Latif, 2017). Water deficit has a direct relationship with the amount of malondialdehyde (MDA) (Petridis et al., 2012). MDA is a main compound in making damage on membranes and cell death in stressed plants subjected to drought (Wu et al., 2015).

Soil salinization resulting from the accumulation of water-soluble salts in the soil (Munns and Tester, 2008). Worldwide, salt stress affects approximately 20% of the land and this rate has been steadily enhancing for a few decades (Khan et al., 2022). Upon exposure to salinity, the structure of cell wall changes. Leaf turgor pressure and photosynthesis exhibit the significant reduction and overall, leaf water and leaf area index decrease (Rodriguez Dominguez et al., 2016). The decrease of growth parameters like the reduced shoot length and diameter, the number of new shoots and dry weight of shoot and root was reported due to enhanced salinity level (Zhu et al., 2015). Salimpour et al. (2019) implied salt stress caused to decrease of leaf RWC as well as potassium (K) in 20-years fig stocks. Likewise, the increased electrolyte leakage (EL) as a result of salinity stress was confirmed by Akhter et al. (2021). In salinity stress and activation of reactive oxygen species (ROS), lipid peroxidation enhanced in membranes, the lipid peroxidation rate could be exhibited by MDA content. MDA rate is evident of cell stability in exposition to oxidative damage (Chen et al., 2018).

as a member of the dicot Bigniniaceae family, is considered as an endemic plant of South America. Then it distributed to the other tropical areas around the world (Sanchez, 2011). This deciduous tree often reach 20 m in height and can produce abundant, imazing, and long-lasting violet flowers (Pasiecznik, 2014).

To enrich the local plant species diversity, the introduction of new trees for urban landscape is inevitable necessity (Coban et al., 2021). To successfully cultivate a tree outside its natural environment, the assessment of its acclimation and good match with new condition is reasonably imperative (Lenzner et al., 2021). In order for a new plant to adapt to a new environment, it must be able to resist the limiting factors of this environment. Since the main limiting factors in the arid and semi-arid regions are the saline soil and water deficit, therefor, evaluation the resist of the new plant to these factrors is necessity for determining the adaptability rate to this regions. Therefore, it is essential to investigate Jacaranda compatibility with the limiting factors of different regions such as Ahvaz condition, which has a hot and dry climate with salty soil.

## Materials and Methods

### Experimental Site, Plant Materials, and Treatments

This experiment was conducted at the experimental field of the Horticultural Sciences Department in Shahid Chamran University of Ahvaz (31º19′ N, 48º40′ E, elevation above sea level: 20 m) in Iran (Figure 1). Murashige and Skoog medium (MS) free of hormones and sterile conditions were used for *in vitro* sowing of the seeds which had low germination capacity (Figure 2 A and B). After germination, the seedlings were maintained in controlled conditions including 25 °C and 16 h photoperiod for 6 months (Figure 2 D and E) and then transplanted to pots containing a mixture of agricultural soil, sand, and animal manure. After the seedlings were established in the field, low irrigation and salinity treatments were applied (Figure 2 F and G).

The treatments consisted of 90 days of low irrigation regimes including 100%, 80% and 60% FC, and salinity levels including 1 dS/m, 2.5 dS/m, 4 dS/m, and 5.5 dS/m NaCl. Also, the depth of irrigation water was 41 mm for all treatments. The maximum root depth was 27 cm and the pot area was 25 cm (Tables 1). Cosidering that the maximum tolerance to water salinity in this plant was 4 ds/m, and the salinity of the Karun River irrigation water between 2.5 to 4 dS/m, these salinity levels were selected.

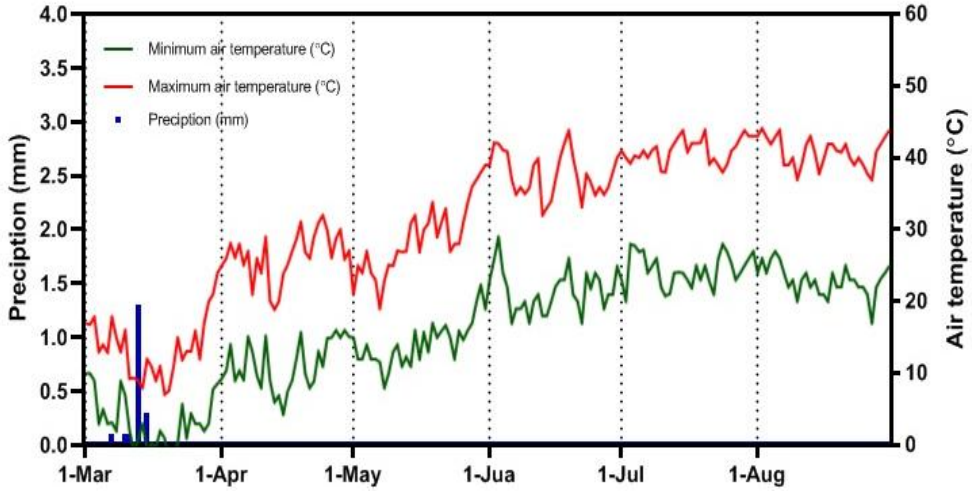



**Fig. 1- Air temperature and precipitation during applying the treatments.**




**Fig. 2- Steps of the experiment: Desinfected jacaranda seeds (A), In vitro seed germination (B), Ex-vitro seedling (C), Seedlings transered to the soil (D), Seedlings ready to transfer to field (E), Seedlings under different Treatments (F) and the seedling after the end of the experiment (G).**

**Table 1- Soil property table**

| *K (Exe) (mg.Kg$^{-1}$)* | *P (mg)* | *N (%)* | *Na (mg.L$^{-1}$)* | *K (mg.Kg$^{-1}$)* | *Ca (mg.L$^{-1}$)* | *CCE (%)* | *OC (%)* | *CEC (mol.Kg$^{-1}$)* | *EC (ds.m$^{-1}$)* | *pH* | *Texture* |
|---|---|---|---|---|---|---|---|---|---|---|---|
| 275 | 16 | 0.036 | 23 | 0.56 | 13.76 | %48 | 0.53 | 14.4 | 3.8 | 7.72 | Clay |

**Measured traits**

At the end of the experiment, various morphological characteristics of the plants including the fresh and dry weight of aerial part and root, shoot and root diameter, internode distance, length of auxiliary shoot and root length, and RWC, MDA, EL, and sodium (Na) and K content were measured.

Na and K content were meausered in the dry-ashed jacaranda leaves were digested through the method of Benton-Jones (1977) by flame photometer (Jenway PSP7, England) at 500ºC. The MDA content was meausred according to Stewart and Bewley, 1980.

EL was measured according to Lutts et al. (1996). Leaf discs of the middle part of completely developed leaves washed three times with distilled water to eliminate surface contaminants, and were located in distilled water. The samples were shaken (150 rpm) at room temperature for 24 h. The EL of the solution (EL1) was determined by EC-meter (Jenway 4330, USA). The same samples were then autoclaved at 121 °C for 20 min, and after cooling, again EL measured (EL2). EL was calculated using equesion (1) and expressed as percentage.

$$EL1 \times 100 / EL2 \quad (1)$$

To measure the leaf RWC, initially, leaves were weighed (FW). Afterwards, the leaf samples were rehydrated for 20 hours and then weighted to obtain leaf turgid weight (TW). Eventually, dried for 48 hours at 80ºC and then weighted to attain dry weight (DW). RWC was calculated using equation (2) (Gucci et al., 1997).

$$RWC\ (\%) = [(FW - DW)/(TW - DW)] \times 100 \quad (2)$$

The water use efficiency was calculated based on ratio of leaf dry weight (Kg) on the water consumption ($m^3$) (Amanullah and Stewart. 2013).

**Statistical analysis**

The experiment was carried out based on a complete randomized block in a factorial arrangement with 4 replications. The experimental data were analyzed using SAS software (v.9.4). Statistical significance at $\rho$=0.05 level was elucidated with Duncan's multiple range test. Before starting the statistical tests, the obtained data was checked for normality and homogeneity of variance, then the statistical test was performed.

## Results and Discussion

**Fresh and dry weights of aerial part and root**

The changes in morphological characteristics in Jacaranda affected by different salinity and drought levels are presented in Tables (2, 3 and 4). In 5.5 $dS.m^{-1}$ NaCl, aerial part fresh and dry weight revealed a 49% and 63% reduction respectively, versus 1 $dS.m^{-1}$ NaCl (Table 2). Additionally, exposure to salinity stress caused a significant decrease in root fresh and dry weight in a level-dependent manner with a 54% and 29% decline in 5.5 $dS.m^{-1}$ NaCl against 1 $dS.m^{-1}$ NaCl respectively.

Regardless of salinity stress, severe drought stress at 60% FC reduced the fresh and dry weight of the aerial parts as well as the fresh and dry weight of the roots by an average of 25%, 34%, 30% and 47% compared to 100% FC, respectively. In terms of significant interaction effects between drought and salinity, the combination of 1 $dS.m^{-1}$ NaCl and 100% FC resulted in the highest aerial part fresh and dry weight as well as root dry weight (Table 2). Sabah et al. (2022) found that reducing the salt concentration of the Murashige and Skoog (MS) medium to half or one-quarter of the standard level enhanced the shoot and root growth indices of Jacaranda plantlets respectively, *in vitro*.

**Table 2- Effects of salinity and drought on aerial part fresh and dry weight and root fresh and dry weight of *Jacaranda mimosifolia***

| Source of variance | Aerial part fresh weight (g) | Aerial part dry weight (g) | Root fresh weight (g) | Root dry weight (g) |
|---|---|---|---|---|
| Salinity | | | | |
| 1 ds.m$^{-1}$ NaCl | 68.59±8.37 a | 52.84±8.32 a | 42.24±8.70 a | 20.62±6.73 a |
| 2.5 ds.m$^{-1}$ NaCl | 58.98±6.99 b | 43.48±7.31 b | 32.75±6.95 b | 18.41±5.24 b |
| 4 ds.m$^{-1}$ NaCl | 48.49±10.36 c | 34.79±10.58 c | 29.03±6.87 c | 17.84±4.51 b |
| 5.5 ds.m$^{-1}$ NaCl | 34.81±5.13 d | 19.41±5.56 d | 19.37±2.86 d | 14.59±3.42 c |
| Drought | | | | |
| 100% FC | 59.86±14.10 a | 44.69±14.17 a | 36.14±11.01 a | 23.35±3.84 a |
| 80% FC | 53.45±13.48 b | 38.65±13.32 b | 31.28±9.52 b | 17.92±3.38 b |
| 60% FC | 44.84±12.95 c | 29.55±12.61 c | 25.11±7.93 c | 12.32±2.37 c |
| Salinity*Drought | | | | |
| 1 ds.m$^{-1}$ NaCl*100% FC | 77.19±2.53 a | 61.34±3.00 a | 50.11±3.72 a | 28.45±1.14 a |
| 1 ds.m$^{-1}$ NaCl*80% FC | 68.71±3.83 b | 52.55±3.25 b | 42.56±4.41 b | 19.98±2.42 cd |
| 1 ds.m$^{-1}$ NaCl*60% FC | 59.88±6.25 c | 44.62±6.93 c | 34.04±8.01de | 13.42±3.89 e |
| 2.5 ds.m$^{-1}$ NaCl*100% FC | 63.01±5.74 bc | 47.22±5.16 bc | 37.42±4.62 c | 23.38±1.70 b |
| 2.5 ds.m$^{-1}$ NaCl*80% FC | 60.75±4.24 c | 46.54±6.05 bc | 34.91±5.69 e | 19.62±3.60 d |
| 2.5 ds.m$^{-1}$ NaCl*60% FC | 53.17±6.52 d | 36.67±5.24 d | 25.91±4.26 fg | 12.22±1.49 e |
| 4 ds.m$^{-1}$ NaCl*100% FC | 59.43±3.41 c | 46.15±3.57 bc | 35.63±5.24 d | 22.89±1.47 bc |
| 4 ds.m$^{-1}$ NaCl*80% FC | 50.05±5.31 d | 35.97±5.41 d | 28.02±4.29 f | 18.23±1.35 d |
| 4 ds.m$^{-1}$ NaCl*60% FC | 35.98±1.94 ef | 22.24±2.36 e | 23.43±4.45 g | 12.41±1.38 e |
| 5.5 ds.m$^{-1}$ NaCl*100% FC | 39.81±5.61 e | 24.05±6.51 e | 21.39±2.80gh | 18.68±2.14 d |
| 5.5 ds.m$^{-1}$ NaCl*80% FC | 34.29±0.98 ef | 19.52±2.15 ef | 19.65±2.43h | 13.84±1.05 e |
| 5.5 ds.m$^{-1}$ NaCl*60% FC | 30.33±1.08 f | 14.65±1.30 f | 17.06±1.18hi | 11.24±0.96 e |
| Significance | | | | |
| Salinity | ** | ** | ** | ** |
| Drought | ** | ** | ** | ** |
| Salinity*Drought | * | * | ns | * |

ns, *, ** non-significant or significant at $p \leq 0.05$ and 0.01, respectively. Values represent means ± standard deviation of four independent replications (n = 4). Different letters within the same column indicate significant differences at $p \leq 0.05$ among the treatments, according to Duncan's multiple range test.

**Table 3- Effects of salinity and drought on shoot diameter, number of node, average internode distance and average length of auxiliary shoot in *Jacaranda mimosifolia***

| Source of variance | Shoot diameter (mm) | Number of node | Average internode distance (mm) | Average length of auxiliary shoot (cm) |
|---|---|---|---|---|
| Salinity | | | | |
| 1 ds.m$^{-1}$ NaCl | 8.74±1.59 a | 20.33±6.65 a | 20.93±6.41 a | 7.76±1.96 a |
| 2.5 ds.m$^{-1}$ NaCl | 7.77±1.82 b | 17.92±5.25 b | 18.30±5.29 b | 5.99±1.69 b |
| 4 ds.m$^{-1}$ NaCl | 5.69±1.81 c | 17.50±4.39 b | 17.97±4.51 b | 4.28±1.49 c |
| 5.5 ds.m$^{-1}$ NaCl | 4.60±1.39 d | 14.08±3.43 c | 14.32±3.50 c | 3.36±1.87 d |
| Drought | | | | |
| 100% FC | 8.25±2.02 a | 22.94±3.85 a | 23.36±4.11 a | 7.19±1.96 a |
| 80% FC | 6.62±2.09 b | 17.44±3.39 b | 17.80±3.36 b | 5.49±1.91 b |
| 60% FC | 5.24±1.83 c | 12.00±2.42 c | 12.48±2.35 c | 3.36±1.73 c |
| Salinity*Drought | | | | |
| 1 ds.m$^{-1}$ NaCl*100% FC | 10.22±0.70 a | 28.00±1.22 a | 28.42±1.07 a | 9.86±0.72 a |
| 1 ds.m$^{-1}$ NaCl*80% FC | 8.96±0.66 b | 19.75±2.49 cd | 20.27±2.41 c | 8.09±0.60 ab |
| 1 ds.m$^{-1}$ NaCl*60% FC | 7.04±1.24 bc | 13.25±3.96 e | 14.09±3.62 d | 5.33±0.53 c |
| 2.5 ds.m$^{-1}$ NaCl*100% FC | 9.25±0.97 a | 23.00±1.73 b | 23.47±1.85 b | 7.48±1.34 a |
| 2.5 ds.m$^{-1}$ NaCl*80% FC | 7.77±1.59 b | 19.00±3.54 d | 19.32±3.49 c | 6.13±0.97 ab |
| 2.5 ds.m$^{-1}$ NaCl*60% FC | 6.30±1.45 c | 11.75±1.48 e | 12.11±1.46 d | 4.35±0.96 c |
| 4 ds.m$^{-1}$ NaCl*100% FC | 7.81±1.11 b | 22.50±1.50 bc | 23.28±1.67 b | 5.90±0.73 b |
| 4 ds.m$^{-1}$ NaCl*80% FC | 5.06±0.80 c | 17.75±1.09 d | 17.95±0.94 c | 4.35±0.44 c |
| 4 ds.m$^{-1}$ NaCl*60% FC | 4.21±0.90 d | 12.25±1.30 e | 12.67±1.08 d | 2.59±0.69 e |
| 5.5 ds.m$^{-1}$ NaCl*100% FC | 5.71±1.47 c | 18.25±2.17 d | 18.26±2.93 c | 5.53±0.97 bc |
| 5.5 ds.m$^{-1}$ NaCl*80% FC | 4.68±0.92 d | 13.25±0.83 e | 13.66±0.77 d | 3.37±0.23 d |
| 5.5 ds.m$^{-1}$ NaCl*60% FC | 3.41±0.38 e | 10.75±0.83 e | 11.05±0.93 d | 1.18±0.19 f |
| Significance | | | | |
| Salinity | ** | ** | ** | ** |
| Drought | ** | ** | ** | ** |
| Salinity*Drought | ns | * | * | ns |

*ns, *, ** non-significant or significant at $p \leq 0.05$ and 0.01, respectively. Values represent means ± standard deviation of four independent replications (n = 4). Different letters within the same column indicate significant differences at $p \leq 0.05$ among the treatments, according to Duncan's multiple range test.*

**Table 4- Effects of salinity and drought on root diameter, root volume, root length and electrolyte leakage in *Jacaranda mimosifolia***

| Source of variance | Root diameter (mm) | Root volume ($cm^3$) | Root length (cm) | Electrolyte leakage (%) |
|---|---|---|---|---|
| Salinity | | | | |
| 1 $ds.m^{-1}$ NaCl | 13.06±6.35 a | 49.01±8.40 a | 52.57±7.91 a | 19.07±7.67 d |
| 2.5 $ds.m^{-1}$ NaCl | 10.81±5.40 b | 39.72±6.85 b | 44.06±6.99 b | 27.12±11.38 c |
| 4 $ds.m^{-1}$ NaCl | 10.21±4.24 b | 29.36±10.49 c | 35.57±10.43 c | 39.41±8.89 b |
| 5.5 $ds.m^{-1}$ NaCl | 6.42±3.38 c | 15.55±5.21 d | 19.80±5.56 d | 50.21±6.98 a |
| Drought | | | | |
| 100% FC | 15.53±3.81 a | 40.50±14.12 a | 44.68±13.79 a | 26.65±13.19 c |
| 80% FC | 10.10±3.60 b | 33.98±13.58 b | 38.97±13.34 b | 34.26±13.50 b |
| 60% FC | 4.74±2.34 c | 25.75±12.78 c | 30.35±12.49 c | 40.96±14.12 a |
| Salinity*Drought | | | | |
| 1 $ds.m^{-1}$ NaCl*100% FC | 20.25±0.74 a | 57.41±3.95 a | 59.70±4.20 a | 13.55±3.99 g |
| 1 $ds.m^{-1}$ NaCl*80% FC | 12.81±2.86 cd | 49.22±4.28 b | 52.99±4.17 b | 17.63±4.73 f |
| 1 $ds.m^{-1}$ NaCl*60% FC | 6.11±3.47 e | 40.40±5.77 cd | 45.03±6.70 d | 26.11±7.50 ef |
| 2.5 $ds.m^{-1}$ NaCl*100% FC | 16.18±1.90 b | 44.05±5.78 bc | 48.14±5.21bc | 17.71±4.56 f |
| 2.5 $ds.m^{-1}$ NaCl*80% FC | 11.84±3.23 d | 40.77±4.13 cd | 46.46±5.07cd | 28.94±9.15 e |
| 2.5 $ds.m^{-1}$ NaCl*60% FC | 4.41±1.55 e | 34.32±6.44 de | 37.57±5.40de | 34.72±11.59cd |
| 4 $ds.m^{-1}$ NaCl*100% FC | 15.15±1.53 bc | 40.01±3.93 cd | 46.58±3.98 cd | 32.24±9.49 d |
| 4 $ds.m^{-1}$ NaCl*80% FC | 10.14±1.38 d | 31.12±6.37 e | 36.69±5.82 de | 40.21±4.04 c |
| 4 $ds.m^{-1}$ NaCl*60% FC | 5.33±1.24 e | 16.95±1.89 fg | 23.45±2.69ef | 45.77±6.18 bc |
| 5.5 $ds.m^{-1}$ NaCl*100% FC | 10.55±1.97 d | 20.52±5.91 f | 24.31±6.62 e | 43.11±3.95c |
| 5.5 $ds.m^{-1}$ NaCl*80% FC | 5.61±0.89 e | 14.80±1.34 fg | 19.74±2.59 f | 50.27±3.07 b |
| 5.5 $ds.m^{-1}$ NaCl*60% FC | 5.11±0.99 e | 11.32±1.27 g | 15.35±1.45fg | 57.24±4.62 a |
| Significance | | | | |
| Salinity | ** | ** | ** | ** |
| Drought | ** | ** | ** | ** |
| Salinity*Drought | * | * | ns | ns |

*ns, *, ** non-significant or significant at $p \leq 0.05$ and 0.01, respectively. Values represent means ± standard deviation of four independent replications (n = 4). Different letters within the same column indicate significant differences at $p \leq 0.05$ among the treatments, according to Duncan's multiple range test.*

**Shoot diameter, number of node, average internode distance and average length of auxiliary shoot**

Salinity induced level-dependent reductions in shoot diameter, number of nodes, average internode distance and average length of auxiliary shoots in 5.5 $dS.m^{-1}$ NaCl, displaying a 47%, 31%, 31%, and 57% decrease respectively, compared to the respective 1 $dS.m^{-1}$ NaCl.

Severe drought (60% FC) induced the lowest shoot diameter and number of nodes, with a remarkable reduction of 36% and 48% compared to the respective controls respectively. Likewise, in 60% FC compared with 100% FC, significant retardation was realized in the average internode distance and average length of auxiliary shoots by 46% and 53% respectively.

The interaction effect of salinity and drought was significant in the number of nodes as well as the average internode distance, and the highest amounts of these traits were obtained in 1 $dS.m^{-1}$ NaCl × 100% FC (Table 3). Fauerharmel et al. (2020) reported similar results consistent with this study regarding Jacaranda shoot length and diameter under one-quarter strength Hoagland low-nutrient solution with a salt concentration of 1.5 $dS.m^{-1}$.

**Root diameter, volume and length and electrolyte leakage**

In Table (4), three morphological characteristics including root diameter, volume and length were significantly affected by salinity, with a severity-dependent decrease. After subjecting the Jacaranda plants to 5.5 $dS.m^{-1}$ NaCl, these traits declined by 51%, 68% and 62% in comparison with 1 $dS.m^{-1}$ NaCl respectively. In contrast, EL showed a considerable enhancement in dependence of salinity severity by 163% in 5.5 over 1 $dS.m^{-1}$ NaCl (Table 4).

Additionally, treatment with 60% FC (severe drought) caused a significant decrease in root diameter, volume, and length by 69%, 36% and 32% respectively, compared to the control (100% FC), while EL displayed a remarkable increase in 60% FC by 54% versus control (Table 4).

As shown in Table (4), the combination of salinity and drought showed a significant interaction effect on root diameter and volume. The highest amounts were achieved in 1 dS.m$^{-1}$ NaCl at 100% FC, similar to other morphological parameters. Our results was in consistent with Fauerharmel et al. (2020).

**RWC, MDA, sodium and potassium content**

The RWC and K content significantly decreased due to salinity treatment by 43% and 21% and conversely, MDA and Na content increased by 33% and 48% in 5.5 dS.m$^{-1}$ NaCl, respectively (Table 5).

Similar consequences were observed in the drought treatment by severity-dependent changes. The use of 60% FC induced a significant decrease in RWC and K content by 19% and 70% compared with the control (100% FC). In 60% FC, MDA exhibited the highest content with a 3-fold enhancement compared to 100% FC, and Na content showed a remarkable increase by 95% in severe drought conditions compared to natural conditions.

Significant interaction effects were observed only on MDA and Na content in Table (5), and the highest amounts were obtained in 5.5 dS.m$^{-1}$ NaCl × 60% FC.

**Table 5- Effects of salinity and drought on relative water content, malondialdehyde, sodium and potassium content in *Jacaranda mimosifolia***

| Source of variance | Relative water content (%) | Malondialdehyde content (µM.g$^{-1}$ FW) | Sodium content (%) | Potassium content (%) |
|---|---|---|---|---|
| Salinity | | | | |
| 1 ds.m$^{-1}$ NaCl | 79.26±7.55 a | 3.30±1.92 d | 0.23±0.06 c | 4.23±1.68 a |
| 2.5 ds.m$^{-1}$ NaCl | 69.96±7.09 b | 3.83±1.77 c | 0.30±0.08 b | 4.04±1.86 a |
| 4 ds.m$^{-1}$ NaCl | 61.46±9.57 c | 4.19±1.93 b | 0.30±0.10 b | 4.14±1.57 a |
| 5.5 ds.m$^{-1}$ NaCl | 45.40±5.73 d | 4.39±1.76 a | 0.34±0.11 a | 3.33±1.93 b |
| Drought | | | | |
| 100% FC | 70.46±13.57 a | 1.46±0.52 c | 0.20±0.04 c | 5.77±0.41 a |
| 80% FC | 64.37±13.83 b | 4.47±0.35 b | 0.30±0.07 b | 4.31±0.26 b |
| 60% FC | 57.22±13.27 c | 5.85±0.51 a | 0.39±0.07 a | 1.72±1.04 c |
| Salinity*Drought | | | | |
| 1 ds.m$^{-1}$ NaCl*100% FC | 86.61±3.42 a | 0.64±0.01 h | 0.18±0.03 e | 6.11±0.10 a |
| 1 ds.m$^{-1}$ NaCl*80% FC | 80.21±2.96ab | 4.15±0.00 e | 0.23±0.01 e | 4.51±0.22 c |
| 1 ds.m$^{-1}$ NaCl*60% FC | 70.95±5.16bc | 5.10±0.06 c | 0.30±0.04 d | 2.05±0.07fg |
| 2.5 ds.m$^{-1}$ NaCl*100% FC | 74.05±5.54 b | 1.49±0.17 g | 0.21±0.03 e | 6.14±0.08 a |
| 2.5 ds.m$^{-1}$ NaCl*80% FC | 71.33±4.67bc | 4.25±0.17 e | 0.29±0.03 d | 4.36±0.30cd |
| 2.5 ds.m$^{-1}$ NaCl*60% FC | 64.48±7.04cd | 5.74±0.16 b | 0.39±0.03 b | 1.63±0.05 g |
| 4 ds.m$^{-1}$ NaCl*100% FC | 69.98±4.04 c | 1.66±0.05 g | 0.19±0.03 e | 5.63±0.09 b |
| 4 ds.m$^{-1}$ NaCl*80% FC | 61.33±5.69de | 4.63±0.34 d | 0.32±0.09 cd | 4.27±0.17de |
| 4 ds.m$^{-1}$ NaCl*60% FC | 53.05±9.12ef | 6.28±0.21 a | 0.38±0.03 bc | 2.52±1.58 f |
| 5.5 ds.m$^{-1}$ NaCl*100% FC | 51.20±5.77ef | 2.04±0.07 f | 0.22±0.06 e | 5.21±0.23bc |
| 5.5 ds.m$^{-1}$ NaCl*80% FC | 44.60±1.62fg | 4.85±0.14 cd | 0.34±0.04 bcd | 4.10±0.10 e |
| 5.5 ds.m$^{-1}$ NaCl*60% FC | 40.40±1.81g | 6.27±0.15 a | 0.47±0.02 a | 0.67±0.05gh |
| Significance | | | | |
| Salinity | ** | ** | ** | ** |
| Drought | ** | ** | ** | ** |
| Salinity*Drought | ns | ** | * | ns |

*ns, *, ** non-significant or significant at p ≤ 0.05 and 0.01, respectively. Values represent means ± standard deviation of four independent replications (n =4). Different letters within the same column indicate significant differences at p ≤ 0.05 among the treatments, according to Duncan's multiple range test.*

**Potassium to Sodium Ratio**

The effect of different levels of irrigation water and salinity on the potassium to sodium ratio (K/Na) in the aerial part of the Jacaranda plant was significant at the 1% level. The highest potassium to sodium ratio was observed in the 5.5 dS/m$^{-1}$ salinity and 80% and 60% irrigation water treatment, and the lowest in the 2.5 dS/m$^{-1}$ salinity and 80% irrigation water level treatment (Figure 3). The potassium to sodium ratio in plants has a significant effect on their growth and development, as an increase in sodium in the plant growth environment creates competition for potassium absorption and leads to potassium deficiency. Cheng et al (2024) also reported that the addition of sodium, sodium:potassium (1:1 ratio), or potassium to sunflower plants resulted in increased potassium levels in stem and leaf organs compared to the control. The same results were obtained by Hasani et al. (2021) for olive trees irrigated with water containing different concentrations of NaCl.

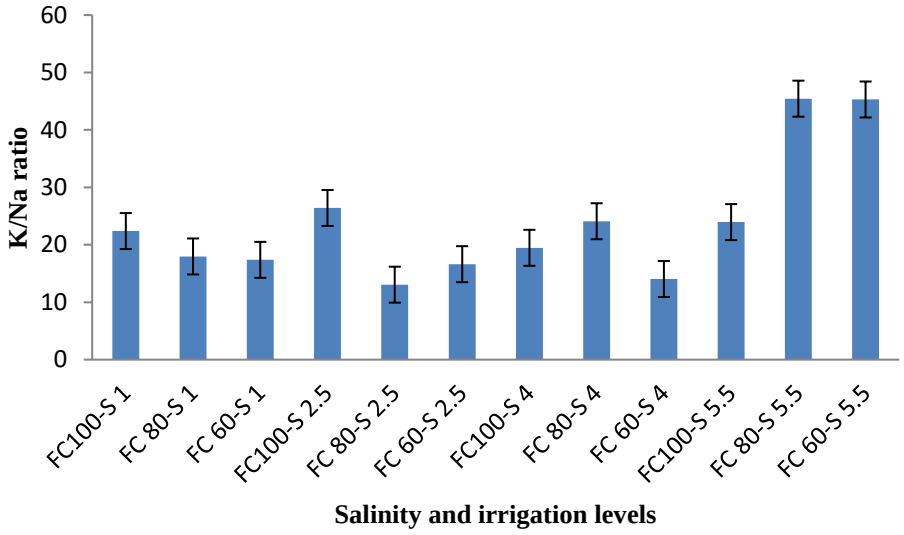



**Fig. 3- Effects of different salinity and irrigation levels on potassium to sodium ratio in Jacaranda seedlings.**

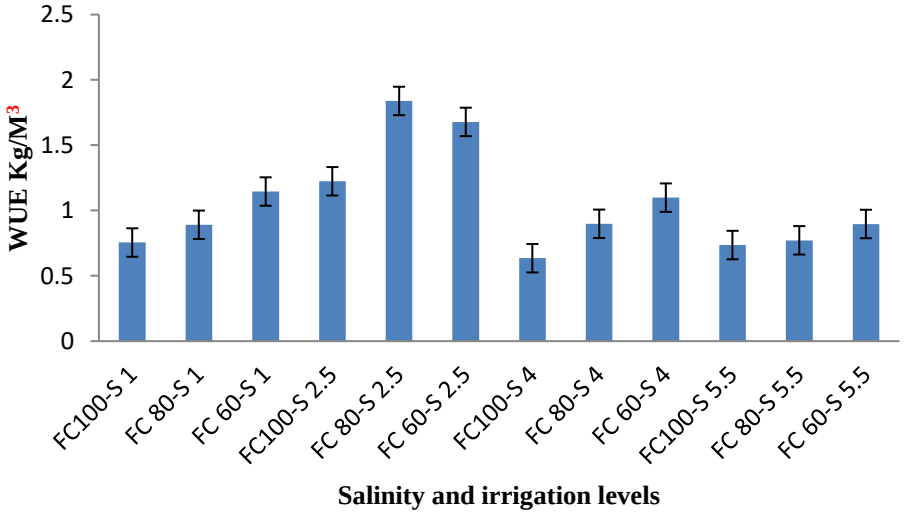



**Fig. 4- Interaction effect of different levels of irrigation and salinity on average water use efficiency in Jacaranda seedlings.**

**Water use efficiency**

The study on Jacaranda demonstrated that water use efficiency (WUE) was significantly influenced by the interaction of salinity and irrigation levels ($p < 0.01$). The highest WUE occurred at 2.5 $dS/m^{-1}$ salinity with 80% FC irrigation, while the lowest was observed at 4 and 5.5 $dS/m^{-1}$ and 80 and 100% FC irrigation (Figure 4). Similar results were found for olive trees by Dindarlou et al. (2019). They observed that the highest intrinsic water use efficiency was achieved under salinity levels of 2.2–7.7 $dS/m^{-1}$ and at 75% of the water requirement. Yuan et al. (2018) also reported that the highest water use efficiency (WUE) in maize was achieved under low salinity conditions (0.71 g/L).

The results obtained indicated that exposure to both types of stress led to a progressive reduction in all morphological characteristics, depending on the severity. Drought stress resulted in a decrease in RWC and water potential in plants (De Campos et al., 2011). The reduction in growth parameters is possibly due to the decline in RWC and subsequent cell shrinkage, decreased meristematic cell division, blocked leaf production, accelerated leaf senescence and ultimately leaf drop (Osuagwu et al., 2010). The ability of the plant to maintain RWC in the optimal range is crucial for its tolerance to drought stress conditions. Proper water distribution in the plant, especially in the leaves, directly affects photosynthesis. Therefore, under conditions of water deficiency, the plant reduces leaf area and keeps the stomata closed in order to maintain RWC (Abdalla and Ahmed, 2021).

The major outcomes of water deficit in plants include a decline in cell division and expansion, differentiation of root and shoot length, changes in foliage dimensions, loss of fruit mass, altered stomatal movements, decreased mineral nutrition, plant yield, and water use efficiency (Aslani et al., 2023; Shomali et al., 2023). Water deficit causes an imbalance between ROS production and their scavenging, resulting in oxidative stress in plant cells. This failure in ROS scavenging leads to the over-accumulation of ROS, resulting in the peroxidation of lipid membranes by active mechanism and increase in MDA (Huang et al., 2023; Ihtisham et al., 2023). The Proline reduces ROS-induced oxidative damage through direct ROS scavenging (Apel and Hirt, 2004; Nkomo et al., 2022). It is documented that drought stress could induce stomatal limitation, directly suppressing photosynthesis throutgh reduce activity of the photosynthetic enzymes and causing chlorophyll degradation due to the release ROS. Likewise, water deficit negatively affects plant growth and development through declined cell division, differentiation, and cell enlargement (Elkelish et al., 2020; Huang et al., 2023). Drought causes a decline in the uptake of various minerals such as K (Ahmad et al., 2018).

The decrease in K uptake was observed under water deficit conditions. As an immediate response of plants exposed to drought and to reduce water loss, stomatal closure occurs, and as a result, the reduction in transpiration leads to a decrease in nutrient uptake along with water absorption ultimately restricting the plant's ability for dry matter production (Singh et al., 2017; Johnson et al., 2022). In other words, the reduction in nutrient uptake due to water deficit could slow the flow of elements and have a negative impact on growth (Hosseini et al., 2021). The reduction in K uptake is attributable to decreased K mobility, weakened function of root membrance transporters and a decreased transpiration rate (Hu and Schmidhalter, 2005; Johnson et al., 2022). Water deficit inhibits genes involved in K transport (Li et al., 2009). Recently, Azeem et al. (2022), found 43 K transport system in cotton genome including 25 transporter and 18 K ion channels.

## Conclusions

The results obtained indicated the detrimental effects of abiotic stresses (deficit irrigation and salinity) on the morphological characteristics and RWC of Jacaranda. The Jacaranda seedlings were sensitive to water salinity and water stress. Therefore, to produce Jacaranda seedlings in tropical and sub tropical nurseries, one should carefully use non-saline water and soil.

**Conflict of Interest**

The authors declared no potential conflicts of interest concerning the research, authorship, and publication of this article.

Confirmation

**Funding**

This study was funded by "Shahid Chamran University of Ahvaz". Research Council of Shahid Chamran University of Ahvaz for financial support (GN: SCU.AH).

**Data availability statement**

The datasets used and/or analyzed during the current study are available from the corresponding author upon reasonable request.

**Authors' contribution**

**First Author:** Khalil Asadivafa, Collecting data and writing the first draft of the article.
**Second Author:** Mousa Mousavi, Reading and revising the initial draft.
**Third Author:** Abdul-kadhm N. S. Al-Showily, Reading and revising the initial draft.
**Fourth Author:** Mohammad Albaji, Reading and revising the initial draft.
**Fifth Author:** Naser Alemzadeh Ansari, Reading and revising the initial draft.

**References**

1- Abdalla, M. and Ahmed, M.A., 2021. Arbuscular mycorrhiza symbiosis enhances water status and soil-plant hydraulic conductance under drought. *Frontiers in Plant Science*, *12*, p.722954.https://doi.org/10.3389/fpls.2021.722954

2- Ahmad ZS, Anjum EA, Waraich MA, Ayub T, Ahmad RMS et al. 2018. Growth, physiology, and biochemical activities of plant responses with foliar potassium application under drought stress-A review. *Journal of Plant Nutrition* 41:1734-1743. https://doi.org/10.1080/01904167.2018.1459688

3- Akhter MS, Noreen S, Mahmood S, Ashraf M, Alsahli AA et al. 2021. Influence of salinity stress on PSII in barley (*Hordeum vulgare* L.) genotypes, probed by chlorophyll-a fluorescence. *Journal of King Saud University-Science* 33 (1):101239. https://doi.org/10.1016/j.jksus.2020.101239

4- Amanullah Jr, Stewart BA 2013. Dry matter partitioning, growth analysis and water use efficiency response of Oats (*Avena sativa* L.) to excessive nitrogen and phosphorus application. *Journal of Agricultural Science and Technology* 15: 479-489

5- Apel K, Hirt H 2004. Reactive oxygen species: Metabolism, oxidative stress, and signal transduction. *Annual Review of Plant Biology* 55: 373-399. https://doi.org/10.1146/annurev.arplant.55.031903.141701

6- Aslani L, Breniere T, Fanciullino AL, Bertin N 2023. Evidence of the very early effects of water deficit on cell division and expansion processes in tomato ovaries. *Environmental and Experimental Botany* 207: 105227 doi.org/10.1016/j.envexpbot.2023.105227.

7- Azeem F, Zameer R, Rashid MAR, Rasul I, Ul-Allah S et al. 2022. Genome-wide analysis of potassium transport genes in *Gossypium raimondii* suggest a role of GrHAK/KUP/KT8, GrAKT2.1 and GrAKT1.1 in response to abiotic stress. *Plant Physiology and Biochemistry* 170: 110-122. https://doi.org/10.1016/j.plaphy.2021.11.038

8- Benton-Jones J 1977. Elemental analysis of soil extracts and plant tissue ash by plasma emission spectroscopy. *Communications in Soil Science and Plant Analysis* 8: 349-365. https://doi.org/10.1080/00103627709366727

9- Bhat MA, Mir, RA, Kumar, V, Shah, AA, Zargar SM 2021. Mechanistic insights of CRISPR /Cas-mediated genome editing towards enhancing abiotic stress tolerance in plants. *Physiologia Plantarum* 172: 1255-1268. https://doi.org/10.1111/ppl.13359

10- Brito C, Dinis, LT, Moutinho-Pereira J, Correia CM 2019. Drought stress effects and olive tree acclimation under a changing climate. *Plants* 232: 1-20. https://doi.org/10.3390/plants8070232

11- Cheng Y, Zhang T, Gao W, Kuang Y, Liang Q, Feng H, Galymzhan S 2024. An excessive K/Na ratio in soil solutions impairs the seedling establishment of sunflower (*Helianthus annuus* L.) through reducing the leaf Mg concentration and photosynthesis. *Agronomy*, *14*(10), 2301. https://doi.org/10.3390/agronomy14102301

12- Chen YE, Mao JJ, Sun, LQ, Huang B, Ding, CB et al. 2018. Exogenous melatonin enhances salt stress tolerance in maize seedlings by improving antioxidant and photosynthetic capacity. *Physiologia Plantarum* 164: 349-363. https://doi.org/10.1111/ppl.12737

13- Coban F, Ozer H, Yilmaz B, Lan Y 2025. Characterization of bioactive compounds in fenugreek genotypes in varying environments: diosgenin, trigonelline, and 4-hydroxyisoleucine. *Front. Plant Sci.*, 16: 1562931. https://doi.org/10.3389/fpls.2025.1562931

14- Darwish DA, El-Berry IM, Mustafa NS, Fatma SM, Laila, FH 2015. Detecting drought tolerance of fig (*Ficus carica* L.) cultivars depending on vegetative growth and peroxidase activity. *International Journal of ChemTech Research* 8 (4): 1520-1532.

15- De Campos MKF, de Carvalho K, de Souza FS, Marur, CJ, Pereira LFP et al. 2011. Drought tolerance and antioxidant enzymatic activity in transgenic 'Swingle' citrumelo plants over-accumulating proline. *Environmental and Experimental Botany* 72: 242-250. https://doi.org/10.1016/j.envexpbot.2011.03.009

16- De Vries FT, Griffiths RI, Knight CG, Nicolitch O, Williams A, 2020. Harnessing rhizosphere microbiomes for drought-resilient crop production. *Science*, *368*(6488), pp.270-274.. https://doi.org/10.1126/science.aaz5192

17- Dindarlou A, Ghaemi AA, Shekafandeh Nobandegani A, Bahrami M, Dastourani M 2019. Interaction of water salinity and different irrigation levels on physiological growth of olive (*Olea europaea* L.). *Journal of Agricultural Science and Technology* 21(6): 1623-1637

18- Elkelish A, Qari SH, Mazrou YSA, Abdelaal KAA, Hafez YM, et al. 2020. Exogenous ascorbic acid induced chilling tolerance in tomato plants through modulating metabolism, osmolytes, antioxidants, and transcriptional regulation of catalase and heat shock proteins. *Plants* 9: 431. https://doi.org/10.3390/plants9040431

19- Fathian F, Morid S, Kahya E 2015. Identification of trends in hydrological and climatic variables in Urmia Lake basin, Iran. *Theoretical and Applied Climatology* 119: 443-464. https://doi.org/10.1007/s00704-014-1120-4

20- Fauerharmel M, Bisognin DA, Lencina KH, Tonetto TS, Meltzer JM, Maggioni JH 2020. Production of jacaranda plantlets by minicutting. *Semina: C iências Agrárias, L ondrina* 41: 1951-1962. https://doi.org/10.5433/1679-0359.2020v41n5Supl1p1951

21- Gucci R, Lombardini L, Tattini M 1997. Analysis of leaf water relations in leaves of two olive (*Olea europaea*) cultivars differing in tolerance to salinity. *Tree Physiology* 17: 13-21. https://doi.org/10.1093/treephys/17.1.13

22- Hasani A, Shirzad H, Marandi R, Samadi A 2021. Morphological and physiological responses of two olive (*Olea europea* L.) cultivars saplings to NaCl salinity stress. *Applied Soil Sesearch* 9(1): 88-101.

23- Hosseini MS, Samsampour D, Zahedi SM, Zamanian K, Rahman MM, et al. 2021. Melatonin alleviates drought impact on growth and essential oil yield of lemon verbena by enhancing antioxidant responses, mineral balance, and abscisic acid content. *Physiologia Plantarum* 172 (2): 1363-1375. https://doi.org/10.1111/ppl.13335

24- Hu Y, Schmidhalter U 2005. Drought and salinity: A comparison of their effects on mineral nutrition of plants. *Journal of Plant Nutrition and Soil Science* 168: 541-549. https://doi.org/10.1002/jpln.200420516

25- Huang C, Qin A, Gao Y, Ma S, Liu Z et al. 2023. Effects of water deficit at different stages on growth and ear quality of waxy maize. *Frontiers in Plant Science* 14: 1069551. https://doi.org/10.3389/fpls.2023.1069551

26- Ihtisham M, Hasanuzzaman M, El-Sappah AH, Zaman F, Khan N et al. 2023. Primary plant nutrients modulate the reactive oxygen species metabolism and mitigate the impact of cold stress in overseeded perennial ryegrass. *Frontiers in Plant Science* 14: 1149832. https://doi.org/10.3389/fpls.2023.1149832

27- Johnson R, Vishwakarma K, Hossen MS, Kumar K, Shackira AM et al. 2022. Potassium in plants: Growth regulation, signaling, and environmental stress tolerance. *Plant Physiology and Biochemistry* 172: 56-69. https://doi.org/10.1016/j.plaphy.2022.01.001

28- Khan AA, Khan MJ, Ijaz M, Hassan SS 2022. Combined effect of organic amendments and seed placement techniques on sorghum yield under salt stressed conditions. *Journal of Soil Science and Plant Nutrition* 22: 4752-4767. https://doi.org/10.1007/s42729-022-00957-y

29- Lenzner B, Magallon, S, Dawson, W, Kreft, H, Konig, C et al. 2021. Role of diversification rates and evolutionary history as a driver of plant naturalization success. *New Phytologist* 229: 2998-3008. https://doi.org/10.1111/nph.17014

30- Li Y, Sun C, Huang Z, Pan J, Wang L et al. 2009. Mechanisms of progressive water deficit tolerance and growth recovery of Chinese maize foundation genotypes Huangzao 4 and Chang 7-2, which are proposed on the basis of comparison of physiological and transcriptomic responses. *Plant and Cell Physiology* 50: 2092-2111. https://doi.org/10.1093/pcp/pcp145

31- Lutts S, Kinet JM, Bouharmont J 1996. NaCl-induced senescence in leaves of rice (*Oryza sativa* L.) cultivars differing in salinity resistance. *Annals of Botany* 78: 389-398. https://doi.org/10.1006/anbo.1996.0134

32- Mohamed HI, Latif HH, 2017. Improvement of drought tolerance of soybean plants by using methyl jasmonate. *Physiology and Molecular Biology of Plants* 23 (3): 545-556. https://doi.org/10.1007/s12298-017-0451-x

33- Munns R, Tester M 2008. Mechanisms of salinity tolerance. *Annual Review of Plant Biology* 59: 651-681. https://doi.org/10.1146/annurev.arplant.59.032607.092911

34- Nadeem M, Li, J, Yahya M, Wang M, Ali A et al. 2019. Grain legumes and fear of salt stress: Focus on mechanisms and management strategies. *International Journal of Molecular Sciences* 20: 799. https://doi.org/10.3390/ijms20040799

35- Nkomo M, Gokul A, Ndimba R, Badiwe M, Keyster M, Klein A 2022. Piperonylic acid alters growth, mineral content accumulation and reactive oxygen species-scavenging capacity in chia seedlings. *AoB PLANTS* 14, 1–10 https://doi.org/10.1093/aobpla/plac025

36- Osuagwu GGE, Edeoga HO, Osuagwu AN 2010. The influence of water stress (drought) on the mineral and vitamin potential of the leaves of *Ocimum gratissimum* (L.). *Recent Research in Science and Technology* 2: 27-33. https://updatepublishing.com/journal/index.php/rrst/article/view/372

37- Pasiecznik N 2014. *Jacaranda mimosifolia* (Jacaranda). *CABI Compendium. Available online*: https://doi.org/10.1079/cabicompendium.29212.

38- Petridis A, Therios I, Samouris G, Koundouras S, Giannakoula A 2012. Effect of water deficit on leaf phenolic composition, gas exchange, oxidative damage and antioxidant activity of four Greek olive (*Olea europaea* L.) cultivars. *Plant Physiology and Biochemistry* 60: 1-11. https://doi.org/10.1016/j.plaphy.2012.07.014

39- Proietti P, Nasini L, DelBuonoa D, D'Amatoa R, Tedeschini E et al. 2013. Selenium protects olive (*Olea europaea* L.) from drought stress. *Scientia Horticulturae* 164: 165-171. https://doi.org/10.1016/j.scienta.2013.09.034

41- Rodriguez-Dominguez CM, Buckley T, Egea G, de Cires A, Hernandez-Santana V et al. 2016. Most stomatal closure in woody species under moderate drought can be explained by stomatal responses to leaf turgor. *Plant Cell, & Environment* 39: 2014-2026. https://doi.org/10.1111/pce.12774

41- Sabah SS, Hosni AM, Abdul Raziq AB, Hewidy M 2022. A comprehensive protocol for *in vitro* propagation and acclimatization of *Jacaranda mimosifolia* trees under the Egyptian conditions. *Egyptian Journal of Agricultural Sciences* 73: 79-92 https://doi.org/10.21608/ejarc.2023.296441

42- Salimpour A, Shamili M, Dadkhodaie A, Zare H, Hadadinejad M 2019. Impact of NaCl on leaf abscission, ion content and photosynthetic indices of seven commercial fig (*Ficus carica* L.) cultivars. *Journal of Plant Process and Function* 8 (31): 9-22. http://jispp.iut.ac.ir/article-1-1196-en.html

43- Sanchez JL 2011. Arboles ornamentales. *Obtenido de _Arboles ornamentales.* Available online: http://www.arbolesornamentales.es/Jacaranda%20mimosifolia.pdf.

44- Shomali A, Das S, Arif N, Sarraf M, Zahra N et al. 2023. Diverse physiological roles of flavonoids in plant environmental stress responses and tolerance. *Plants* 11 (22): 3158. https://doi.org/10.3390/plants11223158

45- Singh R, Parihar P, Singh S, Mishra RK, Singh VP et al. 2017. Redox biology reactive oxygen species signaling and stomatal movement: Current updates and future perspectives. *Redox Biology* 11: 213-218. https://doi.org/10.1016/j.redox.2016.11.006

46- Stewart RRC, Bewley JD 1980. Lipid peroxidation associated with accelerated aging of soybean axes. *Plant Physiology* 65: 245-248. https://doi.org/10.1104/pp.65.2.245

47- Wu L, Zu X, Zhang H, Wu L, Xi Z et al. 2015. Overexpression of ZmMAPK1 enhances drought and heat stress in transgenic *Arabidopsis thaliana*. *Plant Molecular Biology* 88: 429-443. https://doi.org/10.1007/s11103-015-0333-y

48- Yuan C F, Feng S Y, Wang J, Huo Z L, Ji Q Y. 2018. Effects of irrigation water salinity on soil salt content distribution, soil physical properties and water use efficiency of maize for seed production in arid Northwest China. *International Journal of Agricultural and Biological Engineering* 11(3): 137–145.https://doi.org/10.25165/j.ijabe.20181103.3146

49- Zhu M, Zhou M, Shabala L, Shabala S 2015. Linking osmotic adjustment and stomatal characteristics with salinity stress tolerance in contrasting barley accessions. *Functional Plant Biology* 42: 252-263. https://doi.org/10.1071/FP14209.

© 2026 The Author(s). Published by Shahid Chamran University of Ahvaz. This is an open-access article distributed under the terms of the Creative Commons Attribution License (http://creativecommons.org/licenses/by/4.0), which permits unrestricted use, distribution, and reproduction in any medium, provided the original work is properly cited.

Shahid Chamran University of Ahvaz

**Irrigation Sciences and Engineering (JISE)**
**Vol. 48, No. 4, Winter 2026, p. 79-103**
Journal homepage: https://jise.scu.ac.ir

**Research Paper**

# Estimation of Transmissivity and Storage Coefficients in a Dual-Aquifer System Using Combined Field and Analytical Methods

Sheyda Mohammadi Fard[1], Jahangir Abedi-Koupai[2] and Saeid Eslamian[3]

*1*- Corresponding Author, PhD Student, Department of Water Engineeribg, College of Agriculture, Isfahan University of Technology (s.mohammadifard@ag.iut.ac.ir)*
*2 - Department of Water Engineeribg, College of Agriculture, Isfahan University of Technology.*
*3- Department of Water Engineeribg, College of Agriculture, Isfahan University of Technology.*

**ARTICLE INFO**

*Artlcle history:*
Received: 01 July 2025
Revised: 01 September 2025
Accepted: 22 September 2026
Available online: 04 January 2026

*Keywords:*
Aquifer, Groundwater, Transmissivity, Storage.

**TO CITE THIS ARTICLE:**
Mohammadifard, S., Abedi Koupai, J., Eslamian, S. 2026. 'Estimation of Transmissivity and Storage Coefficients in a Dual-Aquifer System Using Combined Field and Analytical Methods', *Irrigation Sciences and Engineering*, 48(4), pp. 79-103. doi: 10.22055/jise.2025.49895.2167

**Abstract**

This study investigates the hydrodynamic coefficients of the Kouhpayeh-Segzi (KSA) aquifer, a vital groundwater resource in Isfahan province in central Iran, located in an arid to semi-arid climate, where surface water is unreliable. The research addresses the increasing dependence on groundwater in the region, driven by population growth, agricultural expansion, and industrial development, which has led to over-extraction, groundwater table depletion, reduced well yields, and land subsidence. The main objective is to accurately estimate the parameters of hydrodynamic coefficients—transmissivity coefficient and storage —essential for sustainable groundwater management. Traditional pumping tests, although standard, are costly and limited by practical constraints, especially in deep or data-poor environments. To overcome these challenges, this study integrates multiple data sources, including grain-size distribution analysis, well drilling logs, geophysical surveys, and exploratory and observational well data. The approach involves re-analyzing pumping test data, determining alluvium thickness, bedrock elevation, and consequently preparing maps of the transmissivity and storage for the aquifer. The studied aquifer has two types of aquifers: confined and unconfined. The results show that the average values of hydrodynamic coefficients such as the transmissivity and storage of the KSA unconfined aquifer are estimated to be 960 m2/day and 3.9% and the transmissivity unconfined aquifer is estimated to be 914 m2/day, respectively. The findings emphasize the necessity of continuous monitoring, adaptive management, and the use of advanced analytical and geophysical techniques to ensure the long-term sustainability of groundwater resources in the KSA region.

## Introduction

One of the essential needs for the growth and development of any country is water, which is not only necessary for the expansion of cities and industries but is also considered a key factor in agricultural development. On the other hand, groundwater resources are among the most important sources of water. The hydraulic study of aquifers is significant because it leads to better utilization of groundwater and, consequently, improved management of water resources. In arid and semi-arid regions, since rainfall occurs only during a short period of the year and evaporation and transpiration rates are high, surface water resources are not a reliable source for water supply. Therefore, in these areas, greater reliance is placed on groundwater resources.

Hydrodynamic coefficients of an aquifer (storage (S) and transmissivity (T)) are the most important hydrogeological information for describing the characteristics of any aquifer. The implementation of most projects

 *DOI:* 10.22055/jise.2025.49895.2167

and research plans in any aquifer depends on the availability of accurate and precise hydrodynamic coefficients. One of the methods to determine these parameters is conducting pumping tests, which are usually very costly and face many limitations, especially in arid regions due to increased drilling depth. Therefore, in recent years, efforts to find the fastest and most economical solutions to perform these tests in most areas have led to the development of various methods. These methods analyze existing data to obtain average values of aquifer coefficients.

The aim of this study is to estimate the hydrodynamic coefficients of the KSA aquifer in Isfahan province in the central part of Iran. Therefore, the objectives of this work are: i) Collecting drilling log data and extracting hydrodynamic coefficients from them ii) Collecting data from pump tests and analyzing them to extract the hydrodynamic coefficient iii) Combining the extracted data in the two above cases to draw maps of both the storage and transportability. Research questions: i) What are the values of hydrodynamic coefficients using the grain-size method? Ii) What values do the hydrodynamic coefficients include in the pumping test method?

There are various methods for measuring the hydrodynamic coefficients of an aquifer, including laboratory methods, groundwater modeling, pumping tests, use of tracers, geophysical methods, and experimental methods such as grain-size, balance. Due to the high cost of pumping tests to estimate hydrodynamic coefficients, the innovation in this study is to use available information and combine the results of two pumping test and grain-size methods to estimate the transportability and storage in the aquifer.

In this study, the inverse solution method was not used to estimate the hydrodynamic coefficients of the aquifer, but the results of this research can be used in the inverse solution method. Because the inverse solution method in estimating the hydrodynamic coefficients of the aquifer is a numerical and optimization method that is used to estimate important hydrodynamic parameters such as transmissivity, storage and hydraulic conductivity. This method is used when there is little direct data or simple analytical models are not suitable. In this method, first, using the equations governing groundwater flow, the behavior that the parameters are expected to have is simulated (Sahranavard et al., 2023). Then, by comparing the simulated model with the actual data (the results of the present study), the difference between the model and observations is defined as the objective function.

Ansarifar et al.(2019) study combines borehole data interpretation with an inverse solution method to estimate hydraulic conductivity (K) and specific yield (Sy) of the Bandar-e Gaz unconfined aquifer in Northern Iran, without pumping test data. A numerical model calibrated and validated over two 12-month periods demonstrates high accuracy using the Nash-Sutcliffe criterion. Results show that K and Sy values range from 5–15 and 0.024–0.036 m/day, respectively, with a spatial pattern decreasing from south to north, aligning with the sediment characteristics of the aquifer.

Pumping tests are one of the most reliable and common field methods for determining the hydraulic properties of aquifers, because this test reflects the hydraulic properties of a relatively large part of the aquifer (the part where the depression cone has formed). A well dewatering test or pumping test is performed to determine the hydraulic properties of an aquifer to study the groundwater status of an area or to determine the amount of dewatering and water level drop in a well. In a pumping test, the goal is to determine the storage and the transportability of the aquifer, and for this purpose, the presence of observation wells or piezometric wells at certain distances from the main well being tested is mandatory. This test is performed under stable and unstable conditions or in a stepwise manner (Lohman, 1972).

One of the methods that can be used to estimate a relatively good estimate of the hydrodynamic coefficients of an aquifer is to use the grain-size method. In this method, by obtaining the permeability coefficient and determining the thickness of the aquifer, the transportability can be calculated. Also, by

obtaining the effective porosity, an estimate of the aquifer storage can be obtained (Domenico and Schwartz, 1990).

Accurate estimation of aquifer parameters is essential for effective groundwater management, but traditional methods face challenges due to subjectivity and non-uniqueness. The proposed Weighted Joint Curve Method (WJCM), based on the Theis equation and optimization, provides unique and reliable parameter estimates by considering both pumping and recovery phases. Application of WJCM to real data demonstrates its efficiency, ease of implementation, and potential for improving groundwater evaluation and management (Li et al., 2025).

Pumping test data are inherently noisy, causing variability in aquifer parameter estimates when analyzed by traditional trial-and-error methods that often yield uncertain, non-unique results. Bashandy et al. (2024) in a study develops a FORTRAN-based tool employing the Markov Chain Monte Carlo (MCMC) algorithm with various likelihood functions to quantify uncertainty and identify the most probable aquifer parameters with high confidence. The tool's effectiveness is demonstrated through hypothetical and real cases, showing improved reliability over standard methods for confined and semi-confined aquifers.

Benson (2023) derives a convolutional solution for pumping tests accommodating any pumping history, improving computational efficiency by using the time derivative of the well function and enabling nonlinear well loss modeling. The method supports simultaneous use of data from multiple observation wells and provides MATLAB and Python codes for parameter optimization. Results highlight the importance of objective function construction and suggest Bayesian inversion for robust estimation of aquifer parameters due to non-uniqueness in step-drawdown test optimization.

Large-scale groundwater models face challenges in parameterization due to limited observational data and scale mismatches. Houben (2022) in research uses spectral analysis of groundwater level fluctuations to derive regional hydraulic parameters, demonstrating that specific aquifer locations can reveal representative parameters. Results show that robust parameter estimation requires long-term data and knowledge of aquifer length and measurement location, enabling effective bridging of scale gaps in groundwater modeling.

Groundwater plays a vital role in securing water resources and ecological stability in semi-arid regions. Li et al. (2019) in a study develops a three-layer hydrogeochemical zoning model for a typical semi-arid basin in western Jilin Province, revealing spatial hydrogeochemical evolution from recharge to discharge zones. The model integrates geological, hydrodynamic, and chemical characteristics, highlighting processes such as leaching, cation exchange, and evaporation that shape groundwater chemistry and elemental distribution.

Accurate hydrogeological parameter estimation is critical for groundwater management. Li and Qian introduced a global curve-fitting method combining pumping and recovery data, showing slightly higher but comparable results to traditional Hantush-Jacob methods, confirming its reliability (Li and Qian, 2012).

A study in China presents a closed-form analytical solution for constant-rate pumping in a confined aquifer affected by a rectangular waterproof curtain, using the image method and superposition principle. A straightforward approach for estimating hydraulic parameters is demonstrated with field data from Wuhan, China, showing good agreement between predicted and observed drawdowns. The solution and parameter estimation method are reliable and valuable for designing dewatering systems in deep excavation projects (Li et al., 2023a).

In another study in China develops a novel dimensionless analytical solution for variable-rate pumping tests using piecewise-constant approximations, addressing limitations of classical constant-rate models. The new type curve method estimates hydraulic conductivity and specific storage by matching observed

 *DOI:* 10.22055/jise.2025.49895.2167

drawdown data with curves dependent on dimensionless inflection time. Application to field data from Wuxi City, China, shows close agreement with PEST calibration and lithology-based validation, providing reliable aquifer parameter estimates (Li et al., 2023b).

In this study, hydrodynamic coefficients of aquifer layers were estimated using grain-size distribution curves, observation well logs, exploratory and production wells, geophysical studies, and pumping tests. The work steps are summarized in the flowchart of Figure (1).

The present research was conducted to achieve the following objectives:

- Collecting pumping test data
- Reviewing and reanalyzing conducted pumping tests to refine the coefficients and verify the accuracy of the data
- Determining the thickness of alluvium and the bedrock elevation based on existing data (including geophysical information, borehole logs, and production and exploratory wells that have reached the bedrock)
- Preparing transmissivity (T) curves and storage maps.

## Materials and Methods

### Study Area

Isfahan Province is located within the arid and semi-arid regions of Iran. Moreover, the timing and location of precipitation in this province do not align with water demand. Most cities in Isfahan Province are situated in areas with limited access to surface water resources; therefore, they primarily rely on groundwater. The presence of numerous deep and semi-deep wells in the aquifers and Qantas in these cities supports this claim. Given these conditions and technological advancements, groundwater exploitation has significantly increased over the past few decades. This has resulted in an imbalance between recharge and withdrawal, leading to a negative groundwater balance and adverse consequences such as declining water table levels, reduced well yields, well displacement and collapse, increased pumping costs due to greater depths, irreversible aquifer volume reduction, and compaction of the aquifer system. These effects cause decreases in transmissivity, storage, and land subsidence. To prevent further quantitative and qualitative decline, proper management of groundwater resources must be seriously considered as a fundamental principle in the planning of Isfahan Province by authorities and stakeholders. The present study was conducted in the KSA area located in the center of Isfahan Province.

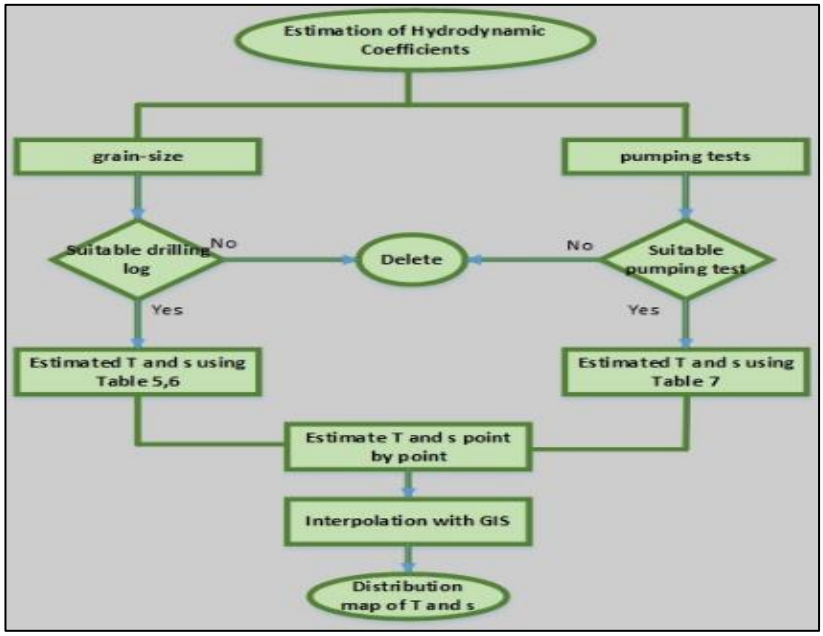



**Fig. 1- Flowchart for work steps**

**Kouhpayeh-Segzi (KSA) Study Area**

The KSA study area is one of the main sub-basins of the Gavkhouni watershed in Iran, located in the eastern part of this watershed, covering an area of approximately 6,678 square kilometers. It extends between longitudes 51°34' to 53°1' east and latitudes 32°11' to 33°13' north. Figure (2) shows the Gavkhouni watershed and the KSA study area in relation to Isfahan Province. Additionally, Table (1) provides detailed information about the KSA.

**Groundwater Characteristics in the KSA Study Area**

Initially, the topography of the KSA study area was examined, as shown in Figure (3). Based on the topographic maps, the elevations and the inflow and outflow points of the aquifers can be identified. As observed, the northern parts of the study area have the highest elevations, which gradually decrease towards the center and east of the area.

For better visualization, Figure (4) presents the KSA study area in Isfahan Province overlaid on a satellite image. This clear image allows the identification of various landforms such as mountains, agricultural lands, rivers, and so on. Understanding the location of these features around the studied aquifers significantly aids in determining the inflow and outflow zones of the aquifers under study.

Further, the characteristics of the KSA study area are analyzed including aquifer discharge and withdrawal, groundwater depth, groundwater level, fluctuations of the groundwater surface, aquifer thickness, saturated thickness, and aquifer storage. Using statistical data, the amount of discharge in the KSA study area through springs, Qantas, and wells is presented in Table (2).

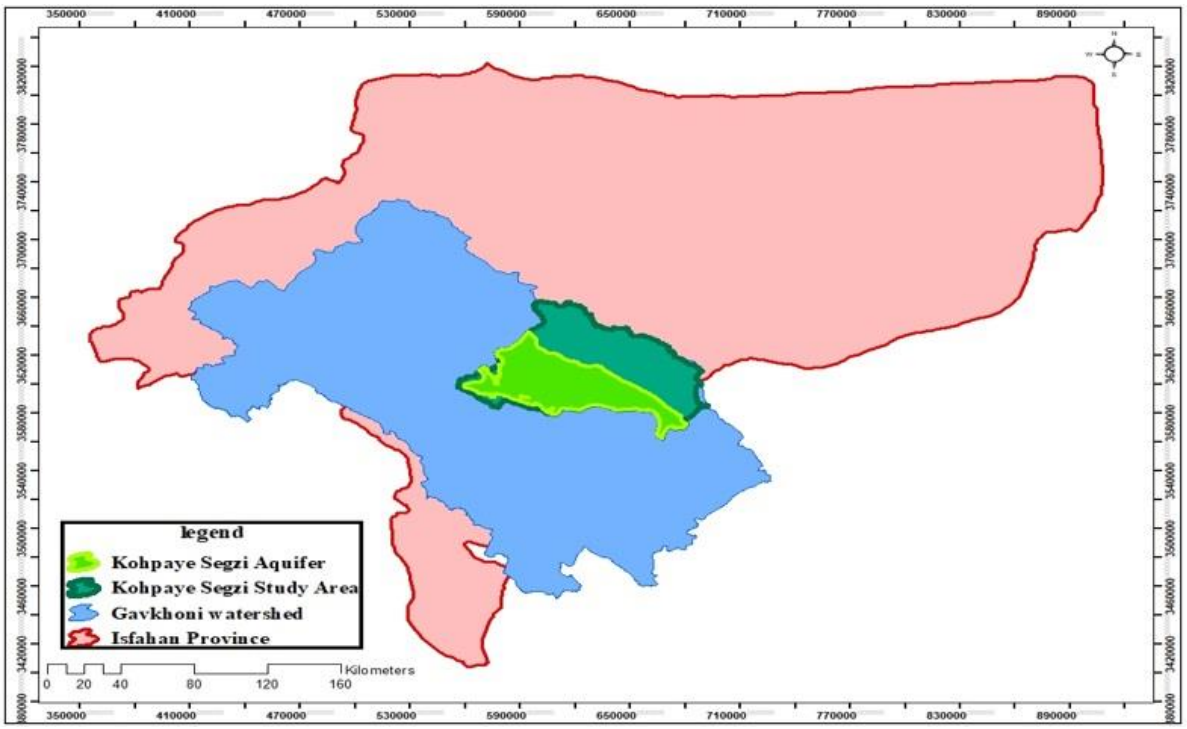



**Fig. 2- The Gavkhouni basin and the KSA study area in Isfahan Province**

**Table 1- Detailed information about the KSA area**

| Watershed Basin | Sub-basin | Study Area ($km^2$) | Plain Area ($km^2$) | Aquifer Area ($km^2$) |
|---|---|---|---|---|
| Gavkhouni | Kouhpayeh-Segzi | 6422 | 4978.3 | 2940 |

 *DOI:* 10.22055/jise.2025.49895.2167

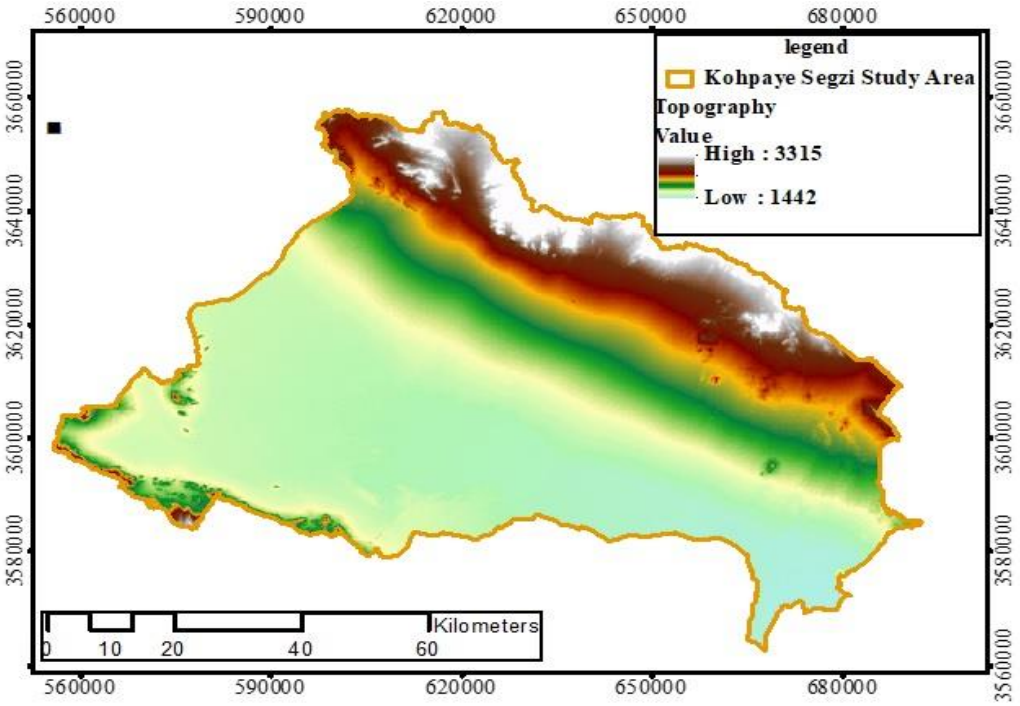



**Fig. 3- Topographic map of the KSA area**

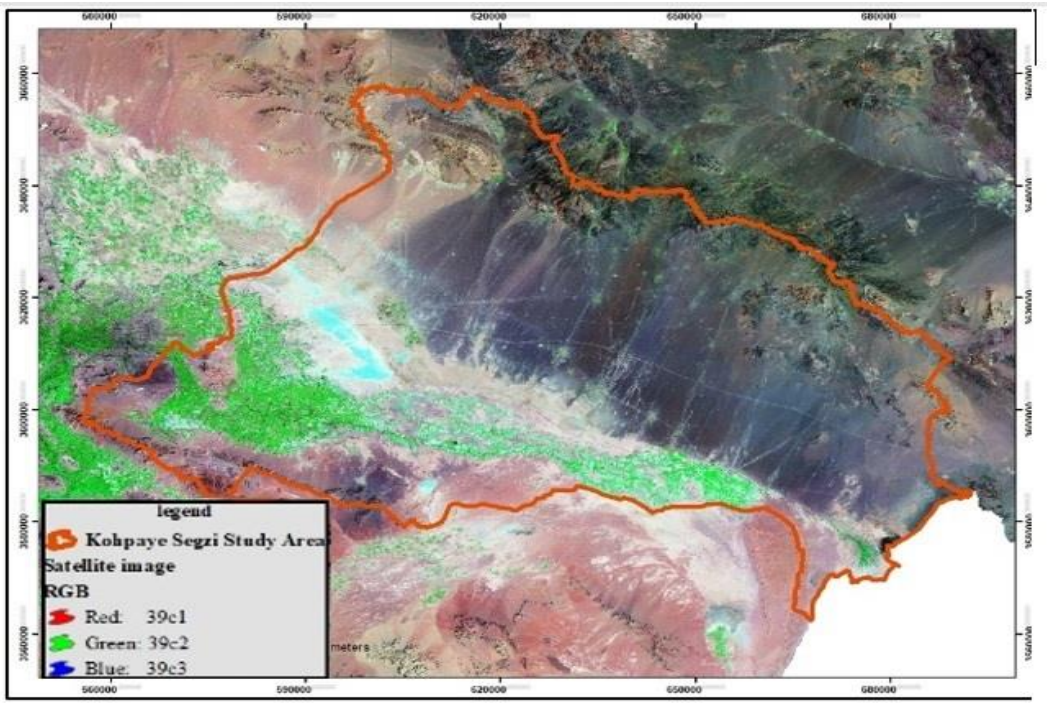



**Fig. 4- Satellite image of the KSA area**

**Table 2- Information on the discharge annual rate of the KSA aquifer**

| Number of Springs | Number of Qanats | Number of Wells | Total Discharge (million cubic meters) |
|---|---|---|---|
| 127 | 263 | 18,094 | 194.58 |

**Table 3- Number of discharge wells by depth in the KSA Area**

| Depth (meters) | Number |
|---|---|
| 1-45 | 18969 |
| 45-90 | 1136 |
| 90-135 | 377 |
| 135-180 | 125 |
| 180-225 | 310 |
| 225-270 | 137 |
| 270-315 | 65 |
| 315-360 | 16 |
| 360-405 | 11 |
| 405-450 | 1 |

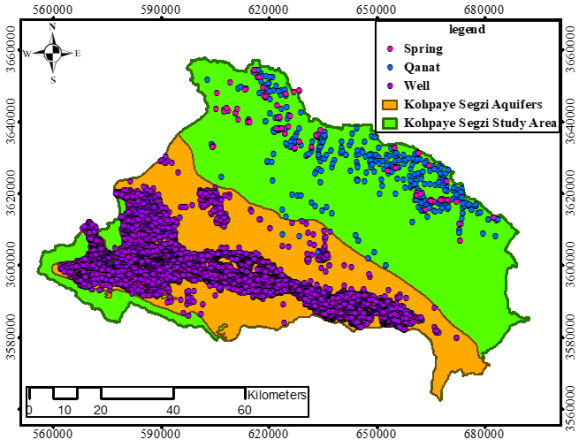



**Fig. 5- Distribution of discharge Wells, springs, and Qanats in the KSA Area**

The depth of the majority of discharge wells within the KSA study area ranges between 20 and 100 meters. Table (3) presents the number of discharge wells categorized by their depth. Additionally, between the years 1991 and 2011, there was a significant increase in the number of drilled wells. This increase has led to a substantial rise in groundwater extraction during this 20-year period, causing a sharp decline in the groundwater level within KSA study area. The drilling of discharge wells plays a crucial role in the direct utilization of groundwater, especially for agricultural water supply in this region. Figure (5) illustrates the spatial distribution of 21,138 discharge wells drilled throughout the KSA study area.

One of the main causes of groundwater level decline is the excessive drilling of numerous wells in the alluvial aquifer and the consequent over-extraction beyond the aquifer's capacity. This overexploitation results in reservoir depletion and further groundwater level reduction in the coming years. Effective groundwater resource management requires a comprehensive assessment of the aquifer's storage capacity relative to the inflows from various sources. Based on the capacity of each aquifer, regulated permits for groundwater withdrawal should be issued to maintain groundwater levels in a balanced state and to prevent adverse phenomena such as land subsidence.

 *DOI:* 10.22055/jise.2025.49895.2167

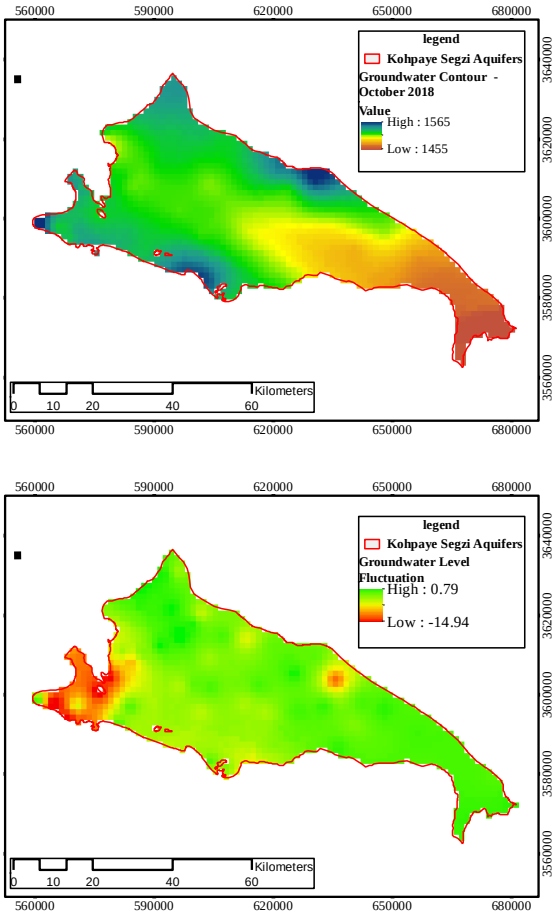



**Fig. 6- Groundwater level fluctuation map comparing October 2008 to October 2018**

Figure (5) shows the spatial distribution of Qanats and springs within the KSA study area. As observed in the figure, the concentration of springs and Qanats is primarily located in the northern and northwestern parts of the study area.

To analyze and identify the inflow and outflow patterns in the KSA aquifer, groundwater level contour maps were drawn for the month of October in the years 2008 and 2018. These maps were also used to delineate groundwater level fluctuations. Figure (6) presents the groundwater contour map for the KSA aquifer based on data from October 2018. According to the map legend, the highest groundwater levels correspond to the recharge areas of the aquifer, including the western regions (southwest, northwest, and west). The area around Isfahan city shows comparatively thinner saturated thickness than other parts of the study area. During the preparation of the groundwater contour map, piezometer well hydrographs from various aquifers were reviewed wherever necessary to verify the accuracy and reliability of the groundwater level data.

To examine groundwater level changes and to draw fluctuation maps, data from the monitoring network of the KSA aquifer for October 2008 and October 2018 were used. The groundwater level fluctuation map between October 2008 and October 2018 is shown in Figure (7). It is observed that the greatest fluctuations in groundwater levels during the ten-year period under study occurred in the western part of the aquifer, which contains a large number of wells and agricultural lands. This area also includes the regions surrounding the Zayandehrud River.

Using geophysical studies conducted across the KSA study area and well log data from exploratory and discharge wells that have

reached the bedrock, the aquifer thickness maps shown in Figures (8 and 9) were prepared for the entire aquifer. The number of exploratory wells within the KSA aquifer is presented in Table (4).

The aquifer thickness in the KSA ranges from approximately 20 meters up to 400 meters in the southern and central parts of the aquifer. The maximum and minimum bedrock elevations observed across the aquifer are 1632 meters and 1057 meters, respectively.

In the previous sections, the groundwater equipotential map based on data from the groundwater monitoring network for October 2018 and the aquifer thickness map were prepared. By combining the groundwater equipotential map and the aquifer thickness map, the saturated thickness map of the aquifer was extracted. This map is presented in Figure (9) for the KSA aquifer.

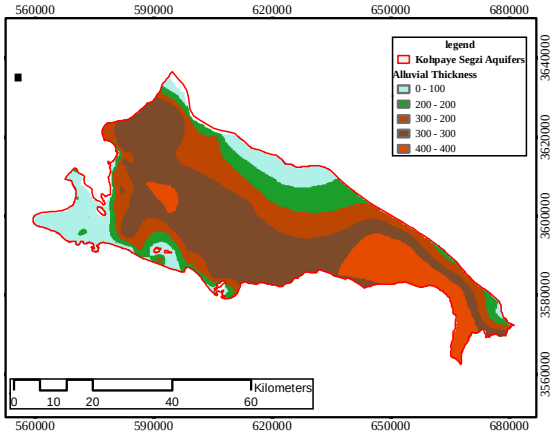



**Fig. 7- Alluvial thickness map**

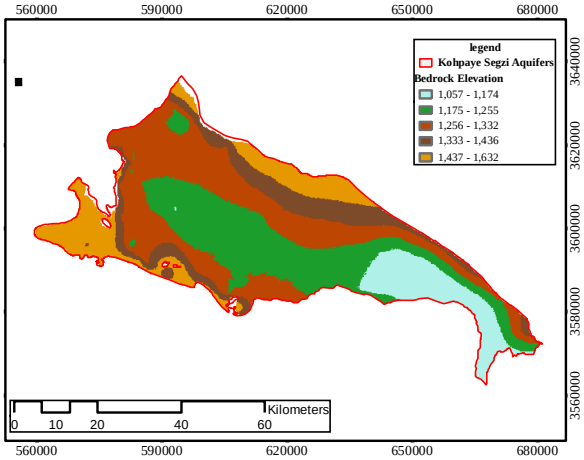



**Fig. 8- Bedrock elevation map**

**Table 4- The Exploratory Wells' data in the KSA Aquifer**

| Number of Exploratory Wells | Exploratory Drilling Depth in Alluvium (m) | Number of Observation Wells Adjacent to Exploratory Wells in Alluvium | Observation Well Depth in Alluvium (m) |
|---|---|---|---|
| 6 | 422 | 2 | 1883 |

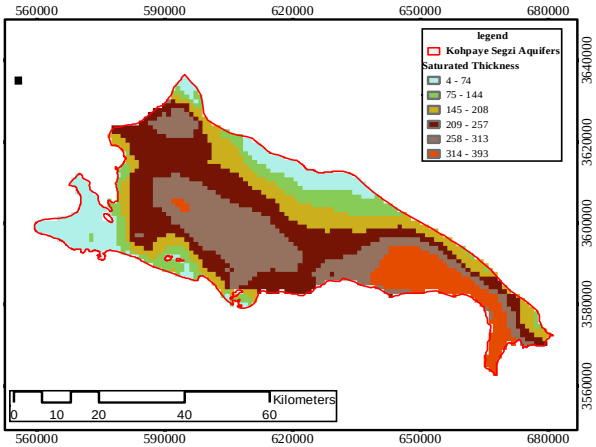



**Fig. 9- Saturated thickness map October 2018**

 *DOI:* 10.22055/jise.2025.49895.2167

**Conventional Pumping Test Methods**

Pumping tests remain the gold standard for determining hydrodynamic parameters like transmissivity and storativity. The Theis (1935) analytical solution forms the foundation:

$S=W(u)Q/4\pi T$ (1)

$u=(r^2 S)/4Tt$ (2)

Here:

s = drawdown (length)

Q = pumping rate (volume per time)

T = transmissivity of the aquifer (length squared per time)

S = storativity (dimensionless)

r = radial distance from the pumping well (length)

t = time since pumping started (time)

W(u) = Theis well function, subsequent developments include:

Type-curve matching (Theis, 1935) for early-time data analysis

Cooper-Jacob approximation (1946) for late-time pumping conditions

Neuman's method (1975) for unconfined aquifers incorporating vertical hydraulic conductivity

**Borehole Logging and Single-Well Techniques**

Recent studies emphasize cost-effective alternatives:

Single-well tests (Hvorslev, 1951; Batu, 1998):

Analyze slug test recovery data using Bouwer-Rice (1976) equations

Borehole geophysical logging:

- Flowmeter logs (Molz et al., 1989) quantify vertical flow variations
- Thermal and resistivity logs infer hydraulic conductivity profiles (Paillet, 2000)
- Acoustic televiewer data enhances fracture network characterization (Williams et al., 2002)

Comparative Studies and Modern Advancements:

Pumping test limitations: High costs and multi-day durations in low-T aquifers (Kruseman and de Ridder, 1990)

Validation studies:

- Quinn et al.(2015) showed <15% discrepancy between pumping tests and combined FLUTe™ liner/flowmeter logging
- Mace (2001) achieved T estimates within 1 order-of-magnitude using pulsed neutron logging

Numerical modeling integration:

- Inverse modeling packages (e.g., MODFLOW-USG, AQTESOLV) resolve heterogeneous parameters
- Machine learning approaches (Xie et al., 2022) reduce interpretation subjectivity

Due to the lack of sufficient data and information related to pumping tests in the study units and their inadequate spatial distribution, this study utilized drilling logs from exploratory, observation, and discharge wells drilled to bedrock, collected from county water authorities and related files, to complete and cover the entire plain area. It is noteworthy that the well logs were prepared based on the theoretical description of the drilled soil. The well drilling logs were obtained from the Isfahan Regional Water Company. Nevertheless, efforts were made to use well logs with higher accuracy, and by referring to grain-size distribution tables Tables (5 and 6), estimates of permeability coefficient (k) and effective porosity. Another important use of the drilling logs was to determine the thickness of the alluvium and the saturated layer.

Since some areas lacked geophysical studies or the geophysical tests were conducted with closely spaced transmitting electrodes that prevented accurate determination of alluvial thickness, drilling logs were used to identify the bedrock and alluvial thickness. Subsequently, based on groundwater equipotential maps drawn from observation well data, the thickness of the saturated layer was determined.

After preparing a thickness map in the KSA aquifer and estimating the permeability coefficient in each of the logs under study using the following equation, the transportability is calculated for each log under study.

$T=k*b$ (3)

In the above equation: T is the transportability, k is the permeability coefficient, and b is the thickness of the aquifer.

**Table 5- Permeability values in various alluvial sediments**

| *Row* | *Sediment Type* | *Permeability (m/d)* | *Group* |
|---|---|---|---|
| 1 | Clay | 0.001–0.1 | K1 |
| 2 | Silt – fine sand, silt and clay | 1–2 | K2 |
| 3 | Mixture of fine sand, coarse sand and clay | 5 | K3 |
| 4 | Clayey fine sand – homogeneous very fine sand – clay, sand and gravel | 7 | K4 |
| 5 | Clayey fine sand – mixture of sand, clay and gravel – sandy clay and sand | 10 | K5 |
| 6 | Mixture of fine, medium sand and some clay – mixture of clayey sand and some gravel – mixture of very fine sand and some gravel | 12 | K6 |
| 7 | Homogeneous fine sand – mixture of sand, sandy clay and gravel – very fine sand, sandy clay, some gravel and pebbles | 15 | K7 |
| 8 | Mixture of fine, medium and coarse sand – mixture of fine gravel, sand and sandy clay | 20 | K8 |
| 9 | Mixture of fine and medium sand – mixture of fine gravel, sand, pebbles and clay | 25 | K9 |
| 10 | Homogeneous medium sand – mixture of pebbles, fine, medium gravel, clay and fine sand | 30 | K10 |
| 11 | Mixture of fine and coarse sand with some gravel | 35 | K11 |
| 12 | Mixture of medium, coarse sand and some gravel – mixture of pebbles, sand, clay and sandy gravel with some gravel | 40 | K12 |
| 13 | Homogeneous coarse sand – mixture of pebbles, gravel and clayey sand | 50 | K13 |
| 14 | Mixture of sand and gravel – mixture of medium and coarse sand, gravel and pebbles | 60 | K14 |
| 15 | Mixture of pebbles, fine, medium gravel and sand | 70 | K15 |
| 16 | Homogeneous fine gravel – mixture of pebbles and medium and fine gravel | 90 | K16 |
| 17 | Clay and medium sand | 110 | K17 |
| 18 | Homogeneous coarse gravel (in terms of size) | 120 | K18 |
| 19 | Homogeneous pebbles | 130 | K19 |

Reference: Kruseman and Ridder, 1990

**Table 6- Effective Porosity Values in Various Alluvial Sediments**

| *Row* | *Sediment Type* | *Effective Porosity (%)* | *Group* |
|---|---|---|---|
| 1 | Clay | 2 | m1 |
| 2 | Sandy clay – sandy silt – clay and fine sand – silt | 4 | m2 |
| 3 | Medium sandy clay | 6 | m3 |
| 4 | Compacted sand – coarse sand and clay – clayey sand – clay, sand and gravel – very fine sand with some gravel – fine compacted gravel, clay | 8 | m4 |
| 5 | Pebbles, gravel, sand and some clay – sandy clay and gravel – fine sand, sandy clay, some gravel and pebbles | 10 | m5 |
| 6 | Gravel, sand and pebbles | 12 | m6 |
| 7 | Sand and pebbles – gravel and pebbles – fine sand | 15 | m7 |
| 8 | Medium sand – coarse sand – fine gravel – gravel and sand | 20 | m8 |
| 9 | Gravel and pebbles | 22 | m9 |

Reference:Batu, 1998

A pumping test is a widely used method to evaluate the hydraulic properties of an aquifer, including its specific yield, transmissivity, and storativity. During the test, groundwater is pumped from a well at a controlled, usually constant rate, while water level drawdowns are measured in the pumping well and nearby observation wells. This process creates a cone of depression around the pumping well, reflecting the aquifer's response to pumping. The drawdown data collected over time allow for the estimation of aquifer parameters by applying analytical or numerical models based on Darcy's law and groundwater flow principles (Singh and Tripura, 2022). How does Figure (11) classify soil textures and show the relationship between grain-size and specific yield.

One important application of pumping tests is the determination of specific yield, which represents the volume of water an aquifer releases from storage per unit decline in the water table. This can be estimated by comparing the volume of water discharged during the test with the volume of dewatered material in the cone of depression. The method involves calculating the volume of the saturated zone that has been drained and relating it to the total pumped volume (Remson and Lang, 1955, Ramsahoye and Lang, 1961). Although the calculation can be complex due to the slow convergence of series solutions, simplified approaches and type-curve methods have been developed to facilitate practical estimation (Gong et al., 2021).

Pumping tests typically last from several hours to days, depending on the aquifer characteristics and the objectives of the test. They provide valuable information not only on specific yield but also on aquifer transmissivity, heterogeneity, and boundary conditions. Moreover, the recovery phase after pumping stops is crucial for verifying the test results and refining parameter estimates (Ramsahoye and Lang, 1961).

Despite their usefulness, pumping tests have limitations, such as assumptions of homogeneous aquifers, no recharge during testing, and idealized boundary conditions. Therefore, combining pumping test results with other methods like grain-size analysis or soil moisture measurements can improve the reliability of specific yield estimates and groundwater resource assessments.

Overall, pumping tests remain a fundamental tool in hydrogeology for characterizing aquifer properties essential for groundwater management and sustainable water supply planning. The different methods of pumping test analysis are listed in Table (7).

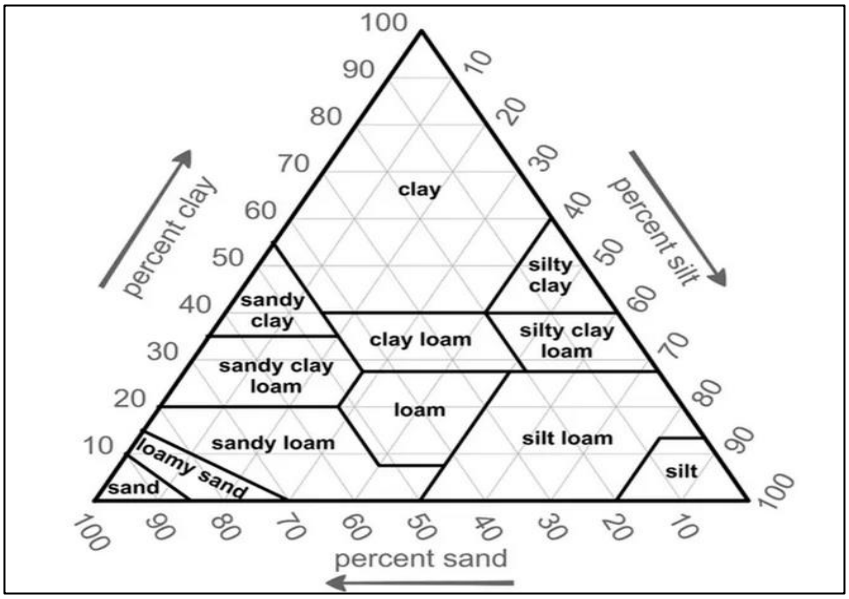



**Fig. 10- Relationship between Grain-Size and Specific Yield (Soil Survey Staff, 1993)**

**Table 4-Pumping test analysis methods**

| Description | Pumping Test Analyses |
|---|---|
| A generalized graphical method for evaluating formation constants and summarizing well field History. (Cooper Jacob Straight Line Method) | Cooper and Jacob, 1946 |
| Constant discharge from a fully penetrating well in a nonleaky aquifer | Theis, 1935 |
| Constant discharge from a fully penetrating well in a nonleaky aquifer | Theis, 1935 (Unconfined) |
| Recovery test after constant discharge from a fully penetrating well in a nonleaky aquifer | Theis, 1946 (Recovery) |
| Constant discharge from a partially penetrating well in a nonleaky aquifer | Hantush, 1961 |
| Constant discharge from a fully penetrating well of finite diameter in a nonleaky aquifer | Papadopulos and Cooper, 1967 |
| Constant discharge from a well in a leaky aquifer with storage of water in the confining beds | Hantush, 1960 |
| Constant discharge from a fully penetrating well in a leaky aquifer | Hantush and Jacob, 1955 |
| Constant discharge from a partially penetrating well in a leaky aquifer | Hantush, 1964 |
| Theory of flow in unconfined aquifers considering delayed response of the water table | Neuman, 1972 |
| Effects of partial penetration on flow in unconfined aquifers considering delayed aquifer response | Neuman, 1974 |
| Double-Porosity Models for a Fissured Groundwater Reservoir with Fracture Skin | Moench, 1984 |
| Transient Flow to a Large-Diameter Well in an Aquifer with Storative Semi Confining Layers | Moench, 1985 |
| Flow to a well of finite diameter in a homogeneous, anisotropic water table aquifer | Moench, 1997 |

Dana and Jwan, (2016)

## Results and Discussion

The minimum thickness of the saturated zone in the piedmont aquifer is 10 meters, with the lowest thickness observed in the southwestern and northern parts of the aquifer. Moving toward the central areas of the aquifer, the thickness of the saturated layer increases. The maximum and average thicknesses of the saturated zone are 392 meters and 224 meters, respectively. The aquifer in this area has two aquifers: confined and unconfined aquifer.

Drilling logs of exploratory, observational, and discharge wells have been analyzed using the grain-size distribution method. In each of the examined logs, the thickness of the first aquifer, the thickness of the impermeable layer between the two aquifers, and the thickness of the confined aquifer must first be determined. In the next step, based on the characteristics and composition of the materials in the unconfined and confined aquifers, the hydraulic conductivity is estimated using reference tables and charts.

Once the thickness of each layer and the estimated hydraulic conductivity for each layer are known, the transmissivities are calculated separately for the first (unconfined) and second (confined) aquifers. Moreover, by identifying the grain-size distribution in the drilling logs, the storage can also be determined using reference charts and tables. However, it should be noted that the storage estimated by the grain-size method is only applicable for the unconfined aquifer, and its estimation for the confined layer using this method is not valid. Confined aquifers have different hydraulic characteristics than unconfined aquifers. The grain-size method doesn't directly account for the compressibility of water and the aquifer matrix, which are the dominant factors in confined aquifer storage. Therefore, using this method for confined aquifers can lead to inaccurate and misleading results.

Figure (12) shows the KSA area with the boundary between the unconfined and confined aquifers. The results obtained from the grain-size analysis method, although

 *DOI:* 10.22055/jise.2025.49895.2167

potentially subject to significant errors due to the theoretical nature of well drilling logs, the inaccuracy in the percentages of soil components, and the unknown physical condition of the soil at depth (such as compaction), have greatly contributed to determining hydrodynamic coefficients when combined with other methods. In other words, from an engineering judgment perspective, comparing the coefficients derived from this method with those from areas where coefficients are known (based on pumping test results in exploratory wells and their comparison with grain-size analysis results from the drilling logs of these wells) has yielded acceptable outcomes. Moreover, the well yields have largely corresponded with the obtained coefficients.

Based on this, out of a total of 65 drilling logs from exploratory, observational, and discharge wells in the second case, 55 logs were selected for examination and analysis using the grain-size distribution method. Additionally, Figure (12) shows the location of the 55 drilling logs under study in relation to the aquifer boundary and the study area.

The estimated hydrodynamic coefficients using the grain-size distribution method have been determined for the drilling logs under study for both aquifers. According to the results obtained, the transmissivity for both aquifers and the storage only for the first (unconfined) aquifer at the water table have been estimated through interpolation methods. In the section “Expansion of Transmissivity”, the section “Interpolation techniques used in GIS” explains the use of different interpolation methods in GIS software as examples. The selection of the best interpolation method is made using aquifer characteristics such as aquifer thickness and annual discharge rate in different areas. It should be noted that the selection of the best method is subject to uncertainty due to limited information. The results, presented in Table (8), show that the minimum, average, and maximum storage at the first aquifer’s water table are estimated to be 2%, 4.6%, and 10%, respectively.

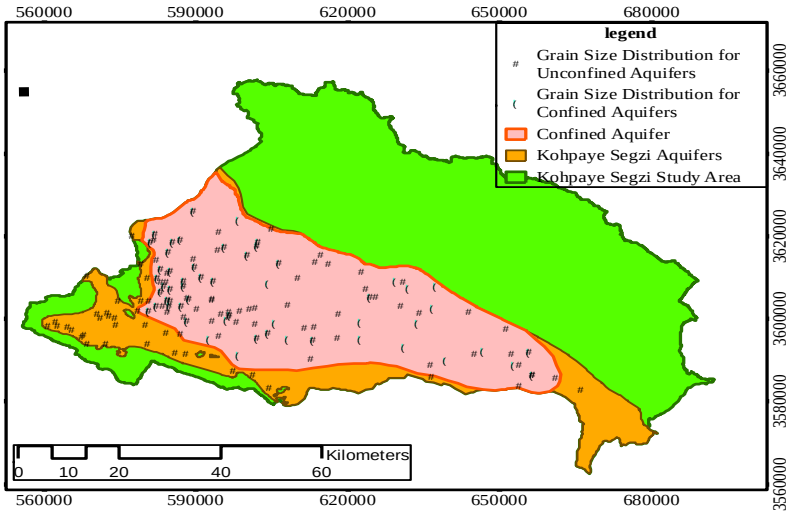



**Fig. 11- Location of the grain-size distribution network for unconfined and confined aquifers**

**Table 5- Results of transmissivity and storage at the KSA Aquifer water table**

| Row | | Transmissivity Coefficient (m²/day) | | | Specific Coefficient (%) | | |
|---|---|---|---|---|---|---|---|
| | | Minimum | Average | maximum | Minimum | Average | maximum |
| 1 | Unconfined Aquifer | 80 | 313.1 | 1237 | 2 | 4.6 | 10 |
| 2 | Confined Aquifer | 177 | 845 | 1704 | - | - | - |

Storativity (*S*) is a dimensionless measure of the volume of water that will be discharged from an aquifer per unit area of the aquifer and per unit reduction in hydraulic head. For a confined aquifer, storativity results only from the rock and fluid compressibilities and is typically very small ($\sim 10^{-4}$–$10^{-5}$). For an unconfined aquifer, the small effect of rock and fluid compressibilities is generally neglected, and *S* is equal to the specific yield ($S_y$), which is defined as the volume of water that will drain under the force of gravity from unit bulk volume of the aquifer. This will be equal to the effective porosity, minus the fractional volume of water retained under gravity drainage by capillary forces (Rackley, 2017).

According to the definitions of storativity and specific yield, the values of storativity coefficients in a confined aquifer using the grain-size method are not valid. Thus, in the present study, only the specific yield in the unconfined has been calculated using the grain-size method. In order to estimate the storativity in the confined aquifer, the pumping test method should be used. The results of two pumping tests are given below. It can be seen that out of the two tests conducted, only test number 2 penetrated the confined layer. However, due to lack of information, the storativity in the confined layer cannot be estimated

Furthermore, the minimum, average, and maximum transmissivity for the first and second aquifers are calculated as 80, 313, and 1237 m²/day, and 177, 845, and 1704 m²/day, respectively.

In Figure (13), the transmissivity map for the second (confined) aquifer is depicted according to the boundary of the second aquifer. Additionally, Figure (14) shows the transmissivity map for the first (unconfined) aquifer derived from the grain-size distribution method, considering the boundary of the first aquifer, which corresponds to the overall boundary of the KSA aquifer.

Two pumping tests have been conducted in the KSA aquifer based on the investigations carried out. As a sample, the analysis of the pumping test using the methods presented in the Materials and Methods section for one of the pumping tests (Well No. 1) is described below. Other pumping tests have also been examined in the same manner, and the final results are presented at the end. Figure (15) shows the locations of two pumping tests conducted in the aquifer. Both tests are located almost near the boundaries of the confined layer.

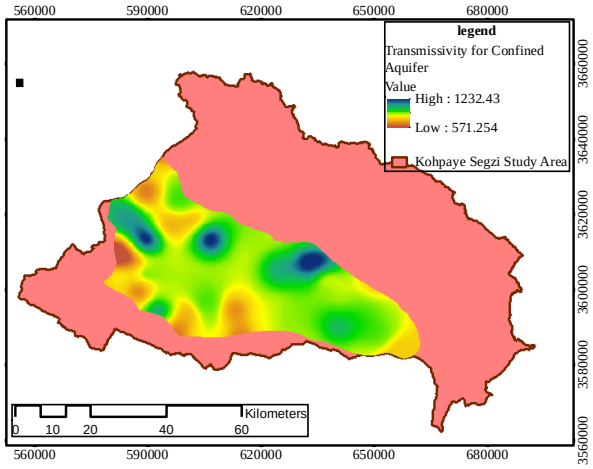



**Fig. 12- Transmissivity map of the confined aquifer based on the grain-size distribution method**

 *DOI:* 10.22055/jise.2025.49895.2167

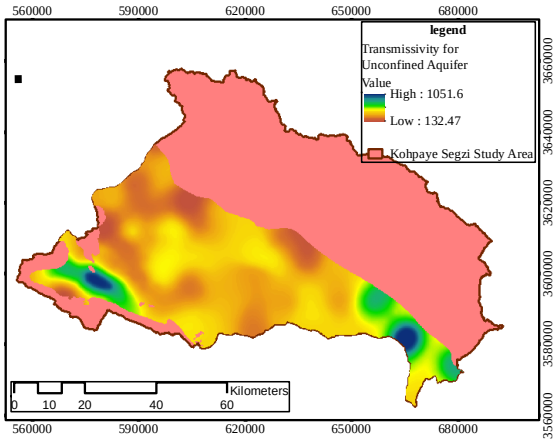



**Fig. 13- Transmissivity map of the unconfined aquifer based on the grain-size distribution method**

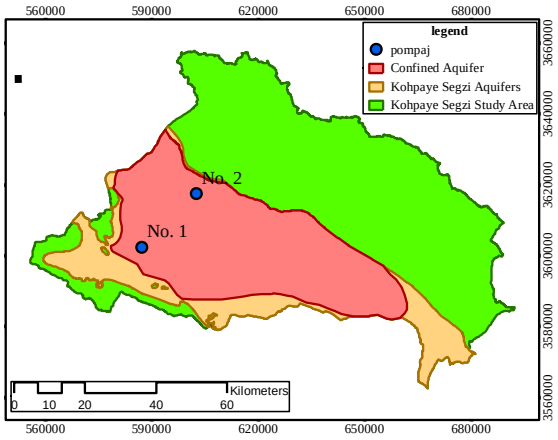



**Fig. 14- Location of pumping tests relative to the KSA aquifer**

**Analysis of Pumping Test for Well No. 1**

The pumping test for Well No. 1 was conducted in 1992 under constant rate conditions (a constant discharge of 1.25 liters per second). The depths of the pumping well and the piezometer were 52 meters and 50 meters, respectively, and the distance between the piezometer and the pumping well was 19 meters. It should be noted that since the pumping and piezometer wells used in this test do not penetrate the entire aquifer—considering that the aquifer thickness at this location is 250 meters—the hydrodynamic parameters of the pumping test need to be evaluated under both unconfined and leaky aquifer conditions for the partially penetrating well. The transmissivity (T) and storage (S) parameters were calculated using the AquiferWin32 software.

Finally, for two reasons, the results of this experiment do not provide a proper estimate of the hydrodynamic coefficients of the aquifer. The first reason is that the well was not drilled through the entire thickness of the aquifer and is not representative of the characteristics of the entire thickness of the aquifer. The other reason is the time of the experiment, which was conducted about 33 years ago, and the groundwater level in this aquifer has decreased significantly in recent years. Therefore, given that the well is located in the first layer (unconfined), the estimation of the hydrodynamic coefficients in this experiment is valid for the first layer. The results of the analysis of pumping test No. 1 using different methods are shown in Figures (16 to 19). Considering the characteristics of the tested well, the best results for estimating hydrodynamic coefficients occurred in the Hantush (leak confined partial penetration) method (Figure 21).

The well depth and aquifer thickness in the second experiment are 165 and 210 meters respectively. In this experiment, the pumping well is not drilled throughout the entire thickness of the aquifer, therefore, the estimated hydrodynamic coefficients in this experiment are slightly lower than reality. The difference between this experiment and experiment number one is that in this experiment, the pumping well is located in the second layer (confined) and the results of the hydrodynamic coefficients represent the characteristics of the confined layer. The characteristics of the two pumping experiments along with the results are shown in Table (9).

**Table 6- Specifications and results of pumping tests**

| Thickness (m) | Q (l/s) | S (%) | T ($m^2$/day) | Depth (m) | zone | Y | X | Name |
|---|---|---|---|---|---|---|---|---|
| 250 | 1.25 | 0.5 | 180 | 52 | 39 | 3602250 | 587250 | No. 1 |
| 210 | 15.2 | 0.9 | 345 | 165 | 39 | 3617480 | 602588 | No. 2 |

**Table 7- Results of the pumping tests in the KSA aquifer**

| Hantush (leak confined partial penetration) | | Hantush | | Neuman | | Recovery | Cooper Jacob | | Theis | | |
|---|---|---|---|---|---|---|---|---|---|---|---|
| T | $S_c$ | T | $S_c$ | T | $S_y$ | T | T | $S_c$ | T | $S_c$ | |
| 180 | 0.005 | 39 | 0.0004 | 34 | 0.0004 | 40 | 43 | 0.0003 | 43 | 0.0003 | No. 1 |
| 345.6 | 0.009 | 139.2 | 0.004 | 75.4 | 0.016 | 300.8 | 192.9 | 0.002 | 153.5 | 0.003 | No. 2 |

Skin effect and partial penetration significantly influence transmissivity estimates by altering the hydraulic conductivity near the well, thus affecting the drawdown behavior during pumping tests. Positive skin reduces effective permeability near the well, causing delayed flow response, while partial penetration limits the vertical extent of flow, both leading to transmissivity variations between methods. These effects must be considered for accurate interpretation (Pasandi et al., 2007).

Table (10) shows the results of the pumping test analysis using the Theis, Cooper and Jacob, Theis Recovery, Neuman, Hantush and Hantush (leak confined partial penetration) methods for the two wells shown in Figure (15). Also, in Figures (16 to 21), the results of the pumping test analysis for pumping test No. 1 are given as an example, and for pumping test No. 2, only the values of the results are included in Table (10). According to the above explanation about the characteristics of the tests performed, among the analyses performed, because the mentioned wells were not drilled throughout the entire thickness of the aquifer, the best analysis is to use the Hantush (leak confined partial penetration) method.

Pumping tests are among the most expensive methods for estimating hydrodynamic coefficients. Because in this method, two wells must first be drilled. One well is used as a pumping well whose depth is equal to the thickness of the aquifer, and the other well is used to record water level information during and after the test. In the KSA aquifer, only two pumping tests have correct information for analyzing the test and estimating hydrodynamic coefficients. Thus, the number and dispersion of pumping tests in the 2940 $km^2$ aquifer are very small. One of the main limitations of this study is the lack of an appropriate number of pumping tests and their dispersion across the KSA aquifer. This makes the grain-size method have the greatest impact on the estimation of hydrodynamic coefficients, which causes uncertainty in the estimation of coefficients.

**Expansion of Hydrodynamic Coefficients by Integrating Results from Grain-size and Pumping Tests**

**Expansion of Transmissivity**

The information used to draw the transmissivity map includes transmissivity values obtained from grain-size and pumping test methods, expansion of transmissivity using geophysical mapping techniques, well discharge distribution maps, and drainage network maps. The significance of each of these data sets is incorporated as different layers within GIS software. As mentioned in the previous sections, the dispersion of information in the grain-size method is much better than the pumping test method. However, in areas where pumping tests have not been conducted, only the results of the grain-size method have been used. In areas where pumping tests are available, the results of both methods have been combined and refined. Finally, using the data imported into the

 *DOI:* 10.22055/jise.2025.49895.2167

software, the priority of utilizing these data, various interpolation methods within the GIS software, and engineering judgment were applied to prepare the transmissivity map, which is shown in Figure (22).

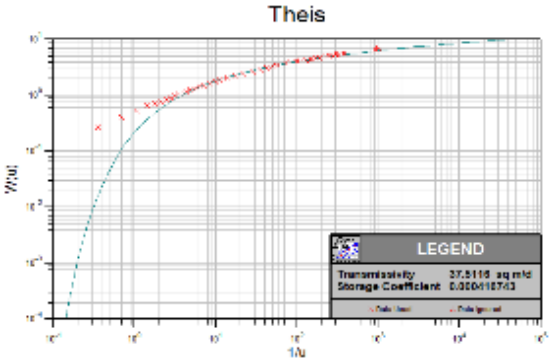



**Fig. 15- Estimation of the storage and transmissivity of Pumping Well No. 1 using the Theis method**

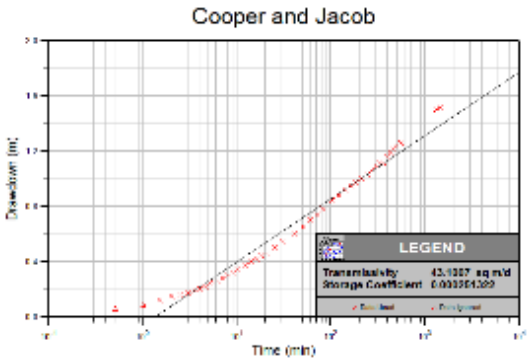



**Fig. 16- Estimation of the storage and transmissivity of Pumping Well No. 1 using the Cooper-Jacob method**

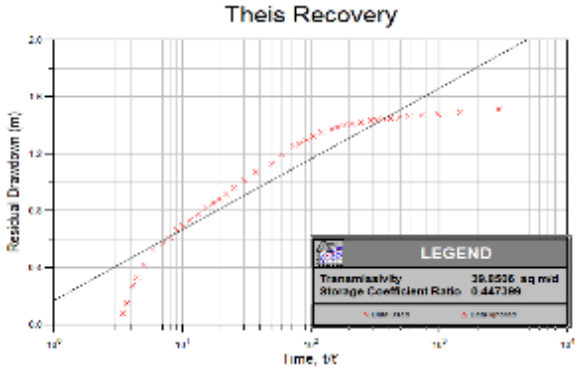



**Fig. 17- Estimation of the transmissivity of Pumping Well No. 1 using the Thiem recovery method**

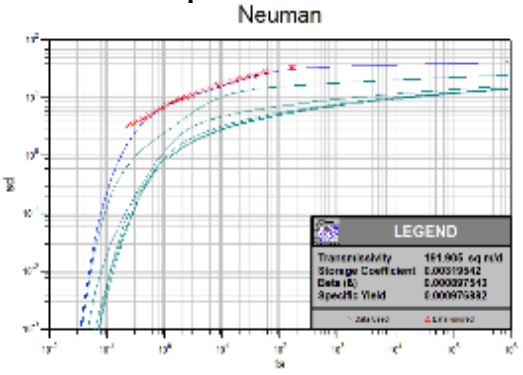



**Fig. 18- Estimation of the storage and transmissivity of Pumping Well No. 1 using the Neuman method**

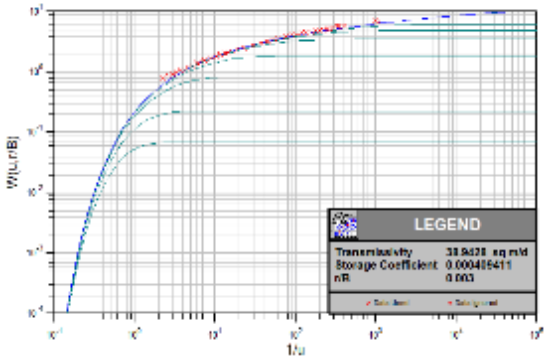



**Fig. 19- Estimation of the storage and transmissivity of Pumping Well No. 1 using the Hantush method**

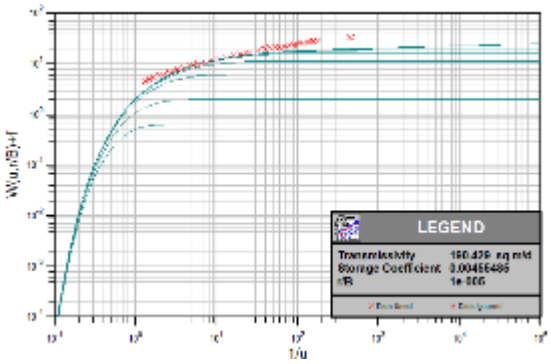



**Fig. 20- Estimation of the storage and transmissivity of Pumping Well No. 1 using the Hantush (leak confined partial penetration) method**

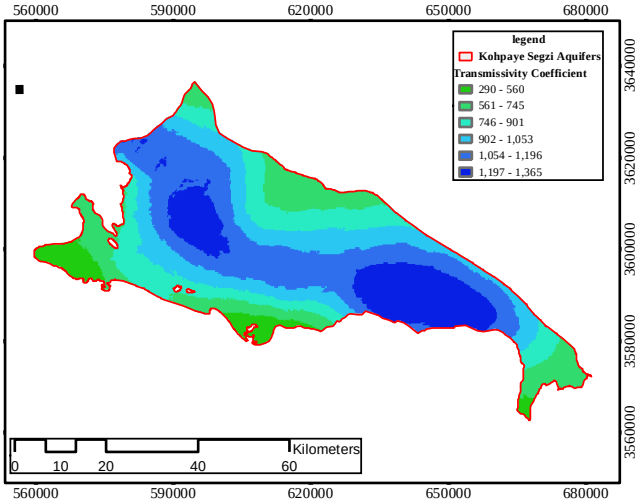



**Fig. 21- Distribution map of transmissivity (Unconfined Aquifer)**

**Table 8- Values of error evaluation criteria for each interpolation method**

| Row | Error evaluation method | Interpolation method | | | | | | | |
|---|---|---|---|---|---|---|---|---|---|
| | | IDW | GPI | RBF | LPI | OK | SK | UK | EBK |
| 1 | MARE | 0.04 | 0.53 | 0.09 | 0.15 | 0.12 | 0.14 | 0.35 | 0.13 |
| 2 | RMSE | 45.92 | 293.86 | 81.01 | 120.78 | 80.19 | 91.08 | 190.53 | 86.81 |
| 3 | R | 0.99 | 0.5 | 0.96 | 0.92 | 0.96 | 0.95 | 0.79 | 0.96 |

**Interpolation techniques used in GIS**

This section explains the steps for selecting the best interpolation method in GIS software for mapping the transportability. For this purpose, the Geostatistical Analyst tool in ARCGIS software was used to apply deterministic and geostatistical methods for interpolation. The methods used include eight methods: IDW, GPI, RBF, LPI, OK, SK, UK, and EBK. The selection of the best interpolation method was based on cross-evaluation criteria and estimation errors such as MARE, RMSE, and R.

The choice of interpolation method depends primarily on the nature of the variable and its spatial variations. Although it is influenced by other factors, it is very difficult to provide a correct and general rule for choosing a method. Among the methods used, the UK, GPI and RBF methods have a weaker distribution of the transportability than the other methods, because in the eastern and border areas of the watershed, high values for the coefficient have been estimated, which is inconsistent with the reality of the region. The changes in the transmission in the OK, SK, EBK, IDW and LPI methods have greater suitability with the characteristics of the study area. However, to achieve the best method, the three UK, GPI and RBF methods are eliminated at this stage and the best interpolation method must be selected from the five OK, SK, EBK, IDW and LPI methods.

In the next step, based on selected points from the available data, the values of error criteria were used to evaluate the interpolation methods. In this study, three validation methods for each of the deterministic and geostatistical interpolation methods were evaluated and investigated to achieve this goal. The results obtained in Table (11) show that the lower the estimated errors and the higher the data correlation, the more suitable the interpolation method is for preparing the transportability zoning maps. Therefore, considering the error evaluation criteria, the best interpolation method is the inverse distance weighting (IDW) method.

To realistically estimate maps generated from interpolation, it is essential to provide an uncertainty estimate for these maps. Uncertainty estimation refers to the process of

 *DOI:* 10.22055/jise.2025.49895.2167

quantifying the degree of doubt associated with the results. This process typically involves identifying various sources of error and conducting statistical analyses. The goal of uncertainty estimation is to provide a range of possible values within which the model outputs are likely to lie with a high probability. This aids decision-makers in considering the confidence level of the results and making better-informed decisions. One of the simplest methods to assess uncertainty involves using statistical metrics such as the MARE (Beven, 2001). In this study, the MARE statistic was employed to estimate the uncertainty of the generated maps. Therefore, the uncertainty in the transmissivity maps is estimated to be ±0.04 (±4%).

To draw other maps using the interpolation method in GIS software, the above steps were performed similarly to select the best interpolation method.

The map of the KSA aquifer indicates that the highest values of this coefficient occur along and around the Zayandehrud River. Despite the considerable thickness of the aquifer in the northern boundaries and areas adjacent to the Gavkhouni wetland, the significant increase in clay and silt content in the grain-size distribution of the sediments indicates a low transmissivity in these regions.

Based on the final results, the average, minimum, and maximum values of the transmissivity in unconfined aquifer are 961, 290, and 1364 square meters per day (Figure 22) and the average, minimum, and maximum values of the transmissivity in confined aquifer are 914, 571, and 1232 square meters per day Figure (23), respectively.

**Expansion of Storage**

To prepare an integrated map of the storage across the KSA aquifer, various data obtained from grain-size analysis and pumping test interpretations were first imported into GIS software. According to the groundwater flow equations under steady-state and transient conditions presented below, in steady-state conditions (related to the first equation), hydraulic conductivity and ultimately transmissivity can be calculated by knowing the saturated thickness of the aquifer. However, to calculate the storage, a time series of available data is required, in which case the second equation describing transient flow conditions is used.

1. Steady-State Flow Equation (Fetter, 2001):

$$\left[K_x \frac{\partial h}{\partial x}\right] + \left[K_y \frac{\partial h}{\partial y}\right] + \left[K_z \frac{\partial h}{\partial z}\right] = 0 \quad (4)$$

2. Transient Flow Equation (Todd, 1980):

$$\left[K_x \frac{\partial h}{\partial x}\right] + \left[K_y \frac{\partial h}{\partial y}\right] + \left[K_z \frac{\partial h}{\partial z}\right] = S_y \frac{\partial h}{\partial t} \quad (5)$$

To prepare an integrated map of the storage across the KSA aquifer, various data obtained from grain-size analysis and pumping test interpretations were first imported into GIS software. One useful dataset aiding the creation of the integrated storage map is the fluctuations observed in piezometer wells within the aquifer.

Initially, based on the available statistical period from the provincial piezometer monitoring network, a hydrological year with complete data was selected. Then, for the selected year, the groundwater level for each well was considered on a monthly basis. Using the groundwater level data for the 12 months of the selected hydrological year for each piezometer, the annual standard deviation of groundwater levels was estimated for each well. The standard deviation values of groundwater levels have been used as a qualitative guide to draw an integrated map of the storage.

Based on the calculated standard deviation for each piezometer, a map of the groundwater level standard deviation for the piezometers in the selected year was drawn. It is worth noting that the groundwater level standard deviation

map can only be used to estimate the storage if the aquifer is in a state of equilibrium.

In such conditions, areas with low groundwater level fluctuations correspond to higher storage values, while areas with high fluctuations in groundwater levels correspond to lower storage values.

Finally, based on the estimated data and the aforementioned explanations, by directly using the storage values estimated from both grain-size analysis and pumping tests, as well as expanding this coefficient using the aforementioned maps in areas lacking direct storage estimates, an integrated storage map for the KSA aquifer was prepared and is shown in Figure (24). Changes in the storage in the KSA aquifer varies between 1.3% and 9.3%, with an average value of 3.9%.

As mentioned in the previous sections, the storage coefficient in a confined aquifer cannot be calculated using the grain-size method, and more pump tests must be conducted within the aquifer to estimate the storage coefficient of the confined layer.

Studies conducted in recent years show that the two methods of pumping tests and grain-size are capable of accurately estimating the hydrodynamic coefficients of an aquifer. Most studies that have dealt with groundwater modeling have used the results and analysis of pumping tests to obtain real information and have examined the efficiency of their model using the results of pumping tests (Li et al., 2025; Muauz et al., 2024; Singh and Tripura, 2022). Hydrodynamic coefficients estimated from pumping test analysis have very high acceptability in confined and unconfined aquifers (Bashandy et al., 2024).

Houben et al. (2022) used the drilling logs of observation wells to estimate and identify aquifer layers for groundwater modeling. The above-mentioned studies are among the studies that used the pumping test or grain-size method to estimate the initial and actual transportability and storage in the aquifer.

In the present study, both pumping test and grain-size methods were used to estimate the transportability and storage in the KSA aquifer in Isfahan province, Iran. Finally, the maximum, minimum, and average values of hydrodynamic, such as the transmissivity and storage of the KSA aquifer, are described in Table (12).

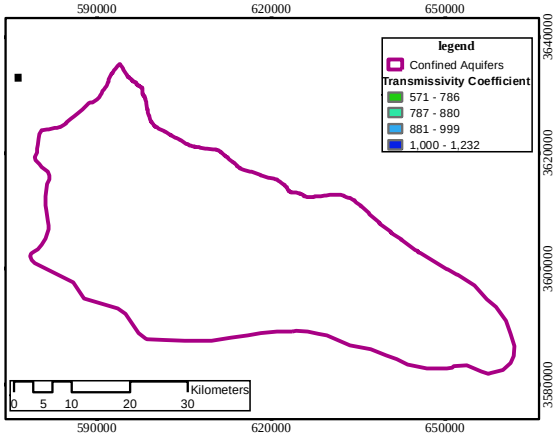



**Fig. 22- Distribution map of transmissivity (confined Aquifer)**

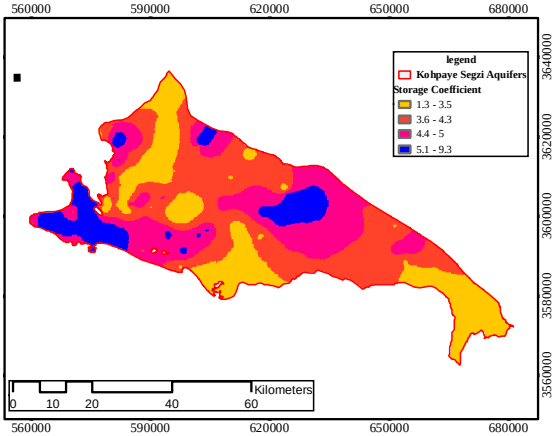



**Fig. 23- Distribution map of storage (Unconfined Aquifer)**

**Table 9- Final values of hydrodynamic coefficients**

| Row | | *Transmissivity Coefficient (m²/day)* | | | *Storage Coefficient (%)* | | |
|---|---|---|---|---|---|---|---|
| | | Minimum | Average | maximum | Minimum | Average | maximum |
| 1 | Unconfined Aquifer | 290 | 1364 | 961 | 1.3 | 9.3 | 3.9 |
| 2 | Confined Aquifer | 571 | 1232 | 914 | - | - | - |

 *DOI:* 10.22055/jise.2025.49895.2167

**Conclusions**

- Based on the conducted investigations, the greatest saturated layer thickness is approximately 390 meters near the Gavkhouni wetland, while the smallest saturated thickness in the KSA aquifer occurs in the mountainous slopes near the city of Isfahan, estimated at about 10 meters.
- In total, 206 well logs were collected across the studied aquifers, of which approximately 186 logs were deemed suitable for estimating hydrodynamic coefficients.
- In the grain-size analysis method, by examining the drilling logs of exploratory, observational, and production wells, the suitability of each log was first evaluated using parameters such as geological maps, the drainage network of production wells, groundwater flow lines, and groundwater level contours. Subsequently, based on charts and tables from references, hydraulic conductivity and storage values were estimated.
- The Results obtained from the analysis of pumping tests in perfectly permeable wells or wells assumed to be perfectly permeable show that the storage values in most of the cases analyzed indicate that the Hantush (leak confined partial penetration) method provides more reliable storage estimates compared to the Theis, Cooper-Jacob, and Neuman methods.
- According to the final studies, the average storage in the KSA aquifer is estimated at 3.9%, the average alluvial thickness is 200 meters, and the average transmissivity of the aquifer is estimated at 960 square meters per day.

The methods used in this study are pumping test and grain-size to estimate hydrodynamic coefficients in the KSA aquifer. It is necessary to consider uncertainty in estimating the transferability and storage. However, in this study, computational errors have been minimized. In the grain-size method, well drilling logs that have been prepared with high accuracy and quality have been used. The number of pumping tests is limited due to the aquifer area. Also, an attempt has been made to select the best interpolation method for extracting transportability and storage maps using error evaluation criteria.

**Recommendations**

Given the importance of the hydrodynamic coefficients of the aquifer, it is necessary to conduct various studies in the future to increase the accuracy of the calculations. Given that pumping tests are expensive, in order to achieve better results in the analysis of pumping tests, it is recommended to improve the quality of pumping tests. Before performing a constant-speed pumping test, a step test should be performed in the pumping well for 24 hours and the drop in the same pumping well should be recorded in order to obtain well information. After calculating the well specifications, including efficiency, critical flow rate, maximum allowable flow rate, critical drop, etc., pumping should not be performed in the well for 24 hours until the water level returns to the initial level. Then, in the next step, a constant-flow pumping test can be performed and the drop in the piezometer well can be measured.

In order to increase the accuracy of estimating hydrodynamic coefficients by the grain-size method, it is recommended that when drilling any new well, whether exploratory, observational, or operational, the well drilling supervisor prepares disturbed or undisturbed samples during drilling and takes the said samples to the geophysical laboratory to accurately determine the amount and percentage of different particles in the composition of the sample taken. Also, in this regard, a grain-size curve can be prepared for the samples under test. In this case, a drilling log can be prepared with much higher accuracy than in the past.

In future studies, it is suggested that the results of the present study be used as baseline information to develop and calibrate a numerical groundwater flow model in the KSA aquifer. This will provide a powerful tool for sustainable water management in the study basin.

**Acknowledgment**

This research has no acknowledgments.

**Conflict of Interest**

The authors declared no potential conflicts of interest concerning the research, authorship, and publication of this article**.** Confirmation.

**Funding**

The authors received no financial support for the research, authorship, and publication of this article.

**Data Availability Statements**

Data Availability Statement: All information and results are presented in the text of the article.

**Authors' contribution**

**First Author**: Sheyda Mohammadi Fard, Data analysis.

**Second Author:** Jahangir Abedi-Koupai Results and Discussion.

**Third Author:** Saeid Eslamian, Article writing.

**References**

1- Ansarifar, M., Salarijazi, M., Ghorbani, K. and Kaboli, A., 2019. Spatial estimation of aquifer's hydraulic parameters by a combination of borehole data and inverse solution. *Bulletin of Engineering Geology and the Environment*. DOI:10.1007/s10064-019-01616-w

2- Batu, V., 1998. *Aquifer Hydraulics: A Comprehensive Guide to Hydrogeologic Data Analysis*. Wiley, New York.

3- Bashandy, A.M., Bekhit, H.M. and Radwan, H.G., 2024. Uncertainty assessment of aquifer hydraulic parameters from pumping test data. *Appl Water Sci, 14(84).* DOI: 10.1007/s13201-024-02134-1

4- Benson, D.A., 2023. Automated Estimation of Aquifer Parameters from Arbitrary-Rate Pumping Tests in Python and MATLAB. *Groundwater, 62 (2),* pp. 285-294. DOI: 10.1111/gwat.13338

5- Beven, K., 2001. *Rainfall-Runoff Modelling: The Primer*. Wiley.

6- Bouwer, H. and Rice, R.C., 1976. Slug test for determining hydraulic conductivity of unconfined aquifers with completely or partially penetrating wells. *Water Resources Research, 12(3),* pp.423–42.

7- Cooper, H.H. and Jacob, C.E., 1946. A generalized graphical method for evaluating formation constants and summarizing well-field history. *Trans. Am. Geophys. Union, 27, 526-534.*

8- Dana, K. M. and Jwan, S. M., 2016. Performing Pumping Test Data Analysis Applying Cooper-Jacob's Method for Estimating of the Aquifer Parameters. *Mathematical Modelling in Civil Engineering, 12(1),* pp.9-20. DOI: 10.1515/mmce-2016-000

9- Domenico, P.A. and Schwartz, F.W., 1990**.** *Physical and Chemical Hydrog*eology. Wiley.

10- Fetter, C.W., 2001. *Applied Hydrogeology* (4th ed.). Prentice Hall. ISBN: 978-0130882394.

11- Gong, C., Zhang, Z., Wang, W., Duan, L. and Wang, Z., 2021. An assessment of different methods to determine specific yield for estimating groundwater recharge using lysimeters. *Science of The Total Environment, 788,* pp.147799. DOI: 10.1016/j.scitotenv.2021.147799

12- Houben, T., Pujades, E., Kalbacher, T., Dietrich, P. and Attinger, S., 2022. From Dynamic Groundwater Level Measurements to Regional Aquifer Parameters— Assessing the Power of Spectral Analysis. *Water Resources Research, 58, pp.* DOI: 10.1029/2021WR031289

13- Hvorslev, M.J., 1951. Time lag and soil permeability in groundwater observations. Waterways Experiment Station, Corps of Engineers, Vicksburg, Mississippi, Bulletin 36.

14- Kruseman, G. P. and de Ridder, N.A., 1990. Analysis and Evaluation of Pumping Test Data. International Institute for Land Reclamation and Improvement (ILRI), Wageningen, The Netherlands.

15- Li, M., Wang, H., Gu, H. and Chi, B., 2025. Weighted joint curve inversion of aquifer parameters in pumping tests with multiple observation wells. *Desalination and Water Treatment*. *321, 101040.* DOI:10.1016/j.dwt.2025.101040

16- Li, M., Liang, X., Xiao, C., Cao, Y. and Hu, S., 2019. Hadrochemical Evolution of Groundwater in a Typical Semi-Arid Groundwater Storage Basin Using a Zoning Model. *Water, 11, 1334*. DOI: 10.3390/w11071334

17- Li, P. and Qian, H., 2012. Global curve-fitting for determining the hydrogeological parameters of leaky confined aquifers by transient flow pumping test. *Arab J Geosci, 6*, pp.2745‑2753. DOI: 10.1007/s12517-012-0567-9

18- Li, Y., Xie, W., Wang, H., Peng, B., Xiong, F. and Zhu, C., 2023a. Hydrogeological Parameter Estimation of Confined Aquifer within a Rectangular Shaped Drop Waterproof Curtain. *Water, 15, 356.* doi: DOI: 10.3390/w15020356

19- Li, Y., Zhou, Z., Zhuang, C. and Dou, Z., 2023b. Estimating Hydraulic Parameters of Aquifers Using Type Curve Analysis of Pumping Tests with Piecewise-Constant Rates. *Water, 15(9),* pp.1661. DOI: https://doi.org/10.3390/w15091661

20- Lohman, S.W., 1972**.** *Ground-Water Hydrauli***cs**. U.S. Geological Survey Professional. pp 708.

21- Mace, R.E., 2001. *Estimating transmissivity using specific-capacity data.* Geological Circular 01-2Affiliation: Bureau of Economic Geology, The University of Texas at Austin.

22- Molz, F.J., Melville, J.G. and Johnson, M.M., 1989. Using flowmeter logs to quantify vertical flow variations in wells. *GroundWater, 27(5),* pp.631–638.

23- Muauz, A., Behailu, B. and Bediru, H., 2024. Application of surface geophysical investigations and pumping test data analysis for better characterization of aquifer hydraulic parameters, Upper Awash Sub-Basin, Central Ethiopia. *Journal of Hydrology: Regional Studies, 55, 101933*. DOI: https://doi.org/10.1016/j.ejrh.2024.101933

24- Neuman, S.P., 1975. Analysis of pumping test data from anisotropic unconfined aquifers considering delayed gravity response. *Water Resources Research, 11(2),* pp.329-342.

25- Paillet, F. L., 2000. Hydraulic conductivity estimation from borehole flow and thermal logs. *Ground Water, 38(6),* pp.885–894.

26- Pasandi, M., Samani, N. and Barry, D.A., 2007. Effect of wellbore storage and finite thickness skin on flow to a partially penetrating well in a phreatic aquifer. *Journal of Applied Geophysics*, 63(1), 27-38. DOI: 10.1016/j.jappgeo.2007.09.003

27- Quinn, P., Cherry, J.A. and Parker, B.L., 2015. Combined use of straddle packer testing and FLUTe profiling for hydraulic testing in fractured rock boreholes. *Journal of Hydrology, 524, pp. 439-454.* DOI: 10.1016/j.jhydrol.2015.03.008

28- Rackley, S., 2017. 15 - Hydrological and environmental features, events, and processes. *Carbon Capture and Storage (Second Edition).* pp 387-406. DOI:10.1016/B978-0-12-812041-5.00015-5

29- Ramsahoye, L.E. and Lang, S.M., 1961. A Simple Method for Determining Specific Yield from Pumping Tests.

31- Remson, I. and Lang, S.M., 1955. A pumping-test method for the determination of specific yield. *Eos, Transactions American Geophysical Union. 36(2),* pp.321-325.

32- Sahranavard, H., Mohtashami, A., Mohtashami, E. and Akbarpour, A., 2023. Inverse modeling application for aquifer parameters estimation using a precise simulation–optimization model. *Applied Water Science*, pp. 1-12. DOI: 10.1007/s13201-022-01864-4

33- Singh, S. and Tripura, J., 2022. Pumping test analysis for assessment of hydraulic parameters and aquifer system formation in hilly terrain. *Water Practice & Technology, 00 (0),* pp.1-11. DOI: 10.2166/wpt.2022.002

34- Soil Survey Staff., 1993. *Soil Survey Manual. U.S.* Department of Agriculture, Handbook 18.

35- Theis, C.V., 1935. The relation between the lowering of the piezometric surface and the rate and duration of discharge of a well using groundwater storage. *Transactions, American Geophysical Union, 16(2),* pp.519-524.

36- Todd, D.K., 1980. *Groundwater Hydrology (2nd ed.).* John Wiley & Sons. ISBN: 978-0471058574.

37- Williams, J.H., Paillet, F.L. and Kuniansky, E.L., 2002. Use of acoustic televiewer data to characterize fracture networks in boreholes. *Hydrogeology Journal, 10(2),* pp.238–247.

38- Xie, Z., Liu. W., Chen, S., Yao, R., Yang, C., Zhang, X., Li, J., Wang, Y. and Zhang, Y., 2022. Machine learning approaches to reduce interpretation subjectivity in hydrogeological modeling. *Journal of Hydrology: Regional Studies, 58,* pp-102227. DOI: 10.1016/j.ejrh.2025.102227

© 2026 The Author(s). Published by Shahid Chamran University of Ahvaz. This is an open-access article distributed under the terms of the Creative Commons Attribution License (http://creativecommons.org/licenses/by/4.0), which permits unrestricted use, distribution, and reproduction in any medium, provided the original work is properly cited.

Shahid Chamran University of Ahvaz

**Irrigation Sciences and Engineering (JISE)**
**Vol. 48, No. 4, Winter 2026, p. 105-115**

Journal homepage: https://jise.scu.ac.ir

**Research Paper**

# Debris Blockage Risk of Modified Stepped Spillways: A Laboratory Study on Obstacle Configuration

Seyed Amin Asghari Pari[1], Seyed Ali Asghari Pari[2*], Mohammad Amin Mokarram[3] and Mojtaba Kordnaeij[4]

*1- Department of Civil Engineering, Faculty of Engineering, Behbahan Khatam Alanbia University of Technology, Behbahan, Iran.*
*2*- Corresponding Author, Department of Civil Engineering, Faculty of Engineering, Behbahan Khatam Alanbia University of Technology, Behbahan, Iran. (asgharipari@bkatu.ac.ir).*
*3- Department of Civil Engineering, Faculty of Engineering, Behbahan Khatam Alanbia University of Technology, Behbahan, Iran.*
*4- Department of Civil Engineering, Faculty of Engineering, Behbahan Khatam Alanbia University of Technology, Behbahan, Iran.*

**ARTICLE INFO**

*Artlcle history:*
Received: 07 August 2025
Revised: 24 November 2025
Accepted: 14 December 2025
Available online: 04 January 2026

*Keywords:*
Stepped Spillway; Floating Debris; Blockage Risk; Dam Safety; Energy Dissipation; Hydraulic Structures; Experimental Hydraulics; Dam Failure.

**TO CITE THIS ARTICLE:**

Asghari Pari, S. A., Asghari Pari, S. A., Mokarram, M. A., Kordnaeij, M. 2026. 'Debris Blockage Risk of Modified Stepped Spillways: A Laboratory Study on Obstacle Configuration', *Irrigation Sciences and Engineering*, 48(4), pp. 105-115. doi: 10.22055/jise.2025.50358.2173.

**Abstract**

Stepped spillways are critical hydraulic structures for energy dissipation, but their performance can be significantly compromised by floating debris. This study experimentally investigates the hydraulic behavior of floating debris on a stepped spillway under three distinct configurations: (1) an unobstructed baseline, (2) continuous on-step obstacles, and (3) discontinuous on-step obstacles. Experiments were conducted in a 1.2-meter-wide laboratory flume under three flow regimes—nappe, transition, and skimming—corresponding to relative critical depths (dc/h) of 0.47, 0.85, and 1.09, and with varying relative obstacle heights (ho/h) from 0.19 to 0.76. Results demonstrate that, in the baseline configuration, debris passed with only a minor delay of 1–3 seconds. For the continuous obstacle configuration, increasing obstacle height significantly enhanced debris conveyance by promoting a "pooling effect" that reduced trapping probability by up to 90% compared to lower heights, virtually eliminating trapping for ho/h ≥ 0.38. Conversely, discontinuous obstacles, particularly under nappe flow conditions, induced stable and extensive blockages with trapping probabilities exceeding 70% for large debris. The presence of debris in the skimming flow regime led to a minor reduction in energy dissipation (up to 5–10%) due to altered surface flow patterns, but no significant changes in discharge coefficient were observed. The findings reveal a critical design paradox: the hydraulic mechanisms that make discontinuous obstacles effective for energy dissipation (up to 39% increase over baseline) are the same mechanisms that cause catastrophic debris trapping. This research provides crucial insights for risk-based design, suggesting that for catchments with high debris loads, continuous obstacles are a more resilient solution despite their lower energy dissipation efficiency (5–15% decrease compared to baseline).

## Introduction

Stepped spillways are a cornerstone of modern hydraulic engineering, designed to safely convey floodwaters while dissipating the kinetic energy of high-velocity flows, thereby mitigating downstream erosion and

 *DOI:* 10.22055/jise.2025.50358.2173

ensuring dam safety (Bekheet et al., 2025; Chanson, 2002). The energy dissipation is achieved through complex, highly aerated flow dynamics over the steps, which are typically classified into nappe, transition, and skimming flow regimes (Sánchez-Juny et al., 2022). However, the hydraulic performance of these structures can be severely compromised by the presence of floating debris, particularly Large Woody Debris (LWD), which is frequently mobilized during extreme flood events (Hassan, 2000; Rundqvist, 2005). The accumulation and subsequent blockage of spillways by debris is a globally recognized threat to dam safety. Historical incidents, such as the 1978 Palagnedra dam overtopping in Switzerland, underscore its catastrophic potential (Rundqvist, 2005). Debris can obstruct spillway openings, leading to a significant reduction in discharge capacity, increased upstream water levels (backwater effects), and, ultimately, structural failure (Yang and Stenström, 2011). The generation and transport of floating debris are complex phenomena governed by catchment-specific characteristics, including geology, topography, forest cover, and hydrology (Iqbal and Riaz, 2024; Rundqvist, 2005). High-intensity rainfall can trigger landslides and bank erosion, introducing large volumes of woody and vegetative matter into fluvial systems. The interaction of this debris with hydraulic structures is a pervasive issue, impacting not only dam spillways but also bridges, culverts, and in-stream structures like rock weirs (Bezzola et al., 2017; Margetts, 2022; Pagliara and Carnacina, 2011). Effective risk management, therefore, necessitates a holistic approach, integrating strategies for controlling debris yield, intercepting debris upstream, and designing resilient hydraulic structures capable of safely passing debris (Rundqvist, 2005 Al-Jubouri et al., 2022).

A substantial body of research has focused on understanding the fundamental mechanisms of debris blockage. A critical dimensionless parameter identified in numerous studies is the ratio of the debris element's characteristic dimension (D) to the upstream flow depth or head (H). For instance, Mansouri and Ahadiyan (2016) demonstrated that blockage probability is highly sensitive to D/H, approaching 100% for D/H > 1 and becoming negligible for D/H < 0.3. These findings highlight that the relative scale of debris to the flow is a dominant factor, which often leads to significant backwater effects correlated with the approach flow Froude number and the density of the debris accumulation (Hartlieb, 2017). Additionally, scale modeling techniques have been employed to investigate wooden debris accumulation at debris racks, providing insights into accumulation patterns and blockage risks (Schmocker and Hager, 2013).

In recent years, numerous studies have investigated the risk of blockage in non-stepped spillway structures—such as piano key weirs (PKWs) and crown wheel weirs—by floating debris. For instance, Habibi and Lashkar-Ara (2018) demonstrated that the gradual accumulation of floating debris at crown wheel weirs leads to a significant rise in upstream water levels and a marked reduction in discharge capacity. In a related study, they (Habibi and Lashkar-Ara, 2020) examined the influence of the slenderness coefficient of wooden debris on blockage probability at CPK weirs, showing that elongated, slender debris elements are more prone to entrapment within structural gaps. Furthermore, Habibi and Lashkar-Ara (2021) assessed blockage probability across consecutive experimental cycles and highlighted that debris behavior under single-event and cumulative conditions can differ substantially. Collectively, these studies—alongside other research in the field of hydraulic structure blockage—underscore that both the geometric configuration of the structure and the physical characteristics of floating debris play decisive roles in blockage dynamics.

While the issue of debris on conventional spillways has been studied Pfister et al, (2013) and Yang et al, (2009), the literature on stepped spillways has predominantly focused on enhancing their primary function: energy dissipation. Numerous studies have explored on-step modifications such as obstacles, sills, and baffle blocks to increase flow turbulence

and improve energy dissipation rates (Bekheet et al., 2025; Kordnaeij et al., 2023; Mikalsen and Thorsen, 2023). However, a critical research gap exists at the intersection of these two domains. The simultaneous effect of on-step energy-dissipating obstacles on the passage of floating debris remains poorly understood. It is unclear whether these obstacles, designed to enhance turbulence, would exacerbate debris trapping or alter the flow field in a way that facilitates passage. This interaction is crucial, as a design optimized for a single objective (energy dissipation) could inadvertently introduce a critical vulnerability (blockage risk).

This study aims to address this knowledge gap through a systematic laboratory investigation. The primary objectives are: (1) to experimentally analyze the passage and trapping behavior of floating debris on a stepped spillway under various obstacle configurations; (2) to quantify the influence of relative obstacle height and flow regime on the debris-spillway interaction; and (3) to elucidate the underlying hydraulic mechanisms to inform a risk-based design approach that reconciles these potentially conflicting objectives.

To provide a consistent framework, a dimensional analysis was performed considering key parameters such as debris length ($L_d$) and diameter ($D_d$), nondimensionalized with respect to the spillway crest length ($L_c$ = 1.2 m) and critical depth ($d_c$). The nondimensional parameters include $L_d$ / $L_c$ (ranging from 0.04 to 0.21) and $D_d$ / dc (0.1 to 0.5), which influence blockage probability alongside the relative obstacle height (ho/h) and flow regime (dc/h).

## Materials and Methods

### Experimental Setup

The experiments were conducted in a 10-meter-long, 1.2-meter-wide, rectangular flume at the Behbahan Khatam Alanbia University of Technology. The flume is equipped with a closed-loop water circulation system powered by two 6-inch pumps, providing a total capacity of 150 L/s. Discharge was precisely controlled and measured using an ultrasonic flowmeter. Both the flume slope and tailwater depth were adjustable to maintain free-flow conditions over the spillway.

### Stepped Spillway Model

The stepped spillway model was constructed from plexiglass with a slope of 1V:2H ($\theta \approx 26.6°$). It comprised four identical steps, each with a height (h) of 10.5 cm and a length (l) of 21 cm, resulting in a total spillway height of 42 cm. The spillway crest was positioned 1.5 m from the flume entrance to ensure a fully developed flow approach.

### Obstacle Configurations

The selection of the two modified spillway configurations for this study was directly informed by the findings of a comprehensive precursor study on energy dissipation conducted in the same experimental facility by Habibi et al. (2025). That study systematically evaluated the hydraulic performance of discontinuous obstacles with various relative widths (Wo/W) and a full-width continuous obstacle. Here, Wo represents the width of an individual obstacle, and W denotes the total width of the flume. Based on their findings, the following two configurations were chosen to represent two opposing design philosophies:

1. Baseline Configuration: An unobstructed (smooth) stepped spillway served as the control case.
2. Continuous Obstacle (Wo/W = 1.0): A full-width wooden obstacle was installed on the leading edge of each step (Figure 1a). This configuration was identified by Habibi et al. (2025) as being largely ineffective for enhancing energy dissipation.
3. Optimized Discontinuous Obstacle (Wo/W = 0.05): Wooden obstacles with a width of 6 cm were installed in a staggered pattern, with a 6 cm gap between them (Figure 1b). This layout was selected as it was identified by Habibi et al. (2025) as the most effective configuration for maximizing energy dissipation, achieving up to a 39% increase compared to the baseline.

For both modified configurations, four relative obstacle heights were tested: ho/h = 0.19, 0.38, 0.57, and 0.76. This experimental

design allows for a direct evaluation of how configurations optimized for energy dissipation perform when subjected to floating debris loads.

**Floating Debris and Experimental Procedure**

To simulate natural debris, wood and reed bundles were prepared with distinct physical properties. The wood bundles, simulating LWD, were constructed to have a bulk density in the range of 700–900 kg/m³, representative of partially saturated timber found in river systems (Bezzola et al., 2017). The reed bundles, simulating lighter vegetative debris, had a significantly lower bulk density, approximately 200–400 kg/m³, reflecting their porous structure and high buoyancy. These objects were prepared in two distinct size classes: small (5–12 cm in length, diameter 2–4 cm) and large (20–25 cm in length, diameter 2–4 cm) (Figure 2). The sizes were selected based on scaling from field observations in similar studies (Bezzola et al., 2017; Margetts, 2022), representing typical debris mobilized in floods, with nondimensional ratios Ld / h = 0.48–2.38 and Dd / h = 0.19–0.38 to cover a range of blockage potentials.

The experiments were performed under three flow intensities, corresponding to the primary hydraulic regimes on stepped spillways, defined by the relative critical depth (dc/h):

- Nappe Flow: dc/h = 0.47
- Transition Flow: dc/h = 0.85
- Skimming Flow: dc/h = 1.09

For each test, a batch of 10 to 25 debris objects was released into the upstream basin. The debris behavior—including passage, trapping location, and delay time—was documented through visual observation and video recording. Each experimental run was repeated 3 to 5 times to ensure the statistical reliability of the observed phenomena. A sensitivity analysis was conducted by varying debris batch sizes (±20%) and flow rates (±5%), revealing that blockage probability increases nonlinearly with debris size (doubling size increases risk by 50–70%) but is less sensitive to batch size in continuous configurations. The overall experimental methodology is summarized in (Figure 3).

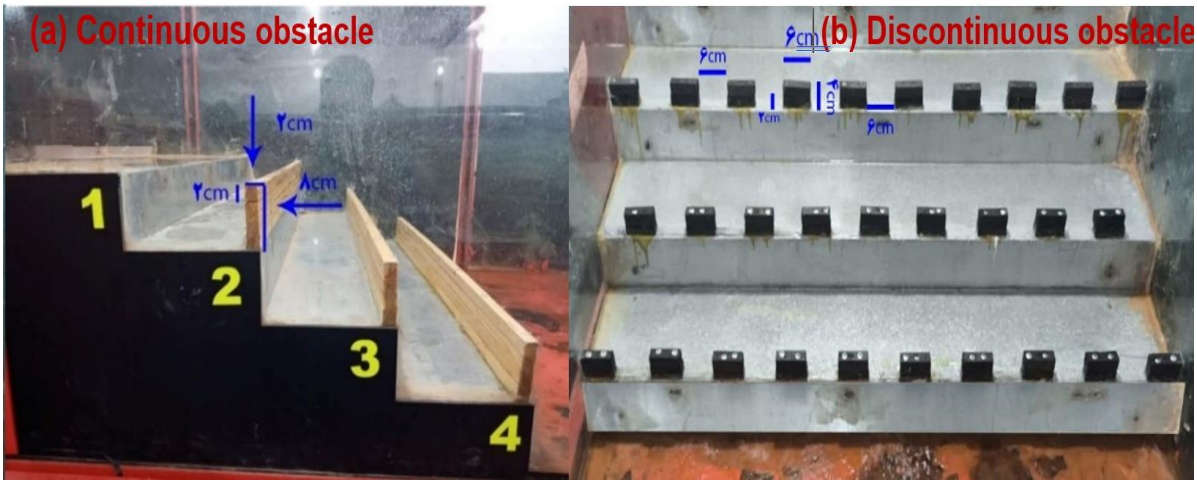



**Fig. 1-The two primary obstacle configurations tested on the stepped spillway model: (a) Continuous obstacle, shown with a relative height of ho/h = 0.76; and (b) Discontinuous (staggered) obstacle, shown with a relative height of ho/h = 0.38.**



**Fig. 2- Representative samples of the large floating debris (20-25 cm) used in the experimental investigation: (a) wood bundles, simulating large woody debris (LWD); and (b) reed bundles, simulating vegetative debris.**

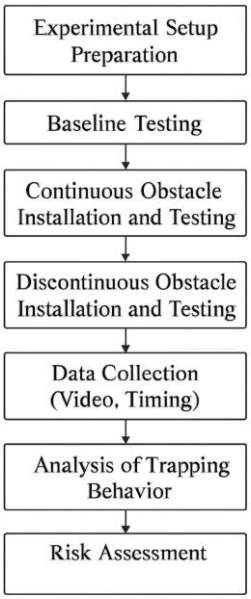



**Fig. 3- Flowchart of the Research Methodology.**

## Results and Discussion

The experimental results reveal a complex interaction between floating debris and the modified spillway hydraulics, governed by the interplay of spillway configuration, obstacle geometry, the prevailing flow regime, and debris characteristics. Quantitative metrics include trapping probability (percentage of runs with trapping), delay time (seconds), and impacts on hydraulic performance.

### Baseline Performance: Spillway Without Obstacles

In the baseline configuration, the stepped spillway exhibited a high capacity for debris conveyance. All types and sizes of debris passed over the steps without any instance of trapping. The only observable hydraulic interaction was a temporary delay (1–3 seconds) as debris navigated the turbulent region of the hydraulic jump at the spillway toe. This finding establishes a crucial baseline: the standard stepped spillway geometry is inherently resilient to debris blockage. No significant changes in flow conveyance or energy dissipation were noted with debris presence.

**Performance with Continuous Obstacles: The Dominance of the Pooling Effect**

The introduction of continuous obstacles fundamentally altered the local hydraulics. As summarized in (Table 1). trapping of large debris (20–25 cm) was a limited phenomenon, occurring only at the lowest obstacle height (ho/h = 0.19) and exclusively within the nappe flow regime (dc/h = 0.47) , with a trapping probability of 30%. This can be attributed to an incomplete development of the key hydraulic mechanism: the "pooling effect." At obstacle heights of ho/h ≥ 0.38, a stable pool of water formed upstream of each obstacle, increasing the local water depth and providing greater buoyant force, which allowed debris to pass over the obstacle crest with trapping reduced to <10%. This aligns with previous research by Asghari Pari and Kordnaeij (2021), who noted that such pooling is highly effective for conveyance. However, this pooling effect reduces turbulence, resulting in lower energy dissipation compared to the baseline configuration, as reported by Habibi et al. (2025). Small debris (5–12 cm) were completely unaffected by continuous obstacles, passing freely under all conditions (Table 2). The presence of debris slightly reduced energy dissipation by 5–8% in skimming flow due to surface disturbances but had negligible impact on discharge coefficient (<2% change).

**Performance with Discontinuous Obstacles: Flow Concentration and Selective Trapping**

The discontinuous obstacle configuration produced the most hazardous and complex results.

**The Primary Trapping Mechanism: Flow Concentration and Jet Impingement**

The gaps between discontinuous obstacles acted as hydraulic nozzles, leading to flow concentration and creating high-velocity jets. These jets exerted a substantial drag force, pinning debris against the downstream faces of the obstacles. This mechanism explains the consistent trapping observed in the nappe flow regime (Table 3), where low initial flow depth made debris highly susceptible to being drawn into these concentrated flow paths, with trapping probabilities of 70–90%.

**The Critical Role of Flow Regime and Debris Properties**

The influence of the flow regime was profound. The transition flow regime (dc/h = 0.85) represented a critical hydraulic threshold where increased turbulent kinetic energy was sufficient to flush all debris and prevent stable blockage. The skimming flow regime (dc/h = 1.09) revealed a nuanced interaction, highlighting the importance of debris properties. At ho/h = 0.76, while wood and mixed debris were trapped (probability 60%), reed debris passed freely due to their higher buoyancy and flexibility, allowing them to ride higher on the skimming flow surface and clear the obstacles. The difference in trapping behavior is attributed to the lower bulk density (200–400 kg/m³) and higher flexibility of reed bundles compared to wood (700–900 kg/m³), which caused wood debris to travel more submerged and be more prone to direct impact with obstacles. In skimming flow, debris presence reduced energy dissipation by 8–10% by disrupting the coherent skimming layer, but flow conveyance remained largely unaffected. Small debris showed minimal trapping, with only minor instances at high obstacles in skimming flow (Table 4).

**Table 1- Trapping Behavior of Large Debris (20-25 cm) with Continuous Obstacles. (✓ = Trapping Occurred on Step 2; ✗ = No Trapping).**

| Debris Type | Obstacle Height (ho/h) | Nappe Flow (dc/h=0.47 | Transition Flow (dc/h=0.85) | Skimming Flow (dc/h=1.09) |
|---|---|---|---|---|
| Wood | 0.19 | ✓ | ✗ | ✗ |
| Reed | 0.19 | ✓ | ✗ | ✗ |
| Mixed | 0.19 | ✓ | ✗ | ✗ |
| All Types | ≥ 0.38 | ✗ | ✗ | ✗ |

**Table 2- Trapping Behavior of Small Debris (5-12 cm) with Continuous Obstacles.**

| Debris Type | Obstacle Height (ho/h) | All Flow Regimes |
|---|---|---|
| Wood, Reed, & Mixed | All Heights (0.19-0.76) | ✗ (No Trapping) |

**Table 3- Trapping Behavior of Large Debris (20-25 cm) with Discontinuous Obstacles. (✓ = Trapping Occurred; ✗ = No Trapping; Location in parentheses).**

| Debris Type | Obstacle Height (ho/h) | Nappe Flow (dc/h=0.47) | Transition Flow (dc/h=0.85) | Skimming Flow (dc/h=1.09) |
|---|---|---|---|---|
| Wood | 0.19 | ✓ (Steps 2&3) | ✗ | ✗ |
| Reed | 0.19 | ✓ (Steps 2&3) | ✗ | ✗ |
| Mixed | 0.19 | ✓ (Steps 2&3) | ✗ | ✗ |
| Wood | 0.38 | ✓ (Steps 2,3,4) | ✗ | ✓ (Step 3) |
| Reed | 0.38 | ✓ (Steps 2,3,4) | ✗ | ✓ (Step 3) |
| Mixed | 0.38 | ✓ (Steps 2,3,4) | ✗ | ✓ (Step 3) |
| Wood | 0.57 | ✓ (All steps) | ✗ | ✗ |
| Reed | 0.57 | ✓ (All steps) | ✗ | ✗ |
| Mixed | 0.57 | ✓ (All steps) | ✗ | ✗ |
| Wood | 0.76 | ✓ (All steps) | ✗ | ✓ (Step 3) |
| Reed | 0.76 | ✓ (All steps) | ✗ | ✗ |
| Mixed | 0.76 | ✓ (All steps) | ✗ | ✓ (Step 3) |

**Table 4- Trapping Behavior of Small Debris (5-12 cm) with Discontinuous Obstacles.**

| Debris Type | Obstacle Height (ho/h) | Nappe Flow (dc/h=0.47 | Transition Flow (dc/h=0.85) | Skimming Flow (dc/h=1.09) |
|---|---|---|---|---|
| Wood, Reed, & Mixed | 0.19 | ✗ | ✗ | ✗ |
| | 0.38 | ✗ | ✗ | ✗ |
| | 0.57 | ✗ | ✗ | ✗ |
| | 0.76 | ✗ | ✗ | ✓ (on step 4) |

**Table 5- Risk Assessment Matrix for Obstacle Configurations**

| Configuration | Energy Dissipation (ΔE %) | Blockage Probability (Pb %) | Recommended for |
|---|---|---|---|
| Baseline | 0 | 0 | Balanced risks |
| Continuous | -5 to -15 | 0-10 | High debris |
| Discontinuous | +20 to +39 | 50-90 | Low debris |

## Discussion: The Design Paradox and Engineering Implications

The results of this study, when synthesized with the established energy dissipation performance from Habibi et al. (2025), reveal a critical design paradox that lies at the heart of optimizing stepped spillway performance. This paradox forces a re-evaluation of design priorities in catchments where both high hydraulic energy and significant debris loads are primary concerns.

### The Fundamental Conflict: Energy Dissipation vs. Debris Conveyance

The results of this study, combined with the energy dissipation findings from Habibi et al. (2025), reveal a critical design paradox for stepped spillways. Habibi et al. (2025) reported that discontinuous obstacles (Wo/W = 0.05) achieved the highest energy dissipation, with up to a 39% increase over the baseline configuration in the skimming regime (dc/h = 1.09), due to intense turbulence and flow separation through the 6 cm gaps between obstacles. In contrast, continuous obstacles (Wo/W = 1.0) exhibited lower energy dissipation than the baseline across all flow regimes (nappe: dc/h = 0.47; transition: dc/h = 0.85; skimming: dc/h = 1.09) due to the formation of stable water pools that reduce turbulence. However, as demonstrated in Sections 3.2 and 3.3, these discontinuous obstacles significantly increase the risk of debris entrapment, particularly for large debris (20–25 cm) in the nappe regime, where high-velocity jets pin debris against obstacles (Table 3). Conversely, continuous obstacles facilitate debris passage through a pooling effect that enhances buoyancy, despite their lower energy dissipation efficiency. The baseline configuration offers moderate energy dissipation and high resilience to debris blockage, serving as a balanced but suboptimal reference. This conflict underscores the need for a catchment-specific design approach, prioritizing either energy dissipation or debris conveyance based on the dominant risk factors. To quantify this paradox, a simple risk assessment matrix is proposed Table (5), where blockage probability (Pb) is weighed against energy dissipation gain (ΔE %). For example, discontinuous obstacles have high ΔE (39%) but high Pb (70%), while continuous have low ΔE (-10%) but low Pb (5%).

**Inversion of Performance: How Hydraulic Mechanisms Dictate a Dual Role** Our findings demonstrate that the very hydraulic mechanisms governing energy dissipation also dictate the success or failure of debris management:

- **The "Pooling Effect" - From Hydraulic Weakness to Conveyance Strength:** The stable pooling behind continuous obstacles, a known detriment to energy dissipation, becomes the primary mechanism for safe debris passage.
- **Flow Concentration - From Dissipative Strength to Blockage Hazard:** The high-velocity jets created by discontinuous obstacles, the source of their superior energy dissipation, become the direct cause of catastrophic debris trapping.

### The Engineering Challenge: A Risk-Based Approach to Reconciling Conflicting Objectives

This presents a significant challenge for hydraulic engineers. The choice of obstacle configuration is a multi-criteria decision based on a holistic risk assessment of the specific catchment:

1. **For catchments dominated by high flood energy but with low debris potential:** Discontinuous obstacles remain a viable and effective option to maximize energy dissipation.

2. **For catchments with high debris loads:** Continuous obstacles are the safer design choice, prioritizing spillway conveyance to prevent severe blockage-induced failure, even at the cost of reduced energy dissipation.
3. **For catchments where both risks are high:** A systems approach is required, involving upstream interception (e.g., debris booms to remove debris before reaching the spillway) or downstream compensation (e.g., a larger stilling basin to manage residual energy). These solutions require careful consideration of costs, maintenance, and environmental impacts, such as potential habitat disruption or sediment accumulation caused by debris interception structures.

While the laboratory experiments provide valuable insights, field justification is limited due to scale effects; however, the nondimensional parameters align with field-scale studies (Rundqvist, 2005), suggesting qualitative applicability, with quantitative scaling requiring further validation.

**Limitations of the Study**

The experimental setup has several limitations that may affect the generalizability of the results. The 1.2-meter-wide flume and four-step spillway model may not fully replicate the scale and complexity of full-scale spillways, which often feature dozens of steps and wider spans, potentially introducing three-dimensional effects in debris accumulation not captured here. Thus, extrapolation to prototype scales should be cautious, and future large-scale or CFD validations are recommended. The use of only two debris types (wood and reed) limits the representation of diverse debris characteristics, such as non-woody materials or varying shapes; for instance, elongated debris with high slenderness (as in Habibi & Lashkar-Ara, 2020) may bridge gaps differently. Additionally, the experiments were conducted under controlled laboratory conditions with single-batch releases, which may not account for real-world complexities like progressive debris accumulation during floods (e.g., cumulative vs. single-event loading as in Habibi & Lashkar-Ara, 2018). Future research should explore larger-scale models, a wider variety of debris types (including slenderness effects), cumulative accumulation dynamics, and field-scale validation to enhance the applicability of these findings.

## Conclusions

This experimental study provides a comprehensive analysis of the interaction between floating debris and on-step obstacles on a stepped spillway. Unobstructed stepped spillways exhibit high resilience to debris blockage, establishing them as a safe baseline for debris conveyance. Continuous obstacles (Wo/W = 1.0) significantly improve debris passage by inducing a "pooling effect," making them a highly recommended solution for catchments where debris conveyance is a higher priority than maximizing on-step energy dissipation. The discontinuous obstacle configuration optimized for energy dissipation (Wo/W = 0.05) poses high blockage risk, particularly for large debris in low-flow regimes, making it unsuitable for debris-prone areas. A critical design paradox is demonstrated: discontinuous obstacles maximize energy dissipation (up to 39% increase over the baseline) but significantly increase blockage risk, while continuous obstacles prioritize safe debris passage at the expense of reduced energy dissipation. The optimal design solution is catchment-specific, requiring a thorough risk assessment of the upstream catchment and downstream valley.

Research Suggestions: Future studies should investigate cumulative debris accumulation, incorporate a broader range of debris shapes and slenderness ratios, validate findings with CFD models or field prototypes, and develop integrated risk models combining blockage probability with hydraulic performance metrics.

## Acknowledgment

This research has no acknowledgments.

## Conflict of Interest

The authors declared no potential conflicts of interest concerning the research,

authorship, and publication of this article **.** Confirmation.

**Funding**

The authors received no financial support for the research, authorship, and publication of this article.

**Data Availability Statements**

Data Availability Statement: All information and results are presented in the text of the article.

**Authors' contribution**

**First Author:** Seyed Amin Asghari, Pari Writing the article, conclusion, and analysis of results (50%).

**Second Author:** Seyed Ali Asghari, Pari Reviewing and controlling results (shared 20% with Mojtaba Kordnaeij).

**Third Author:** Amin Mokaram, Performing experiments (30%).

**Fourthd Author:** Mojtaba Kordnaeij, Reviewing and controlling results (shared 20% with Seyed Ali Asghari Pari).

**References**

1- Al-Jubouri, S.M., Waisi, B.I. and Eslamian, S., 2022. Debris and Solid Waste in Flood Plain Management. In: Eslamian, S. and Eslamian, F. (eds). *Flood Handbook, Vol. 3: Flood Impact and Management*, Ch. 21. Taylor and Francis, CRC Group, USA. DOI: 10.1201/9780429463327-26.

2-Asghari Pari, S.A. and Kordnaeij, M., 2021. Laboratory examination of comparison of the effect of the porous screen, continuous obstacle, and continuous porous obstacle on the edge of a stepped spillway. *Irrigation and Drainage Structures Engineering Research*, 22(83), pp.121-140. DOI: 10.22092/idser.2021.354709.1473. (In Persian).

3-Bekheet, A.A., AboulAtta, N.M., Saad, N.Y. and El-Molla, D.A., 2025. Energy dissipation in stepped spillways: A comprehensive review. *Innovative Infrastructure Solutions*, 10(6), p.253. DOI: 10.1007/s41062-025-02042-6.

4-Bezzola, G.R. et al., 2017. CFD modeling of wood debris accumulation at stepped spillways. *Journal of Hydraulic Engineering*, 143(8), 04017024. DOI: 10.25130/tjes.23.3.01.

5-Chanson, H., 2002. *The hydraulics of stepped chutes and spillways*. Balkema.

6-Habibi, K., Erfani Fard, F., Asghari Pari, S.A. and Azimi, A.H., 2025. Experimental and numerical studies on the hydraulics of stepped spillways with baffle walls and blocks. *ISH Journal of Hydraulic Engineering*, 31(2), pp.217-238. DOI: 10.1080/09715010.2025.2471339.

7- Habibi, S. and Lashkar-Ara, B., 2018. Laboratory evaluation of the effect of floating debris accumulation at crown wheel weirs on the hydraulic characteristics under cumulative test. *Irrigation and Drainage Structures Engineering Research*, 19(73), pp.45-62. DOI: 10.22092/idser.2017.114730.1237. (In Persian).

8-Habibi, S. and Lashkar-Ara, B., 2020. Analyses of slenderness coefficient effect of floating wood on CPK weir blockage in individual test system. *Journal of Civil and Environmental Engineering*, 50(3), pp.89-102. DOI:10.22034/ceej.2020.6955 (In Persian).

9-Habibi, S. and Lashkar-Ara, B., 2021. Two cycle circular piano key weir blocking probability assessment along individual experiment. *Irrigation Sciences and Engineering*, 24(2), pp.115-130. DOI: 10.22055/jise.2017.22015.1575. (In Persian).

10-Hartlieb, A., 2017. Decisive parameters for backwater effects caused by floating debris jams. *Open Journal of Fluid Dynamics*, 7(4), pp.431-441. DOI: 10.4236/ojfd.2017.74029.

11-Hassan, A., 2000. *Handling river floating debris for dam safety – the state of the practice*. Master's thesis, KTH Royal Institute of Technology, Sweden.

12-Iqbal, U. and Riaz, M.Z.B., 2024. Blockage at cross-drainage hydraulic structures – Advances, challenges and opportunities. *Heliyon*, 10(15), e35786. DOI: 10.1016/j.heliyon. 2024.e35786.

13-Kordnaeij, M., Tehrani, M.J.O.M., Pari, S.A.A. and Falahat, H., 2023. Energy dissipation on stepped spillways: The effect of mounted step roughness. In: *Proceedings of the 40th IAHR World Congress*, Vienna, Austria. DOI: 10.3850/978-90-833476-1-5_iahr40wc-p1620-cd.

14-Mansouri, K. and Ahadiyan, J., 2016. Blockage of Piano Key Weirs in debris flow with individual experiments. *Journal of Irrigation and Water Engineering*, 6(2), pp.164-172. DOI: 10.22055/jise.2016.12352. (In Persian).

15-Margetts, K., 2022. *Passage probability of woody debris elements and accumulations at I- and V-shaped rock weirs*. Master's thesis, Utah State University, USA.

16-Mikalsen, L.M. and Thorsen, K.H., 2023. *Improved energy dissipation in stepped spillways–Hydraulic model study applying bubble image velocimetry*. Master's thesis, Norwegian University of Science and Technology (NTNU), Norway.

17-Pagliara, S. and Carnacina, I., 2011. Influence of wood debris accumulation on bridge pier scour. *Journal of Hydraulic Engineering*, 137(2), pp.254-261. DOI: 10.1061/(ASCE)HY.1943-7900.0000289.

18-Pfister, M., Capobianco, B., Tullis, B.P. and Schleiss, A.J., 2013. Debris-blocking sensitivity of piano key weirs under reservoir-type approach flow. *Journal of Hydraulic Engineering*, 139(11), pp.1134-1141. DOI: 10.1061/(ASCE)HY.1943-7900.0000780.

19-Rundqvist, J., 2005. *Debris in Reservoirs and Rivers-Dam Safety Aspects*. CEATI Dam Safety Interest Group.

20-Sánchez-Juny, M., Estrella, S., Matos, J., Bladé, E., Martínez-Gomariz, E. and Bonet Gil, E., 2022. Velocity measurements in highly aerated flow on a stepped chute without sidewall constraint using a BIV technique. *Water*, 14(16), 2587. DOI: 10.3390/w14162587.

21-Schmocker, L. and Hager, W.H., 2013. Scale modeling of wooden debris accumulation at a debris rack. *Journal of Hydraulic Engineering*, 139(8), pp.827-836. DOI: 10.1061/(ASCE)HY.1943-7900.0000714.

22-Yang, J. and Stenström, P., 2011. Ensuring spillway discharge capacity in case of reservoir floating debris. In: *Proceedings of the 11th International Conference on Fluid Control, Measurements & Visualization*, Keelung, Taiwan.

23-Yang, J., Johansson, N. and Cederström, M., 2009. Handling reservoir floating debris for safe spillway discharge of extreme floods – laboratory investigations. In: *Proceedings of the 23rd ICOLD Congress*, Brasilia, Brazil.

© 2026 The Author(s). Published by Shahid Chamran University of Ahvaz. This is an open-access article distributed under the terms of the Creative Commons Attribution License (http://creativecommons.org/licenses/by/4.0), which permits unrestricted use, distribution, and reproduction in any medium, provided the original work is properly cited.

Shahid Chamran University of Ahvaz

**Irrigation Sciences and Engineering (JISE)**
**Vol. 48, No. 4, Winter 2026, p. 117-132**

**Research Paper**

Journal homepage: https://jise.scu.ac.ir

# Environmental Water Diplomacy between Iran and Turkey: Challenges and Strategic Priorities

Fatemeh Lashkari[1], Mir Mehrdad Mirsanjari[2*] and Fatemeh Mohammadyari[3]

*1- M.Sc. of Environmental Sciences and Engineering, Land Assessment and Planning, Department of Environmental Sciences and Engineering, Faculty of Natural Resources and Environment, Malayer University, Malayer, Iran*
*2*- Corresponding Author, Department of Environmental Sciences and Engineering, Faculty of Natural Resources and Environment, Malayer University, Malayer, Iran. (mmmirsanjari@malayeru.ac.ir).*
*3. Department of Environmental Engineering, Faculty of Natural Resources and Earth Sciences, Shahrekord University, Shahrekord, Iran.*

**ARTICLE INFO**

*Artlcle history:*
Received: 23 August 2025
Revised: 24 October 2025
Accepted: 11 November 2025
Available online: 04 January 2026

*Keywords:*
Environmental Water Diplomacy, Sustainable Development Goals, Hydropolitics, Transboundary Rivers, Environmental strategies.

**TO CITE THIS ARTICLE:**

Lashkari, F., Mirsanjari, M. M., Mmohammadyari, F. 2026. 'Environmental Water Diplomacy between Iran and Turkey: Challenges and Strategic Priorities', *Irrigation Sciences and Engineering*, 48(4), pp. 117-132. doi: 10.22055/jise.2025.50717.2184.

**Abstract**

This study investigates the challenges and strategic priorities of environmental water diplomacy in the transboundary river basins shared between Iran and Turkey. Given Iran's significant dependence on inflowing rivers particularly the Aras and Tigris–Euphrates systems and the profound hydrological, ecological, and socio-economic impacts of Turkey's large-scale dam projects (notably GAP and DAP), effective diplomatic engagement over shared water resources has become a critical component of Iran's environmental and national security policy. To address this complex issue, a two-stage analytical framework was employed. First, a SWOT (Strengths, Weaknesses, Opportunities, Threats) analysis was conducted to identify key internal and external factors shaping Iran's hydropolitical position vis-à-vis Turkey. This process yielded five core strategic directions. Second, the Analytic Hierarchy Process (AHP) was applied to prioritize these strategies based on structured pairwise comparisons by 15 domain experts from Bu-Ali Sina, Malayer, and Ilam Universities, selected through purposive sampling for their expertise in environmental diplomacy, hydropolitics, and transboundary water governance. The results reveal a clear preference for inward-oriented institutional strengthening: the highest-priority strategy (weight = 0.532) emphasizes the principled implementation of national land-use planning through the integration of skilled, committed professionals into regional and national decision-making bodies. In contrast, externally focused initiatives such as concluding internationally monitored security and economic agreements with Turkey received the lowest priority (weight = 0.029). Overall, the findings indicate that Iran's prevailing approach aligns with a defensive strategic posture, prioritizing domestic resilience, scientific governance, and border-region capacity-building over confrontational or high-stakes bilateral arrangements. The study concludes that sustainable water diplomacy in this context hinges not on external pressure alone, but on robust internal reforms, evidence-based spatial planning, and investment in local knowledge economies. These insights offer actionable guidance for policymakers seeking to navigate transboundary water tensions while advancing the Sustainable Development Goals and regional environmental security.

## Introduction

Water scarcity, exacerbated by climate change and growing demand, has intensified geopolitical tensions over transboundary freshwater resources (Kummu et al., 2016; IPCC, 2019; Gleeson et al., 2020). In arid and

 *DOI:* 10.22055/jise.2025.50717.2184

semi-arid regions such as West Asia, shared river basins particularly the Tigris-Euphrates and Aras have become focal points of hydropolitical contestation. This context underscores the urgent need for environmental water diplomacy: a strategic framework that integrates diplomatic engagement, scientific cooperation, and legal norms to manage shared waters sustainably and peacefully. While these global issues underscore the urgency of international and regional cooperation, they are paradoxically accompanied by a growing disregard for international agreements and an increasingly prominent role for geopolitics (Eilstrup-Sangiovanni and Hofmann, 2020). These shifts collectively highlight the need for new forms of diplomacy capable of navigating the complex and evolving landscape of foreign policy, particularly where climate change intersects with critical resources such as energy, food, and water (Council of the European Union, 2018 and 2020). Water stands as the most vital natural resource for human societies, transcending national boundaries and being relatively straightforward to quantify. Its transboundary nature often politicizes its use and allocation, prompting the development of diverse cooperative arrangements, especially within river basins shared by multiple countries (McCracken and Wolf, 2019).

Diplomatic efforts have proven particularly effective in resolving land-based water disputes, especially within transboundary river basins. These efforts are often referred to interchangeably as “water diplomacy,” “blue diplomacy,” or “hydro-diplomacy,” reflecting their shared emphasis on cooperative and strategic engagement over shared water resources (MacKay and Collins, 2025). Over the past decade, water diplomacy has garnered increasing attention in both academic research and policy discourse. It reflects a growing awareness of the inherently political nature of transboundary water governance as an aspect not fully captured by the terms “transboundary water management” or “water cooperation.” Rather than relying solely on state-centric explanations, water diplomacy seeks to understand the practices employed by diplomats and other actors engaged in transboundary water cooperation across multiple levels. Most definitions emphasize negotiation as a central component of water diplomacy, particularly in the prevention, mitigation, and resolution of disputes over shared water resources (Sehring et al 2022; Sehring et al 2023).

Water diplomacy is the capacity of beneficiary countries to manage shared waters to achieve a stable political situation, meaning that transboundary and international water resources are used sustainably without any tension or conflict between the riparian countries. Due to constant flow of water from one location or country to another, and also the presence of political borders of different countries along the path of water flows, some disputes, negotiations, and collaborations on the management of these shared resources have emerged within the framework of the foreign policy of the world’s nations, becoming known as “water diplomacy”.Water diplomacy is an emerging as a strategic framework for addressing the political dimensions of transboundary water cooperation and for linking water issues to broader regional collaboration, geopolitical dynamics, and foreign policy agendas. The central argument is that diplomacy as a well-established mechanism through which states engage, collaborate, and exert influence across various diplomatic tracks (Marks and Freema, 2020) can offer additional tools for managing water-related tensions and fostering cooperation among countries that share water bodies. As such, water diplomacy has gained traction both within policymaking circles (Pohl et al., 2014; Council of the European Union, 2018) and among academic communities (Grech-Madin et al., 2018). Water is not only for development, but in today’s world facing the challenge of water scarcity, it is considered a key instrument for securing national interests. In this context, each country’s public diplomacy must evolve into an integrated and inseparable assessment of policies related to water, development, and diplomacy. Water diplomacy focuses on various issues, including the vital nature of water as a resource, virtual

water, water conflicts, international water law, and transboundary water management.

Water diplomacy is crucial for realizing the United Nations' 2030 Agenda for Sustainable Development to implement a global security system. The United Nations has identified water challenges as one of the most significant global issues. As projected, by 2030, the increasing effects of climate change and the lack of sufficient freshwater could lead to substantial human migrations, potentially involving up to 700 million people. By 2040, 25 percent of children under the age of 18 worldwide will face severe shortages of fresh water. Increased water pollution, including chemicals and solid waste, causes many infectious diseases, leading to the rapid spread of microbial contamination among people, impacting entire ecosystems and directly influencing international security policies and structures. In this regard, to prevent these occurrences, implementing a new approach in water diplomacy, presented as part of modern diplomacy, can play a significant role (Klimes et al., 2019). Water diplomacy, as an international network of cooperation, assists governmental and non-governmental actors for water and the promotion of peace in the world (Cuppari, et al., 2017). Actors involved in water diplomacy can build trust and facilitate related processes through joint capacity-building initiatives, collaborative knowledge generation, networking activities, facilitation, and mediation. These efforts contribute to more inclusive and resilient frameworks for transboundary water governance (Niemann et al., 2018; Karjalainen, 2020). Water diplomacy has the potential to become an effective platform for international collaboration in addressing many current and future global water challenges. In fact, water diplomacy is a vital instrument for implementing the Sustainable Development Goals, combining proactive and reactive measures, as well as mediation and the implementation of solutions, which is crucial for regional and global security (Krzymowski, 2021).

Studies conducted in this field include the work of Samei et al. (2020), which addressed a model of regional cooperation based on water diplomacy (a case study of Iran, Turkey, and Iraq). This study was conducted using an analytical-descriptive method. Based on the findings, the necessity of the importance of diplomacy should be given even greater attention. Furthermore, Zaki and Najafi (2020) evaluated Iran's hydropolitical strategies regarding the Arvandrud. In this regard, they gathered the opinions of experts on the environmental factors influencing the hydropolitics of the Arvandrud and prioritized these opinions using SWOT matrix analysis and the Analytic Hierarchy Process (AHP) method. Based on the results, cooperation among the three countries of Iran, Iraq, and Turkey regarding the proper use of the Arvandrud will lead to peace and stability in the region and prevent any future conflicts between Iran and Iraq. Keskinen et al. (2021) also conducted a study on the pathways of water diplomacy to understand water diplomacy actions in shared waters. To this end, they examined the literature, comparatively analyzed water diplomacy approaches, and conducted interviews with selected water diplomacy actors to investigate various dimensions of this issue. Based on the results, this approach, by distinguishing between water-focused and diplomacy-focused activities, as well as considering related tensions and actions, has the potential to support water diplomacy processes. Additionally, Kavianirad et al. (2022) conducted research titled "Water Diplomacy Role in Easing Iran-Iraq Hydropolitical Tensions." The aim of this research was to identify the driving forces effective in transforming hydropolitical tensions into water cooperation between Iran and Iraq. The results of this research indicated that water diplomacy plays a strategic role in reducing hydropolitical tensions.

Iran is situated in an arid, semi-arid, and water-scarce geographical location. Its unique topography and position on the outer edges of mountain ranges have led to increased rainfall in these areas. Consequently, a significant portion of Iran's population, human settlements, and fertile agricultural regions are located in the peripheral areas of the country

 *DOI:* 10.22055/jise.2025.50717.2184

and in proximity to neighboring countries. This has resulted in the dependence of Iranian residents' livelihoods on transboundary water resources. On the other hand, the topography of the country in the western regions has led to a significant volume of water flowing out of Iran and into Iraq, and this is where environmental water diplomacy gains meaning and importance in Iran. Adopting water diplomacy in Iran, considering transboundary resources such as inflow and outflow rivers like the Tigris-Euphrates with Iraq and Turkey; the Kura-Aras with Turkey, Armenia, and the Republic of Azerbaijan; the Atrak with Turkmenistan; the Karakum with Turkmenistan and Afghanistan; the Petergan-Khaf with Afghanistan; the Hamuon-Helmand with Afghanistan and Pakistan; and the Hamoun Mashkil and Rabach-Bahu Kalat with Pakistan, is a necessary and unavoidable matter given our country's geographical situation.

Based on international treaties, no country is allowed to take control of the water resources of international and shared rivers between neighbors. This important point has been explicitly, clearly, and specifically emphasized in the treaties of the United Nations, The Hague, Paris, Geneva, Barcelona, Madrid, and others. The intensification of the water scarcity crisis in the new century underscores the necessity of pursuing "water diplomacy" more prominently in the international arena. Neighboring countries typically share waterways such as rivers, lakes, and seas. Based on multilateral treaties and agreements governing such nations, there should be a mutual understanding and agreement, operating through a clear and specific mechanism, for the joint utilization of these shared waterways for purposes such as agricultural development and the provision of drinking water. From this perspective, the Islamic Republic of Iran shares waterways with Iraq, Turkey, the Republic of Azerbaijan, Armenia, and Afghanistan among its neighbors. However, we are currently witnessing the trampling of the legal rights of countries and existing treaties (Ghaznafarzadeh Kapte, 2018). Turkey has historically emphasized the principle of territorial sovereignty in its water policy, asserting primary rights over rivers originating within its borders (Hekmat Ara, 2022). This stance, reflected in large-scale infrastructure projects such as the Southeastern Anatolia Project (GAP) and the Aras Basin Development Plan (DAP), has raised concerns among downstream states including Iran regarding reduced water flows, ecological degradation, and transboundary equity. While upstream actions by Turkey significantly affect water availability in Iran, domestic water governance challenges including inefficient irrigation practices, over-extraction of groundwater, and fragmented institutional oversight also constrain Iran's capacity to respond effectively to transboundary pressures. A comprehensive hydropolitical strategy must therefore address both external and internal dimensions of water security. Turkey's mega-dam construction projects, aimed at building 22 dams and 19 power plants on the Tigris and Euphrates rivers, have been significantly effective in exacerbating the water scarcity crisis in neighboring countries, ranging from the Republic of Azerbaijan to the Islamic Republic of Iran, Iraq, and Syria, as well as reducing their water rights and damaging the environment of Iran and its neighbors. From this perspective, if Turkey's behavior and dam construction projects (Karakurt, GAP, DAP, and the Ten Mega-Projects) continue, it will cause the closure of river basins to neighboring countries.

Given the inherent complexity of water-related challenges and the interconnected nature of hydrological systems, institutionalized cooperation among riparian states supported by the active participation of all water users is essential for the effective joint management of shared water resources and for the prevention and resolution of conflicts (Honkonen and Lipponen, 2018). Water diplomacy, in the form of a correct, intelligent, and at the same time flexible approach, will be the best solution to claim Iran's water rights from Turkey. This is because if Iran, instead of pursuing water diplomacy and creating joint diplomatic movements with other neighbors, wants to use legal leverage to pressure Turkey,

it will not only fail to achieve its rights but will also create further challenges in its relations with Ankara. Therefore, to prevent a rift in relations with a key neighbor like Turkey, peaceful methods centered on water diplomacy should be employed. This approach would not only reduce the costs of achieving Iran's rights but would also undoubtedly be a shorter path to realizing the country's entitlements. Environmental diplomacy and the clarification of water's role as a key factor in the relations between Turkey and Iran, along with a perspective on Iran's future environmental situation, further highlight the necessity of this study. In this context, the present research was conducted with the aim of evaluating the challenges of modern environmental water diplomacy between Turkey and Iran using a novel approach.

## Materials and Methods

### The study area

The study area in the present research encompasses the transboundary rivers of Turkey and Iran. Due to its geographical location, Turkey possesses numerous natural and artificial rivers and lakes. Some of these rivers, originating in Turkey, flow into Iran, including the Tigris and Euphrates. The Euphrates River originates in the Taurus Mountains of the Anatolian region and, after joining the Tigris River in the Arvandrud, flows into the Persian Gulf. The next river is the Aras River, which originates from the Erzurum region of Anatolian Turkey. This river flows across the border of Turkey, Nakhchivan, Jolfa, and Armenia, and after crossing the Iranian border, enters the Republic of Azerbaijan, where it joins the Kura River and eventually flows into the Caspian Sea. The Aras River forms part of the international boundary between Iran and the Republic of Azerbaijan, a demarcation established by the 1828 Treaty of Turkmenchay following the Russo-Persian War. The river originates in eastern Turkey, flows through Armenia and the Nakhchivan exclave of Azerbaijan, and then delineates the Iran–Azerbaijan border before joining the Kura River and emptying into the Caspian Sea. Turkey's extensive dam construction on these rivers causes and will cause crises and environmental destruction in these regions, both currently and in the near futurethe Aras River was designated as the border between Iran and Syria. Turkey's extensive dam construction on these rivers causes and will cause crises and environmental destruction in these regions, both currently and in the near future (Hekmat Ara, 2022)

### Research Method

The present study is descriptive and analytical in terms of research methodology. After reviewing an extensive literature, examination of scientific documents, and considering the influential factors of the internal environment (strengths and weaknesses) and the external environment (opportunities and threats), along with the opinions and perspectives of relevant experts and specialists, the SWOT (Strengths, Weaknesses, Opportunities, and Threats) matrix analysis method was employed. This method was used to determine our country's strategy and to propose effective hydropolitical strategies for Iran in the transboundary river basins. Following the implementation of the SWOT analysis, the obtained strategies were prioritized using the Analytic Hierarchy Process (AHP).

SWOT analysis serves as a strategic planning and management tool. Despite its simplicity, it offers a robust framework for evaluating internal strengths and weaknesses, as well as external opportunities and threats (Gurl and Merba, 2017). The Analytic Hierarchy Process (AHP) is a quantitative, multi-criteria decision-making approach that relies on pairwise comparisons. Developed by Saaty in the 1970s, AHP has since been extensively researched and applied across various domains. By systematically assessing multiple factors, it facilitates decision-making in complex scenarios. This methodology has found widespread application globally in sectors such as business, education, and public administration (Ha-Vikström & Takala, 2016). The prioritization of alternatives in AHP is derived from a pairwise comparison matrix, as illustrated in Table (1) (Saaty, 1977).

 *DOI:* 10.22055/jise.2025.50717.2184

**Table 1- Saaty's 9-point scale for pairwise comparisons**

| Score | Saaty scales |
|---|---|
| 1 | Equally important |
| 2 | Slightly more important |
| 3 | Moderately more important |
| 4 | Moderately to strongly more important |
| 5 | Strongly more important |
| 6 | Strong to very strong importance |
| 7 | Very strongly more important |
| 8 | Very to extremely strong importance |
| 9 | Extremely more important |

The integration of SWOT and AHP methodologies was selected to combine qualitative strategic diagnosis with quantitative prioritization. SWOT enables systematic identification of contextual factors influencing Iran's hydropolitical position, while AHP provides a structured, transparent mechanism for weighting expert judgments on strategy importance a widely validated approach in environmental policy and resource management (Saaty, 1977; Ha-Vikström & Takala, 2016).

A purposive sample of 15 experts was selected based on their scholarly expertise in transboundary water governance, environmental diplomacy, and Middle Eastern hydropolitics. While the sample size is modest, it aligns with best practices in expert-based AHP studies, where depth of domain knowledge is prioritized over statistical generalizability (Zaki & Najafi, 2020). Participants included faculty from Bu-Ali Sina, Malayer, and Ilam Universities with peer-reviewed publications on Iran–Turkey water relations. Initially, a questionnaire was distributed to the experts to identify the internal and external factors (strengths, weaknesses, opportunities, threats) related to environmental water diplomacy in the study area. Subsequently, another questionnaire was distributed to estimate the impact coefficient and the importance level of each criterion for the internal and external environments separately. The prioritization of criteria was carried out based on pairwise comparisons using Expert Choice software (Zaki & Najafi, 2020). In the first step, the influential factors of the internal environment (5 strengths and 6 weaknesses) and the external environment (11 opportunities and 9 threats) were questioned (Tables 2 to 4). Then, to score and determine the importance coefficients of the components, closed-ended quantitative analysis questionnaires for the matrix of factors were distributed among the experts, and the importance level and impact coefficient of each factor were determined separately. Content validity was established through iterative review by three senior scholars in environmental policy. Construct validity was supported by factor coherence within SWOT categories. Reliability was assessed via Cronbach's alpha = 0.73, which, while modest, is acceptable for exploratory expert judgment studies in social-ecological systems (Nunnally, 1978), particularly given the heterogeneous nature of diplomatic and environmental criteria. Although the 1997 UN Convention on the Non-Navigational Uses of International Watercourses has not been ratified by Turkey or Iran, its core principles equitable and reasonable utilization and the obligation not to cause significant harm reflect customary international law applicable to all states. Iran could strategically invoke these norms in multilateral forums (e.g., UNEP, OIC) to frame Turkey's dam projects as inconsistent with regional environmental obligations, even in the absence of binding adjudication.

In the next stage, to determine the weight of the layers, the AHP method was initially used. After determining the importance of each parameter based on expert opinions, Expert Choice software was employed.

**Results and Discussion**

In this study, after distributing questionnaires among experts and professors and examining the internal and external factors (strengths, weaknesses, opportunities, threats) related to environmental water diplomacy in the study area by these individuals, and distributing another questionnaire, the impact coefficient and the level of importance of each criterion for the internal and external environments were estimated separately. The prioritization of criteria was carried out based on pairwise comparisons using Expert Choice software. After collecting the relevant forms, the average of each factor (in the "Impact Level" column) was obtained. Subsequently, each factor was normalized separately, and finally, the score (final weight) of each factor was obtained by multiplying the normalized value of the "Impact Level" column by the value in the "Importance Coefficient" column, as detailed in Table (5).

**Table 2- Strengths**

| Strengths | Importance Level | Impact Coefficient |
|---|---|---|
| Bilateral Tendencies and Active Diplomacy | | |
| Meetings Focused on Turkey's Dam Construction | | |
| Actions of Influential NGOs and Campaigns Formed in This Area | | |
| Extensive Media Outreach and Use of the Borderless Cyberspace in This Regard and More Executive Actions | | |
| Allocating the Topic of Turkey's Dam Construction Hydropolitics to Relevant Organizations | | |
| Weaknesses | | |
| Turkey's Exploitation of the Weakness of Neighboring Countries (Turkey, Iraq, Syria, Iran) | | |
| Lack of or Insufficient Appropriate Planning and Policies in Environmental and Natural Resources Management | | |
| Weakness in Iran's Diplomatic Apparatus | | |
| Weakness and Negligence of Responsible Organizations and Departments to Prevent the Implementation of Turkey's Dam Construction Projects | | |
| Lack of Sufficient Specialized Knowledge and Literacy of Relevant Experts Regarding the Consequences and Implications of the Implementation of These Projects | | |
| Lack of Proper Education for Iran, Turkey, Iraq, Syria in Dealing with Water Resources | | |

 *DOI:* 10.22055/jise.2025.50717.2184

**Table 3- Opportunities**

| Opportunities | Importance Level | Impact Coefficient |
|---|---|---|
| Iran can strive to utilize the tool of water diplomacy to manage shared water resources by virtue of its power in the region. | | |
| Iran's efforts towards achieving a comprehensive and sustainable regional agreement accompanied by a specific management mechanism. | | |
| A dispute resolution mechanism along with the establishment of an institution with an independent legal personality and representatives from relevant governments, experts, scientific specialists, and designated workshops that can pave the way for win-win strategies. | | |
| The preparation of a collaborative plan by Iran to foster cooperation among all beneficiary governments (Iran, Turkey, Iraq, Syria) in the context of reversing desertification with an economic approach. | | |
| The formation and development of scientific collaborations among higher education centers of relevant governments in the field of international water law. | | |
| The implementation of joint projects for the management of transboundary water resources with neighboring countries and Iran's role as a key element in achieving the intended goals. | | |
| Utilizing the principle of reasonable and equitable utilization by the states of the shared watercourse basin. | | |
| Utilizing the general obligation for cooperation among the states of the watercourse basin for the adequate protection of the watercourse and the achievement of optimal utilization. | | |
| Utilizing the Convention on Biological Diversity, to which Turkey is also a party. | | |
| Reconsidering all economic and social development programs in the region with a focus on water. | | |
| The legal authority of Iran, Turkey, Iraq, and Syria to file lawsuits in international courts and tribunals against Turkey to determine and obtain water rights. | | |

**Table 4- Threats**

| Threats | Importance Level | Impact Coefficient |
|---|---|---|
| Creation of water crisis (reduction of groundwater aquifers, decrease in the water volume of downstream regional dams, etc.) | | |
| Soil erosion (drying up of wetlands and lakes, drying and reduction of soil moisture, destruction of millions of hectares of agricultural lands, pastures, and forests) | | |
| Creation of wind erosion hotspots and the generation of dust and particulate matter from Turkey and Iraq towards Iran. | | |
| Ecosystem change (imbalance of the ecological equilibrium of dependent regions, including the Caspian Sea, leading to a major environmental catastrophe) | | |
| Reduction of air quality (entry and production of dust and particulate matter, transfer of toxins, and increase in pollution) | | |
| Disruption of social security and widespread migration from border regions to central cities. | | |
| Increase in the cost of guarding uninhabited borders and the emergence of insecurity in border areas | | |
| Increase in unemployment and the creation of economic problems for the residents of border regions | | |
| Spread of microbial and viral diseases due to water shortages resulting from the closure of incoming waters from Turkey. | | |

**Table 5- Evaluation Matrixs (Strengths, Weaknesses, Opportunities and Threats) of Turkey's Hydropolitical with Iran**

| Evaluation Matrixs | | | |
|---|---|---|---|
| Strengths | Importance Level | Impact Coefficient | Final Weight |
| Factor 1 | 4 | 0.24 | 0.96 |
| Factor 2 | 2 | 0.21 | 0.42 |
| Factor 3 | 2 | 0.17 | 0.34 |
| Factor 4 | 3 | 0.21 | 0.63 |
| Factor 5 | 3 | 0.17 | 0.51 |
| Weaknesses | | | |
| Factor 1 | 5 | 0.18 | 0.9 |
| Factor 2 | 4 | 0.21 | 0.84 |
| Factor 3 | 4 | 0.21 | 0.84 |
| Factor 4 | 3 | 0.1 | 0.3 |
| Factor 5 | 2 | 0.09 | 0.18 |
| Factor 6 | 3 | 0.18 | 0.54 |
| Opportunities | | | |
| Factor 1 | 3 | 0.07 | 0.21 |
| Factor 2 | 3 | 0.06 | 0.18 |
| Factor 3 | 5 | 0.13 | 0.65 |
| Factor 4 | 3 | 0.9 | 0.27 |
| Factor 5 | 4 | 0.12 | 0.48 |
| Factor 6 | 4 | 0.16 | 0.64 |
| Factor 7 | 3 | 0.07 | 0.21 |
| Factor 8 | 2 | 0.07 | 0.14 |
| Factor 9 | 2 | 0.07 | 0.14 |
| Factor 10 | 3 | 0.07 | 0.21 |
| Factor 11 | 3 | 0.09 | 0.21 |
| Threats | | | |
| Factor 1 | 2 | 0.11 | 0.22 |
| Factor 2 | 3 | 0.1 | 0.3 |
| Factor 3 | 4 | 0.15 | 0.6 |
| Factor 4 | 2 | 0.09 | 0.18 |
| Factor 5 | 3 | 0.09 | 0.27 |
| Factor 6 | 4 | 0.1 | 0.4 |
| Factor 7 | 3 | 0.13 | 0.39 |
| Factor 8 | 4 | 0.13 | 0.52 |
| Factor 9 | 2 | 0.1 | 0.2 |

Subsequently, Iran's pairwise strategies regarding the hydropolitics of its border rivers with Turkey were calculated using a brainstorming session. The calculated pairwise strategies from this session are presented in Table (6).

Subsequently, considering the aforementioned pairwise strategies and their combination and integration, fundamental strategies were proposed Table (7).

 *DOI:* 10.22055/jise.2025.50717.2184

**Table 6- Initial (pairwise) Calculated Strategies**

| |
|---|
| SO Strategies (Aggressive Strategy – maxi-maxi) |
| Enhancing the security provision capabilities of Iran's border rivers with Turkey by Iranian military forces and denying entry to the armed forces of other powers into this region.<br>Concluding security, trade, and economic memoranda of understanding between Iran and Turkey under the supervision of international monitoring bodies, including the United Nations, based on international conventions. |
| ST Strategies (Contingency Strategy – Maxi-Mini) |
| Investing and striving to grow and enhance the knowledge and economic capacity of the country's border regions to counter potential environmental and security threats, including the risk of desertification in Azerbaijan due to the drying up of the Aras River caused by Turkey's dam construction. |
| WO Strategies (Adaptive Strategy – Mini-Maxi) |
| Joint collaborations with Turkey in the field of environmental problems under the supervision of the United Nations Environment Programme and other relevant organizations. |
| WT Strategies (Defensive Strategy – Mini-Mini) |
| Emphasizing to government officials, and especially the Supreme National Security Council, the correct and principled implementation of national land-use planning schemes and the employment of expert and committed Iran-oriented personnel in provincial and national positions. |

**Table 7- Fundamental Strategies**

| Code | Strategies |
|---|---|
| 1 | Enhancing the security provision capabilities of Iran's border rivers with Turkey by Iranian military forces and denying entry to the armed forces of other powers into this region |
| 2 | Joint collaborations with Turkey in the field of environmental problems under the supervision of the United Nations Environment Programme and other relevant organizations |
| 3 | Emphasizing to government officials, and especially the Supreme National Security Council, the correct and principled implementation of national land-use planning schemes and the employment of expert and committed Iran-oriented personnel in provincial and national positions |
| 4 | Concluding security, trade, and economic memoranda of understanding between Iran and Turkey under the supervision of international monitoring bodies, including the United Nations, based on international conventions |
| 5 | Investing and striving to grow and enhance the knowledge and economic capacity of the country's border regions to counter potential environmental and security threats, including the risk of desertification in Azerbaijan due to the drying up of the Aras River caused by Turkey's dam construction |

In this stage, the strategies were prioritized Table (8), and the opinions of experts were obtained and entered into Expert Choice software. Figure (1) illustrates the average pairwise judgments of the experts and the inconsistency ratio of the pairwise comparison of these criteria, which shows a value of 0.06. Given that this value is less than 0.1, the acceptable accuracy of this pairwise comparison is confirmed.

In this software, calculations were performed using the vector method, and the final weight of each calculated strategy was determined Table (8).

Subsequently, the results obtained from the Analytic Hierarchy Process calculations and the final weight of the strategies were extracted as shown in Figure (2) (output of Expert Choice software). Ultimately, the final prioritization of hydropolitical strategies was carried out Table (9).

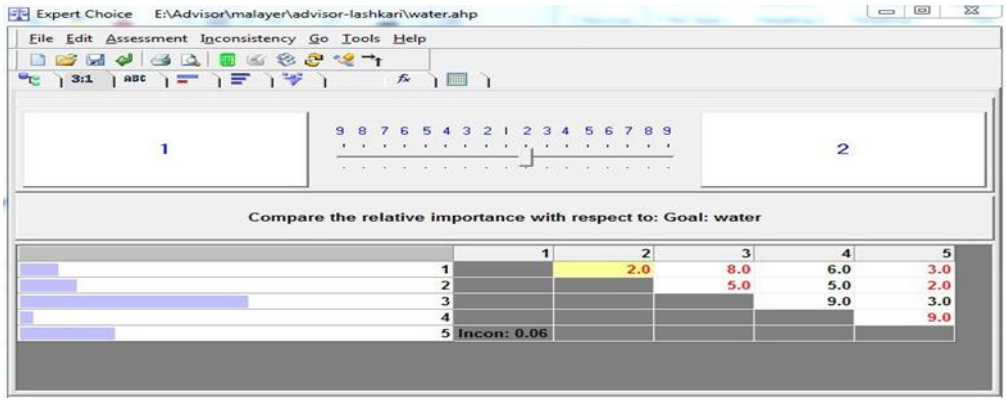



**Fig. 1- Pairwise Comparisons in Expert Choice Software and the Resulting Inconsistency Ratio**

**Table 8- Final Weight of Fundamental Strategies**

| Code | Strategies | Final Weight |
|---|---|---|
| 1 | Enhancing the security provision capabilities of Iran's border rivers with Turkey by Iranian military forces and denying entry to the armed forces of other powers into this region | 0.089 |
| 2 | Joint collaborations with Turkey in the field of environmental problems under the supervision of the United Nations Environment Programme and other relevant organizations | 0.126 |
| 3 | Emphasizing to government officials, and especially the Supreme National Security Council, the correct and principled implementation of national land-use planning schemes and the employment of expert and committed Iran-oriented personnel in provincial and national positions | 0.532 |
| 4 | Concluding security, trade, and economic memoranda of understanding between Iran and Turkey under the supervision of international monitoring bodies, including the United Nations, based on international conventions | 0.029 |
| 5 | Investing and striving to grow and enhance the knowledge and economic capacity of the country's border regions to counter potential environmental and security threats, including the risk of desertification in Azerbaijan due to the drying up of the Aras River caused by Turkey's dam construction | 0.224 |

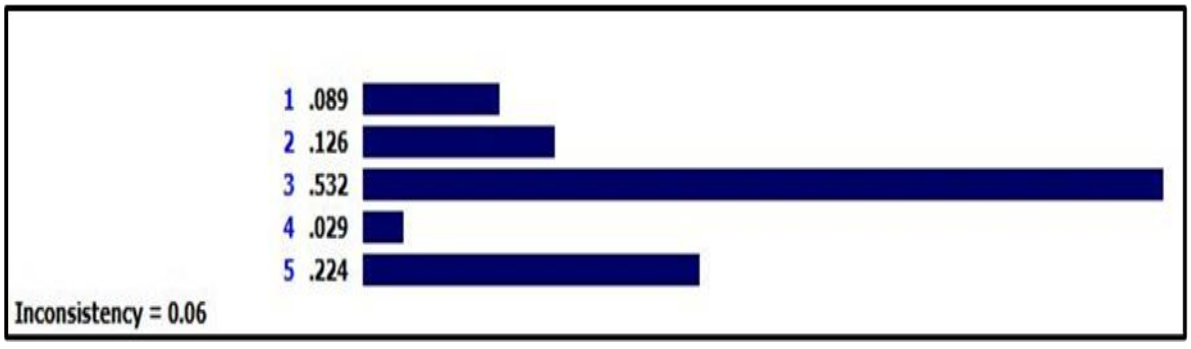



**Fig. 2- Final Weights of Fundamental Strategies in Expert Choice Software Output**

 *DOI:* 10.22055/jise.2025.50717.2184

**Table 9- Final Prioritization of Hydropolitical Strategies**

| Strategy Code | Priority |
|---|---|
| 1 | 4 |
| 2 | 3 |
| 3 | 1 |
| 4 | 5 |
| 5 | 2 |

The current trend in environmental protection is such that many natural resources are now facing serious threats and even extinction. Furthermore, in recent decades, preventive measures that could reverse this trend have not been taken. Turkey's expansionist actions in the field of dam construction and control over water resources, with the aim of exerting power in the region, have created a multitude of environmental, economic, and social challenges. The findings of research and related studies indicate that Turkey's two major dam construction projects, known as DAP in the Aras basin and GAP in the Tigris-Euphrates basin, threaten the region's water security and infringe upon the water rights of downstream countries. Environmental impact assessments reveal that Turkey's GAP and DAP dam construction projects do not fall within the scope of domestic sovereignty and have trans-regional effects. Dependence of water security on water resources outside the country effectively ties a portion of the country's national security to the region.

The absence of managerial structures in the utilization of these resources can become a factor in creating crises between countries. While the implementation of these projects meets national-level water needs, the political objectives of these projects appear to be more significant, or at least it can be inferred that these plans have the potential to be used as a tool of pressure on downstream countries, to the extent that water could be leveraged against the oil of Iraq and Syria as a trump card. It seems that Turkey seeks to establish itself as the (water power) of the region by controlling the water arteries, thereby consolidating its power over neighboring countries. Given that the West Asia region is located in the arid belt and has experienced successive droughts and reduced rainfall in recent years, the final operation of the dams has meant that Syria, Iraq, and Iran, as downstream countries in the Tigris-Euphrates and Aras River basins, have not been spared the environmental consequences.

As observed in Table (5), the total score (final weight) of the factors related to strengths, weaknesses, opportunities, and threats are 0.57 for strengths, 0.60 for weaknesses, 0.28 for opportunities, and 0.34 for threats. This indicates that currently, the net effect of the existing opportunities and threats is neutral. Although the threats are not critical, there are no particularly significant or golden opportunities either. Furthermore, as observed in Figure (2), Strategy 3 has the highest weight (0.532) and is of the greatest importance, while Strategy 4 has the lowest weight (0.29). Therefore, the strategy of "Emphasizing to government officials, and especially the Supreme National Security Council, the correct and principled implementation of national land-use planning schemes and the employment of expert and committed Iran-oriented personnel in provincial and national positions" is identified as the most prioritized and effective hydropolitical strategy for Iran, warranting the attention of relevant authorities Zaki and Najafi (2020) also alluded to this in their study.

The prioritization results reveal a clear policy preference among experts: Strategy 3 focused on institutional reform and expert-driven land-use planning received the highest weight (0.532). This reflects a consensus that Iran's most effective leverage lies in strengthening domestic governance capacity rather than pursuing high-risk diplomatic or military postures. The low priority assigned to Strategy 4 (internationally monitored economic agreements, weight = 0.029)

suggests skepticism about Turkey's willingness to accept external oversight or the feasibility of such frameworks under current geopolitical conditions. Moreover, the relatively high weight of Strategy 5 (0.224) investing in border region resilience indicates recognition that local socio-ecological stability is a prerequisite for effective transboundary engagement. This aligns with recent scholarship emphasizing "bottom-up" water diplomacy that empowers subnational actors (Keskinen et al., 2021).

**Conclusion**

This study demonstrates that Iran's optimal path forward in managing transboundary water tensions with Turkey lies not in confrontation, but in institutional consolidation, expert-led planning, and sub-national resilience-building. The top-ranked strategy implementing scientifically informed land-use policies with qualified personnel addresses both environmental sustainability and national security by reducing vulnerability to upstream disruptions. Future research should expand the expert pool to include Turkish and Iraqi scholars, incorporate hydrological modeling of dam impacts, and explore the role of non-state actors (e.g., NGOs, academia) in Track II water diplomacy. Although, according to the results and the opinions of experts and specialists, the country's current strategy regarding hydropolitics vis-à-vis Turkey is a defensive strategy, it is very close to the center due to its position on the border of the SO region in the SWOT matrix. Therefore, employing aggressive strategies in this situation is not very reasonable.

While it is true that Iran has an advantage over its competitor, Turkey, in terms of both internal and external environments, this advantage is not very significant. Consequently, considering that a review of the historical behavior of the neighboring country, as well as its specific geography and limited access to open waters, indicates that if Turkey gains superiority in economic and military fields over Iran, it could pose an actual threat to our country. As a first step, it is most appropriate for our country's government officials, especially the Supreme National Security Council, to strive for the correct and principled implementation of national land-use planning schemes and the employment of expert and committed Iran-oriented personnel in provincial and national positions. The second step involves investing and striving to enhance the country's knowledge and economic capacity to counter potential environmental and security threats, including the risk of desertification in Azerbaijan due to the drying up of the Aras River. The third step involves paying special attention and allocating appropriate budgets to enhance and develop the country's industrial, infrastructural, strategic economic, nuclear, and military equipment, utilizing domestic scientific, technical, and academic capacities and capabilities to achieve balance and relative superiority over Turkey. In the fourth step, Iranian officials and government authorities should, within a complementary approach, with prudence, policy, and the adoption of smart diplomacy, strive to expand bilateral relations with Turkey and develop the shared water basin regions and areas.

Given that the complementary strategy is a model and framework for resolving issues and problems in geographical locations, and the fundamental assumption in this approach is based on the existence of differences and inequalities among geographical locations, in this regard, Turkey, due to its specific geographical situation regarding easy and convenient access to open waters, has at certain historical junctures sought to overcome this geographical problem, the result of which has been the creation of tension and conflict with its neighboring countries (Turkey, Iraq, and Kuwait). Based on the complementary strategy, the development of the transboundary water basin with the participation of Turkey should be on the agenda of Iran's diplomatic apparatus and foreign policy. Efforts should be made to identify areas of interaction, cooperation, and partnership between the two countries based on the four domains of the complementary approach (political, economic, security, and cultural) to mitigate Turkey's geographical disadvantage and limitations as

much as possible. To this end, the relevant authorities and officials should create incentives and motivation for the Turkish government to participate in the management and utilization of the shared water basin.

## Acknowledgment

The authors of this article would like to thank editor and anonymous reviewers.

**Conflict of Interest**

The authors declared no potential conflicts of interest concerning the research, authorship, and publication of this article.

**Funding**

The authors received no financial support for the research, authorship, and publication of this article.

**Data Availability Statements**

Data Availability Statement: All information and results are presented in the text of the article.

**Authors' Contribution**

**First Author:** Fatemeh Lashkari, Conceptualization, Methodology, Software, Investigation, Writing

**Second Author:** Mir Mehrdad Mirsanjari, Writing - Review & Editing, Visualization, Supervision

**Third Author:** Fatemeh Mohammadyari Conceptualization, Software, Writing - Review & Editing.

**References**

1- Council of the European Union, 2018. *Council Conclusions on Water Diplomacy*.

2- Council of the European Union, 2020. *Council conclusions on Climate Diplomacy*.

3- Cuppari, R., Schmeier, S. and Demuth, S., 2017. *Preventing conflicts, fostering cooperation*–The many roles of water diplomacy. https://www.waterandchange.org/wp-content/uploads/2018/02/PUB_Water-Diplomacy_Bericht.

4- Eilstrup-Sangiovanni, M. and Hofmann, S.C., 2020. Of the contemporary global order, crisis, and change. *Journal of European Public Policy*, *27*(7), pp.1077-1089. https://doi.org/10.1080/13501763.2019.1678665

5- Ghaznafarzadeh Kapte, H., 2018. Environmental Impacts of Turkey's Anatolian Project on Iran's Climate. *In National Conference on Climate Change and Aquatic Ecosystems*.

6- Gleeson, T., Wang-Erlandsson, L., Zipper, S.C., Porkka, M., Jaramillo, F., Gerten, D., Fetzer, I., Cornell, S.E., Piemontese, L., Gordon, L.J. and Rockström, J., 2020. The water planetary boundary: interrogation and revision. *One Earth*, *2*(3), pp.223-234. https://doi.org/10.1016/j.oneear.2020.02.009

7- Grech-Madin, C., Döring, S., Kim, K. and Swain, A., 2018. Negotiating water across levels: A peace and conflict "Toolbox" for water diplomacy. *Journal of Hydrology*, *559*, pp.100-109. https://doi.org/10.1016/j.jhydrol.2018.02.008

8- Gurl, E. and Merba, T., 2017. SWOT analysis: A theoretical review. *Journal of International Social Research*. 10(51):994-1006. https://doi.org/10.17719/jisr.2017.1832

9- Hekmat Ara, H., 2022. Water Dispute between Iran and Turkey in the Aras Basin and How to Manage Them. *IRAS (Institute for Iran and Eurasia Studies).* https://www.iras.ir/p=6432

10- Honkonen, T. and Lipponen, A., 2018. Finland's cooperation in managing transboundary waters and the UNECE Principles for Effective Joint Bodies: Value for water diplomacy?. *Journal of Hydrology*, *567*, pp.320-331. https://doi.org/10.1016/j.jhydrol.2018.09.062

11- IPCC, 2019. Climate Change and Land: An IPCC Special Report on climate change, desertification, land degradation, sustainable land management, food security, and greenhouse gas fluxes in terrestrial ecosystems -*Summary for Policymakers (Intergovernmental Panel on Climate Change IPCC)*

12- Karjalainen, T., 2020. EU peace mediation in the 2020s: *From intervention to investment*.

13- Kavianirad, M., Sadrania, H., Nasri Fakhredavood, S. and Hamid, H., 2022. Water Diplomacy Role in Easing Iran-Iraq Hydropolitical Tensions. *Geopolitics Quarterly*, 18(4), pp.71-93. 20.1001.1.17354331.1401.18.68.4.6

14- Keskinen, M., Salminen, E. and Haapala, J., 2021. Water diplomacy paths–An approach to recognise water diplomacy actions in shared waters. *Journal of Hydrology*, 602, p.126737. https://doi.org/10.1016/j.jhydrol.2021.126737

15- Klimes, M., Michel, D., Yaari, E. and Restiani, P., 2019. Water diplomacy: The intersect of science, policy and practice. *Journal of Hydrology*, 575, pp.1362-1370. https://doi.org/10.1016/j.jhydrol.2019.02.049

16- Krzymowski, A., 2021. Water diplomacy and its strategic significance for sustainable development goals and global security architecture. *Sustainability*, 13(24), p.13898. https://doi.org/10.3390/su132413898.

17- Kummu, M., Guillaume, J.H., De Moel, H., Eisner, S., Flörke, M., Porkka, M., Siebert, S., Veldkamp, T.I. and Ward, P.J., 2016. The world's road to water scarcity: shortage and stress in the 20th century and pathways towards sustainability. *Scientific reports*, *6*(1), p.38495. https://doi.org/10.1038/srep38495

18- Marks, S. and Freeman, C.W., 2020. Diplomacy. *Diakses pada*, *12*.

19- MacKay, K. and Collins, R., 2025. Reorienting approaches to maritime boundary disputes: A case for hydro-diplomacy?. *Marine Policy*, *171*, p.106442. https://doi.org/10.1016/j.marpol.2024.106442.

20- McCracken, M. and Wolf, A.T., 2019. Updating the Register of International River Basins of the world. *International Journal of Water resources development*, *35*(5), pp.732-782. https://doi.org/10.1080/07900627.2019.1572497.

21- Niemann, A., Haastrup, T. and Bergmann, J., 2018. Motives, Roles, Effectiveness and the Future of the EU as an International Mediator. *International Negotiation*, *23*(2), pp.319-330. http://booksandjournals.brillonline.com/content/journals/15718069.

22- Nunnally, J. C. 1978. Psychometric Theory: 2d Ed. McGraw-Hill

23- Pohl, B., Carius, A., Conca, K., Dabelko, G., Kramer, A., Michel, D., Schmeier, S., Swain, A. and Wolf, A., 2014. The rise of hydro-diplomacy: *Strengthening foreign policy for transboundary waters.* https://doi.org/10.13140/2.1.4035.5848

24- Saaty, TL. 1977. A scaling method for priorities in hierarchical structures. *Journal of mathematical psychology*. 15 (3), 234-281. https://doi.org/10.1016/0022-2496(77)90033-5

25- Ha-Vikström, T. and Takala, J., 2016. Knowledge management and analytical modeling for transformational leadership profiles in a multinational company. *In Successes and failures of knowledge management* (pp. 151-173). Morgan Kaufmann.

26- Samei, S., Akhbari, M. and Heydari, G., 2020. Regional Cooperation Between Iran and Western Neighbors based on Water Diplomacy (Case Study: Iraq and Turkey). *Geography (Regional Planning)*, 10(2-3), pp.605-619. 20.1001.1.22286462.1399.10.39.7.4

27- Sehring, J., Schmeier, S., Ter Horst, R., Offutt, A. and Sharipova, B., 2022. *Diving into water diplomacy–exploring the emergence of a concept. Diplomatica, 4 (2), 200–221.* https://doi.org/10.1163/25891774-bja10082.

27-Sehring, J., ter Horst, R. and Said, A., 2023. Water diplomacy: A man's world? Insights from the Nile, Rhine and Chu-Talas basins. *Journal of Hydrology X*, *20*, p.100152. https://doi.org/10.1016/j.hydroa.2023.100152.

28-Zaki, Y. and Najafi, S., 2020. Determining Iran hydropolitics strategies in Arvandrood basin. *Human Geography Research*, *52*(4), pp.1529-1549. https://doi.org/10.22059/jhgr.2020.296172.1008070.

© 2026 The Author(s). Published by Shahid Chamran University of Ahvaz. This is an open-access article distributed under the terms of the Creative Commons Attribution License (http://creativecommons.org/licenses/by/4.0), which permits unrestricted use, distribution, and reproduction in any medium, provided the original work is properly cited.

Shahid Chamran University of Ahvaz

**Irrigation Sciences and Engineering (JISE)**
**Vol. 48, No. 4, Winter 2026, p. 133-144**
Journal homepage: https://jise.scu.ac.ir

**Review Paper**

# Modern Filtration Technologies for Nutrient Removal from Domestic Wastewaters: A Review

Saeid Eslamian[1*] and Mousa Maleki[2]

*1*- Corresponding Author, Full Professor, Department of Water Science and Engineering, College of Agriculture, Isfahan University of Technology, Isfahan, Iran (Saeid@iut.ac.ir).*
*2- PhD Student, Department of Water Science and Engineering, College of Agriculture, Isfahan University of Technology, Isfahan, Iran.*

**ARTICLE INFO**

*Article history:*
Received: 12 February 2025
Revised: 30 March 2025
Accepted: 23 April 2025
Available online: 04 January 2026

*Keywords:*
Modern technologies, Domestic wastewater, Nitrogen, Phosphorus, Filtration Technologies.

**TO CITE THIS ARTICLE:**
Eslamian, S., Maleki, M. 2026. 'Modern Filtration Technologies for Nutrient Removal from Domestic Wastewaters: A Review', *Irrigation Sciences and Engineering*, 48(4), pp. 133-144. doi: 10.22055/jise.2025.49471.2163.

**Abstract**

Nitrogen and phosphorus are essential for the growth and vitality of living organisms; hence they are called nutrients. However, the discharge of nutrient-rich waste streams into aquatic ecosystems leads to eutrophication. Therefore, nutrient removal from wastewater is critical to meet strict nutrient discharge standards. In general, the management of water and wastewater resources is essential to achieve sustainable development. Today, with the progress of urbanization, the necessity to remove nutrients from domestic wastewater that threaten human health is strongly felt. Therefore, it is necessary to develop current methods in addition to using previous methods in nutrient removal to be economically viable and also to increase the efficiency of the system. Due to the presence of nutrients such as nitrogen and phosphorus, domestic wastewater causes the rapid growth of all kinds of algae after being discharged into the water and finally ends in the phenomenon of enrichment. As a result, it is necessary to reduce the amount of phosphorus and nitrogen as much as possible before discharging the wastewater into water sources. Therefore, in this study, a new perspective of modern filtration technologies in the removal of phosphorus and nitrogen is given. It is necessary to explain that most of the following methods are relatively new methods that are converted into methods with higher efficiency and lower costs for domestic wastewater treatment by combining or modifying the main process.

## Introduction

The global water consumption has doubled in the recent decades (Van Vliet et al., 2017). Currently, humanity has endangered by water-related issues, which are increasing due to population growth, rapid urbanization and the growing crisis of climate change (Koop and van Leeuwen, 2017). Wastewater is produced as the result of various agricultural, domestic and industrial operations, and in addition to inorganic and organic chemicals that are released into the atmosphere, it contains human-made pollutants and nutrients (Patwardhan, 2017; Le et al., 2021; Mofijur et al., 2021). If these pollutions are not properly treated, they lead to the destruction of the environment and pose risks to human health (Prosser and Sibley, 2015). Therefore, wastewater management and treatment are one of the main programs in many parts of the world to prevent threats to water quality and availability (Abdel-Raouf et al., 2012). Many countries have focused on improving domestic wastewater treatment technologies, especially regarding the reduction of phosphorus (P) and

nitrogen (N) in wastewater effluents (Connor et al., 2017).

In order to achieve a more sustainable society, it is necessary to rethink the approach to dealing with waste; however, it can also lead to some opportunities. On the other hand, it is necessary to produce clean energy and move towards a carbon-free future. In particular, there is a growing interest in the development of new renewable energy technologies that, unlike solar or wind energy, produce a predictable and stable amount of energy regardless of the weather. For example, Statkraft's prototype osmotic power plant in Tofte, Norway, was the world's first osmotic or salinity gradient power generation plant (Skilhagen et al., 2008; Statkraft, 2013). However, implementing resource recovery technologies is a challenge. Because in the past, wastewater treatment plants were designed and built in a centralized manner with the sole purpose of reducing the pollutant load. To move from pollution removal to recovery sources, existing treatment facilities must be redesigned and modified with the help of governments, scientific institutions, private stakeholders and end users (Kehrein et al., 2020). In addition, socio-economic challenges caused by the past and future of the country's political and socio-economic situation are also a big obstacle (Montwedi et al., 2021).

The presence of nutrients (phosphorus and nitrogen) in wastewater can be a challenge or an opportunity (Eslamian, 2016). The discharge of nutrients from wastewater into the environment can contaminate land and water and cause eutrophication in natural surface water environments, which can lead to algal blooms and other environmental challenges (Dube et al., 2016; Vu et al., 2019).The findings show that while nutrients are essential for healthy ecosystems, there is a link between nutrient overload and harmful algal blooms (HABs) (Heisler et al., 2008, United States Environmental Protection Agency, 2015). Consequently, strict rules have been established in many countries to protect aquatic ecosystems and human health (Jafarinejad, 2019a; Jafarinejad and Jiang, 2019; United States Environmental Protection Agency, 2009; Liu et al., 2011 and Xue et al., 2015).

In the current decade, the concept of nutrient removal/recovery has been used as a sustainable solution to develop and design a variety of modern wastewater treatment technologies to recover nutrients from waste streams and is one of the high-priority research areas (Xue et al., 2015). On the other hand, forward osmosis (FO) membrane technology has grown significantly in the past decade, but application in wastewater treatment has been slower due to some specific limitations. In this study, nutrient removal processes, FO membrane technology, main factors affecting FO process performance, water source for nutrient recovery, previous studies on FO membrane process for nutrient removal/recovery from wastewater and sludge, membrane fouling, and recent developments in FO membranes for nutrient removal/recovery are briefly and critically reviewed. Then, proposed possible schemes for applying the FO process in conventional wastewater treatment plants (WWTPs) were theoretically presented. Finally, based on the gaps identified in the region, the challenges ahead, future prospects and conclusions were discussed.

**Aims and Objectives**

In this study, different types of modern nutrient removal filtration technologies will be introduced and assessed. With regards to the global water and energy crisis, and on the other hand the global warming and intensive climate change, the most cost-effective methods will be of higher attention and consideration in this study. In other words, high energy-consuming methods are disregarded in this review paper. Details of each method and technology will be discussed and at the end, it is expected to have a comprehensive comparison between the methods and distinguish which method would perform better in each unique situation.

**Modern Nutrient Removal Technologies**

Modern nutrient removal technologies combine treatment steps with judicious design and create conditions to enable a high degree of nutrient removal and differ from

conventional nutrient removal technologies in several ways (Anjali and Sabumon, 2024; Do et al., 2020; Rene et al., 2020). Recently, emerging nutrient removal technologies, including phosphorus and nitrogen removal exclusively have been developed to enhance nutrient removal efficiency and save energy and operating cost, such as simultaneous nitrification/denitrification (SND), anaerobic oxidation of ammonium (anammox), single reactor for ammonia removal with high activity from nitrite (SHARON) etc. (Ahn, 2006; Andalib, 2011; Shammas and Wang, 2010; Lee et al., 2021, Kwak et al., 2020). Each of the aforementioned methods will be discussed in the following sub-sections.

**Simultaneous Nitrification/Denitrification SND)**

Simultaneous nitrification, denitrification and phosphorus removal (SNDPR) process has elicited significant attention for high-efficient and low-cost simultaneous nitrogen and phosphorus removal (Chen et al., 2024; Takeda et al., 2025; Wu et al., 2023 and Kwak et al., 2020) Besides relying on conventional phosphorus-accumulating organisms (PAOs) and denitrifying microbes, slow-growing and autotrophic nitrifying bacteria, and heterotrophic nitrifying PAOs (DNPAOs) and glycogen-accumulating organisms (DGAOs and enriched in nitrophores) can also contribute to nitrogen removal (He et al., 2016; Sun et al., 2024; Yang et al., 2016; Roy et al., 2021, Zhao et al., 2018).

The simultaneous nitrification, denitrification and phosphorus removal (SNDPR) system has attracted much attention due to its economy and efficiency (Wu et al., 2023). The main functional microorganisms in the SNDPR system include ammonia-oxidizing bacteria (AOB), nitrite-oxidizing bacteria (NOB), glycogen-accumulating organisms (GAOs), glycogen-accumulating organisms (DGAOs), polyphosphate-accumulating organisms (PAOs), polyphosphate-accumulating organisms (DPAOs), and ordinary heterotrophic denitrifying organisms (OHOs) (Rosas-Echeverría et al., 2023; Carvalho et al., 2007, Wang et al., 2020).

The SNDPR process is usually operated with anaerobic/microaerobic (A/MO) or anaerobic/microaerobic/anoxic (A/MO/A) operation mode and combines simultaneous nitrification (SND) with enhanced biological phosphorus removal (EBPR). A single reactor during the anaerobic period, DGAOs, PAOs and DPAOs store simple organic substances such as low-chain fatty acids in water in the form of poly-β-hydroxy alkenoate (PHA) in the cell, meanwhile, PAOs and DPAOs They can break down and release intracellular polyphosphate and phosphorus into the environment (De Kreuk et al., 2005; Freitas et al., 2005). Under aerobic conditions, AOB and NOB oxidize ammonia nitrogen and nitrogen to nitrate nitrogen, respectively. DGAOs carry out the denitrification process by degrading intracellular PHA, in addition, PAOs/DPAOs use oxygen/nitrite as electron acceptors and absorb excess phosphorus (Rubio-Rincón et al., 2017; He et al., 2018., Freitas et al., 2005). Nitrate and nitrite removal depends on DGAOs and DPAOs, and phosphorus removal by PAOs and DPAOs is more than absorption and discharge of phosphorus-rich residual sludge.

**Anaerobic Oxidation of Ammonium (Anammox)**

With the increasing development of urbanization, the total amount of wastewater discharge continues to increase (Yu et al., 2019). For example, the wastewater discharge of China reached 69.97 billion tons in 2017 (Normative Documents on the Guidance of Prices, 2017). By the end of 2018, more than 5000 municipal wastewater treatment plants have been built in China (Qu et al., 2019). In particular, a large amount of municipal wastewater containing ammonium is typically discharged after treatment, thus intensifying the eutrophication of water bodies and damaging the ecological environment (Qiu, 2021; Wang et al., 2022 , Chen et al., 2021a). Therefore, an efficient and stable reduction of the effluent concentration of ammonia nitrogen is very important for the control of eutrophication (Ma et al., 2020). By far, the conventional biological nitrogen removal (BNR) from wastewater mainly relies on two independent processes including nitrification

and denitrification. With regards to these processes, ammonia nitrogen in municipal wastewater is finally converted to dinitrogen (N2) and discharged into the atmosphere under the synergistic action of multiple microorganisms (Faraji et al., 2017; Pourmohammad et al., 2020; Li et al., 2024; Singh et al., 2025, Chen et al., 2021b). Unfortunately, the BNR process has come under increasing criticism because it is considered economically and environmentally unsustainable in terms of energy consumption, sludge production, and greenhouse gas emissions (Zhang et al., 2019, Zhan et al., 2020).

To cope with such engineering challenges, people have begun to devote themselves to research on the autotrophic anaerobic ammonium oxidation (anammox) process, which is a process in which nitrite and ammonium are simultaneously converted into dinitrogen through the function of anammox bacteria, taking nitrite as the electron acceptor and ammonium as the electron donor (Yan et al., 2024 , Van de Graaf et al., 1996). At the end of the 20th century, new biological nitrogen removal technologies based on the principle of anammox have been rapidly developed. For example, the partial nitrification-anammox (PN-AMX) as a complete autotrophic process has been employed to achieve nitrification and anammox in the reactor and thus result in nitrogen removal through the synergistic action of ammonium oxidizing bacteria (AOB) and anammox bacteria (Jafarinejad, 2019b; Liu et al., 2017; Ma et al., 2015, Ma et al., 2016).

Up to now, more than 110 anammox plants have been established in full-scale applications worldwide, most of which are used for treating high ammonium wastewater with low C/N and high temperatures (Ma et al., 2016). Nevertheless, when PN-AMX is applied to mainstream municipal wastewater treatment, the concentration of free ammonia (FA) and free nitrous acid (FNA) is low that cannot effectively inhibit the activity of nitrite-oxidizing bacteria (NOB), leading to the gradual decrease of the accumulation rate of $NO_2^- - N$ and even a poor nitrogen removal rate (Mao et al., 2017). Moreover, as the total nitrogen (TN) concentration in municipal wastewater is low (20-75 mg $L^{-1}$), containing organic matter, and the temperature might fluctuate greatly (below 10°C in winter), it is made difficult to remove nitrogen using the PN-AMX process. In summary, the unstable accumulation of nitrite has been the bottleneck of PN-AMX in mainstream municipal wastewater treatment (Wang et al., 2016).

**Single Reactor for Ammonia Removal with High Activity from Nitrite (SHARON)**

The SHARON filtration process is a partial nitrification process where the ammonia is oxidized to nitrite (Wei et al., 2017; Wang et al., 2016., Ganigué et al., 2009) The study conducted by Liang (2007) determined the optimal conditions to acquire constant SHARON process for leachate treatment in a bench-scale fixed bed biofilm reactor. The results showed that both dissolved oxygen and ammonium volumetric loading rate had effects on the SHARON process. In the SHARON process, rejection water from dewatering of digested sludge is treated for N-removal. It concerns a highly active process operating without sludge retention (Guan, 2024). The single tank reactor is intermittently aerated. Due to differences in growth rate nitrite oxidizers are washed out of the system while ammonia oxidizers can be maintained, resulting in N-removal over nitrite (Mulder et al., 2001).

Previously, before the SHARON process was developed, a broad range of process factors such as: pH, DO, temperature, $NH_4$, $HNO_2$ and other inhibitors have been tested to achieve nitrification/denitrification with nitrite as intermediate. Most of them initiated the formation of nitrite but could not prevent the formation of nitrate after longer periods. It seemed probable that all these process factors were not successful for full-scale application. The SHARON process is the first successful technique by which nitrification/denitrification with nitrite as intermediate under stable process conditions was achieved (Mulder et al., 2001).

The SHARON filtration process has been described in detail by Hellinga et al. (1998).

This process (patented) distinguishes itself from other biological wastewater treatment processes by a complete absence of sludge retention. Growth and washout of sludge are in equilibrium. The process has the following characteristics.

• Developed for biological nitrogen removal over nitrite in concentrated wastewater.

• Due to high temperatures (30–40 ºC) fast growing micro-organisms will develop in the reactor. The aerobic retention time may be limited to 1 day.

• Micro-organisms show high activity; however, the Ks value is rather high. As a result, effluent concentrations will be several tens of milligrams. The effluent concentration is independent of the influent concentration, the removal efficiency increases with higher inlet concentrations. In case of WWTP Dokhaven ($NH_4$–N>1 g/l) this results in removal efficiencies of over 90%.

• Nitrite oxidation can be prevented since at higher temperatures the NO2-oxidizing bacteria grow slower than the $NH_4$-oxidisers (Hunik et al., 1993). In a system without biomass retention (SRT=HRT) it is simple to limit the SRT in such a way that ammonium will be oxidised and nitrite will not be oxidised. Ammonia removal over nitrite instead of over nitrate has the following advantages:

• Oxidation to nitrite requires only 75% of the aeration energy.

• Denitrification starting with nitrite requires only 60% of the BOD addition.

• pH control is very important, due to the high concentrations and to high reaction rates.

The biocarbonate in the anaerobic effluent and the denitrification process compensate the acidifying effect of the nitrification. Both will take 50% of the alkalinity requirement. In the process however, the CO2 stripping needs to be sufficient to allow full use of the biocarbonate.

• Heat production is significant due to the high inlet concentrations. This had to be considered in the process design.

• As the process functions without sludge retention there is no influence of the presence of suspended solids in the reject water, for example, due to temporary malfunction of the sludge dewatering.

• Simple single reactor (CSTR) system required.

**Conclusion**

The current review paper provides an overview of major nutrients, their environmental and health effects, and their sources. With many distinct advantages, including operational simplicity, cost-effectiveness, extensive energy efficiency, and minimal need for pH control, SND is a desirable alternative for nutrient removal from domestic wastewater. Phosphorus removal denitrification appears to be a very promising process that leads to significant energy savings, less sludge production, improved efficiency, and reduced carbon source requirements, thus, it can effectively use limited carbon resources used in domestic sewage The incorporation of DPAOs in a SND process is recommended to realize DPAO mediated denitrification in a simultaneous nitrification–denitrification-phosphorus removal (SNDPR) system. It is also recommended that the coupling of archaeal ammonium oxidation-anammox-modified denitrifying phosphorous removal processes to intensify nitrogen removal and phosphorous recovery from low carbon/nitrogen wastewater in mainstream application with no external carbon source addition (Rouzitalab et al., 2020).

**Recommendations**

Drawing from the key insights of this review, the following recommendations aim to support researchers, engineers, and policymakers in advancing nutrient removal technologies in domestic wastewater treatment systems:

**Move from Lab to Field**

Many of the innovative technologies discussed such as SND, Anammox, SHARON, and forward osmosis have shown great promise in the lab. However, their real potential lies in how they perform at pilot and full-scale levels. More field-based studies are needed to evaluate their reliability, cost, and long-term

performance under actual operational conditions.

**Think Beyond Removal, Focus on Recovery**

Instead of just removing nutrients, future systems should aim to recover and reuse them. Nitrogen and phosphorus, for example, can be turned into valuable fertilizers(Volpin et al., 2018). Technologies like struvite precipitation and FO-based nutrient capture should be refined to support circular and sustainable practices.

**Make Energy Efficiency a Priority**

As energy costs and environmental concerns grow, it's important to prioritize low-energy, low-input solutions. Processes that pair biological nutrient removal with energy recovery (like anaerobic digestion) can make treatment plants more self-sufficient and eco-friendlier.

**Bring in Smart Technology**

Incorporating real-time sensors, automated monitoring, and AI-driven decision tools could help treatment plants react more quickly and operate more efficiently. Smart systems can also support predictive maintenance and early warning for process disruptions.

**Tackle Membrane Fouling Head-On**

Forward osmosis has great potential, but membrane fouling is still a big challenge. Developing better membrane materials with antifouling properties and finding practical cleaning solutions should be a research priority.

**Evaluate the Bigger Picture**

Life cycle assessments (LCAs) and techno-economic analyses (TEAs) are essential. These tools can help determine the true environmental and economic impacts of new technologies, guiding smarter investments and long-term planning.

**Support Small-Scale, Localized Systems**

In many rural or underserved areas, large centralized systems aren't feasible. Modular, decentralized treatment units that use these filtration technologies could offer effective, affordable solutions especially if tailored to local conditions.

**Align with Policy and Institutional Frameworks**

For these technologies to take off, supportive policies and funding mechanisms are crucial. Governments should revise discharge standards, incentivize innovation, and provide financial and technical support for transitioning to more advanced and sustainable treatment options.

**Acknowledgment**

This research has no acknowledgments.

**Conflict of Interest**

The authors declared no potential conflicts of interest concerning the research, authorship, and publication of this article. Confirmation.

**Funding**

The authors received no financial support for the research, authorship, and publication of this article.

**Data Availability Statements**

Data Availability Statement: All information and results are presented in the text of the article.

**Authors' contribution**

**First Author:** Saeid Eslamian, Led the research and manuscript preparation.

**Second Author:** Mousa Maleki, Provided analytical support and contributed to manuscript revisions.

**References**

1- Abdel-Raouf, N., Al-Homaidan, A.A. and Ibraheem, I., 2012. Microalgae and wastewater treatment. *Saudi Journal of Biological Sciences*, *19*(3), pp.257-275. https://doi.org/10.1016/j.sjbs.2012.04.005.

2- Ahn, Y.H., 2006. Sustainable nitrogen elimination biotechnologies: a review. *Process Biochemistry*, *41*(8), pp.1709-1721. https://doi.org/10.1016/j.procbio.2006.03.033.

3- Andalib, M., 2011. *Biological Nutrient Removal from Municipal and Industrial Wastewater Using a Twin Circulating Fluidized Bed Bioreactor*. The University of Western Ontario (Canada). https://ir.lib.uwo.ca/etd/119.

4- Anjali, G. and Sabumon, P.C., 2024. Revolutionizing Wastewater Treatment: Cutting-Edge Technologies for Biological Nutrient Removal. In *Biological and Hybrid Wastewater Treatment Technology: Recent Developments in India* (pp. 125-158). Cham: Springer Nature Switzerland. https://doi.org/10.1007/978-3-031-63046-0_6

5- Carvalho, G., Lemos, P.C., Oehmen, A. and Reis, M.A., 2007. Denitrifying phosphorus removal: linking the process performance with the microbial community structure. *Water research*, *41*(19), pp.4383-4396. https://doi.org/10.1016/j.watres.2007.06.065.

6- Chen, H., Wang, H., Chen, R., Chang, S., Yao, Y., Jiang, C., Wu, S., Wei, Y., Yu, G., Yang, M. and Li, Y.Y., 2021(a). Unveiling performance stability and its recovery mechanisms of one-stage partial nitritation-anammox process with airlift enhanced micro-granules. *Bioresource Technology*, *330*, p.124961. https://doi.org/10.1016/j.biortech.2021.124961.

7- Chen, H., Wang, H., Yu, G., Xiong, Y., Wu, H., Yang, M., Chen, R., Yang, E., Jiang, C. and Li, Y.Y., 2021(b). Key factors governing the performance and microbial community of one-stage partial nitritation and anammox system with bio-carriers and airlift circulation. *Bioresource Technology*, *324*, p.124668. https://doi.org/10.1016/j.biortech.2021.124668.

8- Chen, J., Yu, Z., Cheng, P., Tan, Y., Fan, X., Xu, X. and Zhu, L., 2024. Microbial synergy achieving simultaneous nitrification-denitrification (SND) in salt-tolerant aerobic granular sludge. *Journal of Water Process Engineering*, *60*, p.105138. https://doi.org/10.1016/j.jwpe.2024.105138

9- Connor, R., (2017). United Nations Economic and Social Commission for Western Asia, Economic and Social Commission for Asia and the Pacific and United Nations Economic Commission for Latin America and the Caribbean, . The United Nations World Water Development Report, Wastewater: the Untapped Resource. https://wedocs.unep.org/20.500.11822/20448

10- De Kreuk, M.K., Heijnen, J.J. and Van Loosdrecht, M.C.M., 2005. Simultaneous COD, nitrogen, and phosphate removal by aerobic granular sludge. *Biotechnology and Bioengineering*, *90*(6), pp.761-769. https://doi.org/10.1002/bit.20470.

11- Do, M.H., Ngo, H.H., Guo, W., Chang, S.W., Nguyen, D.D., Liu, Y., Varjani, S. and Kumar, M., 2020. Microbial fuel cell-based biosensor for online monitoring wastewater quality: a critical review. *Science of The Total Environment*, *712*, p.135612. https://doi.org/10.1016/j.scitotenv.2019.135612.

12- Dube, P.J., Vanotti, M.B., Szogi, A.A. and García-González, M.C., 2016. Enhancing recovery of ammonia from swine manure anaerobic digester effluent using gas-permeable membrane technology. *Waste Management*, *49*, pp.372-377. https://doi.org/10.1016/j.wasman.2015.12.011.

13- Eslamian, S, 2016, (ed.) Urban Water Reuse Handbook, Taylor and Francis, CRC Group, USA, 1141 Pages.

14- Faraji, M., Noormohammadi, F., Jafarinejad, S. and Moradi, M., 2017. Supramolecular-based solvent microextraction of carbaryl in water samples followed by high performance liquid chromatography determination. *International Journal of Environmental Analytical Chemistry*, *97*(8), pp.730-742. https://doi.org/10.1080/03067319.2017.1353088.

15- Freitas, F., Temudo, M. and Reis, M.A., 2005. Microbial population response to changes of the operating conditions in a dynamic nutrient-removal sequencing batch reactor. *Bioprocess and Biosystems Engineering*, *28*, pp.199-209. https://doi.org/10.1007/s00449-005-0029-9.

16- Ganigué, R., Gabarró, J., Sànchez-Melsió, A., Ruscalleda, M., López, H., Vila, X., Colprim, J. and Balaguer, M.D., 2009. Long-term operation of a partial nitritation pilot plant treating leachate with extremely high ammonium concentration prior to an anammox process. *Bioresource Technology*, *100*(23), pp.5624-5632. https://doi.org/10.1016/j.biortech.2009.06.023.

17- Guan, R.C., 2024. Single-Reactor Nitritation for High Strength Landfill Leachate Treatment. https://doi.org/10.7939/r3-c45c-p289.

18- He, Q., Song, Q., Zhang, S., Zhang, W. and Wang, H., 2018. Simultaneous nitrification, denitrification and phosphorus removal in an aerobic granular sequencing batch reactor with mixed carbon sources: reactor performance, extracellular polymeric substances and microbial successions. *Chemical Engineering Journal*, *331*, pp.841-849. https://doi.org/10.1016/j.cej.2017.09.060.

19- He, Q., Zhang, S., Zou, Z., Zheng, L.A. and Wang, H., 2016. Unraveling characteristics of simultaneous nitrification, denitrification and phosphorus removal (SNDPR) in an aerobic granular sequencing batch reactor. *Bioresource Technology*, *220*, pp.651-655. https://doi.org/10.1016/j.biortech.2016.08.105.

20- Heisler, J., Glibert, P.M., Burkholder, J.M., Anderson, D.M., Cochlan, W., Dennison, W.C., Dortch, Q., Gobler, C.J., Heil, C.A., Humphries, E. and Lewitus, A., 2008. Eutrophication and harmful algal blooms: a scientific consensus. *Harmful Algae*, *8*(1), pp.3-13. https://doi.org/10.1016/j.hal.2008.08.006.

21- Hellinga, C.S.A.A.J.C., Schellen, A.A.J.C., Mulder, J.W., van Loosdrecht, M.V. and Heijnen, J.J., 1998. The SHARON process: an innovative method for nitrogen removal from ammonium-rich waste water. *Water Science and Technology*, *37*(9), pp.135-142. https://doi.org/10.1016/S0273-1223(98)00281-9.

22- Jafarinejad, S. and Jiang, S.C., 2019. Current technologies and future directions for treating petroleum refineries and petrochemical plants (PRPP) wastewaters. *Journal of Environmental Chemical Engineering*, *7*(5), p.103326. https://doi.org/10.1016/j.jece.2019.103326.

23- Jafarinejad, S., 2016. *Petroleum waste treatment and pollution control*. Butterworth-Heinemann. https://www.google.com/books/edition/INDUSTRIAL_WASTEWATER_TREATMENT/k84nDwAAQBAJ?hl=en&gbpv=0

24- Jafarinejad, S., 2017. Cost estimation and economical evaluation of three configurations of activated sludge process for a wastewater treatment plant (WWTP) using simulation. *Applied Water Science*, *7*(5), pp.2513-2521. https://doi.org/10.1007/s13201-016-0446-8.

25- Jafarinejad, S., 2019(a). Cost-effective catalytic materials for AOP treatment units. *Applications of advanced oxidation processes (AOPs) in drinking water treatment*, pp.309-343. https://doi.org/10.1007/698_2017_77.

26- Jafarinejad, S., 2019(b). Simulation for the performance and economic evaluation of conventional activated sludge process replacing by sequencing batch reactor technology in a petroleum refinery wastewater treatment plant. *ChemEngineering*, *3*(2), p.45. https://doi.org/10.3390/chemengineering3020045.

27- Jafarinejad, S., Faraji, M., Jafari, P. and Mokhtari-Aliabad, J., 2017. Removal of lead ions from aqueous solutions using novel-modified magnetic nanoparticles: optimization, isotherm, and kinetics studies. *Desalination and Water Treatment*, *92*, pp.267-274. https://doi.org/10.5004/dwt.2017.21562

28- Kehrein, P., Van Loosdrecht, M., Osseweijer, P., Garfí, M., Dewulf, J. and Posada, J., 2020. A critical review of resource recovery from municipal wastewater treatment plants–market supply potentials, technologies and bottlenecks. *Environmental Science: Water Research & Technology*, *6*(4), pp.877-910. https://doi.org/10.1039/C9EW00905A.

29- Koop, S.H. and van Leeuwen, C.J., 2017. The challenges of water, waste and climate change in cities. *Environment, development and sustainability*, *19*(2), pp.385-418. https://doi.org/10.1007/s10668-016-9760-4.

30- Kwak, W., Rout, P.R., Lee, E. and Bae, J., 2020. Influence of hydraulic retention time and temperature on the performance of an anaerobic ammonium oxidation fluidized bed membrane bioreactor for low-strength ammonia wastewater treatment. *Chemical Engineering Journal*, *386*, p.123992. https://doi.org/10.1016/j.cej.2019.123992.

31- Le, V.G., Vo, D.V.N., Tran, H.T., Duy Dat, N., Luu, S.D., Rahman, M.M., Huang, Y.H. and Vu, C.T., 2021. Recovery of magnesium from industrial effluent and its implication on carbon capture and storage. *ACS Sustainable Chemistry & Engineering*, *9*(19), pp.6732-6740. https://doi.org/10.1021/acssuschemeng.1c00754.

32- Lee, E., Rout, P.R. and Bae, J., 2021. The applicability of anaerobically treated domestic wastewater as a nutrient medium in hydroponic lettuce cultivation: Nitrogen toxicity and health risk assessment. *Science of The Total Environment*, *780*, p.146482. https://doi.org/10.1016/j.scitotenv.2021.146482.

33- Li, Y., Pan, Z., Liao, J., Dai, R., Lin, J.G., Ling, J. and Xu, Y., 2024. Micro-aeration and low influent C/N are key environmental factors for achieving ANAMMOX in livestock farming wastewater treatment plants. *Water Research*, *253*, p.120141. https://doi.org/10.1016/j.watres.2023.120141

34- Liang, Z., 2007. Control factors of partial nitritation for landfill leachate treatment. *Journal of environmental sciences*, *19*(5), pp.523-529. https://doi.org/10.1016/S1001-0742(07)60087-4.

35- Liu, T., Ma, B., Chen, X., Ni, B.J., Peng, Y. and Guo, J., 2017. Evaluation of mainstream nitrogen removal by simultaneous partial nitrification, anammox and denitrification (SNAD) process in a granule-based reactor. *Chemical Engineering Journal*, *327*, pp.973-981. https://doi.org/10.1016/j.cej.2017.06.173

36- Liu, Y., Kwag, J.H., Kim, J.H. and Ra, C., 2011. Recovery of nitrogen and phosphorus by struvite crystallization from swine wastewater. *Desalination*, *277*(1-3), pp.364-369. https://doi.org/10.1016/j.desal.2011.04.056.

37- Ma, B., Bao, P., Wei, Y., Zhu, G., Yuan, Z. and Peng, Y., 2015. Suppressing nitrite-oxidizing bacteria growth to achieve nitrogen removal from domestic wastewater via anammox using intermittent aeration with low dissolved oxygen. *Scientific reports*, *5*(1), p.13048. https://doi.org/10.1038/srep13048

38- Ma, B., Wang, S., Cao, S., Miao, Y., Jia, F., Du, R. and Peng, Y., 2016. Biological nitrogen removal from sewage via anammox: recent advances. *Bioresource Technology*, *200*, pp.981-990. https://doi.org/10.1016/j.biortech.2015.10.074.

39- Ma, B., Xu, X., Wei, Y., Ge, C. and Peng, Y., 2020. Recent advances in controlling denitritation for achieving denitratation/anammox in mainstream wastewater treatment plants. *Bioresource Technology*, *299*, p.122697. https://doi.org/10.1016/j.biortech.2019.122697.

40- Mao, N., Ren, H., Geng, J., Ding, L. and Xu, K., 2017. Engineering application of anaerobic ammonium oxidation process in wastewater treatment. *World Journal of Microbiology and Biotechnology*, *33*, pp.1-11. https://doi.org/10.1007/s11274-017-2313-7.

41- Mofijur, M., Fattah, I.R., Kumar, P.S., Siddiki, S.Y.A., Rahman, S.A., Ahmed, S.F., Ong, H.C., Lam, S.S., Badruddin, I.A., Khan, T.Y. and Mahlia, T.M.I., 2021. Bioenergy recovery potential through the treatment of the meat processing industry waste in Australia. *Journal of Environmental Chemical Engineering*, *9*(4), p.105657. https://doi.org/10.1016/j.jece.2021.105657.

42- Montwedi, M., Munyaradzi, M., Pinoy, L., Dutta, A., Ikumi, D.S., Motoasca, E. and Van der Bruggen, B., 2021. Resource recovery from and management of wastewater in rural South Africa: Possibilities and practices. *Journal of Water Process Engineering*, *40*, p.101978. https://doi.org/10.1016/j.jwpe.2021.101978.

43- Mulder, J.W., Van Loosdrecht, M.C.M., Hellinga, C. and Van Kempen, R., 2001. Full-scale application of the SHARON process for treatment of rejection water of digested sludge dewatering. Water Science and Technology, 43(11), pp.127-134. https://doi.org/10.2166/wst.2001.0675.

44- Normative documents on the guidance of prices (NDGP), 2017. China environmental statistics yearbook. https://www.yearbookchina.com/ navibooklist-n3020013264-1. (Accessed 16 March 2021).

45- Patwardhan, A.D., 2017. *Industrial wastewater treatment*. PHI Learning Pvt. Ltd. https://www.google.com/books/edition/INDUSTRIAL_WASTEWATER_TREATMENT/k84nDwAAQBAJ?hl=en&gbpv=0

46- Pourmohammad, M., Faraji, M. and Jafarinejad, S., 2020. Extraction of chromium (VI) in water samples by dispersive liquid–liquid microextraction based on deep eutectic solvent and determination by UV–Vis spectrophotometry. *International Journal of Environmental Analytical Chemistry*, *100*(10), pp.1146-1159. https://doi.org/10.1080/03067319.2019.1650920.

47- Prosser, R.S. and Sibley, P.K., 2015. Human health risk assessment of pharmaceuticals and personal care products in plant tissue due to biosolids and manure amendments, and wastewater irrigation. *Environment International*, *75*, pp.223-233. https://doi.org/10.1016/j.envint.2014.11.020.

48- Qiu, S., Li, Z., Hu, Y., Shi, L., Liu, R., Shi, L., Chen, L. and Zhan, X., 2021. What's the best way to achieve successful mainstream partial nitritation-anammox application? *Critical Reviews in Environmental Science and Technology*, *51*(10), pp.1045-1077. https://doi.org/10.1080/10643389.2020.1745015.

49- Qu, J., Wang, H., Wang, K., Yu, G., Ke, B., Yu, H.Q., Ren, H., Zheng, X., Li, J., Li, W.W. and Gao, S., 2019. Municipal wastewater treatment in China: Development history and future perspectives. *Frontiers of Environmental Science & Engineering*, *13*, pp.1-7. https://doi.org/10.1007/s11783-019-1172-x.

50- Rene, E.R., Ge, J., Kumar, G., Singh, R.P. and Varjani, S., 2020. Resource recovery from wastewater, solid waste, and waste gas: engineering and management aspects. *Environmental Science and Pollution Research*, *27*, pp.17435-17437. https://doi.org/10.1007/s11356-020-08802-4.

51- Rosas-Echeverría, K., Fall, C., Gutiérrez-Segura, E., Romero-Camacho, M.P. and Ba, K.M., 2023. Mechanisms of persistence and impact of ordinary heterotrophic organisms in aerobic granular sludge. Bioresource Technology, 384, p.129346. https://doi.org/10.1016/j.biortech.2023.129346

52- Rouzitalab, Z., Maklavany, D.M., Jafarinejad, S. and Rashidi, A., 2020. Lignocellulose-based adsorbents: A spotlight review of the effective parameters on carbon dioxide capture process. *Chemosphere*, *246*, p.125756. https://doi.org/10.1016/j.chemosphere.2019.125756.

53- Roy, S., Nirakar, P., Yong, N.H. and Stefan, W., 2021. Denitrification kinetics indicates nitrous oxide uptake is unaffected by electron competition in Accumulibacter. *Water Research*, *189*, p.116557. https://doi.org/10.1016/j.watres.2020.116557.

54- Rubio-Rincón, F.J., Lopez-Vazquez, C.M., Welles, L., Van Loosdrecht, M.C.M. and Brdjanovic, D., 2017. Cooperation between Candidatus Competibacter and Candidatus Accumulibacter clade I, in denitrification and phosphate removal processes. *Water Research*, *120*, pp.156-164. https://doi.org/10.1016/j.watres.2017.05.001.

55- Shammas, N.K. and Wang, L.K., 2010. A/O phosphorus removal biotechnology. In *Environmental Biotechnology* (pp. 783-814). Totowa, NJ: Humana Press. https://doi.org/10.1007/978-1-60327-140-0_17.

56- Singh, P., Bisen, M., Kulshreshtha, S., Kumar, L., Choudhury, S.R., Nath, M.J., Mandal, M., Kumar, A. and Patel, S.K., 2025. Advancement in Anaerobic Ammonia Oxidation Technologies for Industrial Wastewater Treatment and Resource Recovery: A Comprehensive Review and Perspectives. *Bioengineering*, *12*(4), p.330. https://doi.org/10.3390/bioengineering12040330

57- Skilhagen, S.E., Dugstad, J.E. and Aaberg, R.J., 2008. Osmotic power—power production based on the osmotic pressure difference between waters with varying salt gradients. *Desalination*, *220*(1-3), pp.476-482. https://doi.org/10.1016/j.desal.2007.02.045.

58- Statkraft, 2013. Statkraft Halts Osmotic Power Investments. https://www.statkraft.com/newsroom/news-and-stories/archive/2013/Statkraft-halts-osmotic-power-investments/.

59- Sun, L., Shewa, W.A., Bossy, K. and Dagnew, M., 2024. Simultaneous nitrification and denitrification framework for decentralized systems: Long-term study utilizing rope-type biofilm media under field conditions. *Science of The Total Environment*, *956*, p.177337. https://doi.org/10.1016/j.scitotenv.2024.177337

60- Takeda, P.Y., Paula, C.T., Carneiro, R.B., do Vale Borges, A., Grangeiro, L.C. and Damianovic, M.H.R.Z., 2025. Challenges in achieving partial nitrification: Simultaneous nitrification-denitrification as the dominant pathway in municipal wastewater treatment. *Journal of Environmental Chemical Engineering*, *13*(2), p.115839. https://doi.org/10.1016/j.jece.2025.115839

61- United States Environmental Protection Agency, 2009. Nutrient Control Design Manual, State of Technology Review Report. Office of research and development, National Risk Management Research Laboratory eWater Supply and Water Resources Division. EPA/600/R-09/012.

62- United States Environmental Protection Agency, 2015. A Compilation of Cost Data Associated with the Impacts and Control of Nutrient Pollution. EPA 820-F-15-096. https://www.epa.gov/nutrient-policy-data/compilation-cost-dataassociated-impacts-andcontrol-nutrient-pollution.

63- Van de Graaf, A.A., de Bruijn, P., Robertson, L.A., Jetten, M.S. and Kuenen, J.G., 1996. Autotrophic growth of anaerobic ammonium-oxidizing micro-organisms in a fluidized bed reactor. *Microbiology*, *142*(8), pp.2187-2196. https://doi.org/10.1099/13500872-142-8-2187.

64- Van Vliet, M.T., Flörke, M. and Wada, Y., 2017. Quality matters for water scarcity. *Nature Geoscience*, *10*(11), pp.800-802. https://doi.org/10.1038/ngeo3047.

65- Volpin, F., Chekli, L., Phuntsho, S., Cho, J., Ghaffour, N., Vrouwenvelder, J.S. and Shon, H.K., 2018. Simultaneous phosphorous and nitrogen recovery from source-separated urine: A novel application for fertiliser drawn forward osmosis. *Chemosphere*, *203*, pp.482-489. https://doi.org/10.1016/j.chemosphere.2018.03.193.

66- Vu, M.T., Price, W.E., He, T., Zhang, X. and Nghiem, L.D., 2019. Seawater-driven forward osmosis for pre-concentrating nutrients in digested sludge centrate. *Journal of Environmental Management*, *247*, pp.135-139. https://doi.org/10.1016/j.jenvman.2019.06.082.

67- Wang, D., Wang, Q., Laloo, A., Xu, Y., Bond, P.L. and Yuan, Z., 2016. Achieving stable nitritation for mainstream deammonification by combining free nitrous acid-based sludge treatment and oxygen limitation. *Scientific Reports*, *6*(1), p.25547. https://doi.org/10.1038/srep25547.

68- Wang, S., Li, Z., Wang, D., Li, Y. and Sun, L., 2020. Performance and population structure of two carbon sources granular enhanced biological phosphorus removal systems at low temperature. *Bioresource Technology*, *300*, p.122683. https://doi.org/10.1016/j.biortech.2019.122683.

69- Wang, Z., Sun, C., Zhou, Y., Yu, Q., Xu, X., Zhao, Z. and Zhang, Y., 2022. Anaerobic ammonium oxidation driven by dissimilatory iron reduction in autotrophic Anammox consortia. *Bioresource Technology*, *364*, p.128077. https://doi.org/10.1016/j.biortech.2022.128077

70- Wei, D., Zhang, K., Ngo, H.H., Guo, W., Wang, S., Li, J., Han, F., Du, B. and Wei, Q., 2017. Nitrogen removal via nitrite in a partial nitrification sequencing batch biofilm reactor treating high strength ammonia wastewater and its greenhouse gas emission. *Bioresource Technology*, *230*, pp.49-55. https://doi.org/10.1016/j.biortech.2017.01.033.

71- Wu, T., Yang, S.S., Zhong, L., Pang, J.W., Zhang, L., Xia, X.F., Yang, F., Xie, G.J., Liu, B.F., Ren, N.Q. and Ding, J., 2023. Simultaneous nitrification, denitrification and phosphorus removal: what have we done so far and how do we need to do in the future?. *Science of the Total Environment*, *856*, p.158977. https://doi.org/10.1016/j.scitotenv.2022.158977.

72- Xue, W., Tobino, T., Nakajima, F. and Yamamoto, K., 2015. Seawater-driven forward osmosis for enriching nitrogen and phosphorous in treated municipal wastewater: effect of membrane properties and feed solution chemistry. *Water Research*, *69*, pp.120-130. https://doi.org/10.1016/j.watres.2014.11.007.

73- Yan, J., Wu, L., Ye, W., Zhou, J., Ji, Q., Gomez, M.A., Hong, Y., Lin, J.G. and Zhang, H., 2024. Ferric and sulfate coupled ammonium oxidation enhanced nitrogen removal in two-stage partial nitrification-Anammox/denitrification process for food waste liquid digestate treatment. *Bioresource Technology*, *398*, p.130533. https://doi.org/10.1016/j.biortech.2024.130533

74- Yang, Q., Shen, N., Lee, Z.M.P., Xu, G., Cao, Y., Kwok, B., Lay, W., Liu, Y. and Zhou, Y., 2016. Simultaneous nitrification, denitrification and phosphorus removal (SNDPR) in a full-scale water reclamation plant located in warm climate. *Water Science and Technology*, *74*(2), pp.448-456. https://doi.org/10.2166/wst.2016.214.

75- Yu, G., Peng, H., Fu, Y., Yan, X., Du, C. and Chen, H., 2019. Enhanced nitrogen removal of low C/N wastewater in constructed wetlands with co-immobilizing solid carbon source and denitrifying bacteria. *Bioresource Technology*, *280*, pp.337-344. https://doi.org/10.1016/j.biortech.2019.02.043.

76- Zhan, X., Yang, Y., Chen, F., Wu, S. and Zhu, R., 2020. Treatment of secondary effluent by a novel tidal-integrated vertical flow constructed wetland using raw sewage as a carbon source: Contribution of partial denitrification-anammox. *Chemical Engineering Journal*, *395*, p.125165. https://doi.org/10.1016/j.cej.2020.125165.

77- Zhang, M., Wang, S., Ji, B. and Liu, Y., 2019. Towards mainstream deammonification of municipal wastewater: Partial nitrification-anammox versus partial denitrification-anammox. *Science of the Total Environment*, *692*, pp.393-401. https://doi.org/10.1016/j.scitotenv.2019.07.293.

78- Zhao, J., Wang, X., Li, X., Jia, S. and Peng, Y., 2018. Advanced nutrient removal from ammonia and domestic wastewaters by a novel process based on simultaneous partial nitrification-anammox and modified denitrifying phosphorus removal. *Chemical Engineering Journal*, *354*, pp.589-598. https://doi.org/10.1016/j.cej.2018.07.211.

© 2026 The Author(s). Published by Shahid Chamran University of Ahvaz. This is an open-access article distributed under the terms of the Creative Commons Attribution License (http://creativecommons.org/licenses/by/4.0), which permits unrestricted use, distribution, and reproduction in any medium, provided the original work is properly cited.

Shahid Chamran University of Ahvaz

**Irrigation Sciences and Engineering (JISE)**
**Vol. 48, No. 4, Winter 2026, p. 145-164**
Journal homepage: https://jise.scu.ac.ir

**Review Paper**

# Microplastics: The Invisible Invaders – Unveiling Sources, Journeys, Impacts, and Cutting-Edge Remedies in a Plastic-Choked World

Fatemeh Elyasi[1], Laleh divband hafshejani[2] and Parvaneh Tishehzan[3*]

*1- Department of Environmental Engineering, Faculty of Water and Environmental Engineering, Shahid Chamran University of Ahvaz, Ahvaz, Iran*
*2- Department of Environmental Engineering, Faculty of Water and Environmental Engineering, Shahid Chamran University of Ahvaz, Ahvaz, Iran*
*3- Corresponding Author, Department of Environmental Engineering, Faculty of Water and Environmental Engineering, Shahid Chamran University of Ahvaz, Ahvaz, Iran*

**ARTICLE INFO**

*Article history:*
Received: 02 October 2025
Revised: 11 November 2025
Accepted: 29 November 2025
Available online: 04 January 2026

*Keywords:*
Microplastics; Polymer Types; Human Health Risks; Detection Technologies; Remediation Innovations.

**TO CITE THIS ARTICLE:**
Elyasi, F., Divband Hafshejani, L., Tishehzan, P. 2026. 'Microplastics: The Invisible Invaders – Unveiling Sources, Journeys, Impacts, and Cutting-Edge Remedies in a Plastic-Choked World', *Irrigation Sciences and Engineering*, 48(4), pp. 145-164. doi: 10.22055/jise.2026.51725.2198.

## Abstract

Microplastics, synthetic polymeric particles under 5 mm, have permeated every environmental niche, from oceanic depths to terrestrial soils and human tissues, posing profound ecological and health risks. This comprehensive review synthesizes current knowledge on their classification, polymer types, primary and secondary sources, and entry pathways driven by human activities such as wastewater discharge, agricultural practices, and urban runoff. It explores transport mechanisms influenced by physical properties, biofouling, and environmental forces, leading to accumulation in hotspots like river deltas and agricultural lands. Ecological impacts include ingestion by wildlife, causing malnutrition and microbial disruptions, while human health concerns encompass chemical toxicity via food chains and systemic exposure, inducing oxidative stress. Detection technologies range from vibrational spectroscopy to AI-powered sensors, and remediation innovations span physical filtration, biological degradation, and nanotechnology hybrids. Challenges like scalability, fouling, and secondary pollution are addressed alongside policy frameworks, including microbead bans and the Global Plastic Treaty. Emphasizing the urgency of a circular economy and harmonized standards, this review calls for integrated strategies to mitigate this Anthropocene hallmark, safeguarding ecosystems and public health.

## Introduction

### Definition and Overview of Microplastics

Microplastics are defined as synthetic polymeric particles typically less than 5 mm in size (Chandra & Walsh, 2024; Gao et al., 2022). These particles can originate from the breakdown of larger plastic items (secondary microplastics) or be directly manufactured for industrial purposes (primary microplastics). They have been found in a variety of environments, including oceans, rivers, soil, atmosphere, and even drinking water. Due to their persistence in the environment and their ability to absorb harmful pollutants, microplastics pose a significant ecological threat, making the development of effective remediation technologies an urgent environmental priority.

### Global Production and Prevalence

The global prevalence of microplastics is significant, driven by a massive increase in plastic production, which rose from 2 million tons in 1950 to approximately 400 million metric tons annually by 2023 (Kumar et al., 2025; Lu et al., 2025; Zielli et al., 2026). This production is projected to reach an

unprecedented 1,520 million metric tons by 2050 (Ramirez-Escarcega et al., 2025; Sepahvand et al., 2025). Much of this plastic is poorly managed; it is estimated that between 4.8 and 12.7 million metric tons of plastic waste enter the oceans from land-based sources every year (Joseph et al., 2025; Lu et al., 2025). Once in the environment, microplastics are ubiquitous, having been detected in all compartments, including remote Arctic ice (Li et al., 2025; Lin et al., 2025), the summit of Mount Everest, and deep-sea trenches thousands of meters below the surface (Kumar et al., 2025; Que et al., 2026; Sumaway et al., 2025).

**Research Focus and Implications**

Research focus is distributed across both aquatic and terrestrial environments. In aquatic environments, oceans, rivers, lakes, and estuaries serve as major transport pathways and reservoirs (Dinku et al., 2025; Joseph et al., 2025; Louvet et al., 2026). Rivers act as "highways" that move microplastics from land-based sources to the sea, where they can accumulate in the water column or settle into the deep-sea sediment (Kholis et al., 2026; Pilechi et al., 2022). Sinking behavior is influenced by particle density, shape, and biofouling, which increases the weight of buoyant polymers like polyethylene and polypropylene, causing them to descend (Dinku et al., 2025; Gkika et al., 2023). In terrestrial environments, soils are increasingly recognized as a major long-term sink for microplastics, receiving 4 to 23 times more annual plastic input than the oceans (Lu et al., 2025; Singh et al., 2025). Key entry routes into soil include the application of sewage sludge (biosolids), agricultural mulching films, and atmospheric deposition (Gao et al., 2025; Kumar et al., 2025). These particles can alter soil properties such as porosity, aggregation, and water retention, potentially hindering plant growth and microbial activity (Samandra et al., 2026; Zhao et al., 2026). These findings lay the groundwork for critical environmental engineering implications, including water purification and soil remediation efforts (Aragón et al., 2025; Gkika et al., 2023; Goh et al., 2025; Joseph et al., 2025; Li et al., 2025; Othman et al., 2021; Samandra et al., 2026). The detection of microplastics in human blood, lungs, and placenta further underscores the urgency of these remediation efforts to protect human health (Que et al., 2026; Sumaway et al., 2025).

## Sources and Types of Microplastics

### Classification and Physical Characteristics

Microplastics refer to a diverse range of small plastic particles, typically defined as those with diameters between 0.1 micrometers and 5 millimeters, though the term often encompasses those smaller than 5 mm (Avinash et al., 2023; Browne et al., 2011; Haque & Fan, 2023). Plastics can be categorized by size as follows: macroplastics (>25 mm), mesoplastics (25–5 mm), microplastics (5 mm to 0.1 micrometers), and nanoplastics (<0.1 micrometers) (Avinash et al., 2023; Browne et al., 2011; Haque & Fan, 2023). From an analytical standpoint, microplastics are usually defined as particles within the micrometer range (1 micrometer to 1 millimeter) (Li et al., 2025; Que et al., 2026; Sumaway et al., 2025). Based on their scale, these plastic contaminants are categorized as follows:

- Large Microplastics: Dimensions ranging from 1 mm to 5 mm (Gkika et al., 2023; Li et al., 2025; Samandra et al., 2026).
- Microplastics (Strict Sense): Particles between 1 µm and 1 mm (or 1000 µm) (Li et al., 2025; Samandra et al., 2026; Zielli et al., 2026).
- Nanoplastics: Particles generally defined as being smaller than 1 µm. Some sources specify a range of 1 nm to 1 µm for these ultra-fine particles (Gkika et al., 2023)(1-18-19).

Physically, these particles appear in various morphologies, including fibers, fragments, films, pellets, spheres, and foams. Their colors are equally diverse, including white, transparent, blue, black, yellow, red, and green, which can influence how they are ingested by aquatic and terrestrial organisms (Burhani et al., 2024; Kholis et al., 2026). Microplastics exhibit a variety of shapes, ranging from spherical to elongated fibers, and come in an array of colors. However, those that differ from natural particles in shape, size, or color (such as blue or red fibers) are more frequently encountered in

environmental studies. Microplastics and mesoplastics can also be categorized based on their shape, including pellets, fragments, fibers, films, and foams. Morphological descriptions of microplastics provide insights into their origin, type, shape, color, and degradation stage. In leachate, microplastics are predominantly found as fibers, granules, and fragments, and fibers are also the most common form found in sewage sludge and wastewater (Golwala et al., 2021; Hidalgo-Ruz et al., 2012; Su et al., 2019).

**Polymer Types and Composition**

These particles originate from the bonding of hydrocarbon atoms in polymers. When plastics degrade or are disposed of improperly, they release various harmful compounds into the environment, such as phthalates, polybrominated diphenyl ethers, and tetrabromobisphenol (Avinash et al., 2023; Browne et al., 2011; Haque & Fan, 2023). The composition of microplastics typically reflects global production trends. The most prevalent polymer types found in environmental samples include:

- Polyethylene (PE): Found in plastic bags, films, and containers; categorized as LDPE (low-density) or HDPE (high-density)(Joseph et al., 2025; Kumar et al., 2024; Othman et al., 2021).
- Polypropylene (PP): Used in packaging, automotive parts, and disposable surgical masks (Ramirez-Escarcega et al., 2025; Shen et al., 2022). (Othman et al., 2021)
- Polyethylene Terephthalate (PET): Primarily used for beverage bottles and synthetic textiles (Pilechi et al., 2022; Ramirez-Escarcega et al., 2025).
- Polyvinyl Chloride (PVC): Common in construction materials and plumbing (23-29-40).
- Polystyrene (PS): Used for food packaging and insulation (Othman et al., 2021; Ramirez-Escarcega et al., 2025).
- Polyamide (PA/Nylon): Frequently derived from clothing and fishing nets (Goh et al., 2025; Othman et al., 2021).
- Technical Polymers: Others include Polyurethane (PU), Polymethyl Methacrylate (PMMA), and Acrylonitrile Butadiene Styrene (ABS) (Othman et al., 2021; Samandra et al., 2026; Zielli et al., 2026). Polymeric plastics like polyethylene (PE), polyethylene terephthalate (PET), polypropylene (PP), polyvinyl chloride (PVC), and polystyrene (PS) are among the most produced materials, and fragments of these polymers are found throughout the environment (Wang et al., 2021). Notably, the behaviors of these plastics in the environment vary. For instance, PVC, nylon, and PET tend to settle, whereas PP, PE, and PS are more likely to float or remain suspended in aquatic environments. However, processes such as biofouling and the absorption of organic materials can alter these behaviors, leading to different distribution patterns in various environmental compartments (Kaiser et al., 2017). As summarized in Table (1), the concentration of microplastics in soil systems is strongly governed by the intensity and type of human activities, highlighting the direct link between anthropogenic land use and terrestrial microplastic pollution.

**Table 1- Physical Properties and Densities of Common Microplastic Polymers (Pilechi et al., 2022)**

| Polymer Type | Abbreviation | Density (kg/m³) | Typical Applications |
|---|---|---|---|
| Polyethylene | PE | 910–950 | Plastic bags, films, containers |
| Polypropylene | PP | 900–920 | Packaging, automotive parts, masks |
| Polystyrene | PS | 1040–1090 | Food packaging, insulation |
| Polyvinyl Chloride | PVC | 1160–1300 | Plumbing, construction materials |
| Polyethylene Terephthalate | PET | 1340–1390 | Beverage bottles, textiles |
| Polyamide (Nylon) | PA | 1130–1150 | Clothing, fishing nets |

 *DOI:* 10.22055/jise.2026.51725.2198

**Primary vs. Secondary Sources**

Microplastics are categorized into primary and secondary types (Joseph et al., 2025; Li et al., 2025). Primary microplastics are intentionally produced in small sizes for specific uses, such as plastic pellets, microbeads in personal care products, particles in paints, and tire wear. Secondary microplastics form when larger plastic items break down through processes like photooxidation, mechanical wear, or biological degradation. Common sources of secondary microplastics include synthetic clothing fibers, urban waste (e.g., bags, plastic bottles), fishing debris, and agricultural films. Tire wear is considered a major contributor to microplastic pollution, particularly due to the increasing global vehicle population (An et al., 2020; Hidalgo-Ruz et al., 2012; Yurtsever, 2019).

**Primary Microplastics (Intentionally Manufactured)**

These are engineered at the micro-scale for specific industrial or consumer uses:

- Microbeads: Found in personal care products such as facial cleansers, toothpaste, and body washes (Joseph et al., 2025; Li et al., 2025; Othman et al., 2021).
- Industrial Abrasives: Used as scrubbers for cleaning or air-blasting (Burhani et al., 2024; Othman et al., 2021).
- Pre-production Pellets (Nurdles): Raw materials for plastic manufacturing that often spill during transport or production (Burhani et al., 2024; Louvet et al., 2026).

**Secondary Microplastics (Fragmentation of Macroplastics)**

These result from the degradation of larger plastic debris (macroplastics) due to environmental stressors:

- Weathering: Breakdown via ultraviolet (UV) radiation, mechanical forces (wave and wind action), and temperature fluctuations (Joseph et al., 2025; Sumaway et al., 2025).
- Synthetic Fibers: Released from clothing and textiles during laundry processes; a single wash can release up to 190,000 fibers (Goh et al., 2025; Shen et al., 2022).
- Tire Wear: Abrasion of tires on road surfaces produces significant quantities of synthetic rubber particles (Sepahvand et al., 2025; Singh et al., 2025).
- Agricultural Residue: Degradation of mulching films, greenhouse covers, and silage wraps (Kumar et al., 2025; Singh et al., 2025).

**Human Activities and Environmental Entry**

Microplastics have been detected in a wide range of environments: the hydrosphere, pedosphere, and atmosphere. Due to improper plastic disposal and inadequate waste management, they are now ubiquitous in seas, lakes, rivers, deltas, the atmosphere, sediments, landfills, and wastewater treatment plants. These particles pose significant risks to ecosystems and human health, especially through the food chain (Browne et al., 2011; Petersen & Hubbart, 2021; Wang et al., 2021). While much of the research has focused on marine systems, land-based sources of microplastics, such as solid waste, remain underexplored. Solid waste sources include buried waste, sewage sludge, and food waste. Microplastics from buried waste and sewage sludge can enter the environment through leachate and runoff, while those from food waste depend on disposal and treatment processes (Golwala et al., 2021).

**Pollution in Aquatic Environments (Rivers, Lakes, Oceans)**

- Wastewater Discharge: Conventional wastewater treatment plants (WWTPs) are not designed to remove microplastics; as a result, millions of particles are released daily into receiving waters (Kumar et al., 2024; Shen et al., 2022).

- Urban and Stormwater Runoff: Rain washes street litter, road markings, and tire wear into drainage systems and rivers (Goh et al., 2025).
- Maritime and Fishing Activities: Direct release from lost fishing gear (ghost nets), ship sewage, ship gray water, and ship ballast water (Kholis et al., 2026; Othman et al., 2021).
- Tourism: Littering by seasonal visitors on beaches and coastal regions (Elawady et al., 2025; Kholis et al., 2026).

**Pollution in Terrestrial Environments (Soils)**

- Sewage Sludge/Biosolids: Treated sludge from WWTPs is often applied as fertilizer in agriculture, directly introducing concentrated microplastics into the soil (Othman et al., 2021; Singh et al., 2025).
- Agricultural Management: The use of plastic mulch films and irrigation with contaminated wastewater (Gao et al., 2025; Kumar et al., 2025).
- Solid Waste Mismanagement: Improper littering, open dumping, and uncontrolled landfills contribute to widespread soil contamination (Goh et al., 2025; Kumar et al., 2025).
- Atmospheric Deposition: Airborne particles derived from urban and industrial zones settle onto the soil surface via wind and precipitation (Samandra et al., 2026; Singh et al., 2025).

Land-use patterns strongly control the distribution and accumulation of microplastics in soil environments. Fig (1) demonstrates that soils associated with intensive human activities—particularly agricultural, urban, and industrial areas in Australia—harbor significantly higher microplastic abundances than less impacted land-use categories, underscoring the critical role of anthropogenic pressure in terrestrial microplastic contamination (Samandra et al., 2026).

## Transport and Accumulation of Microplastics

The transport of microplastics through the environment is complex and not yet fully understood. While microplastics may be transported as dust particles through the air, rivers are considered the primary pathway for their movement, like natural sediments (Rohais et al., 2024). The transport and accumulation of microplastics (MPs) are complex processes governed by the interplay between the physical properties of the particles, environmental forces, and biological interactions across aquatic and terrestrial systems (Joseph et al., 2025; Pilechi et al., 2022).

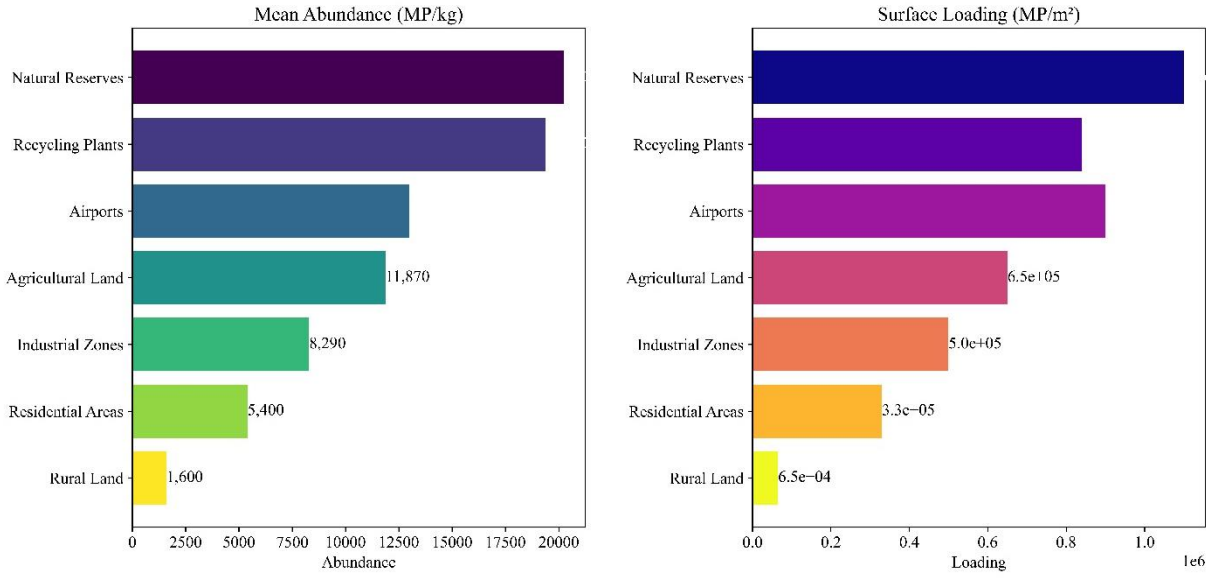



**Fig. 1- Microplastic Abundance in Soils by Land-Use Category (Case Study: Australia) (Samandra et al., 2026).**

**Physical Properties Influencing Movement**

The movement of microplastics is primarily driven by their density, size, and shape, which determines their buoyancy and settling velocity (Joseph et al., 2025; Pilechi et al., 2022):

- Density: Polymers denser than water (e.g., PVC, PET, and PS) tend to sink and accumulate in freshwater and marine sediments (Dinku et al., 2025; Silva & Marques, 2025). Conversely, low-density polymers (e.g., PE and PP) typically float on the surface or remain suspended in the water column (Dinku et al., 2025; Elawady et al., 2025).
- Size: Smaller particles (especially those <1 mm) are more susceptible to transport by wind and water currents (Joseph et al., 2025; Samandra et al., 2026). Decreasing particle size increases mobility, contributing to the widespread occurrence of microplastics in remote areas (Dinku et al., 2025; Samandra et al., 2026).
- Shape: Common morphologies include fibers, fragments, films, and pellets (Burhani et al., 2024; Pilechi et al., 2022). Fibers are notably prevalent in the atmosphere and water but are often more difficult to remove in treatment systems due to their tendency to escape filtration (Elawady et al., 2025; Shen et al., 2022). Irregularly shaped particles with sharp geometry are more likely to remain underwater, whereas spherical particles are more likely to remain on the surface (Zielli et al., 2026).

The behavior of microplastics in the environment is influenced by their physical properties, including polymer type, density, size, and shape. These factors affect buoyancy, drag force, and gravitational forces, all of which influence particle movement. Additionally, the degradation of polymers can affect the effective size of the particles, further complicating their transport. Pollution and deep mixing processes can also influence the long-range movement of microplastics (Shamskhany et al., 2021). In addition to physical properties, biological, chemical, and physical interactions affect the transport and fate of microplastics. Microplastics may remain in one location, incorporated into soil and sediments, or they may cycle between different environments, influenced by weather conditions, currents, and environmental factors (Horton & Dixon, 2018).

**Transport Pathways**

Microplastics utilize several primary conduits to migrate through ecosystems:

- Riverine Transport: Rivers act as the primary "highways" or conduits for transporting land-based plastic waste to the oceans (Joseph et al., 2025). An estimated 1.15 to 2.41 million tons of plastic flow from rivers to the sea annually (Kumar et al., 2025).
- Atmospheric Deposition: Airborne microplastics originate from tire wear, synthetic textile abrasion, and industrial emissions (Joseph et al., 2025; Kumar et al., 2025). These particles can be transported over vast distances by wind and return to the Earth's surface via dry deposition (gravitational settling) or wet deposition (scavenging by precipitation) (Gao et al., 2025).
- Soil Infiltration and Runoff: In terrestrial environments, microplastics enter the soil via sewage sludge application, plastic mulching, and irrigation (Gao et al., 2025; Singh et al., 2025). They can infiltrate deeper soil layers through urban runoff, vertical leaching, and bioturbation by soil fauna like earthworms, potentially reaching groundwater systems (Gao et al., 2025; Singh et al., 2025).

To better understand the fate and transport of microplastics in fluvial systems, predictive modelling approaches have been employed to simulate their distribution across river compartments. As shown in Fig (2), the model captures the movement and accumulation of microplastics along river pathways, providing quantitative support for fate-based assessments of freshwater-to-marine microplastic fluxes.

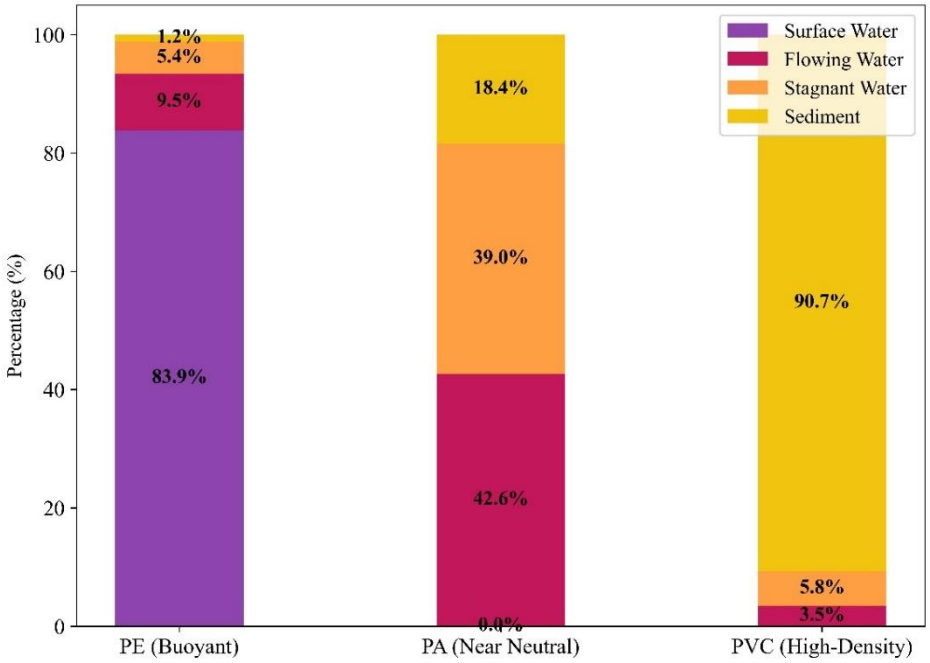



**Fig. 2- Predictive Distribution Model of Microplastics in River Compartments (Domercq et al., 2022).**

**Biological Factors and Biofouling**

Biofouling—the colonization of microplastic surfaces by microbial communities (biofilms)—significantly alters particle dynamics (Domercq et al., 2022; Joseph et al., 2025):

- Altered Density: Biofilm formation increases the effective density and weight of microplastics, causing buoyant polymers to sink into deep-sea habitats or sediments (Domercq et al., 2022; Joseph et al., 2025; Kumar et al., 2025).
- Surface Modification: Biofouling changes the hydrophobicity and surface charge of particles, which influences their aggregation with natural suspended particulate matter (SPM) and their interaction with aquatic organisms (Domercq et al., 2022; Pilechi et al., 2022).

**Accumulation Hotspots**

Specific environments serve as long-term repositories for microplastic accumulation:

- Aquatic Hotspots: These include oceanic gyres (garbage patches), river deltas, and deep-sea trenches. Semi-enclosed seas, such as the Mediterranean, are also significant hotspots (Elawady et al., 2025).
- Terrestrial Hotspots: Agricultural soils are major sinks due to the long-term use of plastic mulches and biosolid fertilizers. Urban roadsides accumulate high concentrations of tire wear and road paint particles (Samandra et al., 2026; Singh et al., 2025).

## Environmental and Health Impacts

Microplastic (MP) pollution has become a significant global threat to ecosystems and human health due to its persistence and capacity to interact with various biological systems (Gao et al., 2025; Lin et al., 2025). These particles, now recognized as indicators of the Anthropocene (or "Plasticene"), infiltrate every environmental compartment, leading to complex hidden damage (Muthulakshmi et al., 2023; Sepahvand et al., 2025).

**Ecological Effects on Aquatic and Terrestrial Wildlife**

Microplastics exert both physical and chemical pressures on a wide range of organisms:

- Ingestion in Aquatic Species: Marine life, from zooplankton and corals to fish and apex predators, mistakenly ingest MPs due to their attractive colors and buoyancy (Kholis et al., 2026). This leads to digestive blockages, internal injuries, reduced feeding

efficiency, and malnutrition (Anene et al., 2025; Gao et al., 2025; Sharma & Vidyarthi, 2024). Specifically, corals have been observed preferentially ingesting MPs over natural food, causing mesenteric atrophy and disrupting their symbiotic relationship with algae (Elawady et al., 2025; Gao et al., 2025).

- Terrestrial Impacts: In terrestrial systems, MPs are ingested by soil fauna like earthworms, causing enterocyte damage and thinning of the intestinal wall (Gao et al., 2025; Lu et al., 2025). Higher up the food chain, apex predators such as gray wolves and Persian leopards accumulate MPs through the consumption of contaminated prey, with higher loads often found in generalist predators closer to human infrastructure (Sepahvand et al., 2025). Poultry also ingests MPs from plastic litter or contaminated feed, leading to accumulation in the gizzard, liver, and muscle tissues, which eventually move into the human food chain (Joseph et al., 2025; Sharma & Vidyarthi, 2024).
- Biodiversity and Microbial Communities: MPs significantly disrupt soil microbial dynamics, particularly nitrogen-fixing bacterial communities. Specific polymers like polyester can reduce soil aggregation and nodule formation in legume plants like red clover, while polypropylene can decrease total bacterial abundance (Zhao et al., 2026).

**Human Health Risks and Toxicity**

Human exposure occurs through ingestion, inhalation, and dermal contact.

- Food Chain Entry: MPs have been detected in a vast array of consumables, including seafood, salt, sugar, honey, milk, beer, and tea (Kumar et al., 2025; Kumar et al., 2024). A single plastic teabag can release billions of micro- and nanoplastics into a single cup (Kumar et al., 2024).
- Chemical Additives and Toxicity: MPs act as vectors for over 16,000 chemicals, including hazardous additives like phthalates, bisphenol A (BPA), and organophosphate esters (OPEs) (Anene et al., 2025; Elawady et al., 2025). These chemicals are often endocrine disruptors linked to reproductive toxicity, reduced fertility, and developmental abnormalities. Furthermore, MPs absorb environmental toxins like heavy metals and persistent organic pollutants (POPs), amplifying their bioavailability to humans.
- Systemic Exposure: Biomonitoring has confirmed MPs in human blood, lungs, placenta, feces, urine, and arterial plaques (Anene et al., 2025; Joseph et al., 2025). Mechanistic studies suggest they induce oxidative stress, inflammatory cytokine release, mitochondrial impairment, and potentially carcinogenic effects (Gao et al., 2025; Joseph et al., 2025).

The detection of microplastics in human tissues and organs provides compelling evidence of direct human exposure. As shown in Table (2), these findings highlight the potential for widespread systemic distribution of microplastics within the human body, underscoring the urgency of assessing long-term health implications.

**Table 2- Detection of Microplastics in Human Tissues and Organs (Joseph et al., 2025; Zielli et al., 2026).**

| Tissue / Organ | Detected Polymers | Detection Method | Potential Health Implications |
|---|---|---|---|
| Blood | PE, PP, PS, PET, PVC | Py-GC/MS, Raman | Circulatory transport; immune activation |
| Lungs | PP, PET, PA, PE | μFTIR, Raman | Inflammation; oxidative stress; fibrosis |
| Placenta | PS, PP, PE, PVC | μFTIR, Raman | Barrier disruption; fetal health risk |
| Stool | PET, PE, PP, PS | FTIR | Gut dysbiosis; intestinal permeability |
| Breast Milk | PE, PVC, PP, PU | FTIR, Raman | Risk to neonatal development |
| Liver & Spleen | PS, PVC, PMMA, PET | Py-GC/MS | Hepatotoxicity; lipid metabolism effects |

**Specific Concerns in Water and Soil Environments**

The impact of MPs is uniquely manifested across these two primary sinks:

- Drinking Water Contamination: Both tap and bottled water are major sources of MP ingestion (Burhani et al., 2024; Kumar et al., 2024). Studies have found up to 5,400 particles/kg in salt and significant concentrations in mineral water, raising concerns for vulnerable populations such as infants consuming formula prepared with contaminated water (Burhani et al., 2024; Gao et al., 2025).
- Soil Fertility and Plant Uptake: In terrestrial environments, MPs alter physical soil properties, including porosity, bulk density, and water retention, often leading to drier, less fertile soil (Samandra et al., 2026; Singh et al., 2025; Zhao et al., 2026). MPs and even smaller Nano plastics are absorbed by plant roots and translocated through the vascular system to edible tissues (Singh et al., 2025). This uptake can inhibit seed germination, reduce chlorophyll content, and hinder nutrient absorption, ultimately lowering crop yield and quality. For example, polystyrene MPs have been shown to reduce biomass in crops like lettuce and rice (Gao et al., 2025; Singh et al., 2025).

**Detection and Monitoring Technologies**

Engineering tools for identifying and monitoring microplastic (MP) pollution span advanced spectroscopic characterization, standardized field sampling, spatial distribution modeling, and emerging real-time sensors. Infrared spectroscopy is widely regarded as the most reliable method for identifying the chemical composition of microplastics. To estimate their abundance, researchers typically use units such as "number per square meter" for sediment and sea surface studies and "number per cubic meter" for water column studies (Hidalgo-Ruz et al., 2012).

**Analytical Techniques and Characterization**

Accurate identification relies on physical and chemical profiling to distinguish polymers from natural debris.

- Vibrational Spectroscopy: Fourier Transform Infrared (FTIR) spectroscopy is the most established tool for identifying unique molecular vibrational signatures (Elawady et al., 2025; Lin et al., 2025). Micro-FTIR (μFTIR) enables spatially resolved detection of particles down to 10–20 μm (Dinku et al., 2025; Lin et al., 2025). Raman spectroscopy offers superior spatial resolution, detecting particles as small as 1 μm, and is less hindered by water interference, making it ideal for aqueous matrices (Lin et al., 2025; Zielli et al., 2026). Surface-Enhanced Raman Spectroscopy (SERS) uses metallic nanostructures to amplify signals, extending detection limits to the nanoscale (Li et al., 2025).
- Laser Direct Infrared (LDIR): This high-throughput system uses a quantum cascade laser for automated identification of chemical composition, size, and shape, typically in the 20–500 μm range (Que et al., 2026).
- Thermoanalytical Methods: Pyrolysis–GC/MS (Py-GC–MS) and Thermal Extraction Desorption (TED-GC–MS) provide mass-based quantification by breaking polymers into volatile fragments. These methods are destructive but can analyze particles smaller than the optical detection limits (Elawady et al., 2025; Li et al., 2025).
- Microscopy: Scanning Electron Microscopy (SEM) and Energy-Dispersive X-ray Spectroscopy (EDS) are used for high-resolution surface characterization and elemental identification (e.g., verifying PVC by detecting chlorine) (Li et al., 2025).

**Sampling and Extraction Methods**

Standardized collection is essential for comparing contamination levels across different environments.

- Water Sampling: Methods include using Rosette Water Samplers at various depths or plankton nets (e.g., 0.8 cm mesh) for surface and riverine transport (Kholis et al., 2026) (19-4). Subsurface sediments are often collected using Van Veen, Ekman, or Ponar grab samplers (Kholis et al., 2026).
- Soil and Sediment Sampling: Tools such as stainless-steel shovels and hand corers are used to collect stratified layers (Samandra et al., 2026).
- Laboratory Extraction: The process typically involves density separation using salt solutions (NaCl, $ZnCl_2$, or NaI) to float

plastic particles away from heavier sediment (Dinku et al., 2025). Chemical digestion (using KOH, $H_2O_2$, or enzymes such as proteinase K) is performed to remove interfering organic matter prior to filtration (Dinku et al., 2025; Sepahvand et al., 2025).

**Quantification Units and Data Reporting**

Microplastic abundance is expressed using several metrics to reflect environmental loading:

- Areal Units: Particles per $m^2$ or $g/m^2$ (surface loading) (Samandra et al., 2026).
- Mass/Volumetric Units: Particles per $m^3$, items per L, particles per kg of dry sediment/soil, or µg/g for mass-based concentrations (Elawady et al., 2025; Samandra et al., 2026).

**Monitoring Strategies and Spatial Modeling**

Engineering applications utilize data-driven approaches to track pollutant movement and identify hotspots.

- GIS and Remote Sensing: Geographic Information Systems (GIS) are integrated with satellite data (e.g., Sentinel-2) to monitor large-scale distributions of floating debris. Spatial modeling correlates MP loads with proximity to anthropogenic features like roads and villages.
- Numerical Fate Models: The SimpleBox4Plastic (SB4P) model estimates MP masses across air, water, and soil compartments (Papavasiliou et al., 2025). CaMPSim-3D is a numerical framework integrating Lagrangian particle tracking with hydrodynamic systems to predict MP transport in rivers and estuaries (Silva & Marques, 2025).

**Emerging Engineering Applications**

New technologies are moving detection from the laboratory to real-time, in situ deployment.

- Biosensors and Smart Sensors: Electrochemical biosensors utilize voltammetry and impedance to provide real-time monitoring of microplastics and adsorbed pollutants (Elawady et al., 2025). Plasmonic sensors integrated with machine learning can classify particle types and sizes in aqueous environments with high accuracy (Elawady et al., 2025; Lin et al., 2025).
- AI-Powered Vision: Real-time artificial intelligence systems, such as the YOLOv5 framework combined with camera systems, are used for automated counting and size estimation of microplastics in dynamic riverine environments (Elawady et al., 2025).
- Point-of-Care (PoC) Tools: Miniaturized devices and smartphone-assisted platforms are being developed for rapid contamination assessment in the field (Lin et al., 2025).

**Innovations in Remediation Technologies**

**Physical Removal Technologies**

Physical methods are typically the primary defence against microplastic pollution, focusing on separating, extracting, or immobilising microplastics through mechanical processes. These techniques have shown high removal efficiencies, even though they were not originally designed specifically for microplastics (Carr et al., 2016).

**Filtration and Membrane Technologies**

Advanced membrane technologies, including ultrafiltration, microfiltration, and membrane bioreactors, demonstrate removal efficiencies that often exceed 99% (Gao et al., 2022). These membranes, which have fine pore sizes, can trap even the smallest microplastic particles. However, they are susceptible to fouling and typically involve high operational costs. Other filtration technologies used in tertiary treatment, such as disc filters (DF), rapid sand filtration (RSF), dissolved air flotation (DAF), and membrane bioreactors (MBR), have also achieved efficiencies of up to 99.9% (Chandra & Walsh, 2024; Gkika et al., 2023; Song & Park, 2024).

## Adsorption-Based Removal

Functional materials like graphene composites, metal-organic frameworks (MOFs), biochar, live and biomass alga, and layered double hydroxides are highly effective adsorbents for types of pollution (Hafshejani et al., 2016; Hafshejani et al., 2015; Hoveizavi et al., 2024; Hooshmand et al., 2024; Menati et al., 2024; Hafshejani & Saeidinia; 2025). Their performance is significantly enhanced through

magnetisation or chemical modification, making them a powerful solution in the fight against microplastic pollution (Tiwari et al., 2020).

**Magnetic Separation**

Iron-based nanoparticles and magnetic carbon nanotubes play a crucial role in the efficient and selective separation of microplastics from various environments. This is especially important when faced with hydrophobic coatings that often hinder traditional separation methods (Li et al., 2025; Tang et al., 2021). These advanced materials utilise their magnetic properties to allow for rapid and effective extraction processes. By incorporating these nanoparticles and nanotubes, we not only significantly reduce the time required for separation but also achieve a remarkable decrease in energy consumption. This makes them invaluable resources in addressing the pressing issue of microplastic pollution while minimising environmental impact.

**Gravitational and Density-Based Separation**

In conventional wastewater treatment plants (WWTPs), the processes of sedimentation and skimming harness the intriguing properties of microplastics (MPs) through their varying densities and buoyancy. High-density particles settle robustly in grit chambers, making their descent like stones sinking to the bottom of a pond. Meanwhile, the low-density plastics rise to the surface, buoyed by their lightweight nature, floating alongside greasy residues and oily film, creating a troublesome scum that requires removal. During the initial stages of treatment, techniques such as screening, scum extraction, and gravity-assisted separation come into play, effectively capturing and eliminating between 35% to 98% of these pesky MPs (Carr & Thompson, 2019; Sarkar et al., 2022).

## Nature-Based Solutions

Constructed wetlands and floating treatment wetlands harness the intricate networks of plant-root systems, combined with the natural process of sedimentation, to efficiently capture microplastics. Through the remarkable process of phytoremediation, these innovative systems not only remove harmful pollutants from water but also revitalise the ecosystem, showcasing nature's power in combating environmental challenges (Ahmad et al., 2024).

Engineering-based removal technologies play a critical role in mitigating water pollution (Naghsh Javaheri et al., 2020; Etemadiasl et al., 2023). As shown in Table 3, the efficiency of physical removal systems differs significantly among filtration, membrane processes, electrocoagulation, and hybrid technologies, emphasizing the importance of technology selection and system optimization.

**Table 3- Efficiency of Engineering Technologies in Microplastic Removal (Song & Park, 2024)**

| Removal Method | Primary Mechanism | Efficiency (%) | Engineering Considerations |
|---|---|---|---|
| Membrane Bioreactor (MBR) | Size sieving + Biodegradation | > 99.4 | High cost; risk of membrane fouling |
| Ultrafiltration (UF) | Pore size separation | 100 | Effective for nanoscale particles |
| Electrocoagulation (EC) | Charge neutralization | 82–99 | Uses Al/Fe electrodes; energy efficient |
| Adv. Oxidation (AOP) | Chemical degradation | ~ 75 | Potential to create smaller fragments |
| Rapid Sand Filtration | Physical entrapment | 29–44 | Low efficiency for particles < 10 µm |

 *DOI:* 10.22055/jise.2026.51725.2198

**Biological and Biochemical Technologies**

Biological solutions effectively harness the power of natural microbial and enzymatic processes to break down microplastics—tiny plastic particles less than five millimetres in size—into benign byproducts such as carbon dioxide and water. These eco-friendly approaches play a vital role in sustainable environmental remediation by addressing the pervasive issue of plastic pollution. While these methods demonstrate significant potential, they do face challenges, particularly regarding the rate at which they can degrade microplastics and their scalability for widespread application. Increasing the efficiency of these biological processes requires ongoing research and development to optimise conditions for microbial activity and enzyme effectiveness. By overcoming these limitations, we can enhance the practicality of biological solutions and move toward a cleaner, healthier planet (Lu et al., 2025; Othman et al., 2021; Shen et al., 2022).

**Microbial Degradation**

Certain bacterial strains, such as Ideonella sakaiensis, have the remarkable ability to break down polyethylene terephthalate (PET), while fungi like Aspergillus niger are adept at degrading polyethylene (Yuan et al., 2020). These microorganisms use complex enzymatic reactions to dismantle harmful plastics, converting them into harmless byproducts such as carbon dioxide ($CO_2$), water ($H_2O$), and biomass. This process not only showcases the incredible potential of nature but also provides promising solutions for tackling plastic pollution in our environment.

**Enzymatic Hydrolysis**

Enzymes such as PETase, MHETase, cutinase, laccase, and hydrolases are powerful tools in the fight against plastic pollution. They can break down plastics by severing ester and carbon-carbon bonds (Dhali et al., 2024; Khairul Anuar et al., 2022). What makes these enzymes particularly remarkable is their ability to function under mild conditions, which makes them effective and environmentally friendly solutions for sustainable remediation strategies. By utilizing enzymatic hydrolysis, we can significantly enhance our efforts to reduce plastic waste and protect the environment.

**Biofilm-Assisted Capture**

In wastewater treatment plants (WWTPs), biofilms play a critical role in tackling microplastic pollution. These natural formations develop on the surfaces of microplastics, significantly changing their density and enhancing their sedimentation (Harrison et al., 2018). Although biofilms do not always completely break down plastics, their ability to effectively capture and immobilize these particles is essential. Additionally, the formation of floc and the active ingestion of microplastics by protozoa during secondary treatments significantly improve the removal process (Sarkar et al., 2022). By harnessing the power of biofilms, we can enhance the efficiency of wastewater treatment, contributing to a cleaner and more sustainable environment.

**Genetic and Synthetic Biology Approaches**

Innovative research in synthetic biology is leading the way in transforming the capabilities of microbes. By utilizing gene editing and pathway engineering, scientists are enhancing the efficiency and precision of these tiny organisms. This groundbreaking work involves fine-tuning enzymes and strategically assembling microbial consortia, enabling them to effectively address various types of plastic. The implications of these advancements are significant, as they offer promising solutions for tackling plastic pollution (Cai et al., 2023).

**Nanotechnology Applications**

Nanotechnology offers a promising solution for addressing the issue of microplastic remediation. It enables precise targeting and has a high surface reactivity, which allows for its integration into hybrid systems. This approach not only improves effectiveness but also fosters further advancements in environmental technology.

**Nano-Adsorbents and Membranes**

Carbon nanotubes, graphene oxide, and nano-enabled membranes are advanced materials that possess exceptionally large

surface areas and customizable surface chemistries. These qualities make them highly effective in capturing a wide variety of microplastic particles from complex environmental mixtures. These nanomaterials can be engineered to interact with different types of microplastics, which enhances their ability to filter out contaminants from water and soil. Their effectiveness in trapping microplastics results from their unique structural properties, which promote strong adsorption, thereby contributing to more efficient environmental cleanup strategies (Kumar et al., 2020).

**Photocatalysis**

Semiconducting nanoparticles, particularly titanium dioxide ($TiO_2$) and zinc oxide (ZnO), play a vital role in the photocatalytic degradation of plastic materials when they are illuminated by ultraviolet (UV) or visible light. This innovative process involves the absorption of light energy by these nanoparticles, which stimulates chemical reactions that break down large plastic polymers into smaller, less harmful molecules, thus reducing their environmental impact (Sacco et al., 2023; Uheida et al., 2021). Despite the promising nature of this approach in addressing plastic waste, several challenges limit its practical application. One major issue is the penetration depth of light, as not all areas of plastic materials receive sufficient exposure to activate the photocatalytic process effectively. Additionally, the high cost associated with producing and implementing these semiconductor materials can hinder their widespread use. Overcoming these obstacles is essential for harnessing the full potential of photocatalytic degradation in real-world applications aimed at minimizing plastic pollution (Ramirez-Escarcega et al., 2025).

**Magnetic Nanoparticles**

Functionalized magnetic nanoparticles offer a promising solution for the targeted and efficient removal of microplastics from various environments. These nanoparticles can be engineered with specific ligands or hydrophobic domains, which enhance their ability to attract and bind to microplastic particles. This selective affinity enables effective capture of microplastics, making the process both efficient and reusable. By utilizing the magnetic properties of these nanoparticles, they can be easily retrieved from mixtures after capturing the microplastics, thereby minimizing waste and facilitating recycling efforts (Li et al., 2025; Sumaway et al., 2025).

**Hybrid Nano-Bio Systems**

New and innovative methods are emerging that combine the unique properties of nanomaterials with the biological effectiveness of enzymes and microbial cells to significantly improve degradation processes. This synergy utilizes the catalytic capabilities of nanoparticles, which can accelerate chemical reactions, while also taking advantage of the specificity of biological agents to target specific substances. By integrating these two approaches, researchers aim to develop hybrid systems that enhance both the efficiency and effectiveness of breaking down complex pollutants and organic materials. These advancements, as noted by Mandeep and Shukla (2020), represent a promising direction in the fields of environmental remediation and bioengineering.

**Challenges, Policies, and Future Directions**

The transition from laboratory-scale research to real-world mitigation of microplastic (MP) pollution is hindered by significant engineering barriers, high economic costs, and a complex regulatory landscape.

**Engineering Barriers and Technical Limitations**

- High Costs and Scalability: Advanced detection methods like micro-FTIR and Raman spectroscopy are labor-intensive, time-consuming, and require expensive instrumentation, making high-throughput monitoring impractical (Elawady et al., 2025; Joseph et al., 2025). Similarly, while photocatalytic degradation and membrane bioreactors (MBR) show high efficiency, their implementation is restricted by high

capital and operational costs, particularly regarding energy consumption (Goh et al., 2025; Ramirez-Escarcega et al., 2025).

- Filter Fouling: A primary challenge in filtration systems (MF, UF, RO) is membrane fouling and pore clogging, where the accumulation of microplastics and organic matter reduces flux and necessitates frequent maintenance or replacement (Aragón et al., 2025; Gkika et al., 2023).
- Secondary Pollution from Nanotechnology: The use of magnetic nanoparticles for MP capture risks secondary contamination if the magnetic sorbents are not fully recovered from the effluent (Li et al., 2025). Furthermore, photocatalysis may unintentionally generate smaller, more bioavailable, and potentially more toxic fragments or chemical byproducts if mineralization is incomplete (Ramirez-Escarcega et al., 2025).
- Slow Biodegradation: Biological removal methods suffer from slow degradation rates (often requiring months or years) and are highly sensitive to environmental factors, making them less reliable for rapid, large-scale treatment (Domercq et al., 2022; Li et al., 2025; Lu et al., 2025).

**Policy Frameworks and Global Regulations**

- Microbead Bans: Many countries, including the USA, UK, Canada, and several EU member states, have enacted bans on the intentional use of plastic microbeads in "rinse-off" personal care products and cosmetics (Elawady et al., 2025; Kumar et al., 2025).
- UN Guidelines and International Treaties: The United Nations Sustainable Development Goal (SDG) 14.1 specifically targets the reduction and prevention of marine pollution, including marine debris, by 2025 (Sumaway et al., 2025). Efforts are also underway to develop a legally binding Global Plastic Treaty to address the full lifecycle of plastics (Sumaway et al., 2025)
- Regional Directives: The EU Single-Use Plastic Directive (SUPD) and the Marine Strategy Framework Directive set ambitious targets for waste reduction, mandatory recycled content, and standardized monitoring of microplastic trends in aquatic bodies (Elawady et al., 2025).

**Roles in Waste Management and Agricultural Control**

- Extended Producer Responsibility (EPR): This policy instrument holds manufacturers accountable for the entire lifecycle of their products, incentivizing the design of more durable, reusable, and recyclable items to minimize environmental leakage (Goh et al., 2025; Kumar et al., 2025).
- Agricultural Regulations: Stricter management is required for agricultural plastics, such as mulching films and greenhouse covers, which are major sources of soil contamination (Kumar et al., 2025; Sepahvand et al., 2025). Additionally, the application of sewage sludge (biosolids) as fertilizer is a significant pathway for microplastics to enter terrestrial ecosystems, necessitating improved sludge treatment or regulation (Goh et al., 2025; Kumar et al., 2025).
- Improved Recycling and Bio-alternatives: Shifting toward a circular economy involves advancing chemical recycling and developing biodegradable alternatives (e.g., PLA, PHA, or starch-based materials) that can naturally decompose without leaving persistent residues (Goh et al., 2025; Kumar et al., 2025)

Despite these developments, the absence of universally accepted standards for monitoring or limiting MPs continues to hamper coordinated global efforts (Silva & Marques, 2025). Establishing internationally harmonized protocols for sampling and reporting is essential to clarify true environmental loads and support effective legislation (Dinku et al., 2025; Zielli et al., 2026).

## Conclusions

Microplastics represent a pervasive and multifaceted environmental challenge, originating from diverse sources and polymers, transported through complex pathways, and accumulating in critical hotspots across aquatic and terrestrial ecosystems. As detailed in this review, their ecological impacts- ranging from wildlife ingestion and microbial disruptions to soil fertility alterations-coupled with human health risks such as systemic exposure and chemical toxicity, underscore the urgent need

for action. Advances in detection technologies, from spectroscopic methods to AI-driven sensors, provide robust tools for monitoring, while remediation innovations in physical, biological, and nanotechnology approaches offer promising solutions, albeit with challenges like scalability and secondary pollution. Policy frameworks, including bans, international treaties, and extended producer responsibility, are essential for prevention, yet require harmonization to be effective. Future research should prioritize integrated, circular economy strategies to reduce plastic production at the source, enhance biodegradation, and mitigate long-term risks, ultimately safeguarding biodiversity and public health in a plastic-dominated world.

**Acknowledgments**

The authors of this paper especially thank the Shahid Chamran University of Ahvaz, Iran.

**Conflict of Interest**

The authors declared no potential conflicts of interest concerning the research, authorship, and publication of this article.
Confirmation

**Funding**

The financial support of this research has been provided by Grant number SCU.WE1403.2589.

**Data Availability Statements**

The datasets generated and/or analyzed during the current study are available from the corresponding author on reasonable request.

**Authors' contribution**

**First Author:** Fatemeh Elyasi, Investigation, Writing – Original.
**Second Author:** Laleh Divband Hafshejani, Visualization, Writing – Review & Editing.
**Third Author:** Parvaneh Tishehzan Conceptualization, Writing – Review & Editing.

**References**

1- Ahmad, H.W., Bibi, H.A., Chandrasekaran, M., Ahmad, S. and Kyriakopoulos, G.L., 2024. Sustainable wastewater treatment strategies in effective abatement of emerging pollutants. *Water*, *16*(20), p.2893. https://doi.org/10.3390/w16202893.

2- An, L., Liu, Q., Deng, Y., Wu, W., Gao, Y., & Ling, W. (2020). Sources of microplastic in the environment. In *Microplastics in terrestrial environments: Emerging contaminants and major challenges* (pp. 143-159). Springer.

3- Anene, D.I., Beltran, M., Tjahjono, B., Schultz, A., McKenzie, M., Stevanovic, S. and Bogush, A., 2025. Microplastics and chemical additives from disposable face masks: Environmental, human health and behavioural impacts. *Science of the Total Environment*, *973*, p.179079. https://doi.org/10.1016/j.scitotenv.2025.179079.

4- Aragón, D., García-Merino, B., Barquín, C., Bringas, E., Rivero, M.J. and Ortiz, I., 2025. Advanced green capture of microplastics from different water matrices by surface-modified magnetic nanoparticles. *Separation and Purification Technology*, *354*, p.128813. https://doi.org/10.1016/j.seppur.2024.128813.

5- Avinash, G.P., Namasivayam, S.K.R. and Bharani, R.A., 2023. A critical review on occurrence, distribution, environmental impacts and biodegradation of microplastics. *Journal of Environmental Biology*, *44*(5), pp.655-664. DOI : http://doi.org/10.22438/jeb/44/5/MRN-5099

6- Browne, M. A., Crump, P., Niven, S. J., Teuten, E., Tonkin, A., Galloway, T., & Thompson, R. (2011). Accumulation of microplastic on shorelines woldwide: sources and sinks. *Environmental Science & Technology*, *45*(21), 9175-9179.

7- Burhani, D., Voet, V.S., Folkersma, R., Maniar, D. and Loos, K., 2024. Potential of Nanocellulose for Microplastic removal: Perspective and challenges. *Tetrahedron Green Chem*, *3*, p.100045. https://doi.org/10.1016/j.tgchem.2024.100045.

8- Cai, Z., Li, M., Zhu, Z., Wang, X., Huang, Y., Li, T., Gong, H. and Yan, M., 2023. Biological degradation of plastics and microplastics: a recent perspective on associated mechanisms and influencing factors. *Microorganisms*, *11*(7), p.1661. https://doi.org/10.3390/microorganisms11071661

9- Carr, S.A. and Thompson, J., 2019. Microplastics: Transport and removal at wastewater treatment plants. *Microplastics in water and wastewater*, pp.45-61. https://doi.org/10.2166/9781789060034_0045.

10- Carr, S.A., Liu, J. and Tesoro, A.G., 2016. Transport and fate of microplastic particles in wastewater treatment plants. *Water research*, *91*, pp.174-182. https://doi.org/10.1016/j.watres.2016.01.002.

11- Chandra, S. and Walsh, K.B., 2024. Microplastics in water: Occurrence, fate and removal. *Journal of contaminant hydrology*, *264*, p.104360. https://doi.org/10.1016/j.jconhyd.2024.104360

12- Dhali, S.L., Parida, D., Kumar, B. and Bala, K., 2024. Recent trends in microbial and enzymatic plastic degradation: a solution for plastic pollution predicaments. *Biotechnology for Sustainable Materials*, *1*(1), p.11.

13- Dinku, D.E., Ndur, S., Gyimah, E., Fosu, S. and Korley, P., 2025. Microplastics in African freshwater sediments: A systematic review of characteristics, abundance and analytical methods. *Cleaner Water*, p.100095.

14- Domercq, P., Praetorius, A. and MacLeod, M., 2022. The Full Multi: An open-source framework for modelling the transport and fate of nano-and microplastics in aquatic systems. *Environmental Modelling & Software*, *148*, p.105291. https://doi.org/10.1016/j.envsoft.2021.105291.

15- Elawady, A., Mohammed, J.A. and bin Abid, M., 2025. Advancements in Microplastics Detection Techniques and Their Multidimensional Impacts on Aquatic Ecosystems and Human Health. *Journal of Hazardous Materials: Plastics*, p.100025. https://doi.org/10.1016/j.hazmp.2025.100025.

16- Etemadiasl, F., Tishehzan, P., Kashefipour, S.M. and Jaafarzadeh Haaghighifard, N., 2023. Investigating and comparing chemical, electrochemical, and photo-electrochemical processes in decreasing dissolved iron from oily wastewaters using steel slag. *International Journal of Environmental Science and Technology*, *20*(9), pp.9881-9900.

17- Gao, T., Jiang, Y., Han, Y. and Wāng, Y., 2025. Intestinal microplastic debris, flora dysbiosis, and insidious combined hazards across diverse aquatic and terrestrial organisms. *Journal of Advanced Research*. https://doi.org/10.1016/j.jare.2025.06.074.

18- Gao, W., Zhang, Y., Mo, A., Jiang, J., Liang, Y., Cao, X. and He, D., 2022. Removal of microplastics in water: Technology progress and green strategies. *Green Analytical Chemistry*, *3*, p.100042. https://doi.org/10.1016/j.greeac.2022.100042.

19- Gkika, D.A., Tolkou, A.K., Evgenidou, E., Bikiaris, D.N., Lambropoulou, D.A., Mitropoulos, A.C., Kalavrouziotis, I.K. and Kyzas, G.Z., 2023. Fate and removal of microplastics from industrial wastewaters. *Sustainability*, *15*(8), p.6969. https://doi.org/10.3390/su15086969.

20- Goh, K.C., Kurniawan, T.A., Sarpin, N., Masrom, M.A.N., Othman, M.H.D., Anouzla, A., Aziz, F., Ali, I., Casila, J.C., Khan, M.I. and Zhang, D., 2025. Combating microplastic pollution in Malaysia's marine ecosystems using technological solutions, policy instruments, and public participation: a review. *Journal of Hazardous Materials Advances*, *17*, p.100542. https://doi.org/10.1016/j.hazadv.2024.100542

21- Golwala, H., Zhang, X., Iskander, S.M. and Smith, A.L., 2021. Solid waste: An overlooked source of microplastics to the environment. *Science of the Total Environment*, *769*, p.14458 https://doi.org/10.1016/j.scitotenv.2020.144581.

22- Hafshejani, L.D., Hooshmand, A., Naseri, A.A., Mohammadi, A.S., Abbasi, F. and Bhatnagar, A., 2016. Removal of nitrate from aqueous solution by modified sugarcane bagasse biochar. *Ecological Engineering*, *95*, pp.101-111. https://doi.org/10.1016/j.ecoleng.2016.06.035

23- Hafshejani, L.D., Nasab, S.B., Gholami, R.M., Moradzadeh, M., Izadpanah, Z., Hafshejani, S.B. and Bhatnagar, A., 2015. Removal of zinc and lead from aqueous solution by nanostructured cedar leaf ash as biosorbent. *Journal of molecular liquids*, *211*, pp.448-456. https://doi.org/10.1016/j.molliq.2015.07.044.

24- Hafshejani, L.D. and Saeidinia, M., 2025. Integrating chemical modification pathways and machine learning for optimization of nitrate removal by rapeseed (Brassica napus L.) biochar. *Scientific Reports*.

25- Haque, F. and Fan, C., 2023. Fate and impacts of microplastics in the environment: hydrosphere, pedosphere, and atmosphere. *Environments*, *10*(5), p.70. https://doi.org/10.3390/environments10050070.

26- Harrison, J.P., Hoellein, T.J., Sapp, M., Tagg, A.S., Ju-Nam, Y. and Ojeda, J.J., 2017. Microplastic-associated biofilms: a comparison of freshwater and marine environments. In *Freshwater microplastics: emerging environmental contaminants?* (pp. 181-201). Cham: Springer International Publishing.

27- Hidalgo-Ruz, V., Gutow, L., Thompson, R.C. and Thiel, M., 2012. Microplastics in the marine environment: a review of the methods used for identification and quantification. *Environmental science & technology*, *46*(6), pp.3060-3075. https://doi.org/10.1021/es2031505

28- Hooshmand, A., Menati, M., Tishehzan, P. and Baghdadi, M., 2024. Comparison of nitrate biosorption in the aqueous solutions by three algae species (Hypnea charaoides Lamx, Cheatomorpha antennina Borgessen, and Champia Kotschyana Harvey) and application of selected alga in a channel. *Water, Air, & Soil Pollution*, *235*(3), p.167.

29- Horton, A.A. and Dixon, S.J., 2018. Microplastics: An introduction to environmental transport processes. *Wiley Interdisciplinary Reviews: Water*, *5*(2), p.e1268. https://doi.org/10.1002/wat2.1268.

30- Hoveizavi, S., Tishehzan, P. and Hooshmand, A., 2024. Investigation of reducing the salinity of agricultural drainage water using cocopeat adsorbent. *Iranian Journal of Irrigation & Drainage*, *18*(3), pp.421-432.

31- Joseph, A.M., Babu, S.K., Shofia, S.I. and Nangan, S., 2025. Assessing the impact of microplastic polymer wastes on environmental fate and human health risks. *Physics and Chemistry of the Earth, Parts A/B/C*, p.104246. https://doi.org/10.1016/j.pce.2025.104246

32- Kaiser, D., Kowalski, N. and Waniek, J.J., 2017. Effects of biofouling on the sinking behavior of microplastics. *Environmental research letters*, *12*(12), p.124003.

33- Khairul Anuar, N.F.S., Huyop, F., Ur-Rehman, G., Abdullah, F., Normi, Y.M., Sabullah, M.K. and Abdul Wahab, R., 2022. An overview into polyethylene terephthalate (PET) hydrolases and efforts in tailoring enzymes for improved plastic degradation. *International journal of molecular sciences*, *23*(20), p.12644. https://doi.org/10.3390/ijms232012644

34- Kholis, N., Manullang, C.Y., Anuar, S.T., Atmadipoera, A.S., Zuraida, R. and Patria, M.P., 2026. Microplastic concentration in the water column of the Banggai Sea, Central Sulawesi, Indonesia. *Water Biology and Security*, p.100553. https://doi.org/10.1016/j.watbs.2026.100553.

35- Kumar, M., Borah, P. and Devi, P., 2020. Priority and emerging pollutants in water. In *Inorganic pollutants in water* (pp. 33-49). Elsevier. https://doi.org/10.1016/B978-0-12-818965-8.00003-2.

36- Kumar, M., Chaudhary, V., Kumar, R., Chaudhary, V., & Srivastav, A. L. (2025). Microplastics, their effects on ecosystems, and general strategies for mitigation of microplastics: A review of recent developments, challenges, and future prospects. *Environmental Pollution and Management*, *2*, 87-105.

37- Kumar, V., Sharma, N., Umesh, M., Gupta, P., Sharma, P., Basheer, T., Huligowda, L.K.D., Thomas, J., Bhagat, S.K. and Pasrija, R., 2024. Microplastics in food: Occurrence, toxicity, green analytical detection methods and future challenges. *Green Analytical Chemistry*, *11*, p.100152. https://doi.org/10.1016/j.greeac.2024.100152

38- Li, M., Zhao, Z., Zhao, Z. and Li, M., 2025. Review of techniques for the detection, removal, and transformation of environmental microplastics and nanoplastics. *ACS Applied Materials & Interfaces*, *17*(14), pp.20560-20589. https://doi.org/10.1021/acsami.5c02306

39- Lin, J.-T., Chung, Y.-P., Lee, Y.-Y., Wu, T.-L., Huynh, T. T. T., Nguyen, P. T., Lu, M.-J., Huang, B.-W., Lin, J.T., Chung, Y.P., Lee, Y.Y., Wu, T.L., Huynh, T.T.T., Nguyen, P.T., Lu, M.J., Huang, B.W., Sriram, B., Wang, S.F. and Chang-Chien, G.P., 2025. Emerging analytical frontiers in microplastic detection: From spectroscopy to smart sensor technologies. *Talanta Open*, *12*, p.100514. https://doi.org/10.1016/j.talo.2025.100514.

40- Louvet, J., Quik, J.T. and Boulay, A.M., 2026. Regionalized characterization factors for microplastic emissions in life cycle assessment considering multimedia fate modelling. *Journal of Cleaner Production*, *538*, p.147217. https://doi.org/10.1016/j.jclepro.2025.147217.

41- Lu, C., Dong, H., Li, H., Huang, X., Du, Y., Ren, Z., Xu, Z., Li, B., Zhu, L., Wang, J. and Wang, J., 2025. Toxicity comparison of multiple biodegradable and conventional microplastics on earthworms: Ingestion, tissue damage, oxidative stress, and transcriptional responses. *Ecotoxicology and Environmental Safety*, *307*, p.119415. https://doi.org/10.1016/j.ecoenv.2025.119415

42- Mandeep and Shukla, P., 2020. Microbial nanotechnology for bioremediation of industrial wastewater. *Frontiers in microbiology*, *11*, p.590631.

43- Menati, M., Tishehzan, P., Hooshmand, A. and Baghdadi, M., 2024. Application of Champia kotschyana Harvey biosorbent for cadmium removal: mechanisms and influencing factors. *Journal of Environmental Research and Technology*, *15*(15), p.83.DOI: 10.61186/jert.46935.9.15.99.

44- Muthulakshmi, L., Mohan, S. and Tatarchuk, T., 2023. Microplastics in water: types, detection, and removal strategies. *Environmental Science and Pollution Research*, *30*(36), pp.84933-84948.

45- Naghsh Javaheri, M., Tishehzan, P. and Moazed, H., 2020. Development of a complete and straightforward hybrid model for gray water treatment. *Clean Technologies and Environmental Policy*, *22*(8), pp.1745-1753.

46- Othman, A.R., Hasan, H.A., Muhamad, M.H., Ismail, N.I. and Abdullah, S.R.S., 2021. Microbial degradation of microplastics by enzymatic processes: a review. *Environmental Chemistry Letters*, *19*(4), pp.3057-3073.

47- Papavasiliou, C., Mintis, D.G., Tsoumanis, A., Karaoli, A., Lynch, I., Krause, S., Varsou, D.D., Melagraki, G., Kavousanakis, M. and Afantitis, A., 2025. MicroPlasticFate web application: Multimedia environmental fate modelling of microplastic particles via the enalos cloud platform. *Bioresource Technology Reports*, p.102157. https://doi.org/10.1016/j.biteb.2025.102157

48- Petersen, F. and Hubbart, J.A., 2021. The occurrence and transport of microplastics: The state of the science. *Science of the Total Environment*, *758*, p.143936. https://doi.org/10.1016/j.scitotenv.2020.143936.

49- Pilechi, A., Mohammadian, A. and Murphy, E., 2022. A numerical framework for modeling fate and transport of microplastics in inland and coastal waters. *Marine pollution bulletin*, *184*, p.114119. https://doi.org/10.1016/j.marpolbul.2022.114119.

50- Que, Y., Zhang, Z., Wu, Y., Cheng, W., Wang, L., Wang, Y., Zhang, Y. and Lu, K., 2026. Detection and Characterization of Microplastics in Commercial Eye Drops: A Novel Ocular Exposure Pathway. *Journal of Hazardous Materials Advances*, p.101019. https://doi.org/10.1016/j.hazadv.2026.101019

51- Ramirez-Escarcega, K.J., Amaya-Galvan, K.J., Garcia-Prieto, J.C., Silerio-Vazquez, F.D.J. and Proal-Najera, J.B., 2025. Advancing photocatalytic strategies for microplastic degradation in aquatic systems: Insights into key challenges and future pathways. *Journal of Environmental Chemical Engineering*, p.115594. https://doi.org/10.1016/j.jece.2025.115594

52- Rohais, S., Armitage, J.J., Romero-Sarmiento, M.F., Pierson, J.L., Teles, V., Bauer, D., Cassar, C., Sebag, D., Klopffer, M.H. and Pelerin, M., 2024. A source-to-sink perspective of an anthropogenic marker: A first assessment of microplastics concentration, pathways, and accumulation across the environment. *Earth-Science Reviews*, *254*, p.104822. https://doi.org/10.1016/j.earscirev.2024.104822.

53- Sacco, N.A., Zoppas, F.M., Devard, A., González Muñoz, M.D.P., García, G. and Marchesini, F.A., 2023. Recent advances in microplastics removal from water with special attention given to photocatalytic degradation: review of scientific research. *Microplastics*, *2*(3), pp.278-303. https://doi.org/10.3390/microplastics2030023.

54- Samandra, S., Mackay, E.S., Alwan, W.S., Ellis, A.V. and Clarke, B.O., 2026. Widespread microplastic contamination in Australian soils: Sources, pathways, and environmental implications. *Chemosphere*, *395*, p.144825. https://doi.org/10.1016/j.chemosphere.2026.144825.

55- Sarkar, D.J., Das Sarkar, S. and Das, B.K., 2022. Occurrence, fate and removal of microplastics in wastewater treatment plants (WWTPs) and drinking water treatment plants (DWTPs). In *Microplastics Pollution in Aquatic Media: Occurrence, Detection, and Removal* (pp. 223-245). Singapore: Springer Singapore.

56- Sepahvand, P., Ghasempouri, S.M. and Moradmand, M., 2025. Hidden Microplastic Pollution in Protected Terrestrial Ecosystems: Evidence from Gray wolves and Persian Leopards. *Journal of Hazardous Materials: Plastics*, p.100026. https://doi.org/10.1016/j.hazmp.2025.100026

57- Shamskhany, A., Li, Z., Patel, P. and Karimpour, S., 2021. Evidence of microplastic size impact on mobility and transport in the marine environment: a review and synthesis of recent research. *Frontiers in Marine Science*, *8*, p.760649. https://doi.org/10.3389/fmars.2021.760649.

58- Sharma, P. and Vidyarthi, V.K., 2024. Impact of microplastic intake via poultry products: Environmental toxicity and human health. *Journal of Hazardous Materials Advances*, *14*, p.100426. https://doi.org/10.1016/j.hazadv.2024.100426.

59- Shen, M., Zhang, Y., Almatrafi, E., Hu, T., Zhou, C., Song, B., Zeng, Z. and Zeng, G., 2022. Efficient removal of microplastics from wastewater by an electrocoagulation process. *Chemical Engineering Journal*, *428*, p.131161. https://doi.org/10.1016/j.cej.2021.131161.

60- Silva, D.B. and Marques, A.C., 2025. $TiO_2$-based photocatalytic degradation of microplastics in water: Current status, challenges and future perspectives. *Journal of Water Process Engineering*, *72*, p.107465. https://doi.org/10.1016/j.jwpe.2025.107465.

61- Singh, D.J., Dikshit, A.K. and Kumar, S., 2025. Impact of Macro-and Microplastic Litter Pollution on Terrestrial Soil-Plant Ecosystems: Pathways, Fate, and Transport. *Current Opinion in Environmental Science & Health*, p.100694. https://doi.org/10.1016/j.coesh.2025.100694

62- Song, M. and Park, J.Y., 2024. Removal of microplastics in a hybrid treatment process of ceramic microfiltration and photocatalyst-mounted PES spheres with air backwashing. *Membranes*, *14*(8), p.169. https://doi.org/10.3390/membranes14080169.

63- Su, Y., Zhang, Z., Wu, D., Zhan, L., Shi, H. and Xie, B., 2019. Occurrence of microplastics in landfill systems and their fate with landfill age. *Water research*, *164*, p.114968. https://doi.org/10.1016/j.watres.2019.114968

64- Sumaway, A.M.N., Rajput, R., Mohan, G., Katsuma, Y. and Pu, J., 2025. A systematic review of microplastics perception and its factors: Implications on SDGs. *Sustainable Futures*, *10*, p.101417. https://doi.org/10.1016/j.sftr.2025.101417

65- Tang, Y., Zhang, S., Su, Y., Wu, D., Zhao, Y. and Xie, B., 2021. Removal of microplastics from aqueous solutions by magnetic carbon nanotubes. *Chemical Engineering Journal*, *406*, p.126804. https://doi.org/10.1016/j.cej.2020.126804

66- Tiwari, E., Singh, N., Khandelwal, N., Monikh, F.A. and Darbha, G.K., 2020. Application of Zn/Al layered double hydroxides for the removal of nano-scale plastic debris from aqueous systems. *Journal of hazardous materials*, *397*, p.122769. https://doi.org/10.1016/j.jhazmat.2020.122769.

67- Uheida, A., Mejía, H.G., Abdel-Rehim, M., Hamd, W. and Dutta, J., 2021. Visible light photocatalytic degradation of polypropylene microplastics in a continuous water flow system. *Journal of hazardous materials*, *406*, p.124299. https://doi.org/10.1016/j.jhazmat.2020.124299.

68- Wang, C., Zhao, J. and Xing, B., 2021. Environmental source, fate, and toxicity of microplastics. *Journal of hazardous materials*, *407*, p.124357. https://doi.org/10.1016/j.jhazmat.2020.124357.

69- Yuan, J., Ma, J., Sun, Y., Zhou, T., Zhao, Y. and Yu, F., 2020. Microbial degradation and other environmental aspects of microplastics/plastics. *Science of the Total Environment*, *715*, p.136968. https://doi.org/10.1016/j.scitotenv.2020.136968

70- Yurtsever, M., 2019. Glitters as a source of primary microplastics: an approach to environmental responsibility and ethics. *Journal of Agricultural and Environmental Ethics*, *32*(3), pp.459-478.

71- Zhao, T., Lozano, Y.M., Li, G., Lammel, D.R., Quensen, J.F. and Rillig, M.C., 2026. Microplastics disrupt the nitrogen-fixing bacterial community with consequences for plant growth. *Applied Soil Ecology*, *219*, p.106772. https://doi.org/10.1016/j.apsoil.2025.106772

72- Zielli, S.O., Pascali, J., Mazzotti, A., Fais, P., Fini, M., Faldini, C. and Pelotti, S., 2026. Microplastics and Nanoplastics in human tissues: systematic review of evidence, analytical protocols, and methodological challenges. *Talanta Open*, p.100615. https://doi.org/10.1016/j.talo.2026.100615.

© 2026 The Author(s). Published by Shahid Chamran University of Ahvaz. This is an open-access article distributed under the terms of the Creative Commons Attribution License (http://creativecommons.org/licenses/by/4.0), which permits unrestricted use, distribution, and reproduction in any medium, provided the original work is properly cited.

Journal of
Irrigation Sciences and Engineering(JISE)
ISSN 2588-5952
Iranian Hydraulic Association
Shahid Chamran University of Ahvaz
Faculty of Water and Environmental Engineering
Vol. 48(4) Winter 2026

Contents

------- Research Papers -------

**Experimental Study of Longitudinal Extension Effects on Scour Patterns Around Single and Grouped Piers** 1
Farinaz Erfani Fard, Seyed Amin Asghari Pari and Lotfollah Emadali

**Evaluating Environmental Impacts of Dam Construction Using an Enhanced Quantitative Checklist: A Case Study of Haleh Dam in Iran** 19
Nader Nabipour and Babak Lashkar-Ara

**Numerical investigation of Semicircular Sharp-Crested Weirs** 37
Abbas Parsaie, Mohammad Bahrami Yarahmadi and Mahziar BasitNejad

**Investigation of Changes in the Green and Blue Water Footprint of Wheat in Drought and Rainy Seasons (A Case Study on Wheat under the Dez Irrigation Network, Southwestern Iran)** 49
Mahkameh Mansouri, Esfandiar Fateh, Amir Aynehband and Ali Shahbazi

**Assesment the adaptability of Jacaranda mimosifolia L. to Ahvaz climete condition under salinity and water stresses** 65
Khalil Asadivafa, Mousa Mousavi, Abdul-kadhm N. S. Al-Showily, Mohammad Albaji and Naser Alemzadeh Ansari

**Estimation of Transmissivity and Storage Coefficients in a Dual-Aquifer System Using Combined Field and Analytical Methods** 79
Sheyda Mohammadi Fard, Jahangir Abedi-Koupai and Saeid Eslamian

**Debris Blockage Risk of Modified Stepped Spillways: A Laboratory Study on Obstacle Configuration** 105
Seyed Amin Asghari Pari, Seyed Ali Asghari Pari, Mohammad Amin Mokarram and Mojtaba Kordnaeij

**Environmental Water Diplomacy between Iran and Turkey: Challenges and Strategic Priorities** 117
Fatemeh Lashkari, Mir Mehrdad Mirsanjari and Fatemeh Mohammadyari

------- Review Papers-------

**Modern Filtration Technologies for Nutrient Removal from Domestic Wastewaters: A Review** 133
Saeid Eslamian and Mousa Maleki

**Microplastics: The Invisible Invaders – Unveiling Sources, Journeys, Impacts, and Cutting-Edge Remedies in a Plastic-Choked World** 145
Fatemeh Elyasi, Laleh divband hafshejani and Parvaneh Tishehzan